QCD Phenomenology of Heavy Particle Dynamics

Emanuel Norrbin

Department of Theoretical Physics
Lund University, Sweden

Thesis for the degree of Doctor of Philosophy

Thesis Advisor: Torbjörn Sjöstrand

Faculty Opponent: Eric Laenen

To be presented, with the permission of the Faculty of Mathematics and Natural Sciences of Lund University, for public criticism in Lecture Hall F of the Department of Theoretical Physics on Friday, the 17th of November 2000, at 10.15 a.m.

Organization **LUND UNIVERSITY** Department of Theoretical Physics Sölvegatan 14A SE-223 62 Lund	**Document Name** **DOCTORAL DISSERTATION** **Date of issue** October 2000 **CODEN:**
Author(s) Emanuel Norrbin	**Sponsoring organization**

Title and subtitle

QCD Phenomenology of Heavy Particle Dynamics

Abstract

In this thesis the phenomenology of Quantum Chromo Dynamics (QCD) is studied in a variety of circumstances from both perturbative and non-perturbative perspectives. The main emphasis is on the production and hadronization of heavy particles, specifically heavy quarks, gauge bosons, leptoquarks and supersymmetric particles.
In the hadroproduction of long-lived heavy quarks (i.e. charm and bottom) in the context of string fragmentation, the pull of a beam remnant at the other end of a string may give a heavy hadron more energy than the perturbatively produced quark. The collapse of a low-mass string to a single hadron is the extreme case of this effect, and gives rise to asymmetries between hadron and anti-hadron spectra. The Lund string fragmentation model is studied and improved by considering fixed-target data and the model is then used to predict the outcome of future experiments.
The describtion of QCD radiation off heavy quarks and supersymmetric coloured particles is improved by using matrix element corrections to the massless parton shower in the event generator Pythia.
In the process $\mathrm{e}^+\mathrm{e}^- \to \mathrm{W}^+\mathrm{W}^- \to \mathrm{q}\overline{\mathrm{q}}\mathrm{q}'\overline{\mathrm{q}}'$, the colour flow can be ambiguous and a transverse momentum based measure of the colour flow is investigated as a tool to determine string topologies. The method is used to study different models of colour reconnection.
QCD aspects of leptoquark production at HERA are discussed with focus on initial- and final-state QCD radiation. By taking into account corrections to this in mass reconstructions of a leptoquark, a narrower mass peak and a better average mass value is obtained.

Key words
QCD, heavy quarks, charm asymmetry, hadronization, string fragmentation, colour reconnection, parton shower, leptoquarks

Classification system and/or index terms (if any)

Supplementary bibliographical information		**Language** English
ISSN and key title		**ISBN** 91-7874-051-7
Recipient's notes	**Number of pages** 224	**Price**
	Security classification	

DOKUMENTDATABLAD
enl SIS 61 41 21

Distribution by (name and address)

Emanuel Norrbin, Dept. of Theoretical Physics, Sölvegatan 14A, SE-223 62 Lund

Signature ____________ **Date** 2000-10-20

Sammanfattning (Summary in Swedish)

Teorin för den starka kraften, kvantkromodynamik eller QCD, behandlas här med både perturbativa och icke-perturbativa metoder. Speciellt produktions- och hadroniseringsdynamiken hos tunga partiklar studeras. Dessa partiklar innefattar tunga kvarkar (charm, botten och top), gaugebosoner, leptokvarkar och supersymmetriska partiklar.

När tunga långlivade kvarkar (d.v.s. charm och botten) produceras vid en hadronkolliderare, kan de producerade kvarkarna växelverka med de kolliderande hadronernas strålrester. Inom strängfragmenteringsmodellen sker denna växelverkan genom att ett färgfält, även kallad en sträng, spänns mellan kvarken och strålresten. När strängen fragmenteras, d.v.s. när hadroner produceras från energin i fältet, kan hadronen som innehåller den tunga kvarken få en större energi (i kollisionens mass-centrum) än den perturbativt producerade tunga kvarken hade. I extrema fall kan en enda hadron ta hela strängens energi, varvid en asymmetri uppstår mellan hadroner som delar en kvarksort med de kolliderande partiklarna, och de som inte gör det. Lunds strängfragmenteringsmodell studeras och förbättras genom att använda information från experiment vid låga energier. Den modifierade modellen används sedan för att förutsäga utgången av experiment vid högre energier.

När färgade partiklar (kvarkar och gluoner, som tillsammans kallas partoner) produceras vid en högenergetisk partikelkollision kommer dessa att utsöndra QCD-strålning. I en partonkaskadsmodell för detta fenomen sker successiv uppsplittring av de ursprungliga, högst virtuella, partonerna till partoner med lägre virtualitet. Denna uppsplittring upprepas tills partonerna är nästan reella, varvid en hadroniseringsmodell tar vid. En speciell implementering av partonkaskaden förbättras genom att matriselement beräknas och används för att korrigera varje uppsplittring i kaskaden. Den nya algoritmen ger en bättre beskrivning av mass-effekter och inför ett processberoende. Några fenomenologiska studier utförs, som botten- och topkvarkproduktion vid en elektron-positron kolliderare. Strålning från färgade supersymmetriska partiklar införs också och några enkla studier genomförs.

I processen $\mathrm{e}^+\mathrm{e}^- \to \mathrm{W}^+\mathrm{W}^- \to \mathrm{q}\overline{\mathrm{q}}\mathrm{q}'\overline{\mathrm{q}}'$ är färgflödet, och därmed strängtopologin, inte entydig. En metod presenteras och studeras för att fastställa vilket färgflöde som har realiserats i en händelse. Metoden baserar sig på antagandet att den transversa rörelsemängden hos en partikel är som minst i vilosystemet för den sträng som producerade den. Metoden används sedan för att studera färgomkopplingar; ett fenomen som skulle kunna påverka massbestämningen av W-bosonen.

För några år sedan observerades några oväntade händelser vid positron-protonkollideraren HERA, där positroner spreds till höga vinklar (stora Q^2). En möjlig förklaring var produktion av en leptokvark, d.v.s. en partikel med både lepton- och kvarkegenskaper som växelverkar direkt med fermionerna i standardmodellen. Här studeras effekterna av QED- och QCD-sstrålning samt hadronisering på en sådan produktionsprocess. Genom att införa korrektioner till dessa effekter skulle en bättre massbestämning av leptokvarken kunna göras. I efterföljande experiment, men nu med elektroner istället för positroner, observerades ingen motsvarande effekt. Endera var den tidigare signalen en statistisk fluktuation, eller så har leptokvarkar med fermiontal 2 andra egenskaper än sådana med fermiontal 0.

To whom it may concern

This thesis is based on the following publications:

I E. Norrbin and T. Sjöstrand
Transverse Momentum as a Measure of Colour Topologies
Physical Review **D 55** (1997) 5

II C. Friberg, E. Norrbin and T. Sjöstrand
QCD Aspects of Leptoquark Production at HERA
Physics Letters **B 403** (1997) 329

III E. Norrbin and T. Sjöstrand
Production Mechanisms of Charm Hadrons in the String Model
Physics Letters **B 442** (1998) 407

IV E. Norrbin and T. Sjöstrand
Production and Hadronization of Heavy Quarks
LU TP 00–16 (hep-ph/0005110)
Accepted for publication in *European Physical Journal* **C**

V E. Norrbin and T. Sjöstrand
QCD Radiation off Heavy Particles
LU TP 00–42 (hep-ph/0010012)
Submitted to *Nuclear Physics* **B**

VI T. Sjöstrand, P. Edén, C. Friberg, L. Lönnblad, G. Miu, S. Mrenna and E. Norrbin
High-Energy-Physics Event Generation with PYTHIA 6.1
LU TP 00–30 (hep-ph/0010017)
Accepted for publication in *Computer Physics communications*

Contents

Introduction

This thesis deals mainly with phenomenological studies of the strong interaction, described by Quantum Chromo Dynamics (QCD), in high energy processes. The main emphasis is on the description of heavy particle dynamics in a variety of circumstances — hadronization of heavy quarks, mass effects in perturbative QCD, colour flow in decays of heavy resonances and more.

The thesis is divided into two main sections: this introduction and the papers. The main technical details of this work are described in the papers, whereas this introduction serves to summarize them and put them in a somewhat broader perspective (at least as far as high energy physics is concerned). It is aimed at a general audience of physicists and physics students with some basic knowledge of particle physics. Even non-physicists could at least get a feeling for the kind of problems addressed in this work by reading the section on the Standard Model. More advanced readers could skip to the section on phenomenological QCD (page 14) and the summary of the papers (page 22), or directly to the papers themselves (see the list on page vi).

The outline of this introduction is as follows. In the first section the Standard Model of particle physics is summarized. The matter contents and the forces of the model is described, emphasizing the parts that are of interest for this work. Subsequent sections describe the main techniques and models used — parton showers, string fragmentation and Monte Carlo event generators. The introduction is concluded by a summary of the papers upon which this thesis is based.

The Standard Model

> The Standard Model has many defects, the most severe being that it agrees with all accelerator data. *John Ellis*

Ever since its completion in the beginning of the seventies, the Standard Model has been very successful in describing experimental data. This chapter serves as a short review of the Standard Model, with emphasis on the aspects which are relevant to the studies in this thesis.

Most people agree that a theory describing the most fundamental aspects of matter should fulfill certain criteria. It ought to be "simple" in the sense that it should possess a simple symmetry, contain few or no free parameters and be able to explain the observed spectrum of indivisible particles together with their masses and interactions. Furthermore, in my opinion, it should be based on a few intuitive principles which any reasonably educated person would be able to grasp. The Standard Model cannot be said to possess any of these virtues. It does, however, provide us with a practical framework within which particle interactions at past, present and future accelerators can be described. Any experimental result which falls out of this framework thus hints at some new physics phenomenon. Most studies in this thesis assume only the physics contents of the Standard Model, but the phenomenology of some extensions are considered, such as leptoquarks (paper II) and supersymmetry (paper V).

Energy

Since this is a thesis on high energy physics it is natural to start with a discussion of energy in general and "high energies" in particular. Energy is a fundamental concept in all of physics. You could even say that physics is the description of different energy forms and processes where energy is transformed between them. Energy is sometimes defined as "work" or the possibility to do work. This, of course, does not tell the whole story, nor does any other single definition. Since energy (E) and mass (m) are intimately related by Einsteins famous formula, $E = mc^2$ (where c is the velocity of light) it is in fact fair to say that *everything* is energy.

Having said this it is still possible to give sensible and precise definitions of energy and energy units. The unit of energy commonly used in everyday life is the Joule (J) which is the energy needed to lift a mass of 1 kg a distance of 1 dm in the earths gravitational field, at the surface of the earth. The standard energy unit used in atomic physics is the electron-Volt (eV) which has a similar definition to the Joule, but this time it is the energy needed to push an electron through an electric potential difference of 1 V (the relation between the two units is 1 J $\approx 10^{19}$ eV, so an eV is a very small energy in ordinary life). In high energy physics the standard unit is 10^9 eV or 1 GeV which is roughly the energy equivalent of 2000 electron masses or the mass of one hydrogen atom. In both of these cases, the energy needed to "lift" the particle or mass is stored as potential energy (either gravitational or electrical) and can therefore be released at a later time. This is a consequence of the general principle that energy can never be destroyed, merely transformed between different forms. In the macroscopic world this is not so obvious because all energy is sooner or later dissipated as heat through friction and has seemingly "disappeared". In particle collisions at small distances, friction is negligible because the colliding particles have no time to interact with bulk matter.

Movement is also an energy called *kinetic* energy and the total energy of a particle is the sum of its kinetic energy and the energy equivalent of its mass, $E = mc^2 + E_{\text{kin}} = \sqrt{m^2c^4 + p^2c^2} \approx mc^2 + \frac{p^2}{2m}$, where the last approximation gives the familiar expression for the kinetic energy, valid in the non-relativistic limit of small velocities. In particle collisions at current experiments, E_{kin} is usually much larger than mc^2. This gives rise to the possibility of creating new particles from the kinetic energy of colliding particles. In high energy physics, the convention of putting $c = \hbar = 1$ is used, where $\hbar$ is Planck's constant. The working units then obtained — called *natural* units — are very useful because *all* relevant, kinematical, quantities can be expressed in powers of GeV (i.e. energy), which makes it even more clear that everything is energy. In this system of units, the mass of an hydrogen atom is roughly 1 GeV. Distances are expressed in GeV^{-1}, where 5 GeV^{-1} is about the size of an atomic nucleus. In this work, collision energies between 25 GeV and 14 TeV (14,000 GeV) are studied. Presently (year 2000), the highest centre-of-mass energy achieved at an accelerator is 2 TeV, and the mass of the heaviest observed particle is 175 GeV.

The Structure of Matter

The Standard Model consists of two parts; one describing the matter particles which build up the visible (and invisible) universe and another describing the interactions between these particles. The concepts needed to describe the smallest building blocks of matter are very far removed from everyday life. Therefore, starting from the atom, which should be familiar to most readers as being the smallest chunk of matter which retains the chemical properties of a material, we work our way down through the different layers of matter. In the end we reach the smallest length scales which so far have been studied experimentally and where the objects investigated in this work are found.

Fig. 1 shows the hierarchy of matter in a very schematic way, ignoring length scales for the moment. The atom consists of a positively charged nucleus, surrounded by a cloud of electrons with a total charge that exactly cancels that of the nucleus, making the atom as a whole seem electrically neutral when viewed from a distance. According to the Standard Model, the electron is an *elementary* particle in the sense that it does not have any internal structure. The electron has only got three static properties: *charge*, *mass* and *spin*. The charge is a measure of the strength of its electromagnetic interaction with other charged particles. The mass is a measure of the strength of its gravitational interaction with other massive particles. The spin describes the magnetic properties of the electron and can have one of two values called "up" and "down". In fact, all elementary particles have very few properties, making them the simplest objects that exist, which is why they are called elementary. They typically all have "charges" (generally called *quantum numbers*), some have mass

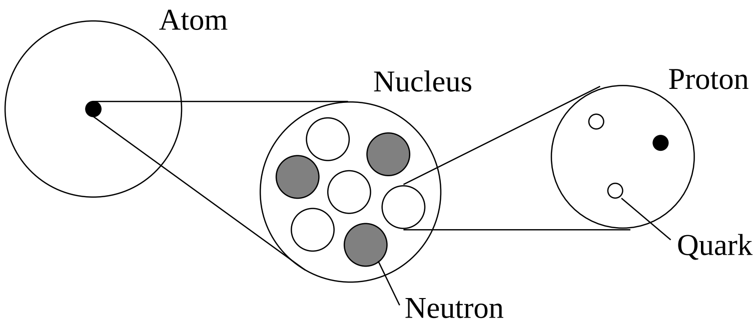

Figure 1: The hierarchy of matter.

and some have spin, some don't.

The size of a typical atom is about 10^{-10} m or ten millionth of a mm. In the centre of the atom, 10,000 times smaller than that, resides the nucleus. The nucleus is so small that when it was first observed it was believed to be without substructure. This of course was a mistake and there is no guarantee that the same mistake has not been made with the electron or the other so called elementary particles described in this chapter. The nucleus was found to consist of even smaller particles, named *protons* and *neutrons*, collectively called *nucleons*. The proton has the same electric charge as the electron but with the opposite sign while the neutron is neutral. They both have masses of the same order of magnitude (about 2000 times larger than the electron), but they are not exactly the same, differing by about 0.1%. For some time the nucleons were also considered to be elementary, but as more and more particles similar to the nucleons — collectively called *hadrons* — were discovered, the concept of *quarks* was introduced to describe the observed plethora of different "elementary" particles. The main idea is that all observed hadrons are built up from three fundamental quarks called *up*, *down* and *strange* (u, d and s are called quark *flavours*) with fractional charges $\frac{2}{3}$, $-\frac{1}{3}$ and $-\frac{1}{3}$ respectively. The observed hadrons then consist of three or two quarks and in fact, at first, no particles were discovered that did not fit into this framework.

From the beginning, the quark was simply regarded as a mathematical convenience, introduced to describe the static symmetry properties of the observed particle spectrum. Later, experiments with electron-proton collisions hinted at the existence of smaller objects within the proton, but were these objects and the quarks identical? The question then is how to observe such small objects. When observing our everyday, macroscopic, objects we direct light emitted by

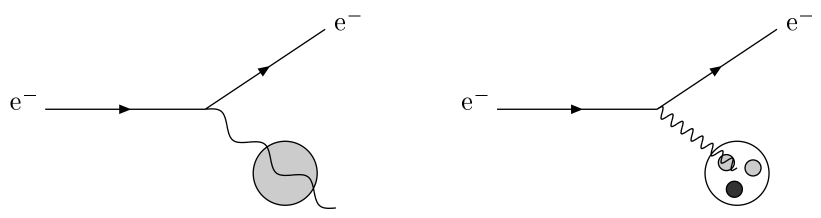

Figure 2: An electron probing the structure of the proton by the exchange of a photon. The wavelength of the photon determines what structures can be resolved.

some source, such as the sun or a light bulb, on the object and the reflected light is detected by our eyes. A perceived image of the object is then formed by our brain. Our eyes can, by definition, only detect "visible" light. The size of the detected object has to be larger than the shortest visible wavelengths of about 400 nm, otherwise the light would not be able to resolve it, just like a big wave of water is not effected by a small pebble. Since protons are so small (about 100 million times smaller than the wavelength of visible light), equally small wavelengths are needed to study them, hence visible light will not be sufficient.

One way to solve this is to use the wave aspect of matter in order to produce beams of very small wavelengths. The wavelength of a beam of particles is given by $\lambda = \frac{hc}{E}$ ($\sim 1/E$ in natural units), where E is the energy of the particle beam. Thus, to probe very small distances, very large energies are needed and this is the main limiting factor when designing an experiment for studying the smallest constituents of matter. When electrons of sufficient energy were scattered off protons, see Fig. 2, the properties of the proton constituents were found to correspond to the properties of the hypothetical quarks — they had the same spin and fractional charges.

The nucleons thus consist of three quarks each (called the *valence* quarks), the proton of two up and one down, and the neutron of one up and two down (uud and udd respectively, adding up to charge +1 and 0). It has also been discovered that about half of the proton momentum is carried by neutral particles, called *gluons*, which are carriers of the strong interaction that binds the quarks together (cf. the next section). To complicate matters further, the gluons can split into quark/anti-quark pairs forming a so called *sea* of quarks besides the valence quarks. Together the quarks and gluons are called *partons* (because they are *parts* of the proton).

The constituents of the proton were found to have several remarkable and important properties not postulated by the original quark model. When an

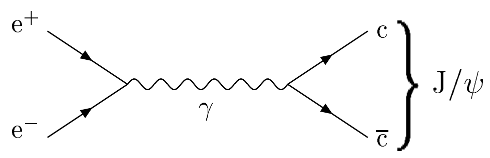

Figure 3: Production of the J/ψ in an e^+e^- experiment.

electron beam strikes the proton, the result depends on the wavelength of the electron. An experiment with electrons of wavelengths above 1 fm (10^{-15} m or the size of the proton) sees the proton as simply a solid, charged, sphere of spin $\frac{1}{2}$. When the wavelength is decreased, the constituent quarks are resolved. Since the gluons are electrically neutral the electron cannot "see" them, but their presence has been inferred by other means, such as proton-proton collisions. Remarkably, quarks and gluons appear to exist as free particles inside the proton. It thus seems that, on the one hand, quarks are confined within the proton but, if probed at small enough distances, appear to move freely inside it. These properties are fundamental to the force that binds quarks together and are called *confinement* (quarks are confined within hadrons) and *asymptotic freedom* (quarks behave as free particles when probed at small distances). The theory of the strong interaction — QCD, described below — accounts for both of these properties and this is a good indication that QCD indeed describes the interaction between quarks and gluons. More indications will be discussed throughout this thesis.

It was not until 1974 that the quark model was accepted by most physicists. The one event that turned the scales in favour of the quark was the discovery of the J/ψ particle. This was done simultaneously in two experiments [1], explaining the double name of this particle. For symmetry reasons a fourth quark, dubbed the *charm* quark, was postulated as a heavier version of the u quark (same charge and spin). If this quark exists, a bound state containing charm (c) and its anti-particle ($\overline{c}$) must also exist. The most straightforward way of producing this particle is to have an e^+e^- pair annihilating, producing a virtual photon which in turn decays into a $c\overline{c}$ pair, see Fig. 3. If this is done at an energy exactly matching the rest mass of the J/ψ, the probability (or cross section) for the production of the bound state is large. If the total probability for the production of hadrons is plotted versus the e^+e^- centre-of-mass energy, a very high and narrow peak should show up, and this was indeed what was seen experimentally. In 1977 a fifth quark called the *bottom* (b) quark was found [2] and almost twenty years later its partner, the *top* (t) quark, was discovered [3]. The reason why it took such a long time to find the top quark is that it is very

$$\begin{array}{cc} \text{quarks} & \text{leptons} \\ \begin{pmatrix} \mathrm{u} \\ \mathrm{d} \end{pmatrix} \begin{pmatrix} \mathrm{c} \\ \mathrm{s} \end{pmatrix} \begin{pmatrix} \mathrm{t} \\ \mathrm{b} \end{pmatrix} & \begin{pmatrix} \nu_{\mathrm{e}} \\ \mathrm{e}^- \end{pmatrix} \begin{pmatrix} \nu_\mu \\ \mu^- \end{pmatrix} \begin{pmatrix} \nu_\tau \\ \tau^- \end{pmatrix} \end{array}$$

Figure 4: The matter particles of the Standard Model.

heavy compared to the other quarks, with a mass of 175 GeV as compared to about 5 GeV for the bottom quark, which is the next heaviest one. The high energies needed to produce the top quark were not achieved until around 1995 at the Tevatron collider outside of Chicago.

In this work, the dynamics of charm and bottom quark production in hadron collisions and the subsequent formation of hadrons containing heavy quarks is studied in some detail (papers III and IV). QCD radiation off bottom and top quarks at high energies is studied in paper V.

This ends the short introduction to the matter contents of the Standard Model. There are, however, a few blanks to fill in before it is complete. In order to build up all the stable matter seen here on earth, all you need is the u and d quarks together with the electron. For some reason Nature is not content with just these particles. In the same way as the up quark is paired with the down quark, the electron has a partner called the electron-neutrino, ν_{e} (collectively they are called *leptons*). Why they are said to come in "pairs" is discussed in the next section. In addition, the pattern of the u and d quarks is copied two times, first in the c and s quarks and then in the t and b. Each quark pair is called a *family*, so there are three quark families. The same goes for the leptons which also appear in three families. There could be more families, but so far this has been ruled out on experimental and theoretical grounds.

In Fig. 4 the known matter particles are summarized; they are 12 in total and counting also their anti-particles this adds up to 24 fundamental particles (there will come more — the interaction particles — in the next section). This multitude of "fundamental" particles suggests that the matter view given by the Standard Model is not the complete one and that some higher symmetry should exist, explaining this complicated and seemingly arbitrary pattern. There are several candidates, such as string theories and supersymmetry, but so far no satisfactory theory has been discovered.

The Fundamental Interactions

Our universe would be pretty boring if it only contained matter, in fact we wouldn't even exist in it. The second part of the Standard Model describes the interactions between the matter particles. Sometimes the word force is used, but interaction is, as we shall see, a much better word. Usually, four interactions are distinguished: *gravity*, *electromagnetism*, the *weak* and the *strong* nuclear forces. At microscopic scales the gravitational force is much weaker than the other ones and is almost always neglected. Also, it has not yet been possible to reconcile it with quantum mechanics; there is no quantum theory of gravity. The remaining three can be derived from a symmetry principle and in this approach the weak and electromagnetic interactions are unified in the *electroweak* force.

The theoretical framework which is currently used to describe all particle interactions (except gravity) is called *quantum field theory*. In this kind of theory, all particles are described in terms of *fields* which basically is the continuum limit of the classical degrees of freedom. When the field is quantized, i.e. quantum mechanical commutation relations are imposed on the fields at different positions, particles (and anti-particles) appear naturally as the quanta of the field. Thus the electron-positron field gives rise to electrons and positrons, and the electromagnetic field gives rise to photons. Any other field can give rise to other particles.

In every quantum field theory the equations of motion of the fields are derived from a *Lagrangian*. The Lagrangian is some function of the particle fields and their derivatives. The main problem then, is to find the Lagrangian. It turns out that the Standard Model Lagrangian can be derived from a gauge (or phase) invariance principle. Postulating that the Lagrangian is symmetric under phase transformations (U(1)) and a set of transformations in an internal space that forms an SU(2) group and one that forms an SU(3) group, the Standard Model Lagrangian can be derived. In general, the SU(n) group can be represented by complex unitary ($U^\dagger U = 1$) $n \times n$ matrices with determinant $+1$ which has $n^2 - 1$ degrees of freedom. After quantization, each degree of freedom gives rise to a *gauge boson* which mediates the interaction. Theories constructed in this way are called *gauge theories*. The symmetry of the Standard Model particle interactions is thus called $\mathrm{U(1)} \times \mathrm{SU(2)} \times \mathrm{SU(3)}$ which gives rise to 12 gauge bosons. Why it is exactly this symmetry that describes the forces of Nature is not known at present. Hopefully, some more fundamental theory will be able to explain this symmetry.

It is not necessarily so that each symmetry corresponds exactly to one of the forces. Indeed, it turns out that the electromagnetic and weak interactions are special mixtures of the U(1) and SU(2) symmetries. This mixture gives rise to the electroweak interaction. SU(3), however, does not mix with the others and gives rise to the strong interaction or QCD, which is the interaction under study in this work.

The modern view of a force is as an exchange of gauge bosons between the interacting particles. Each force has one or several gauge bosons associated with it (one for each degree of freedom of its symmetry) and the differences

Force	Mediators	Properties
Electromagnetic	photon (γ)	Massless, infinite range
Weak	Z^0, W^+, W^-	Massive, short range
Strong	Eight gluons	Massless, self-interacting, short range

Figure 5: The interaction particles (gauge bosons) of the Standard Model.

between the forces stem from the different properties of their gauge bosons. Fig. 5 summarizes the gauge bosons of the three interactions in the Standard Model, listing the special properties that characterize the interaction. Each force has a "charge" associated with it and particles influenced by the force is said to carry an amount of this charge, which quantifies the strength of the interaction. The electromagnetic force is the most familiar example which has the ordinary electrical charge. The weakly interacting particles carry *hypercharge* and strongly interacting ones carry something called a *colour* charge. Particles can be influenced by several different forces and can therefore also carry several charges.

How the exchange of gauge bosons mediates the electromagnetic and weak interactions will be exemplified by e^+e^- scattering and quark decay. QCD will be further described and exemplified in the next section. When an electron and a positron are scattered, they exchange virtual photons, Fig. 6a, or annihilate into a virtual photon and subsequently appear again, Fig. 6b. The photon is called *virtual* because it cannot have its nominal (i.e. zero) mass in this reaction if energy and momentum are to be conserved at each vertex. A virtual photon cannot exist by itself, but only in reactions as this one where it lives for a time, $\tau \sim 1/m_\gamma$, where m_γ is the virtual mass or *virtuality* of the photon. The larger the virtual photon-mass, the smaller the probability will be for the reaction to occur. Since the photon is massless it has an infinite range and the exchange of photons with small virtualities and thus scattering in small angles will be favoured. Actually, since the electromagnetic and weak forces are mixed, the photon in Figs. 6a–b could be a Z^0-boson as well, but at small energies this contribution is negligible. At higher energies however, the Z^0 contribution is very important and it has been verified in many experiments.

The weak interaction is responsible for the decay of unstable particles and radioactive β-decay of nuclei. The charm quark for example, has a finite lifetime and decays by the process in Fig. 6c, among others. In this case the charm quark is transformed into a strange quark by emitting a W-boson. The W-boson is very massive (it has the mass of about 80 protons or 80 GeV) and can only live for a short time until it decays into e.g. $e^+\nu_e$. Now comes the explanation to why the particles in Fig. 5 are said to come in pairs — the members of a pair can be transformed into each other by the emission of a W-

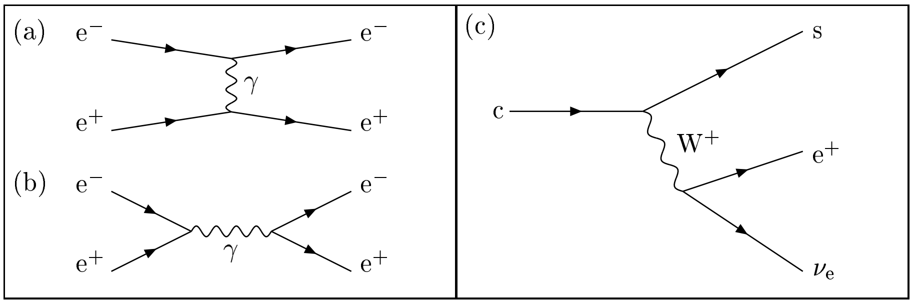

Figure 6: Examples of electromagnetic and weak processes in the Standard Model. (a–b) Electron-positron scattering. (c) Weak decay of a charm quark.

boson. Because the weak eigenstates and the mass eigenstates are not exactly the same, transitions can also occur between the families, e.g. $\mathrm{c} \to \mathrm{dW}^+$. By these decays, all heavy particles will sooner or later be transformed into the lightest u and d quarks, electrons and electron-neutrinos.

The diagrams in Fig. 6 are called *Feynman diagrams*, named after their inventor, and they provide a pictorial and intuitive way of understanding particle interactions. But they are also useful when doing practical calculations, because each diagram can be associated with the quantum mechanical amplitude of the process. When all diagrams contributing to a process have been found, the corresponding amplitudes are summed and squared to give the probability for the process to occur. If this is done in a systematic way, grouping the diagrams in increasing order of the number of vertices, a good approximation to the process can be calculated by only considering the most important diagrams. This way of doing calculations is called *perturbation theory*.

The number of vertices involved in a diagram determines the *order* of the process and e.g. the diagrams in Fig. 6a are the simplest possibilities, thus called the first-order (or leading-order) diagrams of the process $\mathrm{e}^+\mathrm{e}^- \to \mathrm{e}^+\mathrm{e}^-$. When the scattering probability of this process is calculated in perturbation theory it can be written as

$$a_2\alpha^2 + a_3\alpha^3 + \cdots + a_n\alpha^n, \tag{1}$$

where the a_n's come from the diagrams containing n vertices and α is the coupling strength, which in the case of electromagnetism is 1/137 (the fine structure constant). Fig. 7 shows some examples of higher order diagrams for the process $\mathrm{e}^+\mathrm{e}^- \to \mathrm{e}^+\mathrm{e}^-$ which contribute to the a_4 factor above. For this approach to be applicable, the coupling strength, α, has to be sufficiently small so that the contribution from order $n+1$ becomes much smaller than the contribution from order n. In the case of electromagnetism this is fulfilled

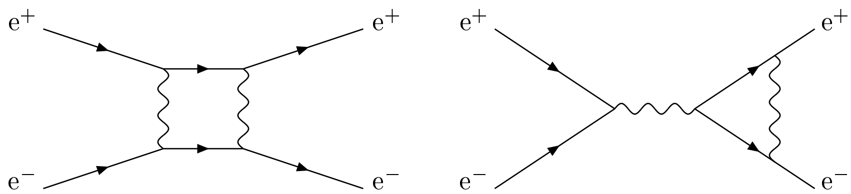

Figure 7: Some examples of second order diagrams in e^+e^- scattering.

because of the smallness of the fine structure constant. In QCD, however, this is not always the case, and the application of perturbation theory becomes impossible in certain circumstances. In this thesis, both perturbative and non-perturbative methods are used to study the formation of heavy hadrons, QCD radiation and other aspects of the strong interaction.

QCD

Quantum Chromo Dynamics (QCD) is the interaction studied in this thesis. Electroweak interactions are also present in the background of the studies but often they are to weak to be significant, or else well known and under control. Particles affected by the strong interaction carry a quantum number (or charge) called colour. This colour has nothing to do with ordinary colours but they do share some properties, e.g that the three fundamental colours add up to white (i.e. colourless or colour neutral). There are three colours, often called red, green and blue (rgb). There are also “anti-colours”: anti-red, anti-green and anti-blue ($\overline{\mathrm{rgb}}$). The known coloured particles are the quarks (q), which carry one of the three colour charges, and the exchange particles of QCD, the gluons (g), which carry two (e.g. $\mathrm{r\overline{g}}$). All other particles, fundamental and composite alike, are colour neutral and thus not directly affected by the strong interaction. The most important consequence of the colour charge of the gluon is that it gives rise to the confinement of quarks and gluons into hadrons. There are other, hypothetical, particles which carry the colour charge and in this thesis, gluon radiation from some of them is studied (paper II and V).

The properties of the QCD field (sometimes called the colour field) differ from the electromagnetic field in a fundamental way. The field between e.g. an electron and a positron fills all of space and the force acting on them vary as $1/r^2$, where r is the separation between the charges, see Fig. 8a, i.e. the potential varies as $1/r$. At small distances between a quark and an anti-quark, the colour field between them behaves in the same way, the potential varying with distance as $1/r$. This is because one gluon exchanges dominate the interaction and it can be described in the same way as electromagnetism, only with a larger

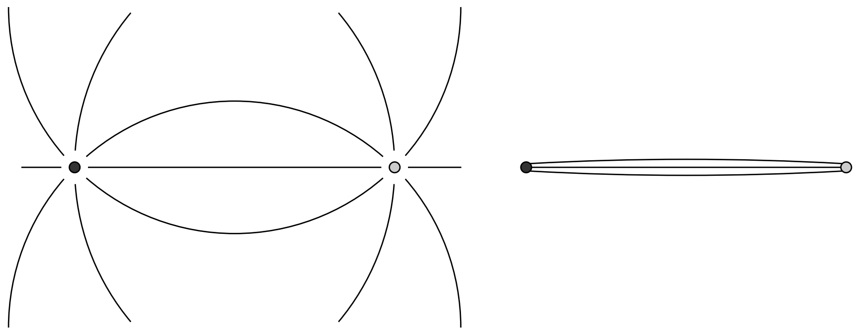

Figure 8: The force field surrounding an e^+e^- and a $q\overline{q}$ pair respectively.

coupling strength. As the distance between the quarks is increased, the self-interaction of the gluons becomes important. This leads to a force field which is compressed into a tube-like region as in Fig. 8b. Now the potential varies linearly (being proportional to r) instead and, consequently, an infinite amount of energy is needed to permanently separate the quarks from each other. Hence, the quarks cannot be separated and they are confined into the bound states of the hadrons (protons, neutrons, etc.). At high energies, however, new particles can be created from the energy in the field. This phenomenon is an important part of this thesis and is further discussed in the section on the Lund string fragmentation model.

This behaviour of the QCD field is intimately related to the fact that the strength of the QCD coupling depends on the scale at which it is studied. Consider the simple diagram

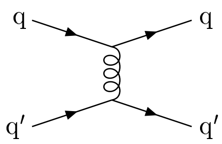

where two quarks interact by the exchange of a gluon (the curly line). The scale at which this exchange takes place is quantified by the invariant mass squared of the virtual gluon, $Q^2 = m_{\mathrm{g}}^2$. Q^2 – which is called the virtuality of the process – is in turn related to the wavelength of the exchanged gluon, $\lambda \sim 1/Q$. The virtual gluon can only resolve structures larger than λ. Each vertex in the Feynman diagram has a coupling with a certain strength $\sqrt{\alpha_{\mathrm{s}}}$ (the equivalent in electromagnetism is the fine-structure constant $\alpha = 1/137$). Now, the strength of the QCD coupling in perturbation theory depends on the resolved scales of the process, so the coupling strength depends on Q^2, thus $\alpha_{\mathrm{s}}(Q^2)$.

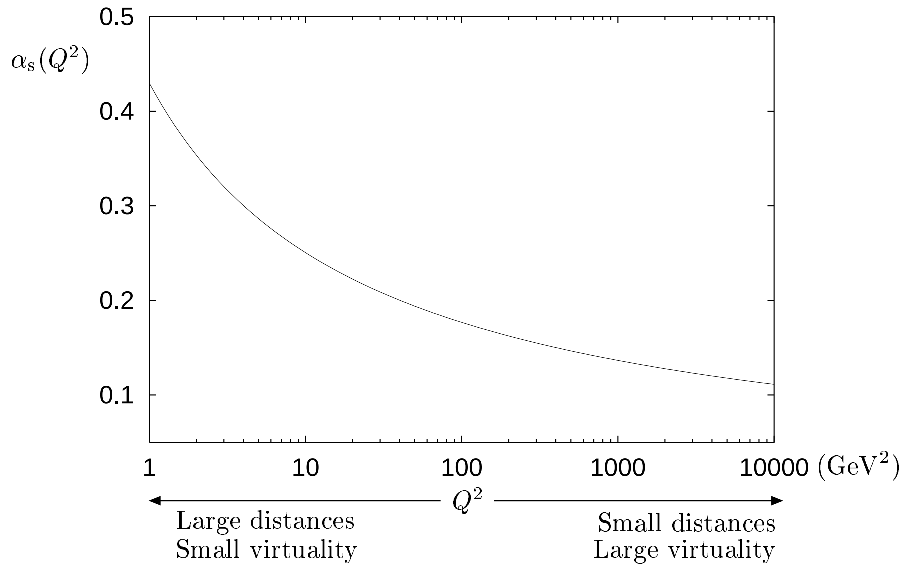

Figure 9: The variation of the strong coupling (α_s) with the resolution scale $Q^2 \sim 1/\lambda^2$.

The qualitative variation of the coupling strength with Q^2 in leading order is shown in Fig. 9. The important thing is that it decreases with increasing Q^2, thus the strength increases at large distances. For distances larger than about 1 GeV^{-1} (remember that distances can be measured in inverse energy units), the coupling increases wildly. Processes that take place at small distances (large Q^2) can be calculated in perturbation theory, because the coupling there is small. For interactions at large distances however, the large value of α_s makes the perturbative expansion of eq. (1) impossible.

Quantities that only depend on small distance physics, like the total probability to produce a $q\overline{q}$ pair in the annihilation of an e^+e^- pair, is straightforward to calculate in perturbation theory. Other quantities that depend on large distance physics, e.g. the probability to produce a specific hadron kind with a certain energy and momentum in a collision between two protons, cannot be calculated in perturbation theory. An example of this situation is investigated in this work, namely the production of heavy quarks and the subsequent formation of hadrons containing these quarks in a hadron collision.

A diagram that contributes to charm production at a hadron collider (in e.g. a proton-proton collision) is

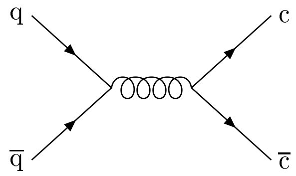

where the incoming (from the left) quarks are part of the incoming hadrons. Since the total mass-squared of the $\mathrm{c}\overline{\mathrm{c}}$ pair is about 12 GeV ($= 4m_c^2$) the virtuality, Q^2, of the gluon has to be larger than that and thus the coupling strength, from Fig. 9, is smaller than about 0.25. This is small enough to make perturbative calculations of the total production rate feasible. The transverse momentum, $p_\perp$, of the produced charm quarks above is related to the virtuality by $Q^2 \sim p_\perp^2$. Therefore the perturbative approach is more reliable for large transverse momenta of the produced charm quarks. Some time after the production, the charm quark pair can start to interact with the environment in which it was produced, by the exchange of low-energy, low-momentum gluons. These processes are not calculable in perturbation theory; instead phenomenological models have been developed to describe the large distance, low-momentum phase of the production. In this work, perturbative and non-perturbative models are combined in order to understand the complete process of charm production in hadron collisions (papers III and IV). The techniques that have been used are described in the following sections.

Phenomenological QCD

A problem in particle physics is that sometimes there seems to be a sharp dividing line between theory and experiment. Phenomenological high energy physics aims at bridging this gap by using theoretical results and developing models in order to predict the outcome of experiments. It is often practically impossible to make predictions directly from theory (in this case QCD) because of the calculational difficulties. Therefore a good deal of approximations, model building, numerical calculations and experimental input is needed. This often involves introducing model parameters and tuning them to present experiments in order to predict the outcome of future ones. This is true also of the studies in this thesis. The aim is of course to minimize the number of parameters and still obtain good agreement with experimental data. Parameters should also, whenever possible, be given some physical interpretation so that the tuned value can give some physical understanding of the process or phenomenon under study. Ideally a parameter should be universal, and in some sense summarize the unknown or approximated aspects of the theory. Then, in the future, this blank can be filled by some improved understanding or calculational tool not available today. The general attitude towards parameters in this work is: introduce as few as possible but don't hesitate to do so if necessary in order to avoid an unknown aspect of the process under study. Then assess its significance by studying variations around sensible values, treating the range of results as a theoretical, or model, uncertainty.

This thesis deals with the phenomenology of QCD using two main techniques. One is a parton shower approximation of QCD which is perturbative in nature and applicable at virtuality scales larger than 1–2 GeV. The second one deals with the hadronization stage where quarks and gluons "dress up" and form hadrons. This process occurs at small virtualities and (relatively) large distances and is therefore not perturbatively calculable. Several models have been developed in order to describe this stage [4, 5] and in this work the Lund string fragmentation model [5] is used and improved in order to describe the hadronization of heavy quarks. This section describes these approaches and ends with a discussion of their implementation in the Monte Carlo event generator PYTHIA [6].

The Parton Shower

The standard way of doing calculations in QCD — or any other gauge theory — is to use fixed order perturbation theory, as described above. In this approach, all the Feynman diagrams up to a given order in the coupling strength (number of vertices in the diagram) are constructed and the corresponding amplitudes are summed and spin averaged. In leading order this is a fairly straight-forward affair, in next-to-leading order (NLO) a lot of work is involved because of the appearance of loop diagrams and the general complexity of the resulting expressions. Performing NNLO calculations is a daunting task and few have been done up till now. In order to describe multi-jet probabilities and structures within jets the probability for multi-parton final states are needed. Clearly some other approach is needed for this task (and others).

Parton shower models utilize the structure of leading order cross sections in order to find the most important parts of the diagrams. Consider e.g. the process $\mathrm{e^+e^-} \to \mathrm{q\overline{q}g}$. The cross section for this process has two singularities, where the cross section grows very large, the *collinear* and the *soft*. The collinear singularity appears when the gluon is parallel to one of the quark directions, independently of the gluon energy, and the soft one when the gluon energy is small. These regions are in some sense the most important ones. Consider the emission of a gluon at small angles with respect to a quark, $\mathrm{q} \to \mathrm{qg}$, Fig. 10a. If the energy fraction taken by the final quark is z, and the virtuality of the initial quark is Q^2, the approximate probability to have an emission at

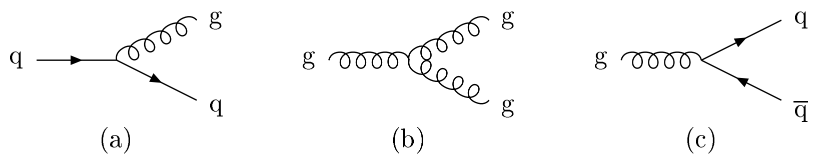

Figure 10: The basic branchings in the parton shower.

z and Q^2 is proportional to

$$\frac{1}{Q^2}\frac{1+z^2}{1-z} \tag{2}$$

This expression favours emissions with $z \approx 1$, i.e. small gluon energies (soft) and small emission angles (collinear).

Other branchings are also possible, Fig. 10b–c, where a gluon can split into two gluons ($\mathrm{g} \to \mathrm{gg}$) or into a quark-antiquark pair ($\mathrm{g} \to \mathrm{q}\overline{\mathrm{q}}$). These branchings have their own splitting probabilities, but they are all quite simple. A complete shower is then built up by subsequently applying these branchings to a parton configuration at high virtuality. In each branching, the virtuality is decreased and the shower is stopped at some fixed scale, Q_0^2, around 1–2 GeV. An example is shown in Fig. 11, where an initial $\mathrm{q}\overline{\mathrm{q}}$ pair is created in a high energy collision between an electron and a positron. A multi-parton final state at low virtuality has been built up, and the probability for a certain kinematical configuration can be calculated numerically by repeating the procedure many times.

This model has been quite successful in describing many features of $\mathrm{e}^+\mathrm{e}^-$ annihilation. The shower approach has problems, however, when it comes to describing well separated parton configurations. This is not so surprising since it is derived in the limit of collinear partons. It is also "process blind" in that the splitting probabilities are the same no matter how the showering particles were produced. In this thesis an attempt is made to remedy some of these problems. The idea is to use first-order (FO) matrix elements for gluon radiation in order to include a correction to the shower. It is easy to overestimate the amount of gluon emission in the shower by modifying the splitting probabilities. Matrix element information can then be used to correct the shower results down to the correct FO level, thereby introducing a process dependence which should give a better overall description. This correction is also applied to all subsequent branchings of the primary quarks as well as to gluon splittings into quarks. This approach is developed in paper V, which also contains a more detailed description of the parton shower implementation used in this work. Several alternatives exist [7], but the basic principles are the same.

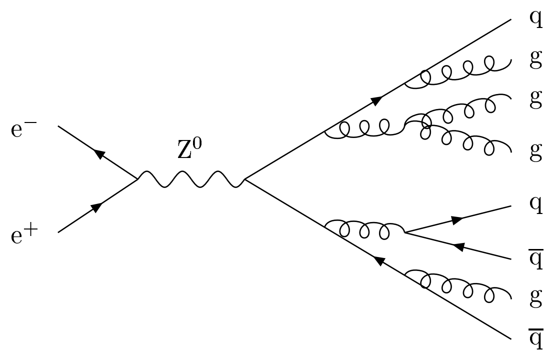

Figure 11: An example of a parton shower in e^+e^- annihilation.

The Lund String Fragmentation Model

Since the strength of the strong coupling depends on the resolution scale (Q^2) — decreasing for small distances (large Q^2) and increasing for large distances (small Q^2) — perturbative methods can only be used for processes occurring at small distances. When the strong coupling increases, many diagrams (ultimately infinitely many) must be calculated which is impossible in practice. It is known that quarks and gluons are confined within hadrons, but at the same time, perturbative calculations are performed on free quarks. The transition between the free state, at small distances, to the confined state at large ones is called *hadronization* or *fragmentation*. It is thus clear that perturbative methods cannot be used to describe all processes in QCD. Several models have been developed to cope with this problem. The most ambitious path is to put the QCD equations on a lattice and then solve them numerically [8]. This approach has so far not been able to tackle the complicated dynamical problems addressed here, but it has been successful in describing the static properties of bound quark states (i.e. hadrons). The linear rise of the inter-quark potential, which is crucial in understanding confinement and the string fragmentation model, has been verified numerically with lattice QCD techniques.

Another approach is to simply factorize the problem in two parts, one which is perturbatively calculable and one which is not. The non-calculable aspects are then parameterized in so called *fragmentation functions* which are then assumed to be universal, meaning that if they are measured in one process, they can be applied to some other process. This method has been used quite successfully in many cases, but no real physical insight into the process of fragmentation is gained. In the model considered in this work, physical assumptions about the nature of the fragmentation process are used in order to derive the fragmentation function. It turns out that only a few, very intuitive, assumptions are needed in order to significantly constrain the fragmentation function, and thereby the hadronization dynamics.

The Lund string fragmentation model is most easily described for e^+e^- annihilation. Consider first the simple process, $e^+e^- \to q\overline{q}$, ignoring the possibility for gluon emission and assuming the quarks to be massless (which is a good approximation at large energies). The initial state is colour neutral and in the final state a colour and an anti-colour charge (carried by the quarks) are produced. The field between these quarks can be approximated by a linear field (as in Fig. 8), i.e. $V(r) = \kappa r$, where r is the inter-quark separation and κ is the so called *string tension* which has a value of about 1 GeV/fm. This means that one fm (10^{-15} m) of the field contains 1 GeV of energy. This colour field is called a string and the motion of the quarks can be approximated by a 1+1 dimensional picture (one space and one time dimension). The massless quarks will move apart, at the speed of light, along a straight line (in the centre-of-mass system of the pair) and the energy in the field will increase at the expense of the kinetic energy of the quarks. When all the kinetic energy is used up, the quarks will turn around and move towards each other until they meet and the field energy is zero again. This movement is then repeated and the result is called the yo-yo state of the string.

If the quarks are produced at high energies, the string field will not stay intact during this motion. Instead, new $q\overline{q}$ pairs will start to form from the energy of the field which will cause the string to split into two separate, independent, pieces. This is then repeated for the two new strings until only string pieces of hadron sizes are left. This is illustrated in Fig. 12 where the linear force field (string) is represented by straight lines. The end product of the process is a set of hadrons which move approximately along the straight line connecting the original quarks. This is the intuitive picture of the string fragmentation mechanism. But to predict the outcome of experiments, the dynamics of the process has to be specified.

What assumptions should then be made about the string fragmentation, or hadronization, process? An obvious property is Lorentz invariance, i.e. the string breakup should look the same for observers in different reference frames. Some implicit assumptions are local flavour conservation (quarks are produced in pairs at each breakup), energy-momentum conservation and confinement (the string ends with a quark). The assumptions that make the Lund model unique is that the breakup points are casually disconnected (no information about one breakup is conveyed to the next) and left-right symmetry (the dynamics of the fragmentation is the same no matter in what end the breakup starts). These assumptions are actually enough to give highly constrained fragmentation dynamics.

The assumptions above are used to derive a fragmentation function for the

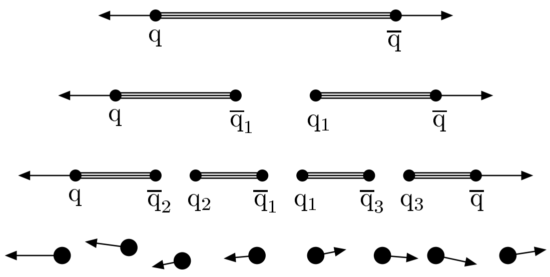

Figure 12: Breaking of the Lund string.

production of hadrons from a parton configuration obtained by other means (e.g. a parton shower). Gluons, which contain two colour charges, are connected to two string pieces and act as excitations of the string. The same picture of string breakups can be used, but the topology of the string will be more complicated. The string fragmentation is an iterative process: from the original string, an energy-momentum fraction z is used to produce an on-shell hadron and a remainder string. The procedure is then repeated on the remainder string until all the energy is used up. The left-right symmetry guarantees that the fragmentation can be performed from any direction and the final result will be the same. The hadronization is a dynamical, quantum mechanical, process (even though it is described in a semi-classical language here) and the outcome will be different each time. The average behaviour, however, is described by the distribution of the z above, which is simply the fragmentation function. The Lund symmetrical fragmentation function is

$$f(z) \propto \frac{1}{z}(1-z)^a e^{-bm_\perp^2/z}$$

with a modification needed for heavy flavours

$$f(z) \propto \frac{1}{z^{1+bm_\mathrm{Q}^2}}(1-z)^a e^{-bm_\perp^2/z},$$

where $m_\perp = \sqrt{m^2+p_\perp^2}$ and m_Q is the heavy quark mass. The two free parameters, a and b are common for all flavours and hadrons.

To be practically useful, the Lund model must be hooked on to a perturbative description of the underlying hard process (such as $e^+e^- \to \mathrm{q}\overline{\mathrm{q}}$ or $\mathrm{gg} \to \mathrm{q}\overline{\mathrm{q}}$) and then tuned to experimental data. Normally, a parton shower approximation is used, where the final state of a LO process is evolved down in virtuality by parton emission to some cut-off scale Q_0. Using a fixed lower scale for the perturbative shower, it has been possible in e^+e^- experiments to fit the two parameters of the Lund model to data and get excellent results. If the Q_0 scale is changed, the non-perturbative parameters of the Lund model will have to be re-tuned, so Q_0 can be seen as the scale at which perturbation theory is abandoned and superseded by the non-perturbative model. In the ideal case, the value of Q_0 should not matter. In practice this is true only as long as it is at the order of 1–2 GeV. Any small change in Q_0 around this value is absorbed by a change of the fragmentation parameters.

Several other models have been developed in order to describe the fragmentation process. They all make some assumptions about the dynamics of the fragmentation process and contain free parameters that need to be fitted to experiments. Often it is wise to use two or several models for the hadronization stage, comparing the results and treating differences as theoretical (or model) uncertainties. Several modifications to the models exist and they can also be used to assess uncertainties.

In this work, the Lund model is used to turn parton configurations into hadron ones in order to study the effects of hadronization (all papers). In papers III and IV the fragmentation model is modified in the region of small string pieces; the process described in this section works only for strings with large invariant masses (above a few GeV). In $\mathrm{e^+e^-}$ annihilation this is normally not a problem since only one primary string is present, taking all the energy. The string can be split into smaller pieces by perturbative $\mathrm{g} \to \mathrm{q\overline{q}}$ branchings in the shower, but these effects are small. In the case of hadron collisions (especially at low energies) small string pieces are often formed and these have to be handled separately. Different assumptions can give non-negligible effects in the final state. One observable consequence is large flavour asymmetries in fixed-target experiments, e.g. $\pi^-\mathrm{p}$ collisions at around 30 GeV centre-of-mass energy.

Monte Carlo Event Generators

As can be seen from the discussions in the preceding sections, the complete description of a particle collision involves quite a few number of steps. Several more complications come into play, such as the need to specify the distribution of quarks and gluons inside a proton in proton-proton collisions and the decay of non-stable hadrons. All this makes analytical calculations untractable. Therefore, to a large extent, computers are used to make numerical calculations and simulations of particle collisions.

In this work, a special kind of computer program, called an *event generator*, has been used and developed. An *event* is the name for a possible outcome (among many other possible outcomes) of a collision between two particles. The object of an event generator is to simulate a collision on a computer, using physical theories and models as input, in order to generate events that correspond to those that could happen in reality. If many events are generated (sometimes very many are needed) distributions of observables can be found and compared to experiment. Event generators are also frequently used by experimentalists as input to detector simulation programs or particle reconstruction routines.

In this work, the event generator PYTHIA [9] is used and further developed in order to describe processes involving heavy particles. An event generated by PYTHIA is typically made up of one or more of the following steps (given in rough "time order" which not necessarily corresponds to the order in which they are handled by the program):

- Specification of the initial state and the structure of incoming particles.
- Initial state radiation.
- Hard interaction.
- Final state radiation.
- Hadronization.
- Decay of unstable particles.

These steps are generally assumed to be independent of each other and performed in sequence. This is of course an approximation; because of the quantum mechanical nature of all steps, interferences will be inevitable, and even the subdivision can be ambiguous.

A computer is inherently a deterministic machine, so how can it be used to simulate quantum mechanical processes? It is possible to construct algorithms that generate pseudo-random numbers on a computer. These are "random" in the sense that if many numbers are generated, they give rise to a random distribution which is very difficult to distinguish from true random sequences (as would have been obtained if e.g. a radioactive decay or some other quantum mechanical device was used to generate them). Random numbers can then be used to generate different distributions, such as cross sections and fragmentation functions. To give a simple example, assume you want to simulate a known, but complicated, probability distribution, $p(x)$, in the variable x. The simplest method is to enclose this function by a constant, say $f(x) = p_{\max}$, and then generate random x values, accepting them with probability $p(x)/f(x) = p(x)/p_{\max}$. The resulting sequence of x values will then be distributed as $p(x)$. If $p(x)$ is very complicated, multi-dimensional or fastly varying, this method will be very inefficient so the approximating function, $f(x)$, must then be chosen with care. This use of random numbers is responsible for the name "Monte Carlo event generator".

The Papers

In this section, a brief overview of the papers presented in the second part of the thesis is given. The description here is slightly more technical but still with few details.

Paper I

In the process $e^+e^- \to W^+W^- \to q\overline{q}q'\overline{q}'$, two distinct colour flows are possible. The colour singlets are either $q-\overline{q}$, $q'-\overline{q}'$ or $q-\overline{q}'$, $q'-\overline{q}$ (ignoring the possibility of gluon emission). A method to determine which colour flow has been realized in an event is developed. In the Lund model, the different colour flows can be mapped onto the string topology of the event. The main assumption of the proposed method is that the transverse momentum of a hadron is minimal in the rest-frame of the string from which it was produced. Experimentally, the string rest-frame is taken to be the centre-of-mass system of a jet pair. The string/jet configuration which minimizes the summed $p_\perp$ of all the hadrons in the event is then assumed to correspond to the "correct" colour flow. Because of the smearing introduced by final state QCD radiation and fragmentation this identification is far from perfect, but still better than guessing. Combined with other methods it could be useful in the determination of colour flows.

The method is then used to study colour reconnections in W^+W^- events and different reconnection scenarios are investigated. The conclusion is that simple reconnection models, especially perturbative ones, can be distinguished. The more sophisticated ones, based on properties of the QCD vacuum and minimization of string lengths, cannot be observed within present statistical limits using this method alone.

Paper II

In 1997 an unexpected amount of high Q^2 events were observed in positron-proton collisions at HERA [10]. In a high Q^2 event, the electron has been scattered to a large angle. One possible explanation for these events is the production of a leptoquark (LQ) resonance in the reaction $e^+q \to LQ \to e^+q$. The LQ is a hypothetical fundamental particle carrying both lepton and quark quantum numbers, which interacts directly with the fermions of the Standard Model. Effects of QCD and QED radiation, especially on the mass determination of the LQ, is studied using Monte Carlo methods. The consequence of LQ-hadron formation is also investigated within the Lund string fragmentation model. A correction procedure to the mass determination of the LQ is proposed which takes some of these effects into account.

Leptoquarks often turn up in different extensions of the Standard Model, where higher symmetries between quarks and leptons are assumed. In the

Standard Model, quarks and leptons cannot be converted into each other so lepton numbers are always conserved. This is not necessarily the case in models with higher symmetries. In this paper we do not try to distinguish between different models but merely investigate the phenomenology of the production of a particle with LQ properties.

In the data taken during 1994–1997 with a positron beam, the LQ signal was seen as a bump in the jet-positron invariant mass distribution at about 200 GeV. In a later run with an electron beam (1998–1999), no corresponding signal was seen [11]. A positron beam is mainly sensitive to the production of a LQ with fermion number F=0 while an electron is sensitive to LQs with F=2, so the second measurement does not necessarily exclude the first. However, several searches for LQs have been performed at other accelerators, all with negative results [12].

Paper III-IV

In the production of heavy, long-lived, quarks (i.e. charm and bottom) at hadron colliders, the assumption is often made that the hard production process and the subsequent formation of hadrons can be modelled without taking the production environment into account. In these papers the underlying hard process is studied, using several different heavy-quark production mechanisms, and the produced quarks are connected to the production environment by strings spanned between the heavy quarks and the beam remnants of the colliding hadrons.

The Lund string fragmentation model is used to hadronize the strings, and this can give rise to heavy hadrons with larger momentum than the perturbatively produced quarks. The extreme case of this effect is when all the energy of a string is taken by a single heavy hadron. The former effect is called "beam-drag" where harder particle spectra than predicted from perturbative calculations is obtained. The latter gives rise to asymmetries between leading and non-leading particles.

In order to describe the flavour asymmetries and other properties, the standard string fragmentation model must be modified when small string pieces are hadronized. The model is then tuned to low energy data to give a good description of the asymmetries there. Several applications are given for different processes where these aspects come into play.

Paper V

A general matrix element correction procedure to the standard massless parton shower in the event generator PYTHIA [9] is studied. Many first-order $a \to bcg$ processes have been calculated and a general comparison between their radiation patterns is included. Two new elements are added to the standard shower routine. First, the evolution variable in the shower has been changed from the standard $Q^2 = m^2$ (the virtual mass of the radiating parton) to $m^2 - m_{\mathrm{q}}^2$, where m_{q} is the nominal mass of the radiating quark, i.e. the evolution variable is now the "off-shellness" of the parton. Second, the splitting functions are slightly overestimated and later corrected down to the level of the calculated cross sections. Furthermore, this correction is applied in all steps of the shower, and also for secondary gluon-splittings into quarks. This procedure correctly includes mass effects and introduces a process dependence of the gluon radiation phenomenon.

Some phenomenological studies are performed using the new algorithm. These include $\mathrm{b\overline{b}}$ and $\mathrm{t\overline{t}}$ production at $\mathrm{e^+e^-}$ colliders, Higgs decay and SUSY processes. Comparisons between processes with similar couplings are studied, such as $Z^0 \to \mathrm{b\overline{b}}$ vs. $\mathrm{H} \to \mathrm{b\overline{b}}$ and $\mathrm{t} \to \mathrm{bW^+}$ vs. $\mathrm{t} \to \mathrm{bH^+}$, in order to demonstrate the advertised process dependence of the new shower algorithm.

Paper VI

This paper is an update note for the Monte Carlo event generator PYTHIA [9] describing the changes in the program since the last major version. My contributions constitute only a small part of these and are listed here:

- Improvement of the hadronization description of low-mass strings.
- Calculation of several first-order matrix elements, used as input to the improved matrix element correction in the final-state parton shower.
- Implementation of a left-right symmetric model [13] containing doubly charged Higgs states. New Higgs states, model parameters and decays to right-handed W's and neutrinos are included.

Most of these issues are covered in papers I–V.

Acknowledgments

First of all I would like to thank my supervisor, Prof. Torbjörn Sjöstrand, for his excellent guidance across the treacherous sea of particle physics. Without him I would surely have capsized long ago! I am also indebted to everyone who has taken an interest in my work, especially our experimentalist friends all over the world. Your participation has been very encouraging.

A big thanks goes to everyone at the department for all the good times, both during and after office hours. It has been a pleasure to share three different offices, big and small, with Christer. I would also like to thank everyone at Rydbergs (you know who you are!) for all the Wednesdays and Torgil for all the lunches (in the future we will eat pork-chops every day!).

Finally, special thanks to my parents for all your support during my first 28 years. I hope to enjoy it for many years to come.

References

[1] J.J Auber et al., Phys. Rev. Lett. **33** (1974) 1404;
J.E. Augustin et al., Phys. Rev. Lett. **33** (1974) 1406.

[2] S.W. Herb et al., Phys. Rev. Lett. **39** (1977) 252.

[3] F. Abe et al. (CDF Collaboration), Phys. Rev. Lett. **74** (1995) 2626;
S. Abachi et al. (D0 Collaboration), Phys. Rev. Lett. **74** (1995) 2632.

[4] R.D. Field and R.P. Feynman, Phys. Rev. **D15** (1977) 2590; Nucl. Phys. **B138** (1978);
B.R. Webber, Nucl. Phys. **B238** (1984) 492.

[5] B. Andersson, G. Gustafson, G. Ingelman and T. Sjöstrand, Phys. Rep. **97** (1983) 31;
T. Sjöstrand, Nucl. Phys. **B248** (1984) 469.

[6] T. Sjöstrand, Comput. Phys. Commun. **82** (1994) 74, LU TP 95-20 (hep-ph/9508391).

[7] G. Marchesini and B.R. Webber, Nucl. Phys. **B238** (1984) 1;
G. Gustafson and U. Pettersson, Nucl. Phys. **B306** (1988) 746.

[8] K. Wilson, Phys. Rev. **D10** (1974) 2445;
M. Creutz, *Quarks, gluons and lattices*, Cambridge University Press (1983);
C. Rebbi, *Lattice gauge theories and Monte Carlo simulations*, World Scientific (1983).

[9] T. Sjöstrand, Comput. Phys. Commun. **82** (1994) 74, LU TP 95-20 (hep-ph/9508391).

[10] H1 Collaboration, C. Adloff et al., Z. Phys. **C74** (1997) 191;
ZEUS Collaboration, J. Breitweg et al., Z. Phys. **C74** (1997) 207.

[11] E. Perez (on behalf of the H1 and ZEUS Collaborations), in International Europhysics Conference on High Energy Physics 99, eds. K. Huitu et al. (IOP Publishing, Bristol, 2000), p. 818.

[12] E. Gross, ibid. p. 144.

[13] K. Huitu, J. Maalampi, A. Pietilä and M. Raidal, Nucl. Phys. **B487** (1997), and private communication;
G. Barenboim, K. Huitu, J Maalampi and M. Raidal, Phys. Lett. **394** (1997) 132.

Transverse Momentum as a Measure of Colour Topologies

Paper I

Transverse Momentum as a Measure of Colour Topologies

Emanuel Norrbin and Torbjörn Sjöstrand
Department of Theoretical Physics
Lund University

Physical Review **D 55** (1997) 5

Several distinct colour flow topologies are possible in multiparton configurations. A method is proposed to find the correct topology, based on a minimization of the total transverse momentum of produced particles. This method is studied for three-jet $Z^0 \to q\overline{q}g$ and four-jet $W^+W^- \to q_1\overline{q}_2q_3\overline{q}_4$ events. It is shown how the basic picture is smeared, especially by parton-shower activity. The method therefore may not be sufficient on its own, but could still be a useful complement to others, and e.g. help provide some handle on colour rearrangement effects.

When high-energy processes produce multiparton states, it is generally believed that the confinement property of QCD leads to the formation of colour flux tubes or vortex lines spanned between the partons. These tubes/vortices are here called strings, in anticipation of our use of hadronization based on the string model [1]. A quark or antiquark is attached to one end of a string. A gluon is attached to two string pieces, one for its colour and one for its anticolour index, and thus corresponds to a kink on the string.

The simplest kind of events, $e^+e^- \to \gamma^*/Z^0 \to q\overline{q}$, gives a single string stretched between the q and the $\overline{q}$. The direction of the colour flow can, in principle, be distinguished by flavour correlations [2], but will not be studied here. In next order, $q\overline{q}g$ events correspond to a string stretched from the q via the g to the $\overline{q}$. The colour topology is unique, but experimentally it is not normally known which of the three jets is the gluon one, so this gives a threefold experimental ambiguity.

From four partons onwards, true ambiguities of the topology exist, even when the identity of the partons is known. In $q\overline{q}gg$ events, the string can be drawn from the q to either of the two gluons, on to the other gluon and then to the $\overline{q}$. This gives two possible topologies. A third topology, not expected to leading order in N_C, is when one string runs directly between the q and $\overline{q}$ and another string in a closed loop between the two gluons. There is an experimental ambiguity, in picking the two quarks among the four partons, which gives a further factor of six, i.e. a total of eighteen possible topologies (reduced to fifteen if single and double strings are not distinguished).

Another four-jet final state is obtained in the process $e^+e^- \to W^+W^- \to q_1\overline{q}_2q_3\overline{q}_4$. Since the W's are colour singlets, in principle each of $q_1\overline{q}_2$ and $q_3\overline{q}_4$ form a separate colour singlet string. However, by soft gluon exchange or some other mechanism, alternatively $q_1\overline{q}_4$ and $q_3\overline{q}_2$ may form two singlets. Since it would not normally be known which of the four jets are quarks and which antiquarks, there is a total of three experimental pairings of four jets, where the third corresponds to the unphysical flavour sets q_1q_3 and $\overline{q}_2\overline{q}_4$.

Among the topologies above, only the three-jet $q\overline{q}g$ events have been studied in detail. It has been shown that the string approach here correctly predicts the topology of particle flow, with a dip in the angular region between the q and $\overline{q}$ jets [3, 4]. This comes about because the qg and $\overline{q}g$ string pieces produce (soft) particles in the respective angular ranges, while there is no string directly between the q and $\overline{q}$. The same effect is also obtained as a consequence of colour coherence in perturbative soft-gluon emission [5] — normally these two approaches give the same qualitative picture. Although by now LEP 1 has produced large samples of four-jet events, the energy flow between these jets have not been studied in detail, presumably because of the large number of possible topologies.

LEP 2 will provide four-jets from W pairs, and here the issue of colour topology may become of great importance [6, 7]. If, by colour rearrangement, an original $q_1\overline{q}_2$ plus $q_3\overline{q}_4$ colour singlet configuration is turned into a $q_1\overline{q}_4$ plus $q_3\overline{q}_2$ one, particle production will be somewhat different. Methods to determine the W mass from LEP 2 four-jet events will then give different results. There is more than one model of the colour rearrangement process; therefore the uncertainty on the W mass could be as high as 100 MeV [8], i.e. larger than the expected statistical error of the order of 40 MeV. The final number will then be dominated by the mixed hadronic–leptonic channel $W^+W^- \to \ell\nu_\ell q\overline{q}$, which has about the same statistics. The hadronic events could be recuperated if colour rearrangement effects could be diagnosed from the data itself. Additionally, the ability to distinguish between various reconnection scenarios could provide information on the nature of the QCD vacuum, and therefore be of fundamental interest. Unfortunately, realistic reconnection scenarios give only very minute effects on the data (remember that the effect on the W mass is at most of the order of one per mille), and so attempts to find useful signals have been rather unsuccessful [7]. There is only one claim for having found a signal [9] where, in a few events, a central rapidity gap separates the particle production from two low-mass colour singlet reconnected systems. It has turned out, however, that neglected angular correlations in the W pair decays tend to reduce this signal to the border of observability [10, 11]. Therefore one would like to devise alternative methods to diagnose the appearance of colour rearrangement.

We now want to propose and study a method to select the correct string topology. The starting point is the observation that, were it not for various smearing effects, hadrons would be perfectly lined up with the string pieces spanned between the partons. In momentum space the hadrons would appear along hyperbolae with the respective endpoint parton directions as asymptotes. In a frame where a string piece has no transverse motion, i.e. where the two endpoint partons are moving apart back-to-back, the hadrons produced by this piece would have vanishing transverse momentum. A hadron could then successively be boosted to the rest frame of any parton pair until the pair is found for which the particle $p_\perp$ is vanishing. When smearing is introduced, this $p_\perp$ will no longer be vanishing, but it still would be reasonable that a "best bet" is to assign each hadron to the string piece with respect to which it has smallest $p_\perp$. The most likely string configuration would be the one where the sum of all hadron $p_\perp$'s is minimal. While the fluctuations for each single hadron is too large for usefulness, it could be hoped that the net effect of all the hadrons would be to single out the correct topology.

To be more precise, here is the scheme proposed, to be carried out for each event:

1. Use some jet clustering algorithm to identify the directions of the number of jets that should be used for the current application.

2. Enumerate the possible colour flow topologies allowed in the process.

3. Form one $\sum p_\perp$ measure for each topology, where the sum runs over all final-state particles in the event. For each particle, its $p_\perp$ is defined as the minimum of the $p_\perp$'s obtained by boosting the particle to the rest frame of each of the string pieces making up the current topology.
4. Identify the correct topology as the one with smallest $\sum p_\perp$.

Several effects could smear the simple picture and lead to incorrect conclusions. The main ones are:

- Errors in the reconstruction of jet directions.
- Additional $p_\perp$ caused by perturbative QCD branchings, predominantly gluon emission.
- The $p_\perp$ generated by the fragmentation process.
- Secondary decays of unstable hadrons.

A convenient test bed for the relative importance of these effects is provided by $q\overline{q}g$ events. In symmetric three-jet events at Z^0 energies, without any parton-shower activity, the gluon is correctly identified in 87% of the cases. This should be compared with the 33% expected from a random picking among the three alternatives. When complete Z^0 events events are generated (with PYTHIA 5.7 and JETSET 7.4 [12]), three jets are found (in 10–20% of the events) and the method above is used, the success rate is around 55–60%. The "correct" answer is here found by tracing the original quark and antiquark through the shower history and associating them with the jets they are closest to in angle. The conclusion of this kind of studies is that the method does work, though maybe not as well as one might have hoped, and that the main cause of errors is the perturbative gluon emission.

The studies can be extended to four-jet $q\overline{q}gg$ events, although the large number of colour flow topologies here makes the method rather inefficient for selecting the correct topology. A more modest objective is to establish differences between string and independent fragmentation [13] models. In the latter approach, particle production is aligned along the direction connecting a parton with the origin in the c.m. frame of the event, again with some smearing effects. This approach is already disfavoured by the three-jet studies [4], but is a convenient reference. We have not completed a full study, but can illustrate with results for a simple four-jet cross topology with q and $\overline{q}$ back-to-back. Fig. 1.1a gives the difference in $\sum p_\perp$ between the worst topology (where none of the string pieces run the way assumed) and the right one. Results are for charged particles, and the $\sum p_\perp$ has been normalized to the number N of charged particles per event. The independent fragmentation distribution is symmetric around the origin, as it should, while the string approach shows a clear offset. Without knowledge of the correct answer, one is reduced to studying a measure such as the difference between the maximal and the minimal $\sum p_\perp$ among all the twelve possible topologies, Fig. 1.1b. By construction this is a positive number, also for independent fragmentation, but an additional

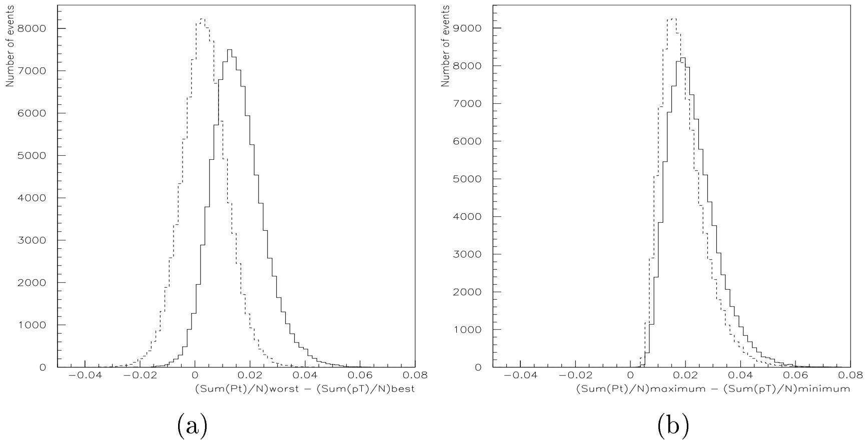

Figure 1.1: The distribution of $\sum p_\perp/N$ for **a**: worst−right, and **b**: maximal−minimal, for Lund string (full) and independent (dashed) fragmentation respectively.

shift is visible for the string approach. Identification of one or both quarks, e.g. by b quark tagging or energy ordering (quarks are likely to have higher energy than gluons), would cut down on the number of topologies to be compared and therefore enhance the signal. Some experimental studies along these lines could therefore be interesting.

We now turn to the main application of this letter, namely four-jet W^+W^- events. Since the two W decay vertices are less than or of the order of 0.1 fm apart, while typical hadronic distances are of the order of 1 fm, the two W decays occur almost on top of each other. QCD interconnection effects could appear at all stages of the process, namely in the original perturbative parton cascades, in the subsequent soft hadronization stage, and in the final hadronic state. It can be shown that perturbative effects are strongly suppressed [7], but no similar arguments hold for the other two. Bose-Einstein effects in the hadronic state could be the largest individual source of W mass uncertainty [14], but it is the least well studied. The presence of such Bose-Einstein effects presumably could be established from the data itself, while reconnection in the hadronization stage is less easy to diagnose. We will study whether the $\sum p_\perp$ measure offers any help here.

The reconnection models used as references in this work are:

1. Reconnection after the perturbative shower stage but before the hadronization, with reconnection occuring at the 'origin' of the showering systems. This 'intermediate' model is the simplest of the more realistic ones.

2. Reconnection when strings overlap based on cylindrical geometry. A 'bag model' based on a type I superconductor analogy. The reconnection probability is proportional to the overlap integral between the field strengths, with each field having a Gaussian fall-off in the transverse direction, the radius being about 0.5 fm. The model contains a free strength parameter that can be modified to give any reconnection probability.
3. Reconnection when strings cross. In this model the strings mimic the behaviour of the vortex lines in a type II superconductor, where all topological information is given by a one-dimensional region at the core of the string.
4. Reconnections occur in such a way that the string 'length' is minimized. As a measure of this length the so-called λ-measure is used, which essentially represents the rapidity range for particle production counted along the string. This can also be seen as a measure of the potential energy of the string.

Models 1 through 3 is described in [7] and the last in [9]. Further models have been proposed [15].

For the study, events should have a clear four-jet structure. To achieve this we demand that each jet must have some minimum energy and that the angle between any jet pair must not be too small [7]. When applied to the expected statistics of LEP 2, the number of events left after the cuts will be about 2500 per experiment; therefore statistics will be a problem when different models are compared with each other.

Three different algorithms are used to identify which jet pairs belong together:

1. The $q_1\overline{q}_2q_3\overline{q}_4$ configuration before parton showers can be matched one-to-one with the reconstructed jets after hadronization. This is done by minimizing the products of the four (jet+q) invariant masses. The original quark information is not available in an experimental situation, so this measure can only be used as a theory reference.
2. The invariant mass of jet pairs from the same W should be close to the known W-mass of about 80 GeV. Among the three possible jet pairings, therefore the one is selected which has minimal $|m_{ij} - 80| + |m_{kl} - 80|$, where i, j, k, l are the four jets. We have picked this method rather than a few similar ones since it has (marginally) the best correlation with the reference method above. This method is mainly probing the electroweak aspect of W pair production, namely the W mass spectrum, while it should be less dependent on the QCD stages of showering and hadronization.
3. The $\sum p_\perp$ method introduced in this letter provides an alternative measure, that rather should be sensitive to the QCD stages and less so to the electroweak one. Without colour reconnection it should (hopefully)

no reconnection			with reconnection (model 1)		
algorithm	1	2	algorithm	1	2
2	85%	–	2	85%	–
3	68%	65%	3	46%	46%

Table 1.1: Fraction of agreement in jet pair identification between the three algorithms.

agree with the previous two, while it could give interesting differences if reconnection occurs.

The agreement between these three methods is shown in Table 1.1, with and without reconnection, the former for model 1. As should be expected, algorithm 2 comes close to the "correct" answer of number 1, and is not significantly affected by colour rearrangement. The $\sum p_\perp$ method, algorithm 3, shows the expected dependence on colour rearrangement, with a smaller success rate when colour rearrangement is included. Note, however, that the success rate does not drop below the naive 33% number, indicating that the $\sum p_\perp$ method is also picking up other aspects of events, such as the jet topology. The results in the table are for a 170 GeV energy, but we do not expect a significant energy dependence.

Both methods 2 and 3 can be applied to data, so therefore the correlation is an observable. The rate of reconnection could be extracted, by interpolation between the two extremes of no and complete colour rearrangement. Statistically it should be feasible to establish a signal for reconnections, if they occur at a rate above the 10–20% level. The systematic errors on the correlation method may be large, however, especially for the model-dependent change when reconnection is included. It is therefore important to study whether a differential distribution would better highlight qualitative differences.

Algorithm 2 can be used to identify the best hypothesis for which jets should be paired to form the two W's, and also the worst hypothesis, where $|m_{ij}-80|+|m_{kl}-80|$ is maximal. The $\sum p_\perp$ can be calculated for each of these two extremes. When the strings are reconnected, the first sum should increase and the second one decrease relative to the no-reconnection case. The signal is therefore enhanced by making use of the difference, $\Delta = (\sum p_\perp)_{\mathrm{worst}} - (\sum p_\perp)_{\mathrm{best}}$, which should decrease in case of reconnection. The subtraction furthermore has the advantage of removing some spurious fluctuations from the comparison. The main example is high-momentum particles, where the assumed string hyperbolae attach well with the four jet directions and therefore all three string hypotheses give the same contribution to $\sum p_\perp$. (Our studies show that particles with momenta above 3 GeV add little to the discrimination

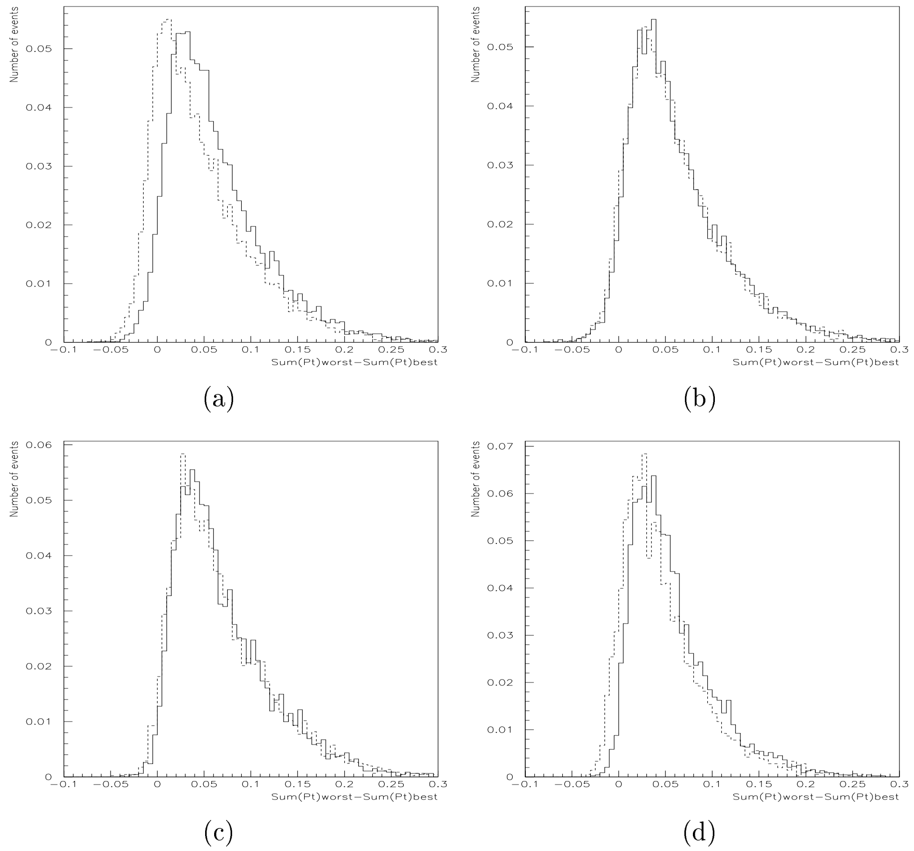

Figure 1.2: Distribution of $\Delta = (\sum p_\perp)_{\mathrm{worst}} - (\sum p_\perp)_{\mathrm{best}}$. Dashed lines are reconnected events according to models **a**: 1 (intermediate), **b**: 2 (bag model), **c**: 3 (type II superconductor), and **d**: 4 (λ-measure), while full lines always are without reconnection.

between the string hypotheses.)

The Δ measure is plotted for models 1–4 in Fig. 1.2. Note that the results for models 1 and 4 correspond to 100% reconnection, while the reconnection rate in models 2 and 3 is about 30%. (The reconnection fraction could be varied in all models, but the effects of reconnection are not linear in this fraction for models 2 and 3, so a reasonable value is preferred here.) All reconnection models show the expected shift towards smaller Δ values, and the magnitude of the shift is comparable once differences in assumed reconnection fractions are removed. Remaining differences imply that one cannot model-independently extract a reconnection rate from the data. The signal for reconnection may be enhanced, compared with the results of Table 1.1, by cuts on Δ, e.g. by only considering the fraction of events with $\Delta < 0$. This is at the price of a reduced statistics, however, so the balance is not so clear. It may be better to use measures that gauge the full shape of the curve, given that the physics of the no-reconnection scenario is presumed well-known (by extrapolation from the Z^0 results).

Prospects look promising to diagnose colour rearrangement along these lines but, as before, the combination of low effects and small statistics could give marginal results. Furthermore, hopes should not be raised too high that this would immediately imply a scheme to correct a W mass measurements for the reconnection effects: of the models above, number 3 shifts the W mass downwards while the others shift it upwards [7, 8], and yet they all shift the Δ distribution in the same direction. Clearly the study of reconnection effects ultimately must be based on a host of different measures, the $\sum p_\perp$ one and others.

It may be of some interest to understand why effects are not larger. Several simulations have been performed with various simplified toy models to study this issue [16]. It turns out that there are two main mechanisms that smear distributions and make them less easily distinguished. One is parton showers, just as for the $Z^0 \to q\overline{q}g$ process studied above. The other is the geometry of the process, namely that the helicity structure of the $W^+W^- \to q_1\overline{q}_2q_3\overline{q}_4$ process is such that q_1 and q_3 tend to go in the same general direction, as do $\overline{q}_2$ and $\overline{q}_4$ [10]. The overall change of string topology by reconnection therefore is not as drastic as if the q_1 had tended to be close to $\overline{q}_4$ and vice versa. Had it been possible to remove these effects, i.e. study events without shower activity and with q_1 and $\overline{q}_4$ reasonably close in angle, the original and the colour-reconnected Δ distributions would almost completely separate. In practice, only a modest reduction of shower activity could be obtained by requiring that all four jets be reasonably narrow, while tagging of quark vs. antiquark (e.g. with charm) would leave very few events. Therefore no simple solutions have been found.

In summary, we have introduced a $\sum p_\perp$ measure as a diagnostic of the colour topology of hadronic events. The fuzzy nature of hadronic final states somewhat limits the usefulness of the method. In particular, the more drastic effects associated with perturbative gluon emission tend to obscure the subtler effects of different colour topologies. Therefore the $\sum p_\perp$ measure is no panacea, but could still be a useful addition to the (not so large) tool box of methods to characterize the nonperturbative stage of hadronic events. Applications include three- and four-jet events at Z^0 energies and, in particular, W pair decay to four jets at LEP 2. In the latter process, it could be possible to detect the effects of colour reconnection with this approach. Further details on the studies reported here may be found in [16].

References

[1] B. Andersson, G. Gustafson, G. Ingelman and T. Sjöstrand, Phys. Rep. **97**, 31 (1983).

[2] B. Andersson and H.-U. Bengtsson, Lund preprint LU TP 87–8 (1987, unpublished).

[3] B. Andersson, G. Gustafson and T. Sjöstrand, Phys. Lett. **94B**, 211 (1980).

[4] JADE Collaboration, W. Bartel *et al.*, Phys. Lett. **101B**, 129 (1981);
J. Fuster, in *International Europhysics Conference on High Energy Physics, Brussels, Belgium, 27 Jul – 2 Aug 1995*, eds. J. Lemonne, C. Vander Velde and F. Verbeure (World Scientific, Singapore, 1996), p. 319;
T. Sjöstrand, *ibid.*, p. 572; and references therein.

[5] Ya.I. Azimov, Yu.L. Dokshitzer, V.A. Khoze and S.I. Troyan, Phys. Lett. **165B**, 147 (1985).

[6] G. Gustafson, U. Pettersson and P. Zerwas, Phys. Lett. **B209**, 90 (1988).

[7] T. Sjöstrand and V.A. Khoze, Phys. Rev. Lett. **72**, 28 (1994), Z. Phys. **C62**, 281 (1994).

[8] Z. Kunszt *et al.*, in *Physics at LEP2*, eds. G. Altarelli, T. Sjöstrand and F. Zwirner, CERN 96–01, Vol. 1, p. 141.

[9] G. Gustafson and J. Häkkinen, Z. Phys. **C64**, 659 (1994).

[10] A. Gaidot, J.P. Pansart and N.K. Watson, OPAL TN320 (1995, unpublished).

[11] J. Häkkinen, Lund University Ph.D. thesis (1996).

[12] T. Sjöstrand, Comput. Phys. Commun. **82**, 74 (1994).

[13] P. Hoyer, P. Osland, H.G. Sander, T.F. Walsh and P.M. Zerwas, Nucl. Phys. **B161**, 349 (1979);
A. Ali, J.G. Körner, G, Kramer and J. Willrodt, Nucl. Phys. **B168**, 409 (2980);
R. Odorico, Comput. Phys. Commun. **72**, 238 (1992).

[14] L. Lönnblad and T. Sjöstrand, Phys. Lett. **B351**, 293 (1995).

[15] L. Lönnblad, Z.Phys. **C70**, 107 (1996);
I.G. Knowles *et al.*, in *Physics at LEP2*, eds. G. Altarelli, T. Sjöstrand and F. Zwirner, CERN 96–01, Vol. 2, p. 103.

[16] E. Norrbin, Lund preprint LU TP 96–15 (hep–ph/9606206).

QCD Aspects of Leptoquark Production at HERA

Paper II

QCD Aspects of Leptoquark Production at HERA

Christer Friberg, Emanuel Norrbin and Torbjörn Sjöstrand
Department of Theoretical Physics
Lund University

Physics Letters **B 403** (1997) 329

If a leptoquark is produced at HERA as a narrow resonance, various effects tend to broaden the measurable mass distribution considerably. These effects are discussed here, with special emphasis on initial- and final-state QCD radiation. A proper understanding is important to assess the significance of data and to devise strategies for better mass reconstruction.

Recently, the H1 and ZEUS Collaborations at HERA have presented evidence for an excess of events at large Q^2 and x [1, 2]. This could be nothing but a statistical fluke. Alternatively, it could be the first signal of the production of an s-channel resonance, a leptoquark (LQ). In order to test such a hypothesis, as further data accumulate, it is important to understand the production characteristics of an LQ at HERA. In particular, it should be noted that an expected narrow mass peak will be smeared by various physics and detector effects. In this letter we want to give a brief survey of the physics components that could contribute to this smearing, and estimate the magnitude of each of these effects. Previous studies of a similar kind have been performed with the LEGO generator [3], which is partly based on PYTHIA [4]. We also want to give some examples of how to improve the reconstruction of the LQ mass.

This is not a study on the physics implications of an LQ observation at HERA [5]. Therefore we do not discuss the origin of an LQ in terms of an underlying theory, be that compositeness, supersymmetry or anything else, but stay with a purely phenomenological description of LQ properties [6]. Even so, several options are possible, and we will restrict ourselves further. An LQ may have spin 0 or 1, with differences in the decay angular distribution, but of little importance for the considerations in this letter, so we stay with the spin 0 alternative. An LQ may have net fermion number 0 ($\mathrm{q}\overline{\ell}$ or $\overline{\mathrm{q}}\ell$) or ± 2 ($\mathrm{q}\ell$ or $\overline{\mathrm{q}}\overline{\ell}$). Given that HERA has been running with an e^+ beam in recent years, the latter kind would be disfavoured by requiring a sea antiquark from the proton. It would have been favoured in the earlier HERA runs with e^-, however, where the valence quark distributions could have been accessed. The ratio in parton distributions between valence and sea at $x \approx 0.5$ being larger than the recorded luminosity ratio $\mathrm{e}^+\mathrm{p}/\mathrm{e}^-\mathrm{p}$, the previous non-observation [7] favours LQ's with vanishing fermion number. A leptogluon scenario is not excluded, but is not favoured [8]. QCD consequences of a $\overline{\mathrm{q}}\overline{\ell}$ LQ or a leptogluon are briefly mentioned later.

Phenomenologically, the production cross section for a leptoquark in the process $\mathrm{q} + \ell^+ \to \mathrm{LQ}$ can be written as [6]

$$\sigma = \frac{\pi\lambda^2}{4s} q(x, M_{\mathrm{LQ}}^2) = k\frac{\pi^2\alpha_{\mathrm{em}}}{s} q(x, M_{\mathrm{LQ}}^2) \ . \tag{2.1}$$

Here λ gives the strength of the unknown Yukawa coupling; the alternative k parameter is normalized such that $k = 1$ corresponds to electromagnetic strength of the coupling. To first approximation $x = M_{\mathrm{LQ}}^2/s$ — corrections to this will be a main theme of the letter — and $q(x, M_{\mathrm{LQ}}^2)$ the parton distribution at a scale given by the LQ mass.

The observed handful of candidate events per experiments, for an integrated luminosity of order 15 pb^{-1} and a detection efficiency around 50% (including a cut $Q^2 > 15000$ GeV^2), would suggest a production cross section of the order of 1 pb. For a ue^+ LQ of around 200 GeV mass this corresponds to $k \sim 0.01$. The width of a scalar LQ,

$$\Gamma_{\mathrm{LQ}} = \frac{\lambda^2}{16\pi} M_{\mathrm{LQ}} = \frac{k\alpha_{\mathrm{em}}}{4} M_{\mathrm{LQ}} , \tag{2.2}$$

then becomes only $\Gamma_{\mathrm{LQ}} \sim 4$ MeV. A de^+ LQ would be somewhat broader, but in either case the width is negligibly small on an experimental scale. Unless the total width is enhanced significantly by decays to exotic channels, the LQ is long-lived enough that it will form an LQ-hadron, made up of the LQ and an antiquark or a diquark.

QCD radiation of gluons and QED radiation of photons in principle can occur in the initial state, off the LQ itself, and in the final state. Including all interference terms, a complicated radiation pattern is then possible. The small width here offers a considerable simplification: interference terms and radiation off the LQ are suppressed for radiated energies above Γ_{LQ} [9, 10]. The region $E \lesssim \Gamma_{\mathrm{LQ}} \sim 10$ MeV giving a very small contribution to the total radiated energy, it is therefore sufficient to consider three main classes of corrections, (i) initial-state radiation, (ii) LQ-hadron formation, and (iii) final-state radiation. We will consider these effects one at a time, roughly in order of decreasing importance.

The main effect of final-state radiation is that the hadronic system of the LQ decay acquires a mass in excess of the naive quark one and that, as a consequence, the energy of the recoiling lepton is reduced. The jet mass phenomenology is not very different from experience in hadronic $\mathrm{e}^+\mathrm{e}^-$ annihilation events. A standard parton-shower description [11] tuned to LEP data predicts an average quark jet mass of about 30 GeV at 200 GeV energy. Taking over the same formalism for the LQ decays then gives an average mass $\langle M_{\mathrm{q}} \rangle \approx 32$ GeV, Fig. 2.1, i.e. somewhat higher since the absence of a radiating final-state partner removes some phase-space competition. In a more detailed study one should include the explicit matrix-element information for the region of well-separated emission, which could introduce some modest dependence on the spin of the leptoquark.

In the rest frame of the LQ the lepton takes an energy

$$E_\ell = \frac{M_{\mathrm{LQ}}}{2} \left(1 - \frac{M_{\mathrm{q}}^2}{M_{\mathrm{LQ}}^2} \right) . \tag{2.3}$$

The rest-frame lepton scattering angle θ^* is only very little affected by the QCD radiation [12]. (Furthermore, for a spin 0 leptoquark, the inclusive decay distribution is isotropic in $\cos\theta^*$ in any case.) Even though the standard DIS variables do not have the traditional meaning related to a spacelike boson propagator, they can be defined purely experimentally. The M_{q} term above then propagates to give

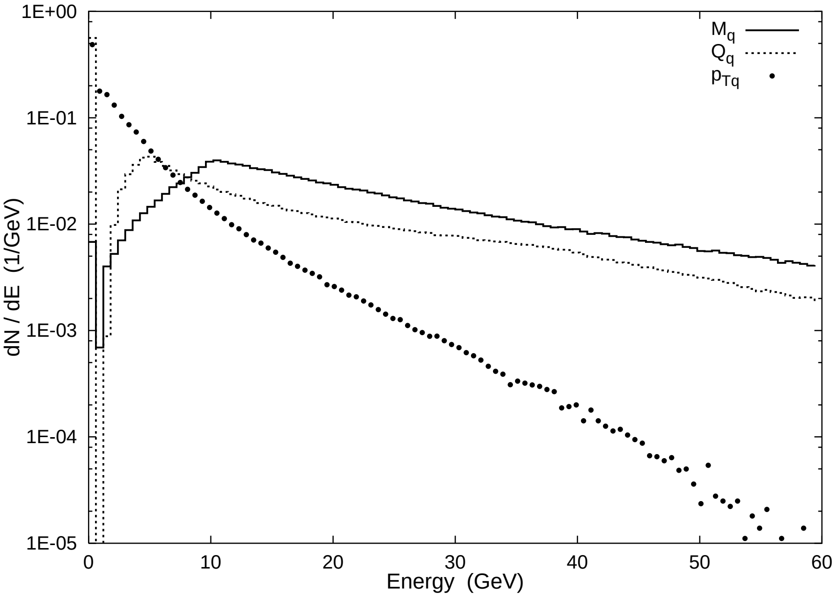

Figure 2.1: Distribution of M_{q} (full), Q_{q} (dashed) and $p_{\perp\mathrm{q}}$ (dots).

$$Q^2 = \frac{M_{\mathrm{LQ}}^2}{2}(1-\cos\theta^*)\left(1-\frac{M_{\mathrm{q}}^2}{M_{\mathrm{LQ}}^2}\right) , \tag{2.4}$$

$$x_{\mathrm{Bj}} = \frac{Q^2}{2Pq} = \frac{M_{\mathrm{LQ}}^2}{s}\frac{Q^2}{Q^2+M_{\mathrm{q}}^2} . \tag{2.5}$$

Defining τ to be the x value relevant for an LQ mass determination,

$$\tau \equiv \frac{\hat{s}}{s} = \frac{M_{\mathrm{LQ}}^2}{s} = x_{\mathrm{Bj}}\left(1+\frac{M_{\mathrm{q}}^2}{Q^2}\right) , \tag{2.6}$$

one finds that $\tau > x_{\mathrm{Bj}}$. In particular note that the denominator of the M_{q} correction factor is Q^2, not M_{LQ}^2. This means that low-Q^2 data would not be expected to show any peak in x_{Bj}. A typical cut $Q^2 > 15000$ GeV^2 reduces the $\langle M_{\mathrm{q}}\rangle$ from 32 GeV to 29 GeV (eq. (2.4)). The $\langle M_{\mathrm{q}}^2\rangle \approx 1430$ GeV^2 then gives an average correction factor in eq. (2.6) of somewhat above 5%. If the experimentally reconstructed LQ mass is taken to be $\sqrt{x_{\mathrm{Bj}}s}$, the original δ function is smeared as shown in Fig. 2.2. Since $Q^2 = x_{\mathrm{Bj}}ys$ is an identity that follows from

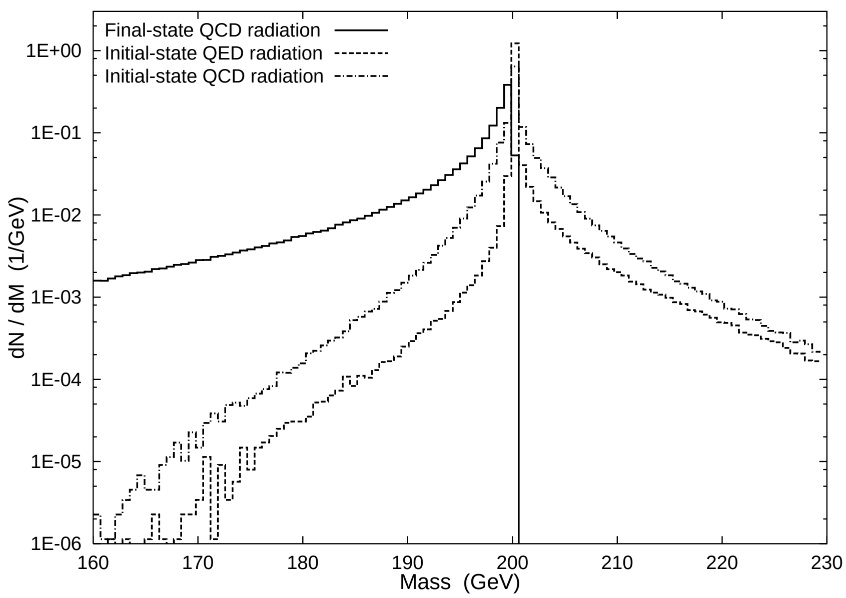

Figure 2.2: The reconstructed LQ mass distribution $m_{\mathrm{recon}} = \sqrt{x_{\mathrm{Bj}} s}$ for an input mass of 200 GeV, with a simple cut $Q^2 > 15000$ GeV^2 on the leptoquark sample. Results are shown with only one component active at a time: final-state QCD radiation (full), initial-state QED radiation off the positron (dashed) and initial-state QCD radiation (dot-dashed).

the definition of the respective variable, the alternative experimental measure $\sqrt{Q^2/y}$ gives the same smearing.

Also photons may be radiated in the final state, both from the lepton and the quark. Owing to the smaller coupling, the amount of radiation is reduced compared with the QCD case above. Radiation almost collinear with the lepton occurs at a significant rate, but is not resolved by the calorimetric definition of lepton energy and so is of little consequence. In our studies we choose not to resolve final-state photons below a 1 GeV invariant mass cut-off.

We next turn to initial-state radiation, i.e. radiation off the incoming quark and lepton lines. This reduces the longitudinal momentum fraction carried by the reacting quark/lepton, and builds up a $p_\perp$ and a spacelike virtuality for it.

Photon radiation off the lepton line is dominated by the almost collinear one. In this limit, one has that $\tau = x_{\mathrm{q}} x_\ell$, where the x_i are the respective momentum fractions. In the leading-log approximation, the positron-inside-positron distribution is roughly [13]

$$D_{\mathrm{e}}^{\mathrm{e}}(x_\ell, M_{\mathrm{LQ}}^2) \approx \beta(1-x_\ell)^{\beta-1} \tag{2.7}$$

with

$$\beta = \frac{\alpha_{\mathrm{em}}}{\pi}\left(\ln\frac{M_{\mathrm{LQ}}^2}{m_{\mathrm{e}}^2} - 1\right) \approx 0.0575.$$

Eq. (2.1) is then modified to

$$\sigma = k\frac{\pi^2\alpha_{\mathrm{em}}}{s}\iint \mathrm{d}x_{\mathrm{q}}\,\mathrm{d}x_\ell\, q(x_{\mathrm{q}}, M_{\mathrm{LQ}}^2)\, D_{\mathrm{e}}^{\mathrm{e}}(x_\ell, M_{\mathrm{LQ}}^2)\,\delta(x_{\mathrm{q}}x_\ell - \tau)\ . \tag{2.8}$$

One obtains $\langle x_\ell\rangle \approx 0.99$ or $\langle x_{\mathrm{q}}\rangle \approx 1.01\tau$. The steep fall-off of $q(x_{\mathrm{q}}, M_{\mathrm{LQ}}^2)$ dampens the tail to large $1-x_\ell$. Therefore typical experimental cuts on photon energy lost in the beam pipe do not make a big difference. The relation between the true and reconstructed masses is

$$\tau = x_{\mathrm{Bj}}\,\frac{x_\ell^2}{1-(1-x_\ell)/y}\ , \tag{2.9}$$

so the mass shift may be in either direction, Fig. 2.2.

Radiation of photons and gluons in the initial state leads to a buildup of spacelike virtualities and transverse momenta for the incoming quark and lepton. The largest effects come on the quark side, Fig. 2.1, where $\langle Q_{\mathrm{q}}\rangle \approx 14.3$ GeV and $\langle p_{\perp\mathrm{q}}\rangle \approx 3.6$ GeV, while $\langle Q_\ell\rangle \approx 0.85$ GeV and $\langle p_{\perp\ell}\rangle \approx 0.15$ GeV for the incoming positron, using the spacelike parton-shower formalism of [14]. (Numbers vary a bit depending on choice of parton distribution parametrizations etc.) The spacelike virtualities can be seen as a kinematical consequence of the $p_\perp$ kicks, so the $Q_{\mathrm{q}(\ell)}$ and $p_{\perp\mathrm{q}(\ell)}$ are strongly correlated. Note that $\langle Q_{\mathrm{q}}^2\rangle \ll M_{\mathrm{q}}^2$: spacelike parton-shower evolution is constrained by the limited phase space and the steeply falling parton distributions at large x. That is, the probability that the daughter quark at x_i comes from the branching of a mother quark at $x_{i-1} > x_i$ is related to the ratio $q(x_{i-1})/q(x_i)$ of parton distributions, and the integral of $q(x_{i-1})$ over $x_{i-1} > x_i$ is small. At each branching one has $p_{\perp i}^2 \approx (1-z_i)Q_i^2$, with $z_i = x_i/x_{i-1}$, so from the argument above it is clear why also $\langle p_{\perp\mathrm{q}}^2\rangle \ll \langle Q_{\mathrm{q}}^2\rangle$.

The consequences of nonzero virtualities and transverse momenta can again be traced through the standard DIS variables. Also including the previous effects, i.e. $M_{\mathrm{q}} \neq 0$ and $x_\ell \neq 0$, gives the relation

$$\tau \quad = \quad \frac{b - 2aQ_{\mathrm{q}}^2 + \sqrt{b^2 - 4ax_\ell Q^2\left(Q_{\mathrm{q}}^2 - p_{\perp\mathrm{q}}^2\right)}}{2sa}\ ,$$

$$\begin{aligned} \text{where} \quad a &= 1 - \frac{1-y}{x_\ell} \\ \text{and} \quad b &= x_\ell Q^2 + M_{\mathrm{q}}^2 + Q_{\mathrm{q}}^2 - 2\overline{p}_{\perp\mathrm{q}}\overline{k}'_\perp \ . \end{aligned} \tag{2.10}$$

(A correction formula in terms of another set of variables is found in [3].) The spacelike virtuality and $p_\perp$ kick may either increase or decrease the estimated LQ mass. In particular, there is an explicit dependence on the azimuthal angle between the $p_{\perp\mathrm{q}}$ of the incoming quark ($= p_{\perp\mathrm{LQ}}$ in this approximation) and the $k'_\perp$ of the outgoing lepton. The resulting spread in reconstructed LQ mass is shown in Fig. 2.2.

A $p_{\perp\mathrm{q}}$ contribution is also given by the primordial $k_\perp$ of the parton-shower initiator inside the proton. This primordial $k_\perp$ is some combination of Fermi motion and initial-state radiation below the soft cut-off of the simulation program. A typical scale for the former would be $\langle k_\perp^2 \rangle \approx 0.25$ GeV^2, but even if this is increased to 1 GeV^2 the net effects are quite negligible, since the $k_\perp$ is added to the much larger $p_\perp$ of the perturbative parton shower. Only in some future study of the LQ $p_\perp$ distribution itself would the low-$p_{\perp\mathrm{LQ}}$ tail be sensitive to the choice.

The effects of LQ-hadron formation are not large, since the LQ is so massive that its motion is not significantly affected by hadronization effects. Data on b and c quarks are consistent with a non-perturbative fragmentation where the LQ-hadron retains an average fraction

$$z \approx \frac{M_{\mathrm{LQ}}}{M_{\mathrm{LQ}} + 1\ \mathrm{GeV}} \approx 0.995 \tag{2.11}$$

of the original LQ momentum, cf. [15]. The antiquark (diquark) contributes a typical fragmentation $p_\perp$ to the net $p_\perp$ of the LQ-hadron. The LQ has some Fermi motion inside the LQ-hadron, of the order of the antiquark constituent mass, that shifts the momentum of the decaying LQ. The net effects of all the hadronization contributions should be a more-or-less random momentum shift at or below the 1 GeV scale, i.e. negligible. A consequence of confinement is that the LQ mass cannot be defined unambiguously, so the detailed effects of hadronization have to be seen in the context of some specific scheme for relating the LQ-hadron mass to the LQ mass itself.

The hadronic system will show some effects of the LQ lifetime. If an LQ-hadron is formed, the hadrons produced from the proton remnant and the initial-state-radiation partons decouple completely from those produced in the decay of the LQ-hadron. This means, e.g., that the charged multiplicity is independent of the LQ decay angle, i.e. of Q^2 (apart from some small trigger-bias effects). By contrast, if the LQ is too short-lived for LQ-hadron formation, the initial- and final-state partons are connected into a common colour string [16]. The string length and hence the multiplicity now depends on the angle between the proton remnant and the LQ hadronic decay products (just like in standard DIS processes, with $W^2 \propto Q^2$ for fixed x_{Bj}). If the initial- and final-state shower effects are neglected, the variation at small Q^2 is significant, but is reduced to $\sim 10\%$ in the $Q^2 > 15000$ GeV^2 region. When showers are included, however, these tend to dominate the particle production characteristics in a global sense. A memory remains in the soft (low-momentum) region, e.g. defined by $|\mathbf{p}| < 1$ GeV in the longitudinal rest frame of the LQ. (The lab frame is unsuitable, since the LQ motion in this frame introduces large spurious effects.) Over the standard high-Q^2 range, and with full inclusion of parton showers, the variation in charged multiplicity is here over 20%. In the unlikely event that the LQ is very short-lived, coherence effects will also appear in the parton-shower stage, and so the multiplicity variation will spread to all $|\mathbf{p}| \lesssim \Gamma_{\mathrm{LQ}}$. It is therefore possible to conclude from the hadronic final state whether an LQ-hadron is being formed or not, given enough statistics. This situation is quite similar to the one for the top quark [10].

All the physics aspects described above are included in the PYTHIA event generator [4].[1] The net distribution of reconstructed LQ masses is shown in Fig. 2.3, where all effects described above have been included. The bulk of the mass spread is given by the effects in eq. (2.10). After correction with this formula, the remaining mass spread is the result of the $k_\perp$ kick and virtuality of the incoming lepton, the QED radiation off the outgoing lepton, and LQ-hadron formation.

A $\overline{\mathrm{q}}\overline{\ell}$ LQ would share most of the features described above. There is enhanced initial-state QCD radiation in those events where a branching chain $\mathrm{q} \to \mathrm{qg}, \mathrm{g} \to \mathrm{q}\overline{\mathrm{q}}$ occurs. However, most events start with a $\overline{\mathrm{q}}$ at the cut-off scale $Q_0 \approx 1$ GeV, and here gluon radiation off the $\overline{\mathrm{q}}$ is suppressed by the steeply falling $\overline{q}(x)$ distribution. That is, parton-shower histories that allow a $\overline{\mathrm{q}}$ to survive at large x and large Q^2 are biased towards lower activity (a bit more than those of the q), and so the $\langle Q_{\overline{\mathrm{q}}} \rangle \approx 12.4$ GeV rather than the 14.3 GeV of the q. For a leptogluon, an increased radiation in the final state follows directly from the higher colour charge, $\langle M_{\mathrm{g}} \rangle \approx 45$ GeV. In the initial state, there is again a suppression from the steeply falling gluon distribution. About half of the events contain a branching step $\mathrm{q} \to \mathrm{qg}$, and this branching is biased towards higher virtualities since the quark line below the branching scale radiates less than the gluon above. The net result is a fairly large mean, $\langle Q_{\mathrm{g}} \rangle \approx 31$ GeV. A leptogluon would hence give a higher hadronic multiplicity than an LQ.

So far we have concentrated exclusively on one method for LQ mass reconstruction, based on the measurement of the scattered positron (Q^2, x_{Bj} and y).

[1] LQ-hadron formation is not part of the standard distribution. Note that `MSTJ(50)=0` and `MSTP(67)=0` should be set to switch off interference between the initial- and final-state radiation.

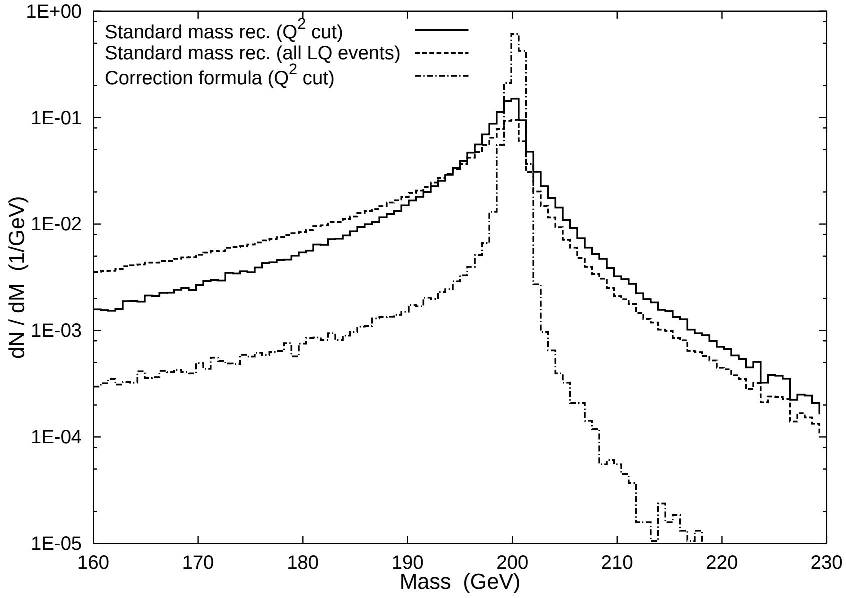

Figure 2.3: The reconstructed LQ mass distribution for an input mass of 200 GeV: all LQ events with $m_{\mathrm{recon}} = \sqrt{x_{\mathrm{Bj}} s}$ (dashed), $Q^2 > 15000$ GeV^2 with $m_{\mathrm{recon}} = \sqrt{x_{\mathrm{Bj}} s}$ (full) and $Q^2 > 15000$ GeV^2 with $m_{\mathrm{recon}} = \sqrt{\tau s}$, eq. (2.10) (dot-dashed).

Alternative methods are used by the H1 and ZEUS collaborations. However, they all share some common assumptions, such as massless partons and $p_\perp$ balance between the scattered positron and the recoiling hadronic system, and therefore do not recover the bulk of the smearing effects noted above. The optimal way to reconstruct a narrow(er) mass peak clearly is detector-dependent, and so must be worked out by the experimental collaborations. We here want to give some very general comments, however.

With an ideal detector, and good separation between the LQ decay products and the hadrons from the proton beam remnant, the four-momentum of the LQ could be reconstructed to give the LQ mass directly. Such an approach suffers from the calorimetric smearing of hadronic momentum measurements. Since the parton-shower activity spreads out hadrons, there is also no clean separation of hadrons. Therefore, alternatively, one could start from the better-measured positron momentum and then add corrections according to eq. (2.10), to give a mass estimate $m_{\mathrm{recon}} = \sqrt{\tau s}$. In practice, some of the required terms turn out to be rather difficult to reconstruct from the observable hadronic

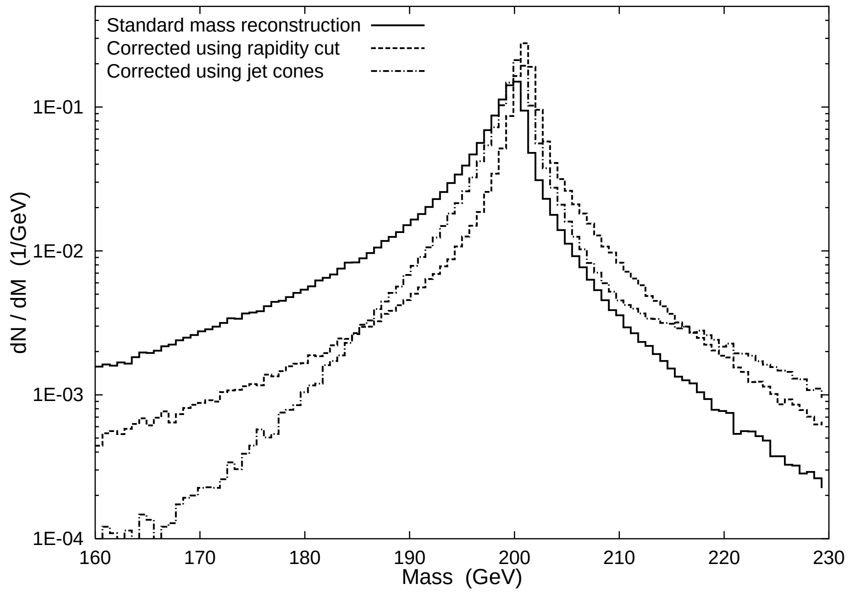

Figure 2.4: The reconstructed LQ mass distribution for an input mass of 200 GeV and with $Q^2 > 15000$ GeV^2. Curves show mass based on x_{Bj} only (full), or corrected for M_{q} either with a pseudorapidity separation (dashed) or a jet-finding strategy (dot-dashed). For details see text.

final state. The most feasible correction is for the final-state QCD radiation, which we have seen to be the largest individual souce of smearing, and which also tends to give a systematic bias in a mass determination. Two alternative methods have been compared for reconstructing M_{q}. In the first, all particles with a (pseudo)rapidity below 1.7 (except the lepton) are used to calculate an invariant mass that is associated with M_{q}. The cut is selected to minimize the misidentification of particles between the LQ-hadron and the remnant system. In the second method, a jet clustering algorithm [4] is used to find jets with an $E_{\perp} \geq 10$ GeV inside an $R = \sqrt{(\Delta\eta)^2 + (\Delta\varphi)^2} < 1$ cone, and an invariant mass is calculated for the particles belonging to the jet or jets. The jet threshold is here selected so that initial-state radiation is less likely to give rise to a jet. The reconstructed M_{q} is then used in eq. (2.6) to give a corrected LQ mass estimate. The distributions in Fig. 2.4 show that either correction factor does result in a narrower mass peak (the width is reduced from 11.1 to 8.2 GeV) and one that contains less systematic bias towards underestimating the correct mass (the average is shifted from 195.3 to 200.6 GeV).

In summary, we have shown that several QCD effects are at play in the production and decay of a leptoquark. These effects are fairly well understood from our experience in other areas of high-energy physics. It is therefore possible to describe in detail the production characteristics. This knowledge may be useful to obtain less biased and narrower mass peaks, and also to devise other tests that could help to distinguish between leptoquark production and ordinary DIS phenomena.

References

[1] H1 Collaboration, C. Adloff et al, DESY 97-024.

[2] ZEUS Collaboration, J. Breitweg et al, DESY 97-025.

[3] K. Rosenbauer, thesis RWTH Aachen, PITHA preprint 95/16, http://www.physik.rwth-aachen.de/group/pitha/1995/pitha1995_16.html.

[4] T. Sjöstrand, Comput. Phys. Commun. **82** (1994) 74.

[5] G. Altarelli, J. Ellis, G.F. Giudice, S. Lola and M.L. Mangano, CERN–TH/97–40;
H. Dreiner and P. Morawitz, hep–ph/9703279;
J. Kalinowski, R. Rückl, H. Spiesberger and P.M. Zerwas, DESY 97–038;
V. Barger, K. Cheung, K. Hagiwara and D. Zeppenfeld, MADPH–97–991.

[6] W. Buchmüller, R. Rückl and D. Wyler, Phys. Lett. **B191** (1987) 442.

[7] ZEUS Collaboration, M. Derrick et al, Phys. Rev. Lett. **75** (1995) 1006;
H1 Collaboration, S. Aid et al, Phys. Lett. **B379** (1996) 319.

[8] J. Bijnens, in 'Proceedings of the HERA Workshop', ed. R.D. Peccei (DESY, 1988), Vol. 2, p. 819.

[9] V.A. Khoze, L.H. Orr and W.J. Stirling, Nucl. Phys. **B378** (1992) 413;
V.S. Fadin, V.A. Khoze and A.D. Martin, Phys. Lett. **B320** (1994) 141;
T. Sjöstrand and V.A. Khoze, Z. Phys. **C62** (1994) 281.

[10] V.A. Khoze and T. Sjöstrand, Phys. Lett. **B328** (1994) 466.

[11] M. Bengtsson and T. Sjöstrand, Phys. Lett. **B185** (1987) 435; Nucl. Phys. **B289** (1987) 810.

[12] R. Kleiss, Phys. Lett. **B180** (1986) 400.

[13] R. Kleiss et al., in 'Z physics at LEP 1', eds. G. Altarelli, R. Kleiss and C. Verzegnassi, CERN 89-08 (Geneva, 1989), Vol. 3, p. 143.

[14] T. Sjöstrand, Phys. Lett. **B157** (1985) 321;
M. Bengtsson, T. Sjöstrand and M. van Zijl, Z. Phys. **C32** (1986) 67.

[15] J.D. Bjorken, Phys. Rev. **D17** (1978) 171.

[16] B. Andersson, G. Gustafson, G. Ingelman and T. Sjöstrand, Phys. Rep. **97** (1983) 31.

Production Mechanisms of Charm Hadrons in the String Model

Paper III

Production Mechanisms of Charm Hadrons in the String Model

Emanuel Norrbin and Torbjörn Sjöstrand
Department of Theoretical Physics
Lund University

Physics Letters **B 442** (1998) 407

In the hadroproduction of charm in the context of string fragmentation, the pull of a beam remnant at the other end of a string may give a charm hadron more energy than the perturbatively produced charm quark. The collapse of a low-mass string to a single hadron is the extreme case in this direction, and gives rise to asymmetries between charm and anticharm hadron spectra. We study these phenomena, and develop models that describe the characteristics not only of the charm hadrons but also of the associated event.

Asymmetries in the production spectra of charm and anticharm hadrons (or generally, asymmetries between leading and non-leading particles) have been observed since long [1]. But it is only in recent years [2, 3, 4] that the precision has improved so as to allow more detailed studies, especially in π^-p events. Perturbative QCD calculations predict only very small asymmetries [5, 6], so the origin of the observed asymmetries has to be sought in nonperturbative physics.

Furthermore, the observed longitudinal momentum spectra of charm mesons are about as hard as or, in some cases, even harder than the perturbatively calculated charm quark spectra. This runs counter to naive expectations, e.g. based on experience from e^+e^- annihilation experiments in the 10 GeV region, where the charm hadrons only keep about two thirds of the original charm quark energy [7]. This number ought to be relevant for the hadroproduced charm events, since the Q^2 scales involved are comparable — by QCD scaling violations, the fraction slowly drops with energy.

Several scenarios have also been proposed to explain the phenomenology [8, 9, 10]. The two most frequently used ones are probably those of string fragmentation [9] and intrinsic charm [10]. In this letter we develop and study the string fragmentation approach. The key objective is to study the collapse of low-mass strings into a single hadron, which provides the main mechanism of flavour asymmetries in our approach. The outline of the letter is as follows. First we classify the different production channels for D mesons in hadron–hadron collisions, from perturbative and nonperturbative perspectives. Then we identify the origin of the charm asymmetry and compare the current model with data. The critical aspects of charm production are thereafter studied in more detail and different model variations are proposed to better understand the data. Further details and applications are intended to appear in a future paper.

The production of a charm hadron can be subdivided into two steps: first the production of a $c\overline{c}$ pair, followed by the hadronization of these quarks. We will assume that the first step of this process is adequately described by standard perturbation theory and conventional parton distributions, i.e. without the inclusion of any intrinsic charm component in the proton wave function. The charm sea is thus assumed perturbatively calculable and peaked at small x values. Intrinsic charm and other modifications to standard perturbative results may well exist at *some* level, but here we want to show that it is possible to understand existing data without invoking new mechanisms for the production stage.

Also with this restriction, it is not possible to obtain unambiguous perturbative predictions: results are sensitive to ill-determined parameters such as the charm mass. As a simplification, we will stay with lowest-order matrix elements for charm production, augmented by a parton-shower approximation to

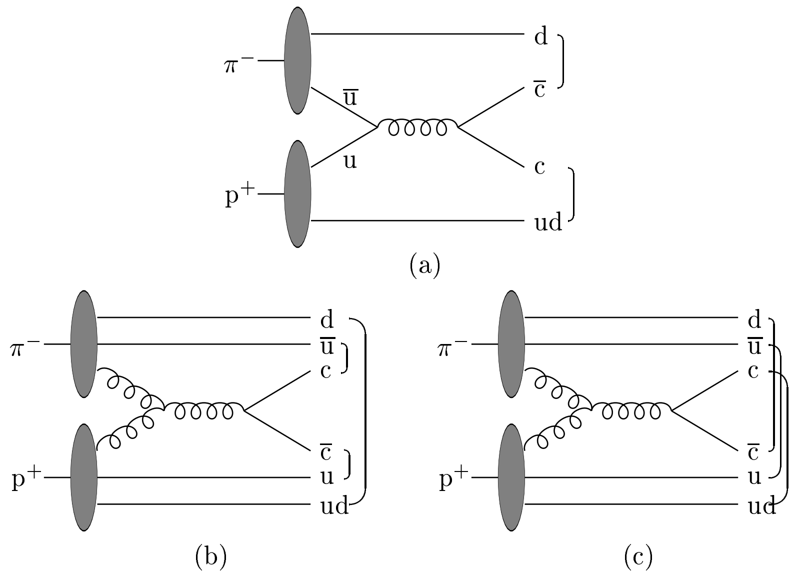

Figure 3.1: Examples of different string configurations in a π^-p collision: (a) $u\overline{u} \to c\overline{c}$ has a unique colour flow; (b,c) $gg \to c\overline{c}$ with the two possible colour flows.

higher-order corrections. Given the uncertainties already noted, this appears adequate.

The interesting phenomenology thus appears in the hadronization stage of our model. Here the partons of the hard interaction and of the beam remnants are connected by strings, representing the confining colour field [11]. Each string contains a colour triplet endpoint, a number (possibly zero) of intermediate gluons and a colour antitriplet end. The string topology can usually be derived from the colour flow of the hard process. For instance, consider the process $u\overline{u} \to c\overline{c}$ in a π^-p collision. The colour of the incoming u is inherited by the outgoing c, so it will form a colour-singlet together with the proton remnant, here represented by a colour antitriplet ud diquark. In total, the event will thus contain two strings, one c–ud and one $\overline{c}$–d (Fig. 3.1a). In $gg \to c\overline{c}$ a similar inspection shows that two distinct colour topologies are possible. Representing the proton remnant by a u quark and a ud diquark (alternatively d plus uu), one possibility is to have three strings c–$\overline{u}$, $\overline{c}$–u and d–ud (Fig. 3.1b), and the other is the three strings c–ud, $\overline{c}$–d and u–$\overline{u}$ (Fig. 3.1c). In addition to the valence $u\overline{u}$ annihilation and gg fusion production mechanisms, there are of course other possibilities, for example events involving sea quarks. These are included in the model but give small contributions to asymmetries and other observables at fixed-target energies, and therefore will not be discussed specifically in the following.

In a process with two (or more) allowed colour flows, such as $gg \to c\bar{c}$, the amplitude for either of them is calculable in perturbation theory, but with a nonvanishing interference term between the two. This term, corresponding to an indeterminate colour flow, fortunately is suppressed by a colour factor $1/N_C^2 = 1/9$. Its contribution to the total charm cross section therefore can be split between the two well-determined colour flows, e.g. according to the pole structure of the terms [12], without much resulting ambiguity. Furthermore, we neglect the possibility of the $c\bar{c}$ pair forming a string, either by a perturbative or nonperturbative colour (re)arrangement. Such mechanisms are likely to play a significant rôle for J/ψ production, e.g., but should be less relevant for the open charm production to be considered here.

Once the string topology has been determined, the Lund string fragmentation model [11] can be applied to describe the nonperturbative hadronization. Assuming that the fragmentation mechanism is universal, i.e. process-independent, the good description of e^+e^- annihilation data should carry over. The main difference between e^+e^- and hadron–hadron events is that the latter contain beam remnants which are colour-connected with the hard-scattering partons. The structure of these remnants is not calculable from first principles, so this introduces some arbitrariness not constrained by e^+e^- data. In the present model these aspects are parameterized in beam remnant distribution functions to be considered later.

Depending on the invariant mass of a string, practical considerations lead to the need to distinguish three hadronization prescriptions:

1. *Normal string fragmentation.* In e^+e^- collisions the string system has a mass equal to the full CM energy, neglecting the not-too-frequent $g \to q\bar{q}$ shower branchings which splits a string in two. This situation is ideal for an iterative fragmentation scheme, for which the assumption of a continuum of phase-space states is essential. The average multiplicity increases linearly with the string 'length' which means, neglecting gluon-emission effects, logarithmically with the string mass. In practice, this approach can be used for all strings above some cut-off mass of a few GeV.
2. *Cluster decay.* In a hadron collision at fixed-target energies it frequently happens that a colour-singlet system contains two partons moving in the same general direction, see Fig. 3.2. This gives the system a small invariant mass, for which maybe only two-body final states are kinematically accessible. The continuum assumption above then is not valid, and the traditional iterative Lund scheme is not applicable. We call such a low-mass string a cluster, and treat it differently from above. When kinematically possible, a c–$\bar{q}$ cluster will decay into a charmed meson and a light meson by the production of a light quark–antiquark pair in the colour force field between

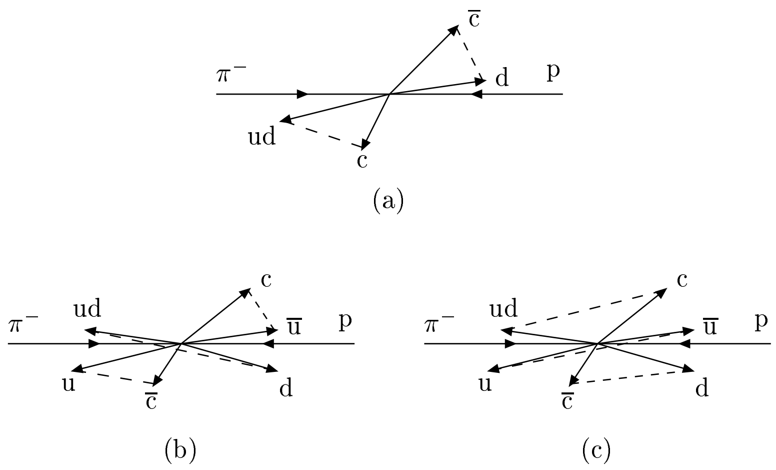

Figure 3.2: Strings (dashed) in a π^-p collision corresponding to the colour flows in Fig. 3.1a, b and c respectively; (a) $u\overline{u} \to c\overline{c}$ and (b,c) $gg \to c\overline{c}$. If e.g. the colour-singlet system c-$\overline{u}$ in (b) has a small invariant mass we will call it a cluster and hadronize it by the procedure described in the text.

the two cluster endpoints, with the new quark flavour selected according to the same rules as in normal string fragmentation. The decay kinematics is for the time being assumed to be isotropic in the rest frame of the cluster, which is the behaviour to be expected in the limit of vanishing phase space.

3. *Cluster collapse.* This is the extreme case of the above situation, where the string mass is so small that the cluster cannot decay into two hadrons. It is then assumed to collapse directly into a hadron resonance, inheriting the flavour content of the string endpoints. The original continuum of string/cluster masses is replaced by a discrete set of hadron masses, mainly D and D*. By local duality arguments [13] we assume that this does not change the total rate of charm production. This is related to the argument used in the $e^+e^- \to c\overline{c}$ channel, that the cross section in the J/ψ and ψ' peaks is approximately equal to a purely perturbatively calculated $c\overline{c}$ production cross section restricted to the below-D$\overline{\text{D}}$-threshold region. Similar relations have also been studied e.g. for τ decay to hadrons [14], and there shown to be valid to good accuracy. In the current case, the presence of other strings in the event additionally allows soft-gluon exchanges to modify parton momenta as required to obtain correct hadron masses. Traditional factorization of short- and long-distance physics would then also protect

the charm cross section. Local duality and factorization do not specify how to conserve the overall energy and momentum of an event, when a continuum of $\bar{c}d$ masses is to be replaced by a discrete D^- one, however. This will therefore be one of the key points to be studied below.

Nature will not be so crude in its classification as we have been here, but hopefully our ansatz should be close enough to give a good first approximation.

Charm cross sections are often presented as functions of Feynman-x, $x_F = p_L/p_{L,max} \approx 2p_L/E_{CM}$, i.e. the longitudinal momentum fraction of the meson in the rest frame of the event [2, 3, 4]. The x_F distribution for the different production channels in the standard Lund model is shown in Fig. 3.3, both for D^- and D^+. We use PYTHIA 6.1 [15] with standard parameters to generate the plots.

In perturbative QCD the x_F spectra of produced charm/anticharm quarks are identical to leading order, and the effects of higher orders are very small in this respect [5, 6]. Therefore any asymmetry between charm and anticharm hadrons is a simple measure of nonperturbative effects. In π^-p experiments the charm asymmetry is traditionally defined as

$$A = A(x_F, p_\perp) = \frac{\sigma(D^-) - \sigma(D^+)}{\sigma(D^-) + \sigma(D^+)} , \tag{3.1}$$

which measures the relative abundance of D^- over D^+ as a function of x_F and $p_\perp$. We will here mainly consider the variation with x_F, integrated over $p_\perp$, since A does not vary much with $p_\perp$ over the experimental range of x_F values [3, 4]. The asymmetry in PYTHIA is compared to experiment in [2, 3, 4], and the model shows general agreement with experiment, except in the region $0 \le x_F \le 0.4$ where the model is predicting a larger asymmetry than found in the data. One collaboration [4] has tuned the parameters of PYTHIA to obtain a good description of data also in this region, see below.

In our model the main source of asymmetry for all $x_F > 0$ is the production of D^- ($\bar{c}d$) mesons via cluster collapse involving a valence d from the pion beam, Fig. 3.3a. This production channel is not open for D^+ ($c\bar{d}$) since the π^- does not contain a valence $\bar{d}$. A number of model aspects influence the rate and character of cluster collapses, and in the following we will review the main ones.

The *charm mass* enters in the perturbative matrix element as well as in the phase space, and so has a strong influence on the total charm cross section, but we have checked that the leading-order x_F distribution is not affected much. It also, together with the *light-quark masses*, sets the threshold of the charm-cluster mass spectrum. The c mass to use need not even be the same in the two applications, cf. the familiar distinction between current algebra and constituent masses. A large combined mass of the charm and light quarks in a cluster dramatically reduces the importance of the cluster collapse mechanism.

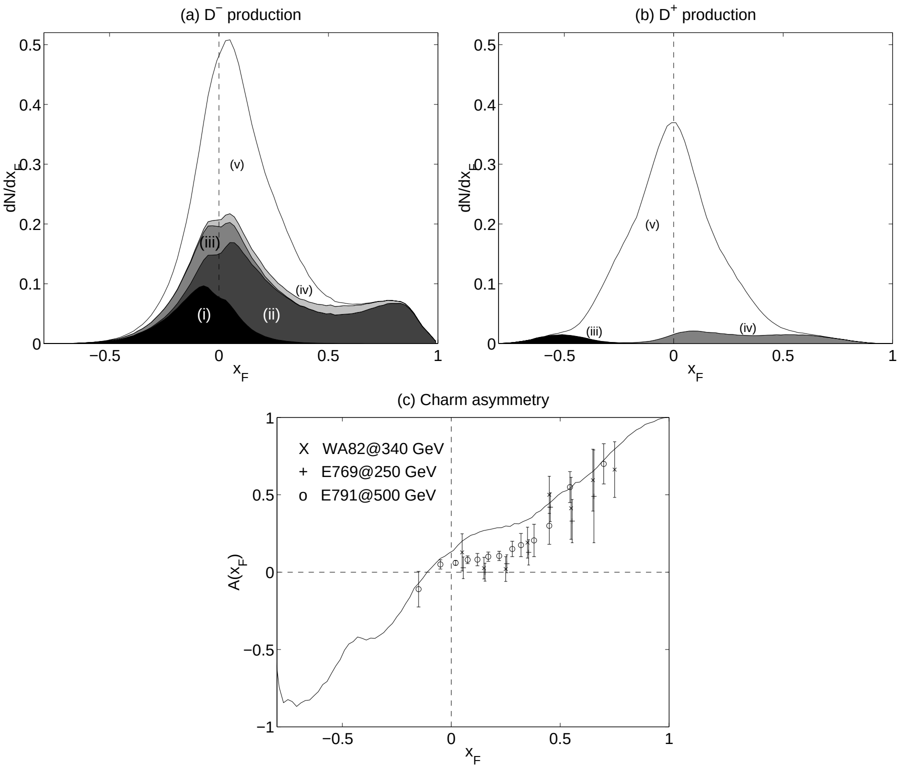

Figure 3.3: $\mathrm{D}^{\mp}$ meson production in a π^-p collision at a π^- beam momentum of 500 GeV, using the default Lund Model. x_{F} distribution (normalized per $\mathrm{c\bar{c}}$ event) of (a) D^- and (b) D^+ for different production channels: (i) Cluster collapse, light quark from p end, (ii) Cluster collapse, light quark from π^- end, (iii) Cluster decay, light quark from p end, (iv) Cluster decay, light quark from π^- end and (v) String fragmentation. (c) The resulting asymmetry, Eq (3.1). Also shown is data from [2, 3, 4].

In the valence $\mathrm{u\bar{u}}$ annihilation mechanism, the π^- beam remnant is a d quark, so no internal structure need be specified. In the gg fusion process, however, the remnant is a $\mathrm{\bar{u}d}$ system in a colour octet state, i.e. attached to two strings. A convenient approach is to imagine this system split into two separate $\mathrm{\bar{u}}$ and d string endpoints. The *beam remnant distribution function* (BRDF) is introduced to describe how the (light-cone) momentum of the remnant is shared between the two, in fractions χ and $1-\chi$, respectively. For an octet meson remnant the χ distribution is always implicitly symmetrized between the q and

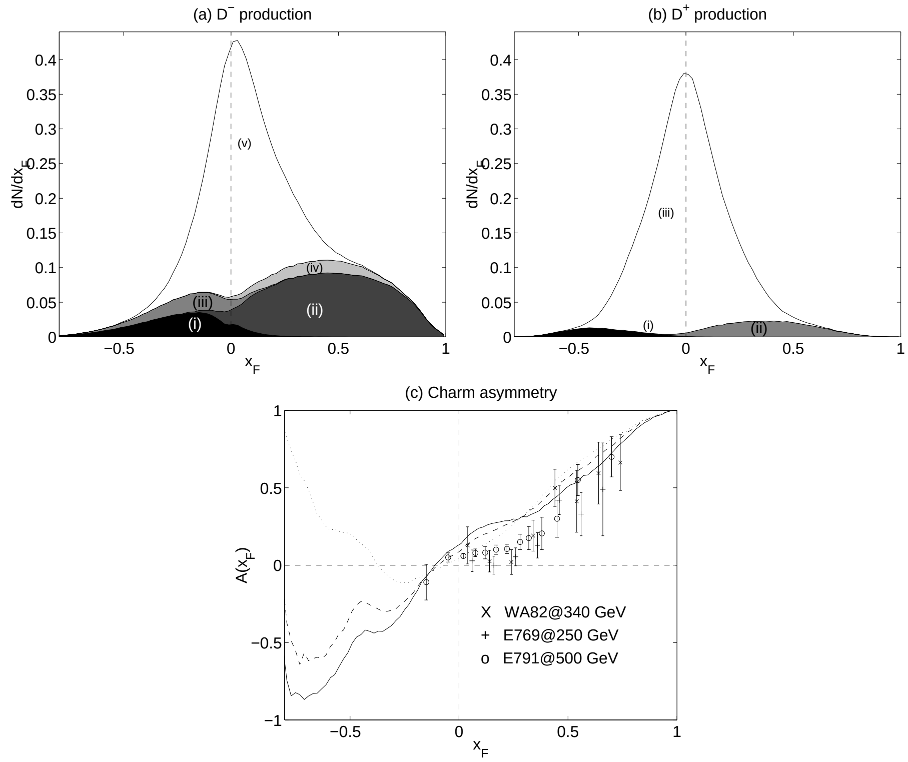

Figure 3.4: x_F distribution of (a) D^- and (b) D^+ for different production channels (cf. Fig. 3.3, which corresponds to the default of extreme uneven sharing) in a $\pi^-\mathrm{p}$ collision at a π^- beam momentum of 500 GeV using an even sharing of energy between the quarks in a beam remnant. (c) the resulting asymmetry using three different choices of BRDF's: $\propto (1-\chi)^k/\sqrt{\chi^2+c_{\mathrm{min}}^2}$, $\propto (1-\chi)^k/\sqrt[4]{\chi^2+c_{\mathrm{min}}^2}$ and $\propto (1-\chi)^l$ respectively, with $(k,l)=(1,0)$ for the pion and $(3,1)$ for the proton remnant, and $c_{\mathrm{min}} = 0.6$ GeV/$\mathrm{E_{cm}}$. They correspond to an uneven (full), intermediate (dashed) and even (dotted) sharing of energy. For the π^- the three cases correspond to $<\chi> = 0.14$, 0.23 and 0.5 respectively. Also shown is data from [2, 3, 4].

$\overline{\mathrm{q}}$, while for an octet baryon remnant one quark (picked at random among the three) takes the fraction χ and the remaining colour antitriplet diquark $1-\chi$. To study the dependence of the asymmetry on the BRDF, we will consider two extreme cases and one intermediate. In one extreme one quark tends to take a small fraction of the available energy, much like the parton distributions in a hadron. In the other extreme, naive counting rules are used and the energy is, on the average, shared evenly between the quarks in the remnant. In Fig. 3.4 the individual spectra as well as the asymmetry is shown for the full x_{F} range.

It is interesting to note the difference between the regions $x_{\mathrm{F}} < 0$ and $x_{\mathrm{F}} > 0$. For $x_{\mathrm{F}} > 0$ the D^- is a leading particle and the asymmetry is attributed to cluster collapses involving a d-quark from the pion beam. In the proton fragmentation region ($x_{\mathrm{F}} < 0$) the D^- is still leading and D^+ non-leading, so naively you would expect the asymmetry to be positive. However, when using an uneven sharing of energy in the proton beam remnant, diquark effects become prominent. As is seen in Fig. 3.2 the c is always connected to diquarks and the $\overline{\mathrm{c}}$ is connected to quarks. Therefore D^+ mesons produced from a cluster (containing a diquark) via cluster decay will, on the average, be harder than D^- from cluster collapses, cf. Fig. 3.3. We see that there are two competing effects for $x_{\mathrm{F}} < 0$, one that favours D^+ (diquark effect), and one that favours D^- (cluster collapse). The strength of the diquark effect depends strongly on the assumed energy sharing in the proton beam remnant. This is seen clearly in Fig. 3.4c where an even sharing makes the asymmetry change sign for $x_{\mathrm{F}} < 0$. If this region could be examined experimentally (p beam on p target) it would give us a hint at which distribution should be used. Possibly one could use data from other (related) experiments to assess a reasonable choice of BRDF.

The partons entering the hard interaction are traditionally taken to have a nonvanishing *primordial* $k_\perp$, seen as a purely nonperturbative Fermi motion of partons inside the incoming hadrons, in addition to whatever is provided by perturbative gluon emission. Typical values should thus be 300–400 MeV. In many connections, also for charm in the current energy range [6], it has been noted that much higher values are required, at or above 1 GeV. This remains somewhat of a mystery, which we do not attempt to solve here. The choice of primordial $k_\perp$ distribution is of non-negligible importance, both by providing a $p_\perp$ kick to the produced charm quarks and, by momentum conservation, an opposite kick to the beam remnants.

The cluster mass spectrum is affected both by the choice of charm mass, of BRDF's and of primordial $k_\perp$ distributions. As a typical example, the $\overline{\mathrm{c}}$–d singlet produced in Fig. 3.2a can have the mass distribution of Fig. 3.5a when calculated on the parton-level with $\mathrm{m}_c = 1.35$ GeV and $\mathrm{m}_d \approx \mathrm{m}_u \approx 0$, or as in Fig. 3.5b if some parameters are varied. But we know that the observed mass spectrum of produced particles consists of peaks at the D^- and D^{*-} masses and then a continuum above the $\mathrm{D}^-\pi^0$ threshold, cf. Fig. 3.5a.

The onset of the continuum depends on the assumed *threshold behaviour*. In one extreme, a $\mathrm{D}\pi$ pair is always formed when the cluster mass allows it. In another, this continuum state is only reached after a succession of thresholds: $\mathrm{D}\pi$, $\mathrm{D}^*\pi$, $\mathrm{D}\rho$, $\mathrm{D}^*\rho$, etc. Thus a fraction of events may collapse to a single

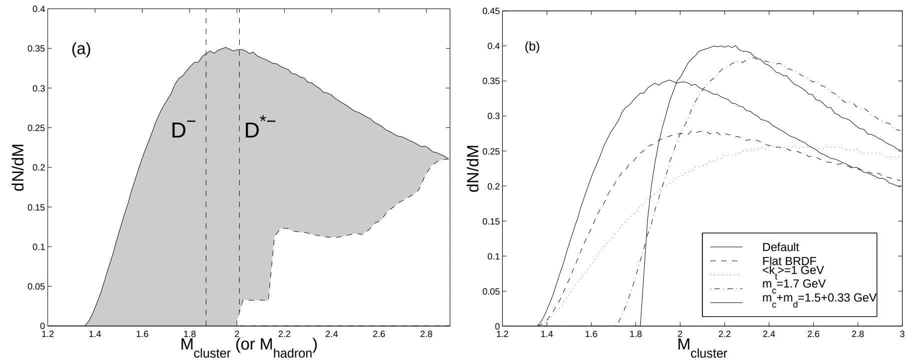

Figure 3.5: (a) Distribution of cluster (full) and meson (dashed) masses in the string model. Clusters within the gray area collapse to D^- or D^{*-}. (b) Dependence of the parton-level mass distribution on some parameters of the model.

resonance also above threshold, cf. the gray area in Fig. 3.5a. In the default implementation, exactly one attempt is made to form two hadrons by a random choice of allowed flavours and spins (using the string fragmentation relative probabilities), and is allowed to succeed if the sum of hadron masses is below the cluster mass. By increasing the number of attempts made before giving up, the behaviour interpolates to the first extreme above. Thus we see that the mass spectrum of collapsing clusters is affected in the low end by quark masses and in the high end by the transition to two-body states, altogether giving a large range of possible cluster collapse rates.

When a collapse occurs, *confinement effects* have to project the continuum of string masses onto the observed hadron mass spectrum. Because of the aforementioned local duality and factorization arguments, the total area of the spectrum should be conserved in the process. How the projection should be done is not known from first principles, however.

One conceivable strategy could be to introduce a weight function consisting of δ function peaks at the D^- and D^{*-} masses, with suitably adjusted normalizations, and then a step function at the $\mathrm{D}^-\pi^0$ threshold. This weight function, when multiplied with the partonic mass spectrum, should then give the hadron-level mass spectrum. Such an approach is not well suited for Monte Carlo simulation, since the string mass is a complicated function of a number of variables and therefore the δ function cannot easily be integrated out. However, on general grounds, we do not expect the overall distribution of event characteristics to differ significantly between events with a $\overline{\mathrm{c}}$–d string mass exactly equal to the D^- one, and events where the string mass is maybe 100 MeV off.

An appealing shortcut therefore is to accept all partonic configurations and thereafter introduce some 'minimal' adjustments to the kinematics to allow hadrons to be produced on the mass shell. Such a strategy would be consistent not only with local duality arguments, but also with the presence of soft final-state interactions, i.e. the exchange of nonperturbative gluons that can carry some amount of momentum between the low-mass string and the surrounding hadronic system. In the following we will therefore adopt the language of 'gluons' transferring energy and momentum between the strings in a collision, while leaving unanswered the question on the exact nature of those 'gluons'. Specifically, we will not address the possibility of changes in the colour structure of events by such 'gluons'.

In this letter we will consider two different choices of energy shuffling schemes that can be said to be of opposite nature. We will further show that, as far as the asymmetry is concerned, the observable differences are small.

The first approach is the standard one in PYTHIA. It consists of shuffling momentum to the parton i in the event that has the largest invariant mass when combined with the cluster cl that is supposed to collapse to a D (say). The new i and D momenta are given by

$$\begin{aligned} p_{\mathrm{D}} &= (1-\delta)p_{\mathrm{cl}} + \epsilon p_i \ , \\ p'_i &= (1-\epsilon)p_i + \delta p_{\mathrm{cl}} \ , \end{aligned} \tag{3.2}$$

where ϵ and δ are determined by the conditions $p_{\mathrm{D}}^2 = m_{\mathrm{D}}^2$ and $p_i'^2 = p_i^2 = m_i^2$. Using the parton furthest away from the cluster has the advantage of minimizing the required momentum transfer, but does not offer a particularly appealing picture physically. In the following we therefore try to formulate a scheme where energy and momentum is shuffled to partons or strings in the vicinity of the cluster.

This problem can be approached in several ways, and we want to mention a few. The basic idea is to emit a soft gluon from the cluster, taking away the energy and momentum needed to put the remainder on the hadronic mass shell. One way to do this is simply to rescale the four-momentum of the cluster in order to give it the correct invariant mass. The gluon can then have both positive and negative masses and energies, which may be conceptually unappealing but not forbidden in principle. Worse is that such a rescaling can give $x_{\mathrm{F}} > 1$, i.e. kinematical inconsistencies. Another approach is to let the cluster decay isotropically into a hadron and a massless gluon. The gluon can still have both positive and negative energies, but this is not a problem in itself since the gluon is connected to the nearest string piece, which is then hadronized according to the standard string-with-gluons scheme [16]. A gluon with positive energy will increase the energy and mass of the string while a gluon with negative energy will decrease it. It is the string which is the physical entity, and it of course has to have a positive energy and mass. The only observable effect of the extra gluon is a slight increase (decrease) in the average multiplicity in the phase space neighbourhood of the inserted positive (negative) energy gluon, but this effect is too small to be seen in an actual experiment. Even so, there are problems with the simple approach. For instance, if a negative-energy gluon is connected to a string that already has a small mass, it can give the string a negative mass and this is not permitted. So, if there are no sufficiently massive strings left in the event, the gluon cannot be connected anywhere, and this method cannot be used. Only if the radiated gluon has positive energy can the mechanism always be used without problems.

In practice, therefore, the negative-gluon approach is too error-prone. When the cluster mass is smaller than the intended hadron mass another approach is instead used to simulate the same effect, i.e. to take up energy from the vicinity of the cluster: a nearby string is allowed to emit a gluon which, when absorbed by the cluster, gives it the right mass. In more detail, imagine a string with endpoints q and $\overline{\mathrm{q}}$. Form a weighted sum of the endpoint momenta

$$p_s = \alpha p_{\mathrm{q}} + \beta p_{\overline{\mathrm{q}}} = \frac{p_{\overline{\mathrm{q}}} p_{\mathrm{cl}}}{p_{\mathrm{q}} p_{\overline{\mathrm{q}}}} p_{\mathrm{q}} + \frac{p_{\mathrm{q}} p_{\mathrm{cl}}}{p_{\mathrm{q}} p_{\overline{\mathrm{q}}}} p_{\overline{\mathrm{q}}} \ , \tag{3.3}$$

so that the end of the string that is closest to the cluster is weighted up relative to the one further away. Thereafter define

$$p_{\mathrm{D}} = p_{\mathrm{cl}} + \delta p_s \ , \tag{3.4}$$

with δ determined by the constraint $p_{\mathrm{D}}^2 = m_{\mathrm{D}}^2$. The meson will then have the correct mass and the string endpoint momenta are scaled down by factors $1 - \delta\alpha$ and $1 - \delta\beta$, respectively. Special cases need to be introduced to avoid e.g. $1 - \delta\alpha < 0$, but these affect only a small fraction of the events, and can be left aside here.

In summary, the new algorithm transfers a 'gluon' from the cluster to the nearest string if the original cluster mass is above the D meson mass, and transfers a 'gluon' the other way if the mass instead is below. Some results are shown in Fig. 3.6. As can be seen, the largest difference is in the distribution of the collapsed mesons at high x_{F}, where the spectrum is somewhat softer in the new scheme than in the old one. Another difference is around $x_{\mathrm{F}} = 0$, where the old algorithm tends to push the meson away from the middle, creating an unphysical dip in the distribution. This effect is seen more clearly in the distributions for a larger charm mass. The distribution with $m_{\mathrm{c}} = 1.7$ GeV is also included to show the relative importance of the collapse mechanism on the asymmetry. Clearly the charm mass — by regulating the amount of collapses — provides a much larger uncertainty (except possibly at very large x_{F}) than the choice of collapse scheme but, if nothing else, the new algorithm remedies some cosmetic problems of the old one. The new algorithm also changes some other characteristics of the event, e.g. the mean multiplicity is changed by ≈ 2

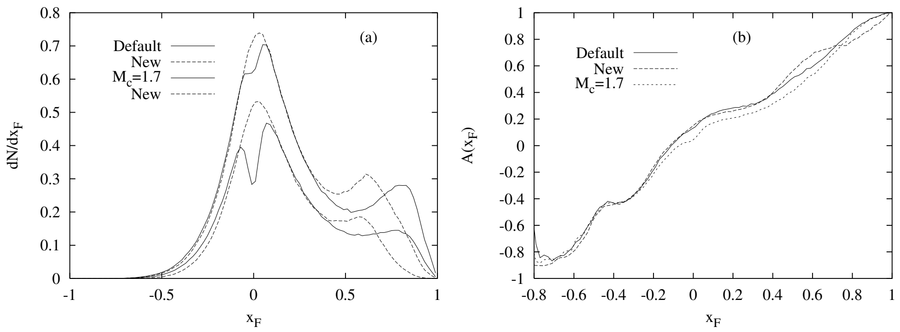

Figure 3.6: Some results for different cluster collapse algorithms: (a) The momentum spectrum for D^- mesons produced from clusters (normalized to the total D^-). The two top curves are with default parameters and the lower ones are with an increased charm mass (from 1.35 to 1.7 GeV). (b) the resulting asymmetry.

%, but this too is a small effect compared to the other uncertainties that we have mentioned.

The E791 collaboration has produced a tuned version of PYTHIA [4]. The specific parameters involved have already been discussed above, so we here only provide a brief summary:

- The charm quark mass is increased from 1.35 to 1.7 GeV. The fraction of cluster collapses is thereby reduced by about 35 %, which reduces the asymmetry considerably for $x_{\mathrm{F}} > 0$, as demonstrated in Fig. 3.6. This large charm mass may appear unrealistic but it is also possible to reduce the number of cluster collapses by increasing the light-quark masses and/or increasing the probability for a cluster with a mass above the $\mathrm{D}\pi$ threshold to decay into two particles. By using constituent masses both for the light quarks and the charm quark (e.g. $m_{\mathrm{c}} = 1.5$ GeV and $m_{\mathrm{d}} = m_u = 0.33$ GeV) and by allowing two attempts to form two hadrons from a cluster, the number of collapses is reduced by a comparable amount. A charm mass of 1.5 GeV is also suggested from calculations of total cross sections for charm production in next-to-leading order QCD [6], and given the theoretical uncertainty regarding quark masses this value is not unreasonable.
- A somewhat less peaked BRDF, like our intermediate scenario. The asymmetry is reduced somewhat in the region $0 < x_{\mathrm{F}} < 0.4$, Fig. 3.4. A photoproduction experiment [17] also seems to indicate flat BRDF's, but these are not determined by any basic principles, and are poorly known, so further studies will be needed here.
- The width of the Gaussian primordial $k_\perp$ distribution is increased from 0.44

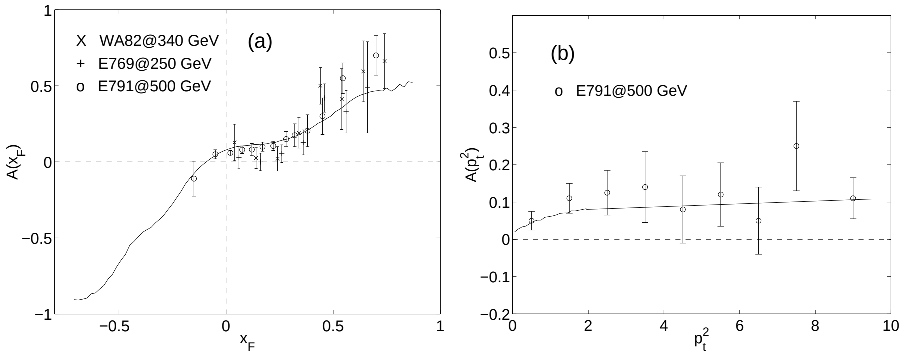

Figure 3.7: The $\mathrm{D}^{\pm}$ asymmetry as a function of (a) x_{F} and (b) $p_{\perp}^2$ for the modified version of PYTHIA described in the text: new cluster collapse mechanism, constituent masses for the quarks ($m_c = 1.5$ GeV, $m_d = m_u = 0.33$ GeV), intermediate BRDF's, primordial $k_{\perp} = 1.0$ and using two attempts to form two particles from a cluster. (a) is for all $p_{\perp}$ and (b) is for $-0.2 \leq x_{\mathrm{F}} \leq 0.8$. Experimental data is from [2, 3, 4].

to 1.0 GeV. As we have noted above, such a number is unexpectedly large, but in agreement with other data, and therefore rather standard these days. This allows cluster collapses between a charm quark and a beam remnant to occur also at fairly large $p_{\perp}$ values, thus leading to an essentially $p_{\perp}$-independent asymmetry. Additionally, the $p_{\perp}$ kick added to charm quarks and beam remnants tend to increase the average invariant mass of the produced clusters, thereby reducing the number of cluster collapses.

Taken together, these parameter changes gives a good fit to data, both for the asymmetry and for the shape of the individual charm meson spectra. Fig. 3.7 shows the asymmetry using default PYTHIA with the following modifications: new cluster collapse mechanism, constituent quark masses, intermediate BRDF's, an increased intrinsic $k_{\perp}$ and with two attempts to form two hadrons from a cluster. The amount of cluster collapse is here reduced by about a factor of three compared with the default, to $\sim 16\%$.

In summary, we have in this letter described the string fragmentation approach to charm production in hadronic collisions. A number of uncertainties have been identified and studied in detail, in particular the transition from a continuous string-mass distribution to a discrete hadron-mass one. The conclusion is that the model can describe much of the existing data, but also that these data do not fully constrain the choice of model parameters. Further data on charm production in π^{-}p collisions may provide further information, as may charm production e.g. in ep collisions. Applications include, among other aspects, bottom production in hadron colliders where the asymmetry between B and $\overline{B}$ mesons has to be understood in order to facilitate a study of CP violation effects [18]. We intend to return to these and other related topics.

References

[1] M. Basile et al., Nuovo Cim. **A66** (1981) 129;
ACCMOR Collaboration, R. Bailey et al., Phys. Lett. **132B** (1983) 237;
NA27 Collaboration, M. Aguilar-Benitez et al., Phys. Lett. **B161** (1985) 400;
NA32 Collaboration, S. Barlag et al., Z. Phys. **C49** (1991) 555.

[2] WA82 Collaboration, M. Adamovich et al., Phys. Lett. **B305** (1993) 402.

[3] E769 Collaboration, G.A. Alves et al., Phys. Rev. Lett. **72** (1994) 812.

[4] E791 Collaboration, E.M. Aitala et al., Phys. Lett. **B371** (1996) 157.

[5] P. Nason, S.Dawson and R.K. Ellis, Nucl. Phys. **D327** (1989) 49;
W. Beenakker, R. Meng, G.A. Schuler, J. Smith and W.L. Van Neerven, Nucl. Phys. **B351** (1991) 507.

[6] S. Frixione, M.L. Mangano, P. Nason and G. Ridolfi, Nucl. Phys. **B431** (1994) 453.

[7] Particle Data Group, C. Caso et al., Eur. Phys. J. **C3** (1998) 1.

[8] V. Barger, F. Halzen and W.Y. Keung, Phys. Rev. **D25** (1982) 112;
P. Mazzanti and S. Wada, Phys. Rev. **D26** (1982) 602;
G.I. Lykasov and M.N Sergeenko, Z. Phys. **C56** (1992) 697;
R.C. Hwa, Phys. Rev. **D51** (1995) 85;
V.A. Bednyakov, Mod. Phys. Lett. **68** (1995) 61;
A.K. Likhoded and S.R. Slabospitsky, hep-ph/9710476;
E. Cuautle, G. Herrera and J. Magnin, Eur. Phys. J. **C2** (1998) 473;
O. Piskounova, Nucl. Phys. **B50** (Proc. Suppl.) (1996) 179;
J. Dias de Deus and F.O. Durães, hep-ph/9803449.

[9] B. Andersson, H.-U. Bengtsson and G. Gustafson, Lund preprint LU TP 83–4 (1983).

[10] S.J. Brodsky, P. Hoyer, C. Peterson and N. Sakai, Phys. Lett. **93B** (1980) 451;
R. Vogt and S.J. Brodsky, Nucl. Phys. **B478** (1996) 311;
G. Ingelman and M. Thunman, Z. Phys. **C73** (1997) 505.

[11] B. Andersson, G. Gustafson, G. Ingelman and T. Sjöstrand, Phys. Rep. **97** (1983) 31.

[12] H.-U. Bengtsson, Comput. Phys. Commun. **31** (1984) 323.

[13] E.D. Bloom and F.J. Gilman, Phys. Rev. **D4** (1971) 2901;
J.J. Sakurai, Phys. Lett. **46B** (1973) 207;
H. Fritzsch, Phys. Lett. **67B** (1977) 217;
R.A. Bertlmann, G. Launer and E. de Rafael, Nucl.Phys. **B250** (1985) 61; and references therein.

[14] E. Braaten, S. Narison and A. Pich, Nucl. Phys. **B373** (1992) 581.

[15] T. Sjöstrand, Comput. Phys. Commun. **82** (1994) 74.

[16] T. Sjöstrand, Nucl. Phys. **B248** (1984) 469.

[17] E687 Collaboration, P.L. Frabetti et al., Phys. Lett. **B370** (1996) 222.

[18] M. Chaichian and A. Fridman, Phys. Lett. **B298** (1993) 218.

Production and Hadronization of Heavy Quarks

Paper IV

Production and Hadronization of Heavy Quarks

Emanuel Norrbin and Torbjörn Sjöstrand
Department of Theoretical Physics
Lund University

LU TP 00–16 (hep-ph/0005110),
Accepted for publication in *European Physical Journal* **C**

Heavy long-lived quarks, i.e. charm and bottom, are frequently studied both as tests of QCD and as probes for other physics aspects within and beyond the standard model. The long life-time implies that charm and bottom hadrons are formed and observed. This hadronization process cannot be studied in isolation, but depends on the production environment. Within the framework of the string model, a major effect is the drag from the other end of the string that the c/b quark belongs to. In extreme cases, a small-mass string can collapse to a single hadron, thereby giving a non-universal flavour composition to the produced hadrons. We here develop and present a detailed model for the charm/bottom hadronization process, involving the various aspects of string fragmentation and collapse, and put it in the context of several heavy-flavour production sources. Applications are presented from fixed-target to LHC energies.

4.1 Introduction

The light u, d and s quarks can be obtained from a number of sources: valence flavours in hadronic beam particles, perturbative subprocesses and nonperturbative hadronization. Therefore the information carried by identified light hadrons is highly ambiguous. The charm and bottom quarks have masses significantly above the Λ_{QCD} scale, and therefore their production should be perturbatively calculable. That is, they are not expected to be produced at any significant rate in nonperturbative processes [1], and they do not occur as valence flavours of the commonly used beam particles. A priori, they are therefore excellent probes of the underlying hard dynamics, whether that involves standard QCD processes or various kinds of new physics. They can also be identified in the data by techniques such as secondary vertices, prompt leptons or kinematical constraints (e.g. the small $m_{\mathrm{D}^*} - m_{\mathrm{D}} - m_{\pi}$).

In order to understand the character of the perturbative process that occurred, it is often necessary to know not only that a c/b quark was produced, but also its original energy and direction of motion. The assumption is then often made that the observed charm/bottom hadron accurately reflects the original quark. For instance, the quark momentum distribution may be scaled down by a convolution with the Peterson fragmentation function [2], while the direction is assumed unchanged. In other cases, like for the study of CP violation in the B^0–$\overline{\mathrm{B}}^0$ system, the produced hadrons are at the focus of attention, and a simple ansatz is that the composition of B hadrons is independent of the production environment and symmetric between particles and antiparticles.

The assumption, that heavy quarks remain rather unaffected by the environment in which they are produced, has some support in the Heavy Quark Effective Theory (HQET) [3], although that framework is more concerned with questions of decay than of production. However, even if many of the effects we will consider here indeed die out roughly inversely to the mass of the heavy quark — the Λ/m_{Q} behaviour of HQET — evidence is that the numerator Λ of such a scaling relation often is large. Thus the large lifetime differences between the D mesons has an analogue in large production asymmetries between D mesons in hadronic collisions [4, 5, 6, 7, 8]. Even with a reduction by a factor 2–3 when moving from charm to bottom, large effects are therefore expected also in the latter case. Only top hadrons would have been reasonably immune, had the top quark been long-lived enough for top hadrons to form.

In order to study and understand the sizeable deviations from the simple picture, of perturbation theory results only minimally modified, it is necessary to have a realistic framework for nonperturbative effects. The Lund string fragmentation model [1] will be the starting point here. In this picture, the colour confinement field between a quark and an antiquark (or a diquark) is squeezed into a tube-like region, corresponding to a linear confinement potential. This couples the hadronization of a c/b quark to the flavour content and momentum of the other string end, i.e. provides an explicit dependence on the production environment. An extreme case is the string collapse, where the mass of a string only allows the production of one single hadron, which by necessity therefore combines the c/b quark with the flavour at the other string end, often one of the valence flavours of the incoming beams. Also less extreme situations can give noticeable effects, and only in the limit of large string masses can one expect to recover a simple description. However, this description can still be counterintuitive, in that the hadronization process can 'speed up' as well as 'slow down' the heavy hadron relative to the heavy quark. In terms of the easily observable consequences, like hadron flavour asymmetries, we therefore go from huge effects at fixed-target experiments to tiny ones at the LHC, but in less obvious ways the effects remain large also at high energies. Furthermore, events at large energies tend to be composed of several strings, so even at the LHC a fraction of small-mass strings is produced.

The presence of such effects is implicit in the Lund model, and was studied qualitatively early on [9]. It is only the more recent higher-precision data sets [5, 6, 7, 8] that allow quantitative comparisons to be carried out, and thereby give the possibility to 'fine-tune' the model with respect to nonperturbative parameters. A study of this kind was presented in a recent letter [10], where we concentrated on the production of charm at fixed-target energies. In this longer description, we will expand the study in several directions: by considering more heavy-flavour production mechanisms, by including bottom as well as charm production, by covering a larger range of energies and by addressing a larger set of observables. In the process, further improvements have also been made in the model.

This paper is organized as follows. Section 4.2 contains the model description, from the perturbative production mechanisms to the various domains of the hadronization process. Sections 4.3 and 4.4 present some results. In Section 4.3 the emphasis is on distributions that help explain how the basic aspects of the model work, with little regard whether distributions are observable or not. In Section 4.4 the emphasis is shifted to observable results for charm or bottom production at some current or planned detectors, although explanations will sometimes rely on non-observable distributions. Finally, Section 4.5 contains a summary and outlook.

4.2 Model Description

Based on the concept of factorization, we here subdivide the process in two distinct phases, the perturbative one, where the heavy quarks are produced, and the nonperturbative one, where these quarks hadronize. Heavy-flavour cross sections thus are completely determined by the former phase, while observable

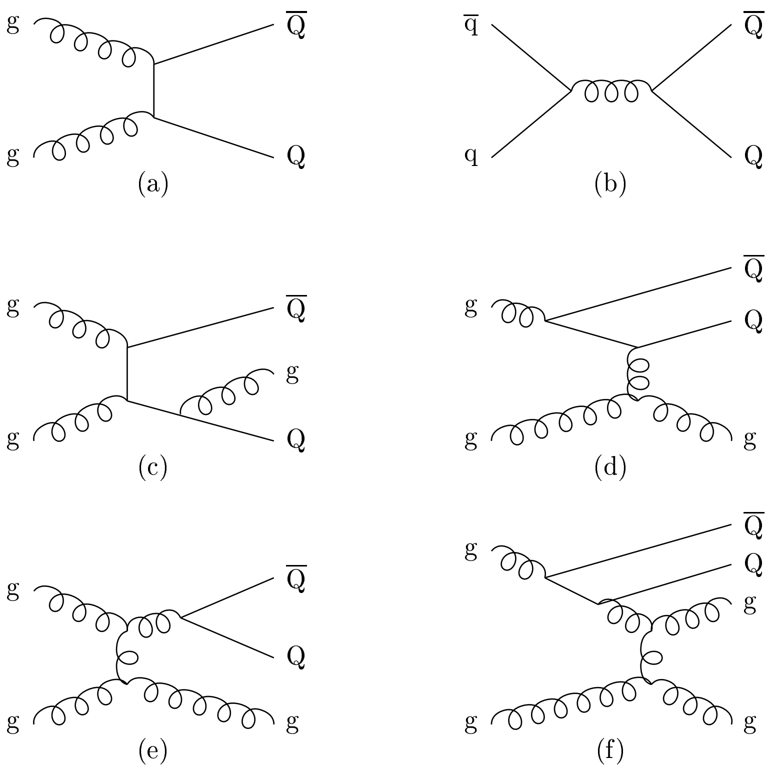

Figure 4.1: Examples of heavy-flavour production diagrams. (a,b) Leading order. (c) Pair creation (with gluon emission). (d) Flavour excitation. (e) Gluon splitting. (f) Events classified as gluon splitting but of flavour-excitation character.

event properties reflect a combination of the two.

4.2.1 Perturbative Aspects

Production Mechanisms

Several different production mechanisms can be envisaged for heavy flavours. Here we will concentrate on QCD processes in hadron–hadron collisions. The $\mathcal{O}(\alpha_s^2)$ leading-order (LO) graphs, $q\overline{q} \to Q\overline{Q}$ and $gg \to Q\overline{Q}$ [11], Fig. 4.1a-b, then form the starting point for the continued discussion.

One way to proceed is to add next-to-leading order (NLO) perturbative processes, i.e the $\mathcal{O}(\alpha_s^3)$ corrections to the above [12]. New graphs are $q\overline{q} \to$

$Q\overline{Q}g$, $qg \to Q\overline{Q}q$ and $gg \to Q\overline{Q}g$. Additionally the leading-order processes are modified by virtual corrections. Depending on the choice of cut-off parameters, the latter may give negative differential cross sections in some regions of phase space. The divergences disappear in sufficiently inclusive distributions, so much phenomenological insight can be gained [13]. However, with our currently available set of calculational tools, the NLO approach is not so well suited for the exclusive Monte Carlo studies we have in mind here, where hadronization is to be added on to the partonic picture. Furthermore, also the NLO results, although exact to $\mathcal{O}(\alpha_s^3)$, would be modified in yet higher orders, e.g. by the resummed effects of multiple gluon emission [14].

As an alternative, the parton-shower (PS) approach offers a different set of approximations. It is not exact even to $\mathcal{O}(\alpha_s^3)$, but it catches the leading-log aspects of the multiple-parton-emission phenomenon. Especially when one goes to higher energy this can offer many advantages. The PS approach is based on a probabilistic picture, wherein the overall $2 \to n$ partonic process is subdivided into three stages: initial-state cascades, hard scattering and final-state cascades. The hard scattering is here defined as the $2 \to 2$ sub-diagram that contains the largest virtuality, i.e. corresponds to the shortest-distance process. It is important to respect this in order to avoid double-counting, as will become apparent in the following. Heavy-flavour events can then be subdivided into three classes, which we will call pair creation, flavour excitation and gluon splitting. The names may be somewhat misleading, since all three classes create pairs at $g \to Q\overline{Q}$ vertices, but it is in line with the colloquial nomenclature.

The three classes are characterized as follows.

1. Pair creation is when the hard subprocess is one of the two LO processes above. Showers do not modify production cross sections, but shift kinematics, Fig. 4.1c. For instance, in the LO description, the Q and $\overline{Q}$ have to emerge back-to-back in azimuth in order to conserve momentum, while the parton shower allows a net recoil to be taken by one or several further partons.
2. Flavour excitation is when a heavy flavour from the parton distribution of one beam particle is put on mass shell by scattering against a parton of the other beam, i.e. $Qq \to Qq$ or $Qg \to Qg$, Fig. 4.1d. When the Q is not a valence flavour, it must come from a branching $g \to Q\overline{Q}$ of the parton-distribution evolution. In most current-day parton-distribution parameterizations, heavy-flavour distributions are assumed to vanish for virtuality scales $Q^2 < m_Q^2$. The hard scattering must therefore have a virtuality above m_Q^2. When the initial-state shower is reconstructed backwards [15], the $g \to Q\overline{Q}$ branching will be encountered, provided that Q_0, the lower cutoff of the shower, obeys $Q_0^2 < m_Q^2$. Effectively the processes therefore become at least $gq \to Q\overline{Q}q$ or $gg \to Q\overline{Q}g$, with the possibility of further emissions. In princi-

ple, such final states could also be obtained in the above pair-creation case, but the earlier advertised requirement on the hard scattering to be more virtual than the showers avoids double-counting.

3. Gluon splitting is when a $\mathrm{g} \to \mathrm{Q}\overline{\mathrm{Q}}$ branching occurs in the initial- or final-state shower, and no heavy flavours enter the hard scattering, Fig. 4.1e. Here the dominant source is gluons in the final-state showers, since timelike gluons emitted in the initial state are restricted to a smaller maximum virtuality. Except at high energy, most gluon splittings in the initial state instead result in flavour excitation, already covered above. An ambiguity of terminology exists with initial-state evolution chains where a gluon first branches to $\mathrm{Q}\overline{\mathrm{Q}}$ and the Q later emits another gluon that is the one to enter the hard scattering, Fig. 4.1f. From an ideological point of view, this is flavour excitation, since it is related to the evolution of the heavy-flavour parton distribution. From a practical point of view, however, we will choose to classify it as gluon splitting, since the hard scattering does not contain any heavy flavours.

In summary, the three classes above are then characterized by having 2, 1 or 0, respectively, heavy flavours in the final state of the hard subprocess. Of course, all this assumes that only one heavy-flavour pair is produced in an event — one could have e.g. double flavour excitation $\mathrm{QQ}' \to \mathrm{QQ}'$ — which normally is a good first approximation. Only in high-$p_\perp$ processes at high energies do profuse shower evolution make the multiple gluon-splitting process relevant.

To the above heavy-flavour sources, one could add the creation in decays of heavier resonances, such as $\mathrm{Z}^0 \to \mathrm{b}\overline{\mathrm{b}}$, $\mathrm{W}^+ \to \mathrm{c}\overline{\mathrm{s}}$, $\mathrm{H}^0 \to \mathrm{b}\overline{\mathrm{b}}$, $\mathrm{t} \to \mathrm{bW}^+$ and, of course, $\mathrm{b} \to \mathrm{c}$. In the current paper we will have little to say about these. However, c and b production at LEP1 clearly provides the basis that we can build on here, by testing both the showering and the hadronization of heavy flavours, although in a different environment. For primary-produced heavy flavours, everything appears to be well understood in the framework of our models. Some discrepancies have been noted in the rate of hard gluon emission off b's [16], i.e. in the region where the shower is not expected to be perfect anyway, and even so discrepancies are tiny compared with typical uncertainties in hadronic collisions. Rather more worrisome is the observed rate of secondary heavy-flavour production, i.e. what we have called gluon splitting above. There the LEP observations exceed the rate predicted by shower programs [17, 18], and also by analytical calculations [19], by maybe as much as 50% [20, 19]. The error bars are large, however, so the true excess could be lower. The possibility of higher rates already exists in some models [21], and one could imagine modifications to others. Currently the data is too poor to tell much about whether the shape agrees or not with models. We will therefore assume that only the rate could be a problem, and then any effect in hadronic collisions could be absorbed under the general heading of K factors, i.e. a rescaling in rate by higher-order corrections.

Parton-Shower Particulars

The perturbative shower approach is implemented in the Pythia program [17] that we will use for the studies in this paper.

Pair creation is easy to generate by itself, by allowing only the two hard processes $q\overline{q} \to Q\overline{Q}$ and $gg \to Q\overline{Q}$, using the LO matrix elements with quark masses included. The full phase space can be populated, i.e. down to $\hat{p}_\perp = 0$, since the quark mass provides the soft cutoff. The Q^2 scale of the process, used to set the range of allowed shower evolution as described below, is here taken to be $Q^2 = m_Q^2 + \hat{p}_\perp^2$.

Flavour excitation can be obtained by only sampling the heavy flavour $Q/\overline{Q}$ from one of the incoming hadrons (a standard option of the program) while allowing all flavours from the other hadron. The two sides of the event are covered by two separate runs, added for the final results. We have not implemented any special matrix elements for the scattering of one heavy quark against another massless parton; instead massless matrix elements are used. Since the heavy-flavour parton distributions vanish for scales $Q^2 < m_Q^2$, where we associate $Q^2 = \hat{p}_\perp^2 = \hat{t}\hat{u}/\hat{s}$ for massless kinematics, it follows that $\hat{s} > 4m_Q^2$. The mass corrections to the matrix elements are therefore not expected to be very large. (In practice, massive four-vectors are constructed from the massless ones by a scaling-down of the three-momenta, in the rest frame of the subprocess, while preserving the energy: $p_i^2 = 0$, $p_i'^2 = m_i^2$, $\mathbf{p}_i' = \alpha \mathbf{p}_i$, $E_1' + E_2' = E_1 + E_2$. The actual $\hat{p}_\perp$ may thus end up somewhat below the nominal cut at m_Q.) The normal backwards shower evolution from the hard subprocess is then supposed to find a preceding $g \to Q\overline{Q}$ branching.

In the earlier Pythia versions, this often failed, and a heavy quark was allowed to form part of the beam-remnant flavour content that entered the nonperturbative description. We have now studied this phenomenon and recognized it as coming from the constrained kinematics that exists inside the shower. To see this point, consider a branching $g \to Q\overline{Q}$ where Q takes a fraction z of the lightcone momentum $p_+ = E + p_z$ of the gluon, and is virtual with $p_Q^2 = -Q^2$. The recoiling $\overline{Q}$ is part of the final state and must thus have mass m_Q, or above that if it radiates final-state gluons. Then conservation of $p_- = m_\perp^2/p_+$ gives

$$\frac{-Q^2 + p_\perp^2}{z} + \frac{m_Q^2 + p_\perp^2}{1-z} = 0 \ , \tag{4.1}$$

and the requirement of a physical transverse momentum in the branching, $p_\perp^2 \geq 0$, translates into

$$z \leq \frac{Q^2}{m_Q^2 + Q^2} \ . \tag{4.2}$$

It may then become kinematically impossible to find a gluon with $x_g = x_Q/z < 1$. Since many common parton distribution parameterizations do not respect the above kinematics constraints, we have introduced a further explicit check, where kinematically impossible configurations are rejected, and the cross section is reduced accordingly. Even when a Q is formally in the allowed region, one may feel threshold effects that make event generation less efficient. As a first approximation for this region, the shower is forced to 'try harder' to find a $\mathrm{g} \to \mathrm{Q}\overline{\mathrm{Q}}$ branching, without any loss of cross section. The end result is that, in the new program version, no c or b quarks remain in the beam remnant, but are always constructed as coming from a shower branching.

Gluon splitting cannot easily be generated by itself, since it could appear e.g. several steps down in a gluonic cascade, which cannot easily be predetermined. Instead it is necessary to attempt to generate the full QCD jet cross section, down to some lower $\hat{p}_{\perp\mathrm{min}}$ cut, and then pick up all events that 'happen' to contain the heavy flavour. Some events fall under the heading of pair creation or flavour excitation and are thus removed in a second step.

Note that the kinematics machinery here is based on massless quarks in the hard scattering, with some post-facto modifications for heavy quarks, so the alternative pair-creation description obtained here is less precise than the one in point 1 above. Masses are included in the description of the shower branching $\mathrm{g} \to \mathrm{Q}\overline{\mathrm{Q}}$, however.

Showers should not populate kinematical regions already covered by the hard scattering. This requirement is not easy to implement exactly. One reason is that several different sets of constraints can appear, such as from virtuality ordering and angular ordering. Here we therefore satisfy ourselves with an approximate matching of Q^2_{max} and M^2_{max}, the maximally allowed virtualities of spacelike and timelike showers, respectively, to $Q^2 = \hat{p}_\perp^2 = \hat{t}\hat{u}/\hat{s}$, the conventional hard-scattering scale. This matching is generic to all branchings in showers, but obviously we give special attention to implications for the heavy-quark production vertices.

With massless kinematics, one may sensibly assume $Q^2 \le Q^2_{\mathrm{max}}, M^2_{\mathrm{max}} \le 4Q^2$. The lower limit would be appropriate for a t-channel graph, where $-\hat{t} \approx Q^2$ sets the maximal virtuality. The upper limit is more relevant for an s-channel graph, where $\hat{s} \ge 4\hat{p}_\perp^2$ sets the scale. So the above range translates into an uncertainty in the amount of shower evolution. However, we can try to be more specific. Timelike parton showers are evolved in terms of M^2, the squared mass of the propagating parton. It is thus akin to the $\hat{s}$ scale of the hard scattering, and $M^2_{\mathrm{max}} = 4Q^2$ is the preferred choice. With both Q and $\overline{\mathrm{Q}}$ having a mass at or above m_Q, the heavy-flavour production threshold at $M^2_{\mathrm{max}} = 4m^2_\mathrm{Q}$ then corresponds to $Q^2 = m^2_\mathrm{Q}$, which agrees with the threshold for pair creation at the hard scattering. Spacelike parton showers instead are evolved in a spacelike virtuality, analogous to $\hat{t}$, and the reasonable choice then is $Q^2_{\mathrm{max}} = Q^2$. Again, this gives a matching threshold for 'flavour excitation' both in the shower and at the hard scattering, at m^2_Q for most heavy-flavour parton distribution parameterizations. Specifically, note that an initial-state shower branching does not have to produce two heavy quarks on mass shell, but only one at a time.

Parameters

The main formal parameters in the perturbative description are the heavy-quark masses. They enter in the description of hard scatterings and parton showers alike, both directly as mass terms in matrix elements or splitting kernels and indirectly in the description of the phase space. Therefore cross sections are especially sensitive to the value selected. Also the nonperturbative phenomenology is significantly affected. In [10], we chose to standardize on $m_{\mathrm{c}} = 1.5$ GeV. Based on conventional mass formulae [22],

$$\frac{3m_{\mathrm{D}^*} + m_{\mathrm{D}}}{4} - m_{\mathrm{c}} = \frac{3m_{\mathrm{B}^*} + m_{\mathrm{B}}}{4} - m_{\mathrm{b}} \ , \tag{4.3}$$

we then obtain $m_{\mathrm{b}} = 4.8$ GeV.

Also the choice of parton distributions gives some leeway, especially since the gluon distribution is not yet so well constrained at small x and moderately small Q^2, where a non-negligible amount of the total charm/bottom cross section at high energies comes from. Unless otherwise specified, we have used the CTEQ 5L parameterized distributions for the proton [23], with $\Lambda^{(4)} = 0.192$ GeV. For the pion we rely on the GRV LO (updated) sets [24]. As already noted, the default factorization scale is $Q^2 = \hat{p}_{\perp}^2$.

4.2.2 Nonperturbative Aspects

The way string fragmentation affects charm production was described in [10]. We will here develop the main points and outline the current status of our modeling, which is slightly modified since the previous publication.

The partonic state that is to be hadronized consists, at the very least, of the outgoing partons from the hard scattering and of the beam-remnant partons. Furthermore, a realistic study has to include the additional partons produced by initial- and final-state showers, and by the possibility of having several hard parton–parton interactions in the same event. These aspects increase in importance with increasing energy, and have to be included in the event description, but will not be at the focus of attention.

Colour Flow

In the string model, confinement is implemented by spanning strings between the outgoing partons. These strings correspond to a Lorentz-invariant description of a linear confinement potential, with string tension $\kappa \approx 1$ GeV/fm. Each

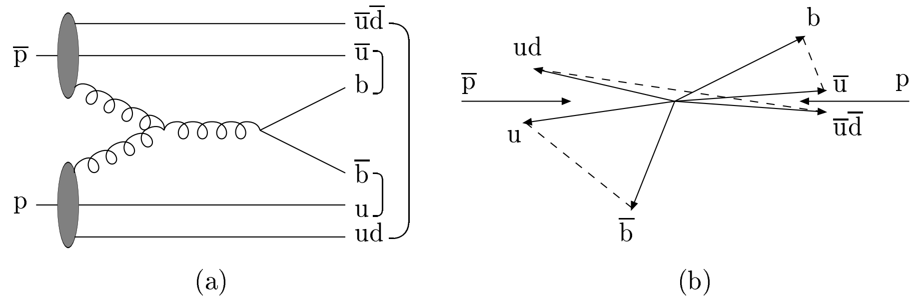

Figure 4.2: Example of a string configuration in a p$\overline{\text{p}}$ collision. (a) Graph of the process, with brackets denoting the final colour singlet subsystems. (b) Corresponding momentum space picture, with dashed lines denoting the strings.

string piece has a colour charge at one end and its anticolour at the other. The double colour charge of the gluon corresponds to it being attached to two string pieces, while a quark is only attached to one. A diquark is considered as being in a colour antitriplet representation, and thus behaves (in this respect) like an antiquark. Then each string contains a colour triplet endpoint, a number (possibly zero) of intermediate gluons and a colour antitriplet end. An event will normally contain several separate strings.

The string topology can be derived from the colour flow of the hard process. For instance, consider the LO process u$\overline{\text{u}}$ → b$\overline{\text{b}}$ in a p$\overline{\text{p}}$ collision. The colour of the incoming u is inherited by the outgoing b, so the b will form a colour-singlet together with the proton remnant, here represented by a colour antitriplet ud diquark. In total, the event will thus contain two strings, one b–ud and one $\overline{\text{b}}$–$\overline{\text{u}}\overline{\text{d}}$. In gg → b$\overline{\text{b}}$ a similar inspection shows that two distinct colour topologies are possible. Representing the proton remnant by a u quark and a ud diquark (alternatively d plus uu), one possibility is to have three strings b–$\overline{\text{u}}$, $\overline{\text{b}}$–u and ud–$\overline{\text{u}}\overline{\text{d}}$, Fig. 4.2, and the other is the three strings b–ud, $\overline{\text{b}}$–$\overline{\text{u}}\overline{\text{d}}$ and u–$\overline{\text{u}}$.

In processes with several possible colour topologies, the relative composition may become nontrivial. For gg → b$\overline{\text{b}}$, the symmetry of the process gives an equal integrated — but not differential — rate for the two topologies. For a more illustrative example, consider e.g. ug → ug, again in p$\overline{\text{p}}$, which contains both s-, t- and u-channel graphs, including interference terms. There are again two possible colour topologies, u–$\overline{\text{u}}$ plus ud–g–$\overline{\text{u}}\overline{\text{d}}$ and u–g–$\overline{\text{u}}$ plus ud–$\overline{\text{u}}\overline{\text{d}}$. The u-channel only contributes to the former and the s-channel to the latter, but the t-channel contributes to both, meaning there is a nontrivial kinematics dependence on the relative probability for the two topologies. Furthermore, the cross section contains an interference contribution that corresponds to an undetermined colour flow, where it is not possible to subdivide the event into two separate colour singlets. Since the hadronic final state consists of singlets, clearly a collapse of this ambiguity must occur at some stage. We therefore subdivide the interference term, in a sensible but not unique way, between the two configurations above [25]. As should be expected, it is suppressed by a factor $1/N_C^2$, where $N_C = 3$ is the number of colours.

The above example carries over to flavour excitation $\mathrm{Qg} \to \mathrm{Qg}$, but additionally the colour flow in the initial- and final-state cascades has to be considered, at the very least the branching $\mathrm{g} \to \mathrm{Q\overline{Q}}$. Since we only work to leading order, where no interference contributions are explicit (implicitly they have been used e.g. to introduce angular ordering in the shower evolution), this is straightforward: a new colour-anticolour pair is created and spanned between the daughters in $\mathrm{g} \to \mathrm{gg}$ and $\mathrm{q} \to \mathrm{qg}$, while the existing colours are split in $\mathrm{g} \to \mathrm{q\overline{q}}$. No special colour rules are needed for heavy flavours. The last vertex, although the most rare of the three, has a special rôle in subdividing one colour singlet into two. With increasing energy and parton-shower activity, it gives an increasing average number of separate singlets in an event.

Hadronization

Once the string topology has been determined, the Lund string fragmentation model [1] can be applied to describe the nonperturbative hadronization. To first approximation, we assume that the hadronization of each colour singlet subsystem, i.e. string, can be considered separately from that of all the other subsystems. Presupposing that the fragmentation mechanism is universal, i.e. process-independent, the good description of $\mathrm{e^+e^-}$ annihilation data should carry over. The main difference between $\mathrm{e^+e^-}$ and hadron–hadron events is that the latter contain beam remnants which are colour-connected with the hard-scattering partons. More about these remnants below, in Sect. 4.2.2.

Depending on the invariant mass of a string, practical considerations lead to the need to distinguish three hadronization prescriptions:

1. *Normal string fragmentation.* In the ideal situation, each string has a large invariant mass. Then the standard iterative fragmentation scheme, for which the assumption of a continuum of phase-space states is essential, works well. The average multiplicity increases linearly with the string 'length', which means logarithmically with the string mass. In practice, this approach can be used for all strings above some cut-off mass of a few GeV.
2. *Cluster decay.* If a string is produced with a small invariant mass, maybe only two-body final states are kinematically accessible. The continuum assumption above then is not valid, and the traditional iterative Lund scheme is not applicable. We call such a low-mass string a cluster, and consider it separately from above. When kinematically possible, a Q–$\mathrm{\overline{q}}$ cluster will decay into one heavy and one light hadron by the production of a light quark–

antiquark pair in the colour force field between the two cluster endpoints, with the new quark flavour selected according to the same rules as in normal string fragmentation. The $\overline{\mathrm{q}}$ cluster end or the new $\mathrm{q}\overline{\mathrm{q}}$ pair may also denote diquarks; for ease of notation we will not always enumerate all the possible combinations covered in the full description.

3. *Cluster collapse.* This is the extreme case of the above situation, where the string mass is so small that the cluster cannot decay into two hadrons. It is then assumed to collapse directly into a single hadron, which inherits the flavour content of the string endpoints. The original continuum of string/cluster masses is replaced by a discrete set of hadron masses, mainly D/B and $\mathrm{D}^*/\mathrm{B}^*$ (or corresponding baryon states). This mechanism plays a special rôle, in that it allows large flavour asymmetries in favour of hadron species that can inherit some of the beam-remnant flavour content.

We assume that the nonperturbative hadronization process does not change the perturbatively calculated total rate of charm production. By local duality arguments [26], we further presume that the rate of cluster collapse can be obtained from the calculated rate of low-mass strings. This is related to the argument used in the $\mathrm{e}^+\mathrm{e}^- \to \mathrm{c}\overline{\mathrm{c}}$ channel, that the cross section in the J/ψ and ψ' peaks is approximately equal to a purely perturbatively calculated $\mathrm{c}\overline{\mathrm{c}}$ production cross section restricted to the below-$\mathrm{D}\overline{\mathrm{D}}$-threshold region. Similar relations have also been studied e.g. for τ decay to hadrons [27], and there shown to be valid to good accuracy. In the current case, the presence of other strings in the event additionally allows soft-gluon exchanges to modify parton momenta as required to obtain correct hadron masses. Traditional factorization of short- and long-distance physics would then also protect the charm cross section. Local duality and factorization, however, do not specify *how* to conserve the overall energy and momentum of an event, when a continuum of $\overline{\mathrm{c}}\mathrm{d}$ masses is to be replaced by a discrete D^- one. This will therefore be one of the key points to be studied below.

A first step towards constructing a model is to decide which mass range a string belongs to. We have above settled for $m_{\mathrm{c}} = 1.5$ GeV and $m_{\mathrm{b}} = 4.8$ GeV. Light quarks are given constituent masses, $m_{\mathrm{d}} = m_{\mathrm{u}} = 0.33$ GeV and $m_{\mathrm{s}} = 0.5$ GeV. Diquark masses are essentially the sum of the constituent masses above, with a spin-splitting term added. If the string invariant mass exceed the sum of the two string endpoint masses by some margin, $\sim$1 GeV, the normal string fragmentation routine can be used. This routine can produce two, three or more hadrons from the string, with the actual multiplicity determined dynamically during the hadronization process. Close to the lower limit, the two-body states dominate, so there should be a smooth transition to the cluster decay description.

For smaller string masses, a special cluster fragmentation procedure is used. Whether this results in the production of one or two hadrons depends on the assumed two-body threshold behaviour. Consider a $c\overline{u}$ cluster, for instance. In one extreme point of view, a $D\pi$ pair should always be formed when above this threshold, and a single D never. In another extreme, the two-body fraction would gradually increase at a succession of thresholds: $D\pi$, $D^*\pi$, $D\rho$, $D^*\rho$, etc., where the relative probability for each channel is given by the standard flavour and spin mixture in string fragmentation. (For instance, D^* and D are assumed to be produced in the 3:1 ratio implied by spin counting, while the big ρ–π mass splitting there gives a mixture more like 1:1.) In our current default model, we have chosen to steer a middle course, by allowing two attempts to find a possible pair of hadrons. Thus a fraction of events may collapse to a single resonance also above the $D\pi$ threshold, but $D\pi$ is effectively weighted up. For instance, a 2.2 GeV string mass might, in a first round, be chosen to decay to $D^*\rho$, and thus fail. If a second attempt instead gives $D\pi$, this two-body state would be accepted, but if $D^*\rho$ is selected again, the cluster would collapse to a single hadron. If a large number of attempts had been allowed (this can be varied as a free parameter), collapse would only become possible for cluster masses below the $D\pi$ threshold.

One might have chosen also to include a phase-space factor close to each two-body threshold, instead of the step function used here. However, measurements of R in e^+e^- above the charm and bottom thresholds [28] indicate that Coulomb final-state interaction effects cancel any such suppression. (Actually, the same data could be used to argue for having only two-body states above the $D\pi$ threshold. However, there is a difference: in a hadronic environment there will be a competition between the production of one or of two hadrons, while collapse to a single particle is not an option in e^+e^- away from the $c\overline{c}$ resonance masses. Within the large error bars of the data, one might also read in some trend towards a larger R a bit further above the $D\overline{D}$ threshold.)

In a cluster decay to two particles, a simplified version of normal string fragmentation is used, in a spirit similar to the machinery for joining the fragmentation chain by the production of two final hadrons somewhere in the middle of a normal string. In the cluster rest frame, a string direction is defined by the momentum vector of the heavy quark Q. As a starting distribution, the cluster is allowed to decay isotropically to the two hadrons. The hadronic transverse momentum with respect to this direction is then used to introduce a Gaussian suppression factor $\exp(-p_\perp^2/2\sigma^2)$, with $\sigma = 0.36$ GeV denoting the standard fragmentation $p_\perp$ width parameter. At threshold the decay thereby remains isotropic, but at (an imagined) large cluster mass one would reproduce the same $p_\perp$ spectrum as when a string breaks by the production of a new $q\overline{q}$ pair. The heavy hadron H could still equally likely be produced in the Q hemisphere as in the opposite one, however. In string fragmentation, these two configurations enter with different relative weights, that can be derived from the space-time history of the process. Applied to the current case, this gives

$$\mathcal{P}_{\mathrm{opposite}} = \frac{1}{1 + e^{b\Delta}} \tag{4.4}$$

with

$$\Delta = \sqrt{(m^2 - m_{\perp\mathrm{H}}^2 - m_{\perp\mathrm{h}}^2)^2 - 4m_{\perp\mathrm{H}}^2 m_{\perp\mathrm{h}}^2} \ , \tag{4.5}$$

where m is the cluster mass, $m_{\perp\mathrm{H}}$ and $m_{\perp\mathrm{h}}$ are the heavy and light hadron transverse masses, and b the string fragmentation parameter, $b \approx 0.9$ GeV^{-2}. $\Delta = \Gamma_2 - \Gamma_1 = \kappa^2(\tau_2^2 - \tau_1^2)$ is the difference in string area Γ_i spanned for the two solutions, which can be related to a difference in decay proper times τ_i by the string tension κ. After this final correction, giving the 'natural' ordering with the heavy hadron usually close to the direction of the heavy quark when well above the threshold, the transition between normal string fragmentation and cluster decay is reasonably smooth.

What is not so smooth is the cluster collapse mechanism. Here confinement effects have to project the continuum of string masses onto the observed discrete hadron mass spectrum. Because of the aforementioned local duality and factorization arguments, the total area of the spectrum should be conserved in the process. How the projection should be done is not known from first principles, however.

One conceivable strategy could be to introduce a weight function consisting of δ function peaks at the single-hadron masses, with suitably adjusted normalizations, and then step functions at the two-particle thresholds. This weight function, when multiplied with the partonic mass spectrum, should then give the hadron-level mass spectrum. Such an approach is not well suited for Monte Carlo simulation, since the string mass is a complicated function of a number of variables and therefore the δ function cannot easily be integrated out. Conceptually, it would also suffer from the problem of having to have a non-universal weight function: the coefficients would have to be adjusted somewhat as a function of energy to ensure exact conservation of the total cross section, since the cluster mass spectrum itself is somewhat energy dependent. However, on general grounds, we do not expect the overall distribution of event characteristics to differ significantly between events with a $\overline{\mathrm{c}}$–d string mass exactly equal to the D^- one, and events where the string mass is maybe 100 MeV off. An appealing shortcut therefore is to accept all partonic configurations and thereafter introduce some 'minimal' adjustments to the kinematics to allow hadrons to be produced on the mass shell. Such a strategy would be consistent not only with local duality arguments, but also with the presence of soft final-state interactions, i.e. the exchange of nonperturbative gluons that can carry some amount of momentum between the low-mass string and the surrounding hadronic system. In the following we will therefore adopt the language of 'gluons' transferring energy and momentum between the strings in a collision, while leaving unanswered the question on the exact nature of those 'gluons'. Specifically, we will not address the possibility of changes in the colour structure of events by such 'gluons'.

The basic strategy will be to exchange some minimal amount of momentum between the collapsing cluster and other string pieces in its neighbourhood. Consider an event in its CM frame, with all partons emerging from an assumed common origin. Partons move out with close to the speed of light, so if they move in the same direction they also stay close to each other for a long time, and therefore have an enhanced chance to exchange momenta. An exchange can also occur to the string pieces spanned between the partons, quarks or gluons. The piece between two partons 1 and 2 spans the set of velocity vectors

$$\mathbf{v}_{\mathrm{string}} = \alpha \mathbf{v}_1 + (1-\alpha)\mathbf{v}_2 \ , \ 0 \leq \alpha \leq 1 \ . \tag{4.6}$$

A closest 'distance' between this string piece and the cluster can then be defined as

$$D^2 = \min_{0\leq\alpha\leq 1} (\mathbf{v}_{\mathrm{cl}} - \mathbf{v}_{\mathrm{string}})^2 \ . \tag{4.7}$$

Based on this measure, the string piece closest to the cluster is found.

The momentum transfer can be in either direction, depending on whether the hadron is heavier or lighter than the cluster it comes from, $m_{\mathrm{H}} \gtrless m_{\mathrm{cl}}$. The hadron species, and thereby hadron mass, is selected according to the standard flavour selection rules. That is, there is no mass dependence, e.g. so that a lighter cluster could have been more likely to form a D/B and a heavier a $\mathrm{D}^*/\mathrm{B}^*$; after all, the mass splitting is not so large that kinematics should come out particularly different for the two.

The simpler situation is when $m_{\mathrm{H}} < m_{\mathrm{cl}}$. Then one may split the cluster four-momentum into two parallel vectors, $p_{\mathrm{H}} = (m_{\mathrm{H}}/m_{\mathrm{cl}})p_{\mathrm{cl}}$ and $p_{\mathrm{g}} = (1 - m_{\mathrm{H}}/m_{\mathrm{cl}})p_{\mathrm{cl}}$. The latter momentum, for an imagined gluon, can be absorbed by the closest string piece found above, i.e. be inserted between the endpoint partons 1 and 2. This gluon has $m_{\mathrm{g}}^2 > 0$, but not too large or a collapse would not have occurred. Such somewhat massive gluons are well modeled by the standard string fragmentation framework [29]. One could have chosen a 'decay' of the cluster into a massless gluon, e.g. with an isotropic angular distribution in its rest frame, but such an ansatz gives the same average behaviour as the one above, and only slight differences in fluctuations.

A worse situation is when $m_{\mathrm{H}} > m_{\mathrm{cl}}$. A negative-energy gluon could be defined and handled as above. Usually this works fine, but it can lead to complete strings (not just string pieces) with negative m^2, or even to hadrons with $|x_{\mathrm{F}}| > 1$, so such an approach is not quite trustworthy. Instead we assume an exchange in the opposite direction, where the nearest string piece emits a gluon that can be absorbed by the cluster to give it the desired hadron mass. To be more precise, form a weighted sum of the endpoint momenta

$$p_s = \alpha p_1 + \beta p_2 = \frac{p_2 p_{\mathrm{cl}}}{p_1 p_2} p_1 + \frac{p_1 p_{\mathrm{cl}}}{p_1 p_2} p_2 \ , \tag{4.8}$$

so that the end of the string that is closest to the cluster is weighted up relative to the one further away. Thereafter define

$$p_{\mathrm{H}} = p_{\mathrm{cl}} + \delta p_s \ , \tag{4.9}$$

with δ determined by the constraint $p_{\mathrm{H}}^2 = m_{\mathrm{H}}^2$. The hadron will then have the correct mass, and the string endpoint momenta are scaled down by factors $1 - \delta\alpha$ and $1 - \delta\beta$, respectively. (Also the endpoint masses are scaled down in the process. This is no problem, since the string fragmentation is not dependent on having partons of a fixed mass.)

In the rare case that, e.g., $1 - \delta\alpha < 0$, the procedure has to be extended. If the parton 1 is a gluon, the string does not end there but extends further to a parton 3. Then the gluon 1 four-momentum can be fully absorbed by the cluster, and the procedure above repeated for the partons 2 and 3. That way, one gluon after the next could be absorbed, at least in principle. If instead a string endpoint is involved, this trick does not work and we there revert to the old scheme, where four-momentum is shuffled between the cluster and the parton furthest away from it, i.e. with the largest cluster+parton invariant mass. This scheme is more robust, and normally requires only small four-momentum transfers, but physically it is not so appealing, since it runs counter to the principle of locality in the hadronization description. In practice, though, there is a good general agreement between results for the new and the older description [10].

Beam Remnants

A characteristic feature of hadronic collisions is the presence of a beam remnant. This remnant is defined by what is left behind of the hadron by the initial-state parton shower initiator. In the simplest case, when a valence quark is picked out of the incoming hadron, the remnant is a single antiquark, for a meson, or a diquark, for a baryon. In either case it is in a colour antitriplet state that can be considered as a unit. For a baryon, simple flavour+spin SU(6) rules can be used, e.g. to select between a ud_0 and a ud_1 diquark.

A more complex situation is when a gluon is picked out of the hadron, so that the remnant is a colour octet, i.e. attached to two strings. A convenient approach is to imagine this system split into two separate string endpoints, one colour triplet and the other antitriplet. For a meson this would correspond to valence quark+antiquark, for a baryon to quark+diquark. The beam remnant distribution function (BRDF) is introduced to describe how the (light-cone) momentum of the remnant is shared between the two, in fractions χ and $1-\chi$, respectively. For an octet meson remnant the χ distribution is always implicitly symmetrized between the q and $\overline{\mathrm{q}}$, while for an octet baryon remnant one quark (picked at random among the three) takes the fraction χ and the remaining

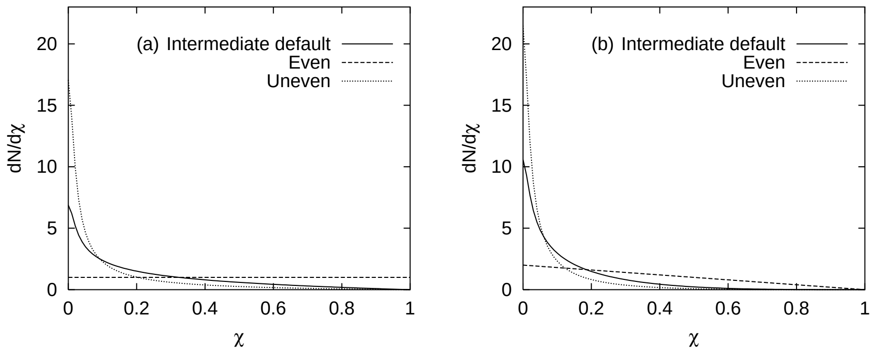

Figure 4.3: Distribution of χ variable at 40 GeV for (a) a meson and (b) a baryon. Full curves show the default intermediate option, dashed the even one and dotted the uneven one, corresponding to $\langle\chi\rangle = 0.22$, 0.50 and .12 for mesons and .13, .33 and .076 for baryons.

colour antitriplet diquark $1-\chi$. There is no first-principles theory for BRDF's, so one has to rely on sensible ansätze. It turns out that asymmetries, e.g. between D and $\overline{\mathrm{D}}$ mesons, are very sensitive to the choices made here, especially in the baryon fragmentation regions [10]. Therefore we will have reason to compare different forms. As an intermediate, default, option we use

$$\begin{aligned} f(\chi) &\propto \frac{1-\chi}{\sqrt[4]{\chi^2 + c_{\mathrm{min}}^2}} && \text{for mesons,} \\ f(\chi) &\propto \frac{(1-\chi)^3}{\sqrt[4]{\chi^2 + c_{\mathrm{min}}^2}} && \text{for baryons,} \end{aligned} \tag{4.10}$$

see Fig. 4.3. Here $c_{\mathrm{min}} = 0.6\ \mathrm{GeV}/E_{\mathrm{CM}} \approx 2m_{\mathrm{q}}/E_{\mathrm{CM}}$ provides an effective damping for χ values so small that a parton ends up in the opposite hemisphere from its mother hadron. Some arguments for the forms above, especially the $1/\sqrt{\chi}$ behaviour, can be found in reggeon phenomenology [30], but basically this is just a compromise between extremes. One such is that of an even sharing between all the valence partons,

$$\begin{aligned} f(\chi) &= 1 && \text{for mesons,} \\ f(\chi) &= 2(1-\chi) && \text{for baryons.} \end{aligned} \tag{4.11}$$

Another is that of an uneven distribution,

$$
\begin{aligned}
f(\chi) &\propto \frac{1-\chi}{\sqrt{\chi^2 + c_{\mathrm{min}}^2}} && \text{for mesons,} \\
f(\chi) &\propto \frac{(1-\chi)^3}{\sqrt{\chi^2 + c_{\mathrm{min}}^2}} && \text{for baryons,}
\end{aligned}
\tag{4.12}
$$

reminiscent of the parton distributions encountered in the process of perturbatively extracting a parton from a hadron.

Also sea quarks/antiquarks may be emitted from a hadron. We here refer to the lighter u, d and s quarks that, unlike the heavier quarks, exist in the parton distributions at the lower shower cut-off scale $Q_0 \approx 1$ GeV. In this case, the remnant is in an (anti)triplet state, which conveniently is subdivided into a colourless hadron plus a simple coloured remnant. For instance, a uuds remnant could become Λ + u. The current default is to assign the hadron a χ lightcone fraction according to the normal string fragmentation function. Differences relative to using simpler expressions, in the spirit e.g. of the even sharing above, are minor for the quantities of interest to us. One reason is that the sea contribution is much smaller than the gluon one above. A questionable but convenient approximation is to assume that any emitted quark that could be a valence quark also is one; a better choice would be to split e.g. the u distribution of the proton into one valence and one sea part that are to be handled differently. This simplification is not so critical, for the same reason as above.

The partons entering the hard interaction are traditionally taken to have a non-vanishing primordial $k_\perp$. In a shower description, such a $k_\perp$ is instead assigned to the initial-state shower initiators. These could be seen as having a purely nonperturbative Fermi motion inside the incoming hadrons. Typical values should thus be 300–400 MeV, consistent with constituent quark masses and fragmentation transverse momenta (σ above). The initial-state shower will add further activity, so the parton that enters the hard $2 \to 2$ subprocess could well have more. However, in many connections [31], also for charm production at fixed-target energies [13], it has been noted that much higher values are required, at or even above 1 GeV. This remains somewhat of a mystery, which we do not attempt to solve here. We will use a Gaussian width of 1 GeV as default. The choice of primordial-$k_\perp$ distribution is of non-negligible importance, both by providing a $p_\perp$ kick to the produced heavy-flavour quarks and, by momentum conservation, an opposite kick to the beam remnants.

When a remnant is split up in two, not only longitudinal but also transverse momentum sharing has to be specified. If the large primordial $k_\perp$ comes from a complicated multigluon emission process, there is no reason why all of it should be taken by one of the remnants. Instead it is assumed shared evenly between the two. Furthermore, a relative kick is added between them, picked according to the standard fragmentation $p_\perp$ width σ, for simplicity and in the lack of any experimental indication.

A further aspect of the beam-remnant physics is the possibility of having multiple parton–parton interactions in an event. This could have an impact in a number of ways. Some of these, like an increase of the underlying event activity and more complicated string drawings, are included in the standard Pythia framework [32], but obviously with several degrees of freedom in the description. Others, like the production of multiple heavy-flavour pairs in separate hard processes and the possibility of even more complicated beam remnants than the ones above, have not (yet) been studied.

Another area not addressed is that of QCD interconnection, wherein a given colour configuration may be rearranged by soft-gluon exchanges [33]. Mechanisms in this spirit have been proposed e.g. to produce closed-heavy-flavour states (J/ψ etc.) from colour-octet heavy-flavour pairs [34].

These examples serve as useful reminders that the modelling, however sophisticated, cannot be considered as complete in the nonperturbative sector. Therefore one cannot hope for perfect agreement between the model and the data. In the following we will show, however, that the current experimental data can be understood qualitatively, and often also quantitatively. This gives some confidence that the modeling described above is a good first approximation, that could also be used for predictions in processes or at energies not yet studied.

4.3 Simple Model Properties

In this section we examine some properties of the model as presented in the previous section. In the first part we study purely perturbative properties of the model such as the total cross section, $\hat{p}_\perp$ of the hard interaction and quark distributions. In the second part we study the properties of the nonperturbative fragmentation. Experimental observables will be presented and confronted with data in the next section.

4.3.1 Properties of the Perturbative Production

Above, three different production channels have been distinguished in the parton-shower description: pair creation, flavour excitation and gluon splitting. In the following we will present their separate contributions, even though this subdivision of course is unobservable and model-dependent. It will still provide helpful insights.

The most basic and inclusive observable is the total heavy-flavour cross section. In Fig. 4.4 we present it as a function of the pp centre-of-mass energy, from the fixed-target régime to LHC and beyond, both for charm and bottom.

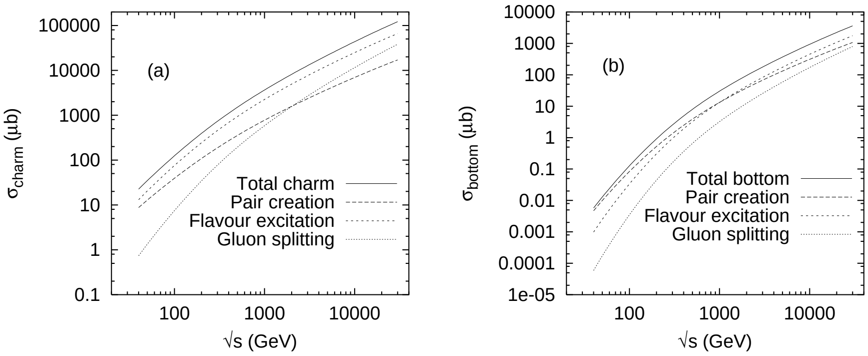

Figure 4.4: The total (a) charm and (b) bottom cross sections for pp collisions as a function of $E_{\mathrm{CM}} = \sqrt{s}$. The contributions from pair creation, flavour excitation and gluon splitting are shown separately.

The cross section is divided into the contributions from the three perturbative production channels. As noted before, we assume that no nonperturbative effects contribute to the total cross section. The level of the total cross section is in sensible agreement with the present data (not shown), indicating that there is no need for any further significant production mechanism.

For small (fixed-target) energies the pair creation cross section is dominating the production, followed by a non-negligible fraction of flavour excitation, whereas gluon splitting is very small. As the energy is increased, flavour excitation overtakes pair production and gluon splitting is catching up. At very large energies gluon splitting becomes the dominant production mechanism, so that the low-energy pattern is completely reversed.

The reason is not so difficult to understand. If we think of any partonic process, it will only contain one hardest $2 \to 2$ scattering whatever the energy, whereas the number of branchings in the associated initial- and final-state showers will increase with energy. This increase comes in part from the the growing phase space, e.g. the larger rapidity evolution range of the initial-state cascades, in part from the increase in accessible and typical virtuality scales Q^2 for the hard subprocess. The multiplication effect is at its full for gluon splitting, whereas flavour-excitation topologies are more restrictive. At small energies, however, the less demanding kinematical requirements for flavour excitation in a shower gives it an edge over gluon splitting.

The total cross section is strongly dependent on QCD parameters such as the heavy-quark mass, parton distributions, and factorization and renormalization scales. It is not our aim here to present theoretical limits and errors — this has been done elsewhere [13]. However, Fig. 4.5 gives some examples of

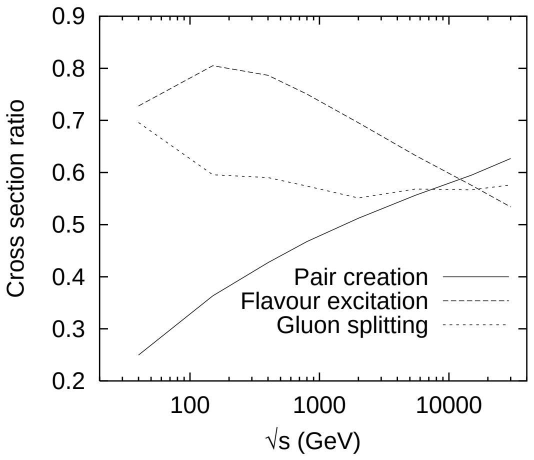

Figure 4.5: Dependence of the charm cross section on model aspects, for pp collisions as a function of $E_{\mathrm{CM}} = \sqrt{s}$. Shown is the ratio of cross sections: pair creation for $m_{\mathrm{c}} = 1.7$ GeV/$m_{\mathrm{c}} = 1.3$ GeV, flavour excitation for GRV 94L/CTEQ 5L parton distributions, and gluon splitting for $Q^2_{\mathrm{max}} = M^2_{\mathrm{max}} = Q^2/Q^2_{\mathrm{max}} = M^2_{\mathrm{max}} = 4Q^2$.

how much results may vary. Clearly, the quark-mass choice is very important, especially for charm. Maybe surprisingly, the charm parton distributions in the proton do not differ by that much, probably reflecting a convergence among the common parton distributions and in the scheme adapted for $\mathrm{g} \to \mathrm{Q}\overline{\mathrm{Q}}$ branchings in the evolution equations. Among the examples given, the largest uncertainty comes from the choice of the heavy quark mass. However, it should be remembered that the variations above have no formal meaning of a '1σ' range of uncertainty, but merely reflects some more or less random variations.

To gain further insight into the properties of the perturbative production processes, one may study 'non-observables' that characterize the hard-scattering process associated with the production, such as the $\hat{p}_\perp$ of the hard interaction. We also show kinematical distributions, like the rapidity and transverse momentum of the heavy quarks, and correlations between them, in order to quantify in which regions the different production processes contribute. As an example, $\mathrm{b}\overline{\mathrm{b}}$ production is studied at a 2 TeV $\mathrm{p}\overline{\mathrm{p}}$ collider, where the three production mechanisms are of comparable magnitude. Since the valence-quark-dependent contribution to hard subprocesses is small at this energy, there is no significant difference between pp and $\mathrm{p}\overline{\mathrm{p}}$.

Fig. 4.6 shows the $\hat{p}_\perp$ distribution of the hard interaction, where $\hat{p}_\perp$ is the transverse momentum of the outgoing partons evaluated in the hard-interaction

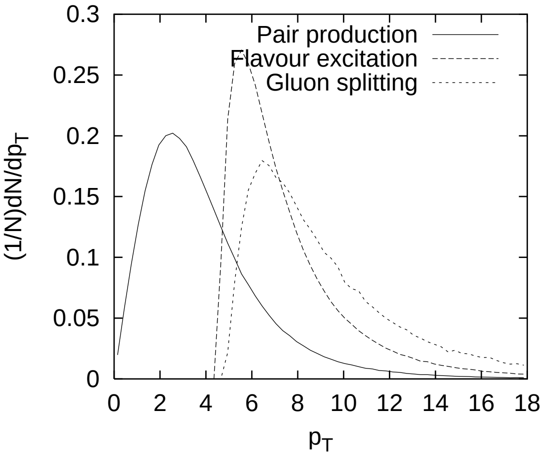

Figure 4.6: $\hat{p}_\perp$ distributions for the hard interaction associated with a $\mathrm{b\overline{b}}$ event at a 2 TeV $\mathrm{p\overline{p}}$ collider. The pair creation, flavour excitation and gluon splitting curves are each normalized to unit area to simplify comparisons of the shape.

rest frame. The main difference is in the behaviour at small $\hat{p}_\perp$. For the pair creation process, massive LO matrix elements are used, so that $\hat{p}_\perp$ goes all the way down to zero. The differential cross section is not divergent and no explicit $\hat{p}_{\perp\mathrm{min}}$ cut is needed. For the other two processes, massless matrix elements are used as a starting point — implying a divergent cross section in the limit $\hat{p}_\perp \to 0$ — and mass constraints are introduced the back door. To be able to resolve a heavy quark inside a hadron, i.e. flavour excitation and initial-state gluon splitting, a virtuality $Q^2 = \hat{p}_\perp^2 > m_\mathrm{Q}^2$ is needed, so the quark mass sets $\hat{p}_{\perp\mathrm{min}}$ in this case. (With a massive quark in the final state, the actually reconstructed $p_\perp$ of the hard scattering is always smaller than the nominal $\hat{p}_\perp$ one.) Also the final-state shower contribution to gluon splitting begins at $\hat{p}_{\perp\mathrm{min}} = m_\mathrm{Q}$. Here the shower evolution scale is set by $M_\mathrm{max}^2 = 4\hat{p}_\perp^2$, but the threshold for gluon splitting is at $M^2 = 4m_\mathrm{Q}^2$, so the two factors of 4 cancel. We remind that the cuts fill a well-defined function: the heavy-flavour-producing part of the graph cannot be the most virtual one in flavour excitation or gluon splitting, or one would double-count with pair creation. Nevertheless, the very sharp thresholds may be somewhat of an artefact, and are certainly smeared when the effects of further QCD emissions are included.

As an illustration, consider Fig. 4.7, where we show the single $\mathrm{b}/\overline{\mathrm{b}}$ transverse momentum ($p_\perp$) and rapidity (y) distributions of the produced quarks for the three production channels. Here the full parton-shower and intrinsic-$k_\perp$ smearing effects are included. Now all the $p_\perp$ spectra extend down to $p_\perp = 0$,

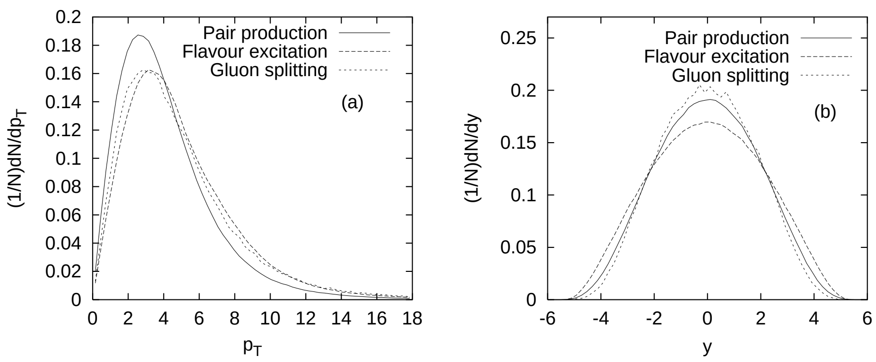

Figure 4.7: Single $\mathrm{b}/\overline{\mathrm{b}}$ quark (a) $p_\perp$ and (b) y distributions at a 2 TeV $\mathrm{p}\overline{\mathrm{p}}$ collider. The curves are each normalized to unit area to simplify comparisons of the shape.

and the shapes are surprisingly similar, although pair creation remains somewhat softer than the other two mechanisms. The rapidity spectra agree even better between the three mechanisms, although flavour excitation gives somewhat more production at larger rapidities and gluon splitting more at central ones, as could be expected. This seems to indicate that the heavy-quark production part of the process is more or less independent of what goes on in the rest of the event. There are indeed also similarities in the descriptions, e.g. gluon splitting $\mathrm{g} \to \mathrm{Q}\overline{\mathrm{Q}}$ is equivalent to the s-channel graph of pair creation $\mathrm{gg} \to \mathrm{Q}\overline{\mathrm{Q}}$, while flavour excitation is closely related to the t-channel graph of pair creation. Furthermore, compensation mechanisms are at play: the $p_\perp$ spectrum of gluon splitting is softened by the Q and $\overline{\mathrm{Q}}$ having to share the $p_\perp$ of the gluon between them, but this is compensated by the relative $p_\perp$ in the $\mathrm{g} \to \mathrm{Q}\overline{\mathrm{Q}}$ branching itself.

Correlations between the produced heavy quarks turn out to be more interesting, since here the difference between the three production channels are better visible. In Fig. 4.8 we present the distributions of $m_{\mathrm{b}\overline{\mathrm{b}}}$, $\Delta y = |y_{\mathrm{b}} - y_{\overline{\mathrm{b}}}|$, $\Delta p_\perp = |p_{\perp\mathrm{b}} - p_{\perp\overline{\mathrm{b}}}|$ and $\Delta\phi = |\phi_{\mathrm{b}} - \phi_{\overline{\mathrm{b}}}|$. The invariant mass spectrum is appreciably more peaked for gluon splitting than for the other two mechanisms. Given that gluon splitting is equivalent to the s-channel exchange of a gluon, while the other two are dominated by t-channel contributions, it is clear why the gluon splitting is more suppressed at large $m^2_{\mathrm{b}\overline{\mathrm{b}}} =$'$\hat{s}$'. As a logical consequence, also the y correlation is more narrow for gluon splitting.

In the Δy distribution the differences are even more marked. Here flavour excitation is depleted at small rapidity differences and approaches the pair production spectrum only at large Δy. The explanation of this involves several

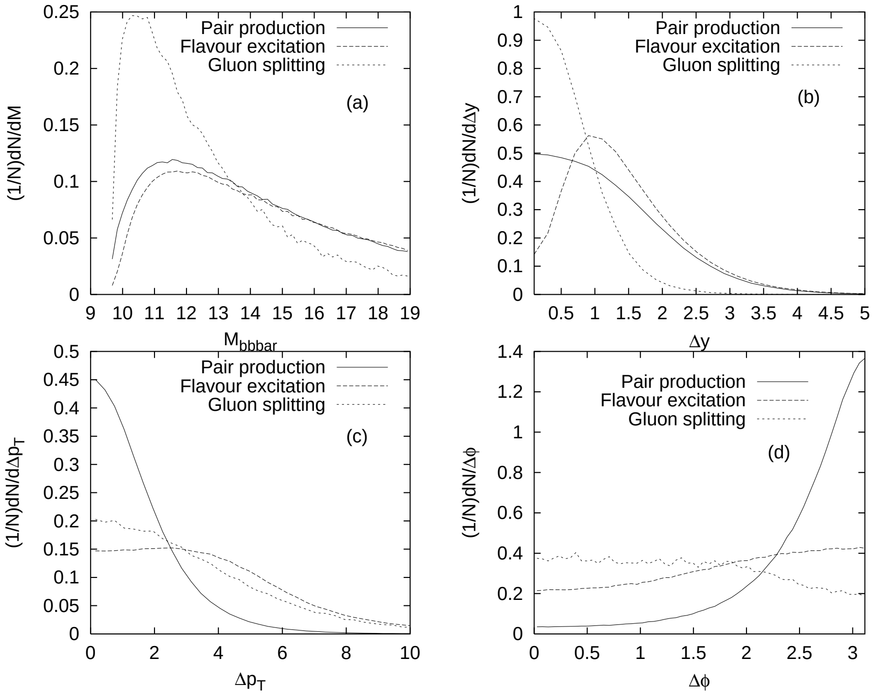

Figure 4.8: Correlations between b and $\overline{\mathrm{b}}$ at a 2 TeV $\mathrm{p\overline{p}}$ collider: (a) $m_{\mathrm{b\overline{b}}}$, (b) $\Delta y = |y_{\mathrm{b}} - y_{\overline{\mathrm{b}}}|$, (c) $\Delta p_{\perp} = |p_{\perp\mathrm{b}} - p_{\perp\overline{\mathrm{b}}}|$ and (d) $\Delta\phi = |\phi_{\mathrm{b}} - \phi_{\overline{\mathrm{b}}}|$. The curves are each normalized to unit area to simplify comparisons of the shape.

mechanisms. When a gluon in the parton-distribution evolution splits into a $\mathrm{b\overline{b}}$ pair this gives them a small initial rapidity separation, with a distribution which is centered around zero much like the gluon splitting distribution in Fig. 4.8b. One of the heavy quarks then enter the hard interaction and is back-scattered by a parton from the other beam. Since the minimum $\hat{p}_{\perp}$ of the hard interaction here is m_{b} and this is the largest scale of the process, the rapidity shift can be fairly large. An additional smearing is introduced by further gluon emissions in the parton shower, but not enough to hide the underlying behaviour.

Differences also appear in transverse momentum correlations. In the $\Delta p_{\perp}$ and $\Delta\phi$ distributions, pair creation is the one most peaked in the region of a heavy-quark pair with opposite and compensating $p_{\perp}$. Thus the basic LO-process behaviour largely survives showers and primordial $k_{\perp}$. In the other two processes the correlations are more smeared. Especially discerning is the $\Delta\phi$ distribution, where gluon splitting gives an almost flat curve, pair creation a clear peak near 180°, and flavour excitation is somewhere in between. In gluon splitting, the $p_\perp$ of the hard scattering favours small angles and the $p_\perp$ of the splitting itself large angles, so the near-flat curve is the result of a non-trivial balance. Needless to say, a cut on the $p_{\perp\mathrm{b}}$ and $p_{\perp\overline{\mathrm{b}}}$ values would distort the $\Delta\phi$ distribution significantly: at large $p_\perp$'s, pair creation becomes more peaked at large angles and gluon splitting peaked at small angles.

To summarize, we note that flavour excitation and gluon splitting give significant contributions to the total heavy quark cross section at large energies and thus must be considered. NLO calculations probably do a better job on the total b cross section than the shower approach, whereas for the lighter c quark, production in parton showers is so large that the NLO cross sections are more questionable. The shapes of single heavy quark spectra are not altered as much as the correlations between Q and $\overline{\mathrm{Q}}$ when flavour excitation and gluon splitting is added to the leading order result. Similar observations have been made when comparing NLO to LO calculations [12, 35].

4.3.2 Properties of the Fragmentation

We now proceed to describe properties of the fragmentation process. In the Lund string fragmentation model no new heavy flavours are produced during the fragmentation, so the model can 'only' map the momentum of a heavy quark onto the momentum and species of a heavy hadron in the final state. This can, however, be dramatic enough, e.g. with hadrons formed at larger momenta than the perturbatively produced quark, or with flavour asymmetries favouring the production of heavy hadrons sharing light valence quark flavours with the incoming beam particles. Such topics will be covered in detail in the following section, so here we only mention a few of the basic aspects.

The fate of a colour singlet system in the string model depends on its mass and on its flavour content. The mass spectrum of strings/clusters containing one heavy flavour and a u or d quark at the other end is shown in Fig. 4.9 for two typical processes. Here we are only interested in the low-mass behaviour where only few primary hadrons are produced. (Secondary decays, of everything from ρ to B^*, is not considered here.) In the high mass region traditional string fragmentation should work well. Technically, the description is split into clusters, giving one or two hadrons, and strings, giving two or more. In total, the area under the curve in Fig. 4.9 splits into these four contributions. The transition from one to two hadrons comes in a set of steps, somewhat smeared e.g. by the ρ Breit-Wigner shape. That from two to three particles is continuous, but still slightly tailor made. Only beyond that is the multiplicity determined fully dynamically, by fragmenting off hadrons of random energies until all has been used up.

The mass spectrum near threshold, and thus the amount of collapses to a single hadron, is sensitive to a large number of parameters, such as the heavy

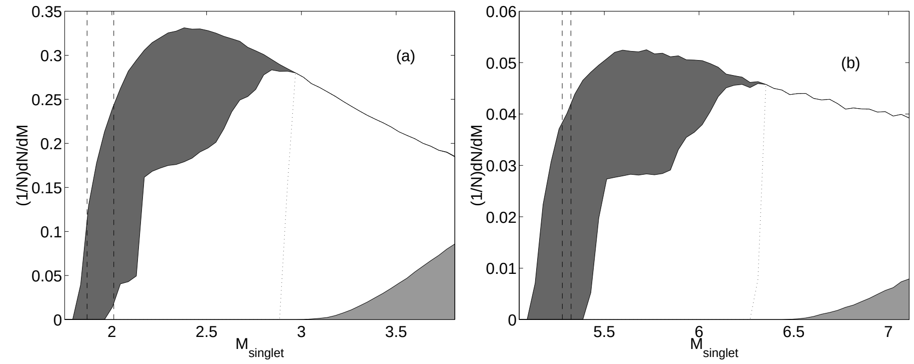

Figure 4.9: The fate of a cluster/string as a function of its mass, (a) for charm in π^-p collisions with a π^- beam momentum of 500 GeV, and (b) for bottom in p$\overline{\text{p}}$ collisions at 2 TeV. The full curve represents the original mass spectrum, for simplicity only from pair creation. Clusters within the gray area to the left collapse to a single particle, predominantly the D/D* or B/B* states indicated by dashed vertical lines. The white middle area gives two primary hadrons, with cluster decay to the left of the dotted curve and with string fragmentation to the right. The rightmost gray area corresponds to the production of three or more primary hadrons from the string.

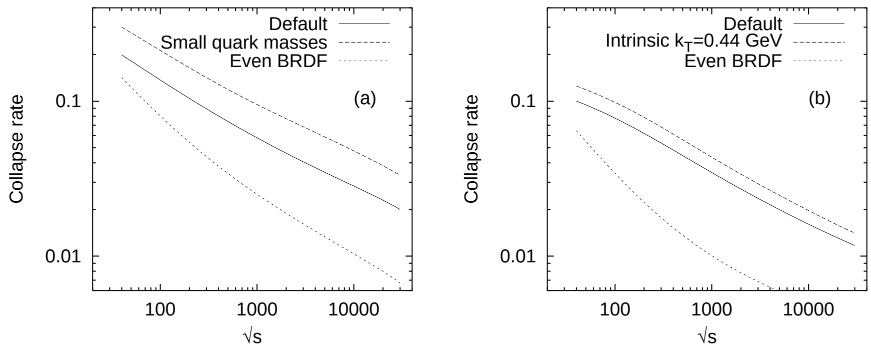

Figure 4.10: The average number of cluster collapses to a single heavy hadron per heavy-quark event, for (a) charm and (b) bottom in a pp collision as a function of $E_{\text{CM}} = \sqrt{s}$. For simplicity, only pair creation is included.

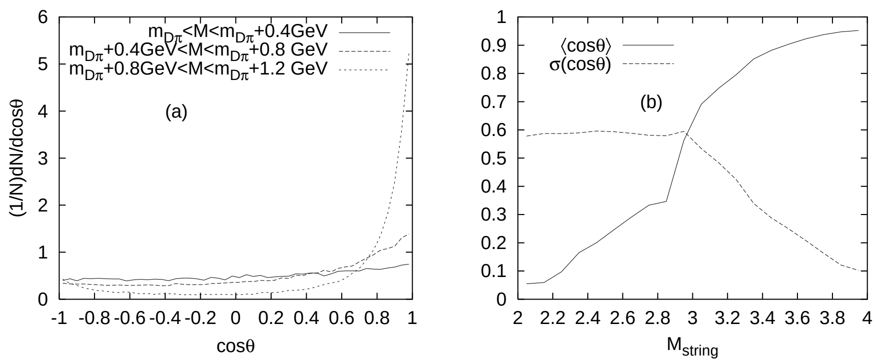

Figure 4.11: Direction of a D/D* hadron in the decay of a c$\overline{\mathrm{d}}$ string/cluster at rest. (a) The distribution $\mathrm{d}n/\mathrm{d}(\cos\theta)$, with θ the angle between the c and D/D*, for a few masses. (b) $\langle\cos\theta\rangle$ and $\sigma(\cos\theta)$ as a function of the string/cluster mass.

and light quark/diquark masses, the average primordial $k_\perp$, and the beam-remnant description [10]. Some of these are constrained by information from other processes, but a significant uncertainty remains. By introducing some piece of experimental data, such as the flavour asymmetries in π^-p collisions, a reasonable overall set of parameters has been found. The energy dependence of the collapse rate is then predicted, Fig. 4.10. The drop with larger energies is a natural consequence of the string mass spectrum then extending to larger values. The collapse rate can be shifted up or down e.g. by varying the charm mass, and shifted in shape by the beam-remnant description, but always follows the same qualitative behaviour. No input has been used from B physics, so here measurements would directly test the universality of the model. Note that the collapse rate is expected to be lower for bottom than for charm, since the mass spectrum near threshold scales roughly with m/m_Q, i.e. the bulk of the mass spectrum is higher above threshold for heavier quarks, while the upper limit for collapse goes like m_Q+constant.

The transition between the cluster and string two-hadron scenarios is purely artificial, and in the best of worlds the treatments should smoothly match at the crossover. In the new Pythia version, an attempt has indeed been made to ensure that. Specifically, the cluster decays anisotropically in a fashion that should mimic the string scheme for the larger cluster masses. We have studied the angular distributions in the transition region and found this to be reasonably well fulfilled, Fig. 4.11.

When a cluster collapses to a single hadron, energy and momentum is redistributed between this system and the rest of the event. The mass shift in the

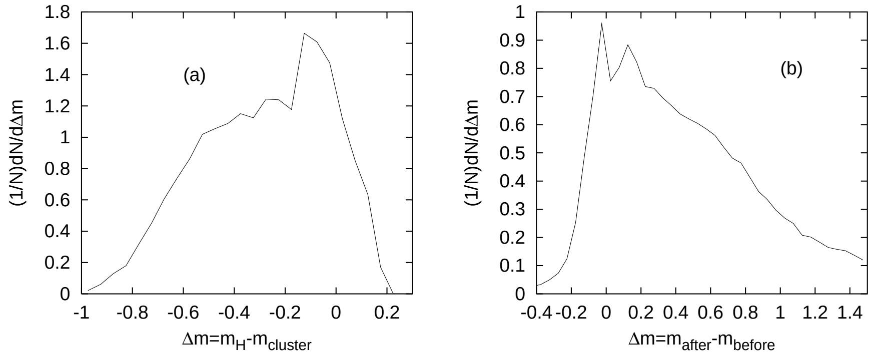

Figure 4.12: Distribution of mass shifts induced by the collapse of clusters to a single charm hadron, in π^-p collisions with a π^- beam momentum of 500 GeV, and for simplicity only including pair creation. (a) For the collapsing system, i.e. $\Delta m = m_{\mathrm{H}} - m_{\mathrm{cluster}}$. (b) For the string taking the momentum recoil, $\Delta m = m_{\mathrm{after}} - m_{\mathrm{before}}$.

collapsing cluster is implicit in the shape of the leftmost gray area in Fig. 4.9, and an explicit illustration is given in Fig. 4.12a. With the current default set of quark masses and form of the two-particle threshold, it is more likely that the produced hadron has a smaller mass than the original cluster. For lower quark masses, it is possible to reverse this asymmetry, but then at the price of a cluster collapse rate in excess of what is indicated by data. The string system that takes the energy/momentum recoil of the collapse clearly will see its mass shifted in the opposite direction, Fig. 4.12b. If the cluster and string are at relative rest, the two mass shifts are exactly compensating, but a relative motion tends to distort this, in the direction of a larger (opposite) string mass shift than cluster mass shift. The reasonably narrow distribution in Fig. 4.12b then indicates that the compensation algorithm is working well.

The colour connection between the produced heavy quarks and the beam remnants in the string model gives rise to an effect called beam remnant drag. In an independent fragmentation scenario, a quark jet fragments symmetrically around the quark direction. The light cone (along the quark axis) energy-momentum of the quark is then simply scaled by some factor, picked from a fragmentation function, in order to give the momentum of the hadron. Thus, on average, the rapidity would be conserved in the fragmentation process. This is not necessarily so in string fragmentation where both string ends contribute to the four-momentum of the produced heavy hadron. If the other end of the string is a beam remnant, the hadron will be shifted in rapidity in the direction of the beam remnant, often resulting in an increase in $|y|$. This beam-

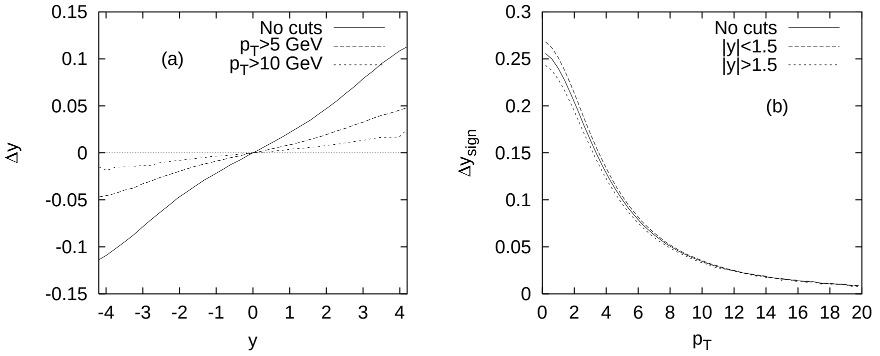

Figure 4.13: (a) Average rapidity shift Δy as a function of y for some different $p_\perp$ cuts for a $\mathrm{p\overline{p}}$ collider at 2 TeV. (b) Average rapidity shift Δy_{sign} as a function of $p_\perp$ for some different rapidity cuts.

drag is shown qualitatively in Fig. 4.13, where the rapidity shift for bottom hadrons in a 2 TeV $\mathrm{p\overline{p}}$ collision is shown as a function of rapidity and transverse momentum. We use two different measures of the rapidity shift. The first is the average rapidity shift $\Delta y = \langle y_{\mathrm{B}} - y_{\mathrm{b}} \rangle$. Here the heavy quark can be connected to a beam remnant on either side of the event, giving rise to shifts in both directions which tend to cancel in inclusive measures. A better definition is therefore

$$\Delta y_{\mathrm{sign}} = \langle (y_{\mathrm{B}} - y_{\mathrm{b}}) \cdot \mathrm{sign}(y_{\mathrm{other\ end}}) \rangle, \tag{4.13}$$

which measures the rapidity shift in the direction of the other end of the string. This shift should almost always be positive. The rapidity shift is not directly accessible experimentally, only indirectly as a discrepancy between the shape of perturbatively calculated quark distributions and the data.

High-$p_\perp$ Asymmetries

There is another possible asymmetry which occurs at large transverse momentum, involving the collapse and drag of scattered valence quarks and heavy quarks produced by gluon splitting in the parton shower. As an illustration, consider Fig. 4.14 where a valence u quark is scattered to high transverse momentum in a high energy pp collision. In such high-$p_\perp$ jets, parton showering will be profuse. If a gluon close to the scattered u quark splits into a heavy quark pair, the heavy antiquark could be in a colour singlet system together with the scattered u quark. If this singlet has a small mass it could collapse into a single heavy hadron. Heavy hadrons with its light quark constituent in common with the beam will thus be favoured. The effect then is due to the

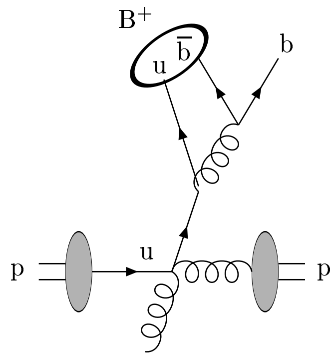

Figure 4.14: Illustration of the high-$p_\perp$ asymmetry.

asymmetry in the composition of jet flavours. At reasonably low $p_\perp$, where gluon (and second to that seaquark) jets dominate, effects therefore are vanishingly small.

This mechanism was studied in [36] and the size of the effect was found to be at the 10^{-3} level. Here we would like to study if the modifications to the model has changed this result. To increase the effectiveness we study high-$p_\perp$ quark jets in a 14 TeV pp collision and look at B mesons produced within the jets. To be specific, and hint at a possible experimental procedure to study the effect, we generate events containing the subprocess $\mathrm{qq}' \to \mathrm{qq}'$ (where q is a scattered valence quark) with $\hat{p}_{\perp,min} > 500$ GeV and look for events containing two high-$p_\perp$ jets. We use a cone algorithm to find the jets and then look for B mesons within these jets which carry at least 20% of the jet $E_\perp$. The asymmetry between B^0 and $\overline{\mathrm{B}}^0$ fulfilling these criteria was found to be 0.019 ± 0.005 and the asymmetry between B^+ and B^- 0.011 ± 0.005. The size of possible collapse asymmetries is limited by the probability for a b hadron within a jet to be produced in a collapse between a scattered valence quark and a b quark. This probability was found to be at the 10^{-3} level. This indicates that another mechanism is at play giving rise to a larger asymmetry. Furthermore, the two asymmetries above might have been expected to be of opposite sign, by equality between the number of b and $\overline{\mathrm{b}}$ quarks, at least if strangeness and baryon production can be neglected.

A possibility is that gluon splittings on the perimeter of the jet-cone give rise to $\mathrm{b}\overline{\mathrm{b}}$ pairs where the $\overline{\mathrm{b}}$ is colour connected to the scattered valence quark and the b is connected to the beam remnant diquark. In the string fragmentation process the $\overline{\mathrm{b}}$ could be dragged towards the scattered high-$p_\perp$ quark at the centre of the jet and the b towards the low-$p_\perp$ beam remnant, i.e. away from the jet, thus lowering the rate of $\overline{\mathrm{B}}^0$ and B^- within the jet and at the same time giving rise to a slightly harder $p_\perp$ spectrum for leading B mesons at high $p_\perp$. This is simply a variation of the drag effect already discussed, only this time the drag is in the transverse direction instead of the longitudinal one.

The total asymmetry then is a convolution of the asymmetry in the composition of jet flavours with the asymmetry in the b hadronization mechanisms. To get an estimate of the total asymmetry the result above must be diluted with all other non-asymmetry-generating QCD processes contributing to high-$p_\perp$ jets containing B mesons, e.g. $\mathrm{gg} \to \mathrm{gg}$ and flavour excitation. The ratio between the cross sections for producing a B meson within a valence quark jet and within any jet is approximately 0.035 in this specific case, so the diluted $\mathrm{B}^0/\overline{\mathrm{B}}^0$ asymmetry is $(6.5 \pm 1.7) \cdot 10^{-4}$. The lesson to be learned is that asymmetries can turn up also when not expected and will depend on the procedure used in studying the effects, like jet $p_\perp$, jet clustering algorithms, and B hadron selection criteria.

4.4 Applications

In this section we apply the model presented in the preceding sections to some typical current and future experiments at both small and large energies. No attempt will be made to be exhaustive, instead different examples will be picked as illustrations of the basic ideas. At low energies the most striking effect is the flavour asymmetries already observed in several experiments [4, 5, 6, 7, 8]. At large energies the most important aspect may be the beam drag effect, suggested in HERA data both for photoproduction [37] and deep inelastic scattering (DIS) [38].

Since the model is available in Monte Carlo form, further studies are left to the interested reader. However, there are some caveats. In particular, nuclear-target effects are not simulated. Instead such a target has to be represented by a single proton or neutron, with total cross sections suitably rescaled. One does not expect large nuclear effects in the heavy-flavour production characteristics, but effects may be non-negligible.

4.4.1 Fixed-target π^-p

Charm production in fixed-target π^-p collisions was already studied in [10, 42], but only using the pair creation mechanism of charm production. Here we will extend the results to the other production mechanisms and to correlations between the two charm hadrons in the event.

We see from Fig. 4.4 that gluon splitting does not give a significant contribution to the total charm cross section for fixed-target energies around 30

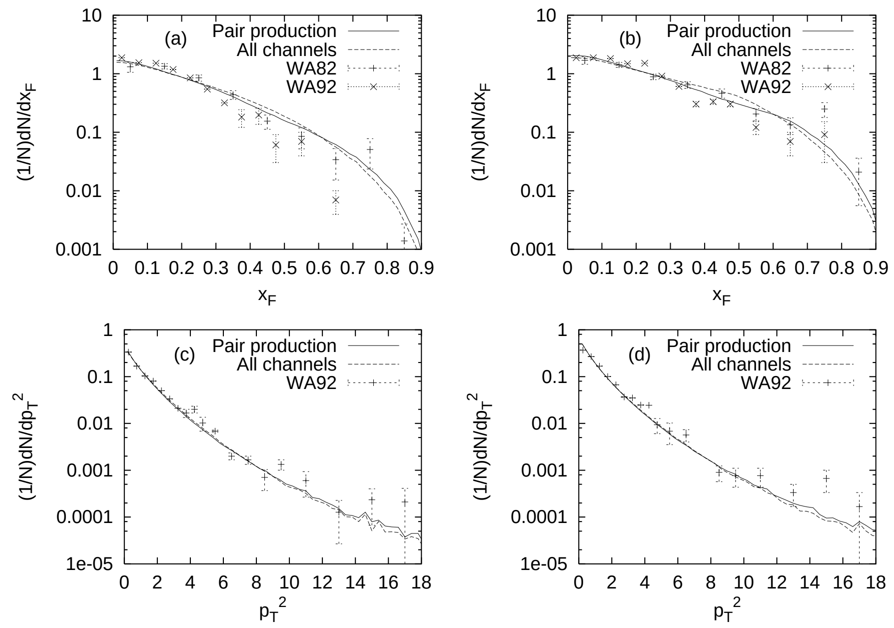

Figure 4.15: D^+/D^- meson spectra in a π^-p collision with $\sqrt{s} = 26$ GeV. (a) Single D^+ x_F distributions. (b) Single D^- x_F distributions. (c) Single D^+ $p_\perp^2$ distributions. (d) Single D^- $p_\perp^2$ distributions. The distributions are normalized to the sum of the experimental D^+ and D^- cross sections in each case.

GeV. Flavour excitation, on the other hand, gives a contribution to charm production which is as large as the pair production one even at these low energies. Fig. 4.15 shows the single heavy hadron x_F and $p_\perp^2$ distributions as predicted by the model, using the default parameters, compared to data from the WA82 [5] and WA92 [6] experiments. The leading order pair creation result and the result with all production channels added together are shown separately. The agreement with data is reasonable, though the x_F spectra are slightly harder than the data, especially for D^+ which is non-leading. The resulting asymmetry as a function of x_F and $p_\perp^2$ is shown in Fig. 4.16. The data are taken at slightly different energies but the energy dependence of the model is small within the experimental energy range. This seems to be true also for the data. As expected from the study in Section 4.3.1, single charm spectra and asymmetries are not significantly altered by the addition of flavour excitation and gluon splitting.

Fig. 4.17 shows the correlation in ϕ, the angle between D^+ and D^- in the

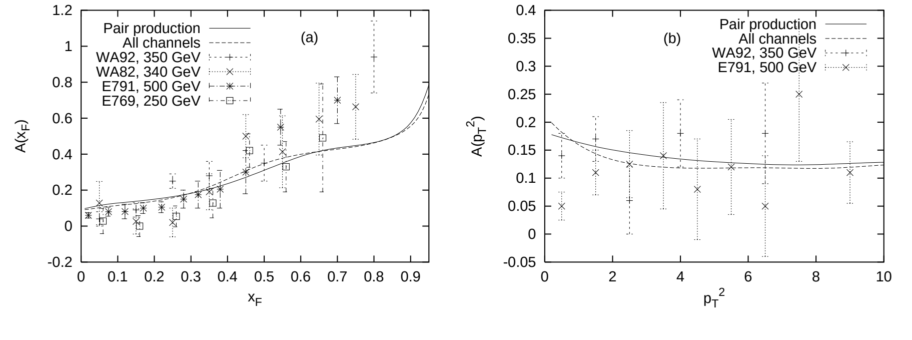

Figure 4.16: The resulting asymmetry as a function of $x_{\rm F}$ and $p_\perp^2$. The theoretical curves are model results for a 340 GeV π^- beam on a proton target ($\sqrt{s} = 26$ GeV).

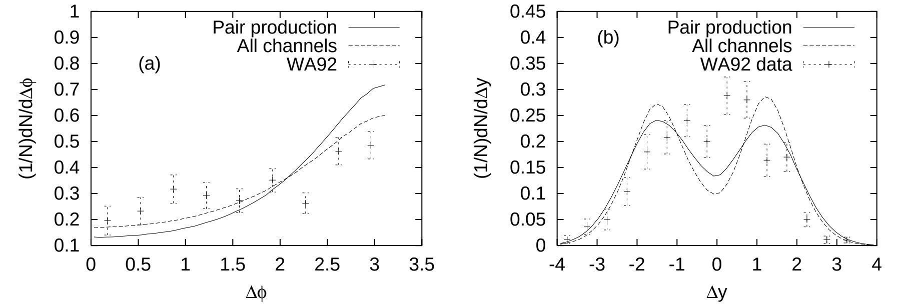

Figure 4.17: Correlations between D^+ and D^- when at least one D meson is produced with $x_{\rm F} > 0$ for a π^-p collision with $\sqrt{s} = 26$ GeV. The figure shows the distribution of (a) $\Delta\phi = |\phi_{\mathrm{D}^+} - \phi_{\mathrm{D}^-}|$ and (b) $\Delta y = y_{\mathrm{D}^+} - y_{\mathrm{D}^-}$. The distributions are normalized to the total $\mathrm{D}^+\mathrm{D}^-$ cross section in each case. The data is taken from the WA92 experiment [39].

transverse direction, and rapidity, y compared to data from the WA92 experiment [39]. The model prediction for correlations is more sensitive to the addition of flavour excitation and gluon splitting than single charm spectra are, again as expected from Section 4.3.1. In this case the description of data is improved for the transverse correlation ($\Delta\phi$) but not for the longitudinal (Δy) one. The large separation in the rapidity distribution is a consequence of the colour connection between the produced charm quarks and the beam remnants, which tend to shift the charm momenta in the direction of the respective

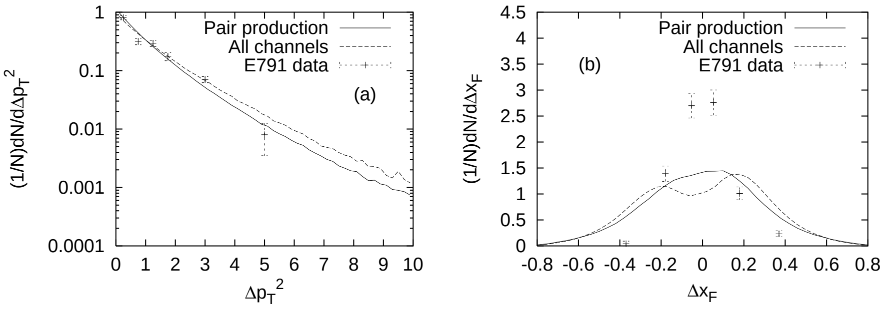

Figure 4.18: Correlations between D and $\overline{\mathrm{D}}$ mesons when both are produced with rapidity $-0.5 < y < 2.5$ for a π^-p collision with $\sqrt{s} = 30$ GeV. The figure shows the distribution of (a) $\Delta p_\perp^2 = |p_{\perp,\mathrm{D}}^2 - p_{\perp,\overline{\mathrm{D}}}^2|$ and (b) $\Delta x_\mathrm{F} = x_{\mathrm{F,D}} - x_{\mathrm{F},\overline{\mathrm{D}}}$. The distributions are normalized to the total $\mathrm{D}\overline{\mathrm{D}}$ cross section in each case. The data is taken from the E791 experiment [40].

beam remnant, thus increasing the rapidity separation. The same pattern is repeated when comparing correlation distributions to the E791 collaboration [40] in Fig. 4.18.

There are two mechanisms which could decrease the rate of connection. The first is gluon splitting into light quarks ($\mathrm{g} \to \mathrm{q}\overline{\mathrm{q}}$) in the parton shower and the other is colour reconnections [33, 34]. Gluon splitting would split the string in two and each would then hadronize independently. The memory of the colour connection is decreasing for each splitting of the string, thus decreasing the drag in the direction of the beam remnants. However, at these low energies the phase space for gluon splitting is limited. Colour reconnection by soft gluon exchange could change the colour structure of the event, thus making the charm quark lose its colour connection to the beam remnant. In the simplest scenario the charm quark pair could be reconnected to form a $\mathrm{c}\overline{\mathrm{c}}$ colour singlet, causing them to pull each other closer, resulting in a drastic decrease in $\langle \Delta y \rangle$. However, this mechanism would increase the production of J/ψ from collapses of low-mass $\mathrm{c}\overline{\mathrm{c}}$ colour singlet systems. Given the experimental ratio of J/ψ to $\mathrm{D}\overline{\mathrm{D}}$ production, $\sigma(\mathrm{J}/\Psi)/\sigma(\mathrm{D}\overline{\mathrm{D}}) \sim 0.02$ [41], and a collapse probability of $\sim$50% in reconnected events (not all to J/Ψ), the colour reconnection probability would thus be limited to 5 – 10 %. More complicated colour reconnections could be imagined, involving also gluons from the parton shower, where the charm quarks are not always in a colour singlet but still not connected directly to the beam remnants. This kind of more sophisticated colour reconnection models have been used with some success to describe J/ψ production and rapidity gaps in hadronic collisions and DIS [34]. The colour reconnection rates needed to

	$\frac{\sigma(D^+,D^-)}{\sigma(D^0,\overline{D}^0)}$	$\frac{\sigma(D_s^+,D_s^-)}{\sigma(D^0,\overline{D}^0,D^+,D^-)}$	$\frac{\sigma(D^-)}{\sigma(D^+)}$	$\frac{\sigma(D^0)}{\sigma(\overline{D}^0)}$
Model	0.33	0.11	1.39	0.94
Experimental average [6]	0.415	0.129	1.35	0.93

Table 4.1: Cross section ratios for π^-p collisions around 26 GeV.

describe the longitudinal correlations would also significantly soften the single charm distributions as well as lower the asymmetry. This is not favoured by the data so in the following we only consider single heavy quark distributions which are well described by the model.

We also compare results on some cross section ratios shown in Table 4.1 and again the description is reasonable but not perfect. The cross sections are interrelated by several model aspects. Consider e.g. the ratio of D_s to D_q. The main parameter that determines the rate of strangeness production in the fragmentation is the ratio between u, d and s production, which by default is set to 1:1:0.3. This number has been fitted to e^+e^-data and can not be changed appreciably. The D_s production ratio is also sensitive to the collapse rate of colour singlets containing charm and a light quark from a beam remnant. A large collapse rate decreases the ratio, because D_s is depleted in favour of D_q when the beam consists of non-strange particles (like in this case π^-).

To summarize, we find good agreement with several fixed target experiments when it comes to single charm spectra and asymmetries. The only case where the model does not perform well is for longitudinal correlations. Similar results were obtained [42] in comparisons with the E791 experiment [40]. In that study the contradiction between single charm and correlation data from different experiments was observed, a problem that as of yet has not been resolved, as we have seen.

4.4.2 HERA-B

The HERA-B experiment at DESY is a fixed-target experiment built especially for bottom studies. The experiment will study pA collisions at a centre-of-mass energy of about 40 GeV. It is therefore an ideal experiment to test the results of Section 4.4.1 for bottom quarks. Predictions for $B\overline{B}$ asymmetries and spectra follow directly from the model using the new updated set of parameters and hadronization mechanisms. The HERA-B experiment collides protons with nuclei but we do not include any simulation of nuclear effects. We take into account the neutrons in the nuclei by simulating pp and pn events separately and use the mean to produce the plots. The only missing pieces are then the bottom quark mass and the proton beam remnant distribution. By the simple ansatz of eq. (4.3) we obtain $m_b = 4.8$ GeV. The BRDF of the proton is

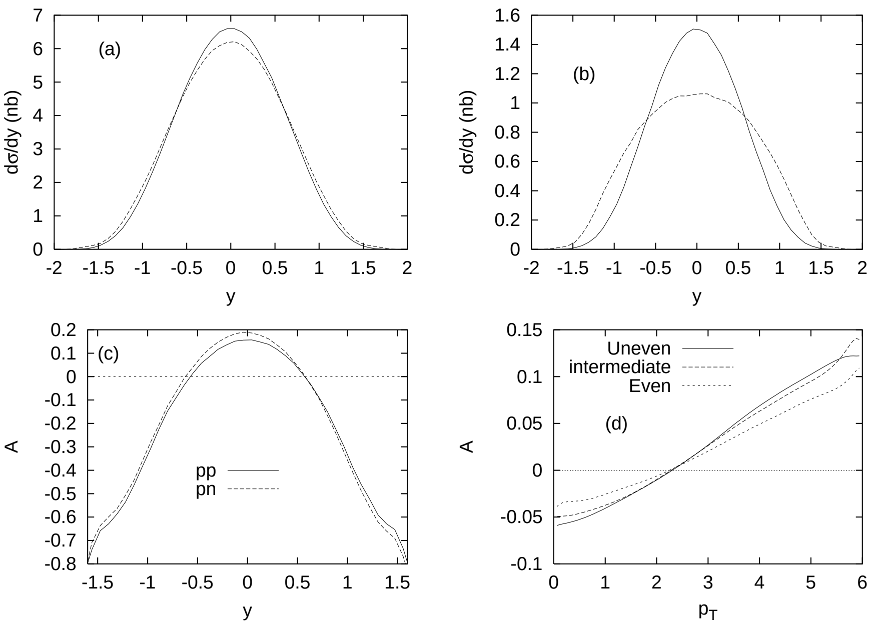

Figure 4.19: Bottom production in a pA collision at HERA-B energies, neglecting nuclear effects. (a) Rapidity distribution of bottom quarks (full) and the B hadrons produced from them (dashed). (b) Rapidity distribution of B^0 (full) and $\overline{\mathrm{B}}^0$ (dashed). (c) The asymmetry $A = \frac{\sigma(\mathrm{B}^0)-\sigma(\overline{\mathrm{B}}^0)}{\sigma(\mathrm{B}^0)-\sigma(\overline{\mathrm{B}}^0)}$ as a function of rapidity comparing pp and pn collisions. (d) The asymmetry as a function of $p_\perp$ for three different parameterizations of the BRDF of the proton. For simplicity, only pair production is included.

more problematic because there is no fundamental understanding of its structure. There are some indications that an even sharing of energy-momentum is favoured by experiments [8, 43]. We have tried different parameterizations but found no significant qualitative differences (see e.g. Fig. 4.19).

Fig. 4.19 shows the distribution of bottom mesons at HERA-B, showing both the size of the drag effect and asymmetries. The asymmetry is significant at all rapidities, not only large ones, and can reach as high as 20% even in the central rapidity region. When the kinematical limit at large rapidities is approached, the asymmetry changes sign for small $p_\perp$ because of the drag-effect; b quarks connected to diquarks from the proton beam remnant which carry most of the remnant energy often produce $\overline{\mathrm{B}}^0$ hadrons which are shifted

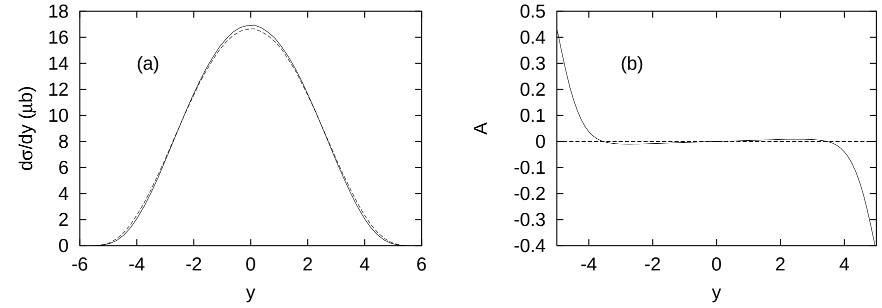

Figure 4.20: Bottom production at the Tevatron. (a) Rapidity distribution of bottom quarks (full) and the B hadrons produced from them (dashed). (b) The asymmetry $A = \frac{\sigma(\mathrm{B}^0)-\sigma(\overline{\mathrm{B}}^0)}{\sigma(\mathrm{B}^0)-\sigma(\overline{\mathrm{B}}^0)}$ as a function of rapidity. For simplicity, only pair production is included.

more in rapidity than the B^0's are. Cluster collapse, on the other hand, tend to enhance the production of 'leading' particles (in this case B^0) so the two mechanisms give rise to asymmetries with different signs. Collapse is the main effect at central rapidities while eventually at very large y, the drag effect dominates. This is also reflected in the $p_\perp$ dependence of the asymmetry which exhibits a sign shift at small $p_\perp$. The $p_\perp$ dependence is, however, partly a consequence of the fact that large $p_\perp$'s imply small $|y|$. Compared to pp, the asymmetry is slightly larger for pn collisions in the negative rapidity region. This is a natural consequence of the larger amount of d quarks in the neutron beam remnant.

4.4.3 The Tevatron Collider

The Tevatron $\mathrm{p\overline{p}}$ collider operating at CM energies up to 2 TeV represent a significant step up the energy ladder and offers a good opportunity to check the energy dependence of our results. We first show some generic distributions for the Tevatron and then consider a scenario where very forward, low-$p_\perp$ bottom hadrons can be detected. We use $2.5 < |y| < 4$ and $p_\perp < 5$ GeV. This would be ideal for studying the drag effect which is inherently a low-$p_\perp$/high-y phenomenon, see Fig. 4.13.

Fig. 4.20 shows the distribution of bottom quarks and the hadrons produced from them, as well as the asymmetry between B^0 and $\overline{\mathrm{B}}^0$ without any kinematical cuts. The trend is similar to that of HERA-B, but the asymmetry is antisymmetric because of the asymmetry of the initial state. Therefore the asymmetry is zero at y=0 and increasing in different directions for

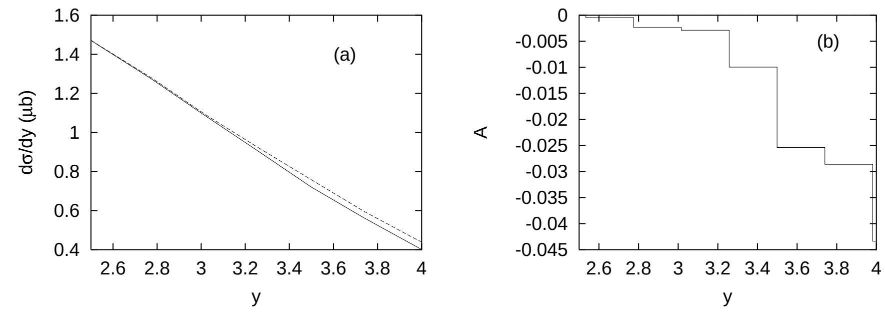

Figure 4.21: Bottom production at the Tevatron for $2.5 < |y| < 4$ and $p_\perp < 5$ GeV. (a) B^0 (full) and $\overline{\mathrm{B}}^0$ (dashed) rapidity spectra. (b) The asymmetry $A = \frac{\sigma(\mathrm{B}^0)-\sigma(\overline{\mathrm{B}}^0)}{\sigma(\mathrm{B}^0)-\sigma(\overline{\mathrm{B}}^0)}$ as a function of rapidity. For simplicity, only pair production is included.

increasing/decreasing rapidities. As expected from Fig. 4.10, the integrated asymmetry has decreased significantly.

In Fig. 4.21 we introduce cuts in order to study the region of large rapidities and small $p_\perp$. $\overline{\mathrm{B}}^0$ is shifted slightly more in the direction of the beam remnant than B^0, but the size of the effect is quite small, approaching 4% at very large rapidities. Still, if large precision is desired in CP violation studies, this effect could be non-negligible.

4.4.4 LHC

The difference between the Tevatron and the LHC collider is mainly that the energy at the LHC is one order of magnitude larger and both colliding particles are protons. Due to the similarities we only give some generic results on asymmetries and try to assess the theoretical uncertainty of the model by looking at some parameter variations.

Fig. 4.22 shows the asymmetry between B^0 and $\overline{\mathrm{B}}^0$ as a function of y for several $p_\perp$ cuts in the string model. The asymmetry is essentially zero for central rapidities, where the beam remnant flavour content is not felt so much. At intermediate rapidities it is then positive (except at small $p_\perp$) only to turn negative at larger rapidities. The reason is the same as for HERA-B, but here the switch over is closer to the kinematical limit at large rapidities.

In Table 4.2 we study the parameter dependence of the asymmetry by looking at the integrated asymmetry for different kinematical regions using three different parameter sets:

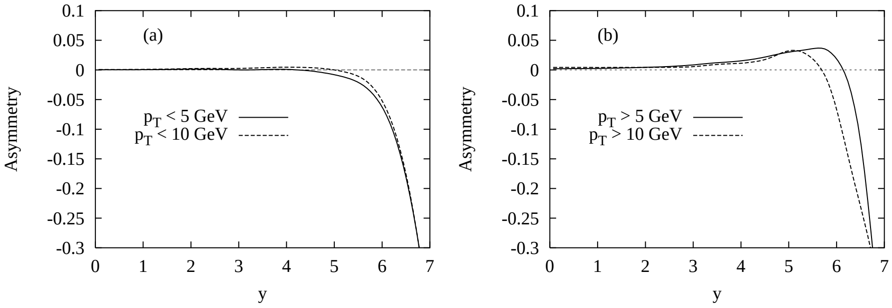

Figure 4.22: The LHC asymmetry, $A = \frac{\sigma(\mathrm{B}^0)-\sigma(\overline{\mathrm{B}}^0)}{\sigma(\mathrm{B}^0)+\sigma(\overline{\mathrm{B}}^0)}$, as a function of rapidity for different $p_\perp$ cuts: (a) $p_\perp < 5, 10$ GeV and (b) $p_\perp > 5, 10$ GeV using parameter set 1 as described in the text. For simplicity, only pair production is included.

Cuts $\rightarrow$ Parameters	$\lvert y\rvert < 2.5$ $p_\perp > 5$ GeV	$3 < \lvert y\rvert < 5$ $p_\perp > 5$ GeV	$\lvert y\rvert > 3$ $p_\perp < 5$ GeV
Set 1	0.003(1)	0.015(2)	−0.008(1)
Set 2	−0.000(2)	0.009(3)	−0.005(2)
Set 3	0.013(2)	0.020(3)	−0.018(2)

Table 4.2: Parameter dependence of the asymmetry in the string model. The statistical error in the last digit is shown in parenthesis (95% confidence). For simplicity, only pair creation is included.

- **Set 1** is the new default as described in Section 4.2.
- **Set 2** The same as Set 1 except it uses simple counting rules in the beam remnant splitting, i.e. each quark get on average one third of the beam remnant energy-momentum.
- **Set 3** The old parameter set, before fitting to fixed-target data, is included as a reference. This set is characterized by current algebra masses, lower intrinsic $k_\perp$, and an uneven sharing of beam remnant energy-momentum.

We see that in the central region the asymmetry is generally very small whereas for forward (but not extremely forward) rapidities and moderate $p_\perp$ the asymmetry is around 1–2%. In the very forward region at small $p_\perp$, drag effects dominates, which can be seen from the change in sign of the asymmetry. The asymmetry is fairly stable under moderate variations in the parameters even though the difference between the old and new parameter sets (Set 1 and 3) are large in the central region. Set 1 typically gives rise to smaller asymmetries. Note also that asymmetries on the perturbative level, calculated to NLO [12], could become relatively more important at LHC energies, where the collapse asymmetries are small. Other non-perturbative effects, such as intrinsic bottom, are also expected to be small at LHC energies [44].

To summarize, we find small asymmetries at the LHC except at large rapidities. Unless the other b in the event is unambiguously tagged, the asymmetry is still not completely negligible for high-precision CP asymmetry studies, especially at LHC-B.

4.4.5 Photoproduction

The model can also be used in the photoproduction of heavy quarks in γp collisions. Here we wish to apply the model to γp physics at HERA. The asymmetries are small in this case because of the high energy and the flavour neutral photon beam. Instead we study beam-drag effects, consequences of the photon structure and higher-order effects.

The photon is a more complicated object than a hadron because it has two components, one *direct* where the photon interacts as a whole and one *resolved* where it has fluctuated into a $\mathrm{q\overline{q}}$ pair before the interaction. This will result in very different event structures in the two cases. This study is constrained to real photons (photoproduction) as modeled by Schuler and Sjöstrand [45] and implemented in the PYTHIA [17] event generator. We include the photon flux and use cuts close to the experimental ones. We first examine the leading-order charm spectra for direct and resolved photons, estimate the cross section in the two cases, and study how the fragmentation process alters the charm spectra in the string model. Then we add flavour excitation and gluon splitting and find that also in this case they give a significant contribution to the charm cross section, especially for resolved photons.

We consider charm photoproduction in an $\mathrm{e^{\pm}p}$ collision (820 GeV protons and 27.5 GeV electrons) with real photons ($Q^2 < 1$ GeV) and rather large energy in the γp CMS system ($130 < W_{\gamma\mathrm{p}} < 280$) using some different $p_\perp$-cuts. The analysis is done in the γp centre-of-mass system using true rapidity ($y = \frac{1}{2}\ln(\frac{E+p_z}{E-p_z})$) as the main kinematical variable. The photon (electron) beam is incident along the negative z-axis.

To leading order, the massive matrix elements producing charm are the fusion processes $\mathrm{g}\gamma \to \mathrm{c\overline{c}}$ (direct), $\mathrm{gg} \to \mathrm{c\overline{c}}$ and $\mathrm{q\overline{q}} \to \mathrm{c\overline{c}}$ (resolved). Fig. 4.23 shows the distribution of charmed quarks and charmed hadrons separated into these two classes. For direct photons the hadrons are shifted in the direction of the proton beam, since both charm quarks are colour-connected to the proton beam remnant. In a resolved event the photon also has a beam remnant, so the charmed hadron is shifted towards the beam remnant it is connected to. Also in this case the drag effect is a small-$p_\perp$ phenomenon.

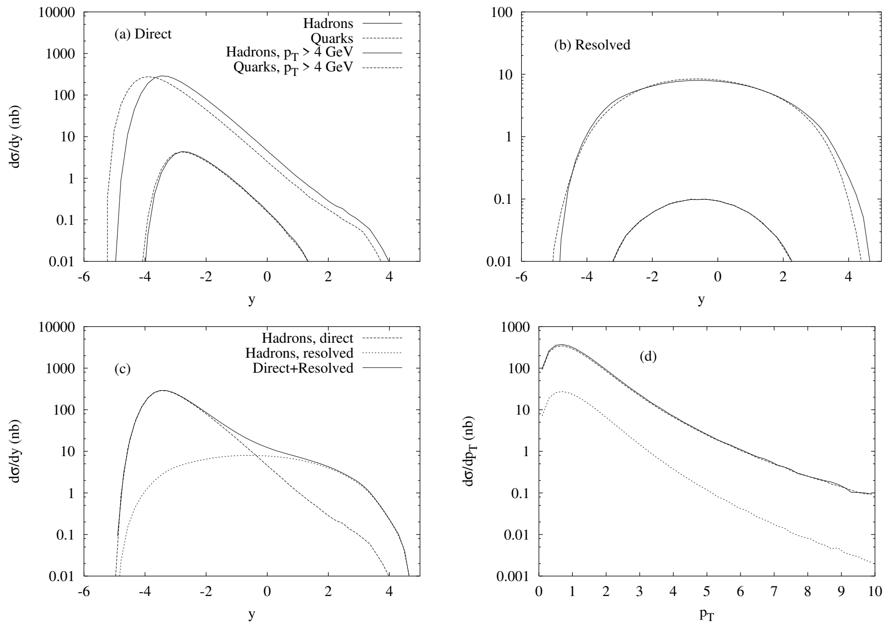

Figure 4.23: Leading order distribution of charmed hadrons and quarks in rapidity: (a) direct and (b) resolved photons. Comparison of resolved and direct processes in (c) rapidity and (d) transverse momentum.

The drag effect is illustrated in Fig. 4.24 where the average rapidity shift in the hadronization, $\langle \Delta y \rangle = \langle y_{\mathrm{Hadron}} - y_{\mathrm{Quark}} \rangle$, is shown as a function of y_{Hadron}. For direct photons and central rapidities the shift is approximately constant. The increasing shift for large rapidities is due to an increased interaction between the proton remnant and the charmed quark when their combined invariant mass is small. At large negative rapidities there is no corresponding effect because there is no beam remnant there. The drop of $\langle \Delta y \rangle$ in this region is a pure edge effect; only those events with below-average Δy can give a very negative y_{Hadron}. For resolved photons the shift is in the direction of the proton and photon beam remnants. Note that what is plotted is only the mean. The width of Δy is generally larger than the mean, so the shift can go both ways. For example the quarks at very small rapidities ($y \lesssim -5$) in Fig. 4.23b will almost all be shifted with $\Delta y > 0$ but hadrons produced there will, on the average, come from quarks produced at larger rapidities (i.e. $\Delta y < 0$). Hence the apparent contradiction with Fig. 4.24b by these edge effects. The differences between these figures and Fig. 4.13 stem exclusively from differences in

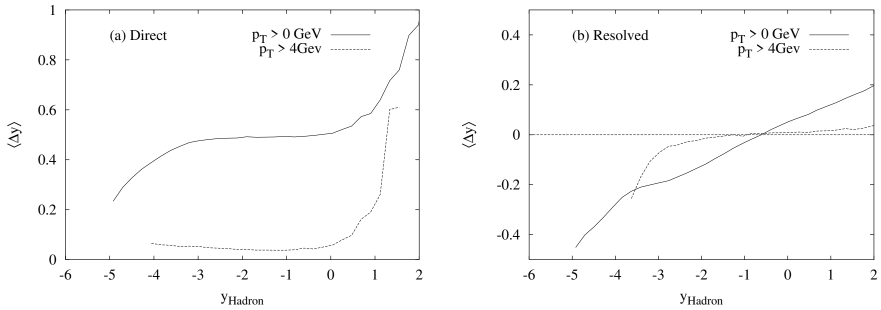

Figure 4.24: Rapidity shift $\langle \Delta y \rangle = \langle y_{\mathrm{Hadron}} - y_{\mathrm{Quark}} \rangle$ for (a) direct and (b) resolved photons as a function of rapidity.

the event topology.

At HERA energies, flavour excitation and gluon splitting give large contributions to the cross section. In Fig. 4.25 the cross section is divided into different production channels for direct and resolved photons. We note that the cross sections are of the same order of magnitude, unlike the results in lowest order, and the major contribution in the resolved case is flavour excitation. The details of course depend on the parameterization of the photon structure.

The double peak structure in the flavour excitation process for direct photons is because the charm quark in the beam remnant at low $p_\perp$ is also included. This peak disappears when a $p_\perp$ cut is introduced (Fig. 4.25c).

4.5 Summary and Outlook

In this study, we have further developed a model for the production and hadronization of heavy quarks in hadronic collisions. While the emphasis lies on the modelling of the nonperturbative phenomena, the two cannot be fully separated and therefore have to be considered in common. Thus the road we take for the production stage — using a three-component picture of pair creation, flavour excitation and gluon splitting together giving the heavy-flavour cross section — is not very economical if viewed in isolation. A next-to-leading-order matrix elements description could do the job much better, at least at current energies; only at higher energies could the possibility of extensive showering histories make a fixed-order approach inferior to our leading-log showering one. The real difference is instead that our approach also defines the environment in which the heavy quarks are produced: partons from the hard interaction, from its associated showers and from beam remnants, joined in a specific order by colour-confinement strings. And, as we have attempted to show, it is essen-

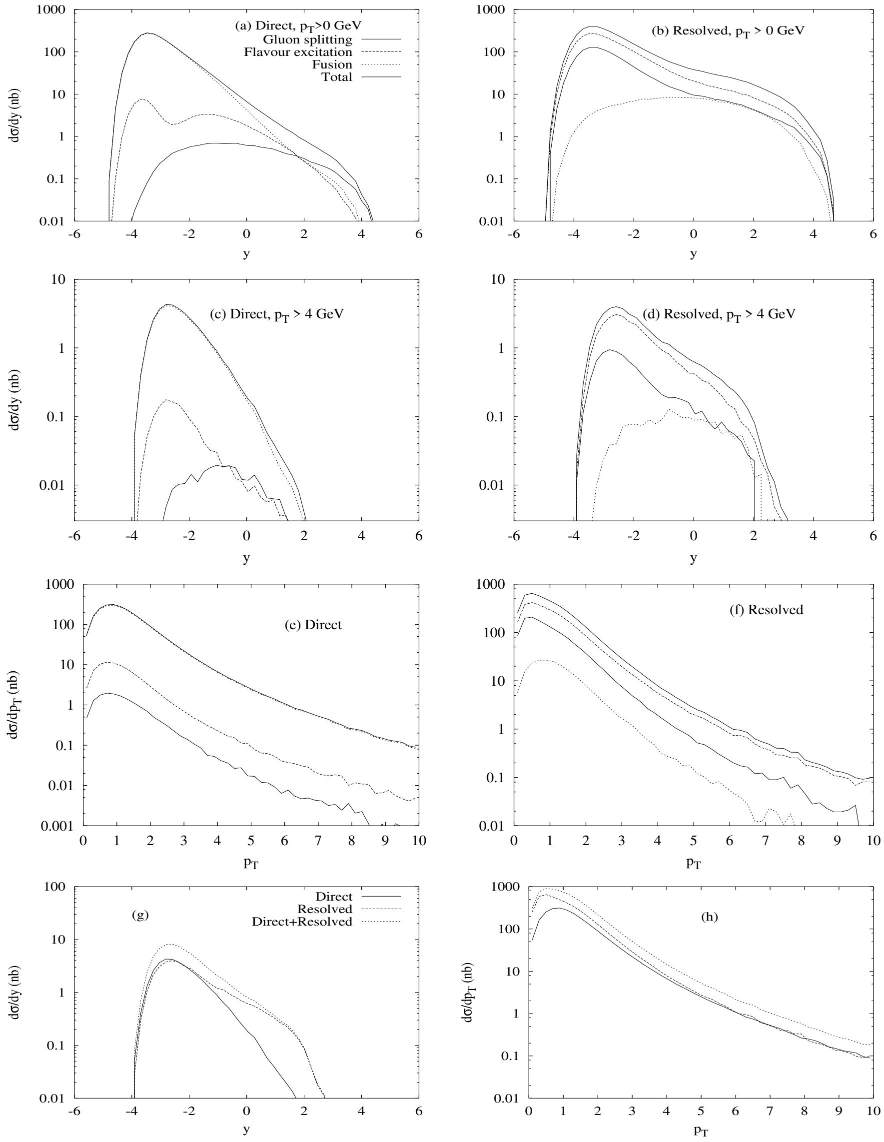

Figure 4.25: The cross section for charm hadrons divided into different production mechanisms and different photon structure. (a) Direct and (b) resolved photons with $p_\perp > 0$ GeV. (c) Direct and (d) resolved photons with $p_\perp > 4$ GeV. (e) Direct and (f) resolved photons in $p_\perp$. We add the components together for (g) rapidity ($p_\perp > 4$ GeV) and (h) transverse momentum.

tial to have that background if one wants to understand the production of the heavy hadrons, not only the heavy quarks.

This article represents the third main one on heavy flavours from the Lund group. The basic ideas were already established almost twenty years ago, so the path taken since has been evolutionary rather than revolutionary. At the time of the first study [9], neither the model nor the data were good enough more than to hint at the validity of the basic principles. In the subsequent years the modelling was gradually improved [17], and fits to some model parameters were performed by at least one experimental collaboration [8]. In our more recent study [10] it was therefore possible to start at a higher level, and introduce a technically somewhat more sophisticated re-implementation of the same basic ideas. This trend is continued in the current article, where some further model details have been improved. The main difference, however, is that we here have considered a wider range of observables, for more different production channels, and for several experimental configurations.

The basic ideas are not particularly controversial today, but the outcome may often be unexpected and counterintuitive. For instance, it is well known, from LEP and other e^+e^- machines, that the heavy hadron only takes a fraction of the heavy-quark energy, i.e. that the pull of the string in the hadronization stage 'slows down' the heavy quark. However, before one has studied the colour topology of heavy-flavour production in hadronic events, and done some trivial Lorentz boost brain gymnastics, it is not equally obvious that exactly the same phenomenon could 'speed up' the heavy quark here. Or: it is not unreasonable that a heavy quark could pick up one of the beam valence flavours to form a hadron, but the extent to which this can happen over a wide range of longitudinal and transverse momenta may come as a surprise.

The studies here have also put the finger on a few other interesting phenomena, such as:

- The extrapolation from charm to bottom quarks.
- The importance of heavy flavour production through flavour excitation and gluon splitting.
- The kinematics of backward evolution in the initial state shower.
- Scale choices in the parton shower.
- The importance of colour flow.
- The matching of cluster decay and string fragmentation of low-mass colour singlets.
- The details of the collapse mechanism.
- The choice and importance of beam remnant distribution functions.
- The choice and importance of intrinsic $k_\perp$ smearing.
- High-$p_\perp$ asymmetries.
- The influence of the photon structure.

- The limitations of the model.

While not as spectacular as the colour drag and flavour asymmetry ones above, they help to put flesh on the bones of our understanding of hadronization. Experimental results on the yet untested features clearly would be welcome.

A topic not discussed in this paper is cosmic ray physics where the momentum spectra of charm and bottom hadrons has implications for the rate of prompt leptons and neutrinos in atmospheric cascades [46]. Also here our improved modelling may affect the traditional flux calculations.

It is important to remember that the predictions can be wrong. Hopefully not in a qualitative fashion, but quite possibly in a quantitative one. For instance, it is all well to assume we can control the colour topologies at fixed-target energies, where there is a very small number of participating partons and thereby of separate string pieces. At high energies, the more extensive parton showers and especially the increased rate of multiple parton–parton interactions could well mess up our tidy picture of colour flow, and thereby of single-particle spectra and correlations. If so, we would like to believe that heavy flavours here could be used as a probe for such effects.

Of course, our approach is not the only one that has been proposed for the hadronization of heavy quarks [47]. Especially the intrinsic charm model [48] is still very actively pursued. It is not unlikely that several mechanisms may coexist, but we have also encountered no evidence to indicate that the ones outlined by us are not the dominant ones. However, as always, more data may provide new insights also in this regard.

A final reflection is that B physics will remain a major topic of study for many years to come, because of the interest in CP violation studies. Furthermore, many of these studies will require a tagging of both beauty hadrons in an event. One can therefore foresee large data sets that will allow many detailed tests, beyond the ones shown here. It also appears plausible that charm hadron samples can be extracted as a by-product, where, as we have seen, many of the predicted effects are larger. Hopefully we will therefore enjoy a gradually improved level of understanding.

References

[1] B. Andersson, G. Gustafson, G. Ingelman and T. Sjöstrand, Phys. Rep. **97** (1983) 31.

[2] C. Peterson, D. Schlatter, I. Schmitt and P. Zerwas, Phys. Rev. **D27** (1983) 105.

[3] T. Mannel, Rept. Prog. Phys. **60** (1997) 1113;
and references therein.

[4] M. Basile et al., Nuovo Cim. **A66** (1981) 129;
ACCMOR Collaboration, R. Bailey et al., Phys. Lett. **132B** (1983) 237;
NA27 Collaboration, M. Aguilar-Benitez et al., Phys. Lett. **B161** (1985) 400;
NA32 Collaboration, S. Barlag et al., Z. Phys. **C49** (1991) 555.

[5] WA82 Collaboration, M. Adamovich et al., Phys. Lett. **B305** (1993) 402.

[6] WA92 Collaboration, M. Adamovich et al., Nucl. Phys. **B495** (1997) 3.

[7] E769 Collaboration, G.A. Alves et al., Phys. Rev. Lett. **72** (1994) 812.

[8] E791 Collaboration, E.M. Aitala et al., Phys. Lett. **B371** (1996) 157.

[9] B. Andersson, H.-U. Bengtsson and G. Gustafson, Lund preprint LU TP 83–4 (1983).

[10] E. Norrbin and T. Sjöstrand, Phys. Lett. **B442** (1998) 407.

[11] B.L. Combridge, Nucl. Phys. **B151** (1979) 429.

[12] P. Nason, S. Dawson and R.K. Ellis, Nucl. Phys. **B327** (1989) 49; erratum ibid. **B335** (1990) 260;
W. Beenakker, R. Meng, G.A. Schuler, J. Smith and W.L. Van Neerven, Nucl. Phys. **B351** (1991) 507.

[13] S. Frixione, M.L. Mangano, P. Nason and G. Ridolfi, Nucl. Phys. **B431** (1994) 453.

[14] E. Laenen, J. Smith and W.L. van Neerven, Phys. Lett. **B321** (1994) 254;
N. Kidonakis and J. Smith, Phys. Rev. **D51** (1995) 6092;
M. Cacciari, M. Greco and P. Nason, J. High Energy Phys. **05** (1998) 007;
F.I. Olness, R.J. Scalise and W.-K. Tung, Phys. Rev. **D59** (1999) 014506.

[15] T. Sjöstrand, Phys. Lett. **157B** (1985) 321.

[16] DELPHI Collaboration, P. Abreu et al., Phys. Lett. **B418** (1998) 430.

[17] T. Sjöstrand, Comput. Phys. Commun. **82** (1994) 74.

[18] G. Marchesini, B.R. Webber, G. Abbiendi, I.G. Knowles, M.H. Seymour and L. Stanco, Comput. Phys. Commun. **67** (1992) 465.

[19] M.H. Seymour, Nucl. Phys. **B436** (1995) 163;
D.J. Miller and M.H. Seymour, Phys. Lett. **B435** (1998) 213.

[20] M.L. Mangano, CERN-TH/99-337, hep-ph/9911256, to appear in the Proceedings of EPS HEP '99, Tampere, Finland, 15-21 July 1999.

[21] L. Lönnblad, Comput. Phys. Commun. **71** (1992) 15.

[22] A. De Rújula, H. Georgi and S.L. Glashow, Phys. Rev. **D12** (1975) 147.

[23] CTEQ Collaboration, H.L. Lai et al., Eur. Phys J. **C12** (2000) 375.

[24] M. Glück, E. Reya and A. Vogt, Z. Phys. **C53** (1992) 651.

[25] H.-U. Bengtsson, Comput. Phys. Commun. **31** (1984) 323.

[26] E.D. Bloom and F.J. Gilman, Phys. Rev. **D4** (1971) 2901;
J.J. Sakurai, Phys. Lett. **46B** (1973) 207;
H. Fritzsch, Phys. Lett. **67B** (1977) 217;
R.A. Bertlmann, G. Launer and E. de Rafael, Nucl.Phys. **B250** (1985) 61;
and references therein.

[27] E. Braaten, S. Narison and A. Pich, Nucl. Phys. **B373** (1992) 581.

[28] Particle Data Group, C. Caso et al., Eur. Phys. J. **C3** (1998) 1.

[29] T. Sjöstrand, Nucl. Phys. **B248** (1984) 469.

[30] A. Capella and J. Tran Thanh Van, Z. Phys. **C10** (1981) 249.

[31] EMC Collaboration, M. Arneodo et al., Z. Phys. **C36** (1987) 527;
L. Apanasevich et al., Phys. Rev.**D59** (1999) 074007;
G. Miu and T. Sjöstrand, Phys. Lett.**B449** (1999) 313;
C. Bálazs, J. Huston and I. Puljak, hep-ph/0002032.

[32] T. Sjöstrand and M. van Zijl, Phys. Rev. **D36** (1987) 2019.

[33] G. Gustafson, U. Pettersson and P. Zerwas, Phys. Lett. **B209** (1988) 90;
T. Sjöstrand and V.A. Khoze, Z. Phys. **C62** (1994) 281, Phys. Rev. Lett. **72** (1994) 28;
G.Gustafson and J.Häkkinen, Z. Phys. **C64** (1994) 659;
L. Lönnblad, Z. Phys. **C70** (1996) 107;
Š. Todorova–Nová, DELPHI Internal Note 96-158 PHYS 651;
J. Ellis and K. Geiger, Phys. Rev. **D54** (1996) 1967, Phys. Lett. **B404** (1997) 230;
B.R. Webber, J. Phys. **G24** (1998) 287.

[34] A. Edin, G. Ingelman and J. Rathsman, Phys.Rev. **D56** (1997) 7317.

[35] M.L. Mangano, P. Nason and G. Ridolfi, Nucl. Phys. **B372** (1992) 295; Nucl. Phys. **B405** (1993) 507.

[36] M. Chaichian and A. Fridman, Phys. Lett. **B298** (1993) 218.

[37] H1 Collaboration, S. Aid et al., Nucl. Phys. **B472** (1996) 32;
ZEUS Collaboration, J. Breitweg et al., Eur. Phys. J. **C6** (1999) 67; hep-ex/0003018.

[38] H1 Collaboration, C. Adloff et al., Nucl. Phys. **B545** (1999) 21;
ZEUS Collaboration, J. Breitweg et al., Eur. Phys. J. **C12** (2000) 35.

[39] WA92 Collaboration, M. Adamovich et al., Phys. Lett. **B385** (1996) 487.

[40] E791 collaboration, E.M. Aitala et al., Eur. Phys. J. **C4** (1999) 1.

[41] D. Barberis, C. Gemme and L. Malferrari, in *Heavy Quarks at fixed target*, eds. H.W.K. Cheung and J.N. Butler p. 179.

[42] E. Norrbin, in *Heavy Quarks at fixed target*, eds. H.W.K. Cheung and J.N. Butler p. 228 (hep-ph/9812460).

[43] E687 Collaboration, P.L. Frabetti et al., Phys. Lett. **B370** (1996) 222.

[44] P. Nason et al., hep-ph/0003142, to appear in the Report of the "1999 CERN Workshop on SM physics (and more) at the LHC", P. Nason, G. Ridolfi, O. Schneider G.F. Tartarelli, P. Vikas (conveners).

[45] G.A. Schuler and T. Sjöstrand, Nucl. Phys. **B407** (1993) 539; Z. Phys. **C73** (1997) 677.

[46] M. Thunman, G. Ingelman and P. Gondolo, Nucl. Phys. Proc. Suppl. **B43** (1995) 274; Astropart. Phys. **5** (1996) 309.

[47] V. Barger, F. Halzen and W.Y. Keung, Phys. Rev. **D25** (1982) 112;
P. Mazzanti and S. Wada, Phys. Rev. **D26** (1982) 602;
G.I. Lykasov and M.N Sergeenko, Z. Phys. **C56** (1992) 697;
R.C. Hwa, Phys. Rev. **D51** (1995) 85;
V.A. Bednyakov, Mod. Phys. Lett. **68** (1995) 61;
A.K. Likhoded and S.R. Slabospitsky, hep-ph/9710476;
E. Cuautle, G. Herrera and J. Magnin, Eur. Phys. J. **C2** (1998) 473;
O. Piskounova, Nucl. Phys. **B50** (Proc. Suppl.) (1996) 179;
J. Dias de Deus and F.O. Durães, hep-ph/9803449.

[48] S.J. Brodsky, P. Hoyer, C. Peterson and N. Sakai, Phys. Lett. **93B** (1980) 451;
R. Vogt and S.J. Brodsky, Nucl. Phys. **B478** (1996) 311;
G. Ingelman and M. Thunman, Z. Phys. **C73** (1997) 505.

QCD Radiation off Heavy Particles

Paper V

QCD Radiation off Heavy Particles

Emanuel Norrbin and Torbjörn Sjöstrand
Department of Theoretical Physics
Lund University

LU TP 00–42 (hep-ph/0010012)
Submitted to *Nuclear Physics* **B**

We study QCD radiation in decay processes involving heavy particles. As input, the first-order gluon emission rate is calculated in a number of reactions, and comparisons of the energy flow patterns show a non-negligible process dependence. To proceed further, the QCD parton shower language offers a convenient approach to include multi-gluon emission effects, and to describe exclusive event properties. An existing shower algorithm is extended to take into account the process-dependent mass, spin and parity effects, as given by the matrix element calculations. This allows an improved description of multiple gluon emission effects off b and t quarks, and also off nonstandard particles like squarks and gluinos. Phenomenological applications are presented for bottom production at LEP, Higgs particle decay to heavy flavours, top production and decay at linear colliders, and some simple supersymmetric processes.

5.1 Introduction

Heavy particles often tend to be in the focus of particle physics research. The search for new physics at the high-energy frontier is an obvious example. Not only are the hypothetical new heavy states here of interest, but often their detection relies on decay chains that involve heavy flavours. Here the b quark is the prime example. By secondary vertices or semileptonic decays it can be tagged. It is a main decay product of top, where the b tag is a standard requirement for top identification above background at hadron colliders. A light Standard Model Higgs ($m_{\mathrm{h}} \lesssim 140$ GeV) predominantly decays to $\mathrm{b\overline{b}}$, and for any Higgs state the $\mathrm{b\overline{b}}$ branching ratio is a key parameter in pinning down its nature. These tagging and identification aspects also appear in other scenarios beyond the standard model.

Many of the potentially new particles carry colour, like squarks, gluinos and leptoquarks. Also colourless states often decay to quarks. Therefore QCD radiation is unavoidable, and the large value of the α_{s} coupling implies that such radiation can be quite profuse. It is well-known, e.g. from LEP, that fixed-order perturbation theory fails to describe QCD radiation effects off light quarks: the rate of a few well separated jets can be reproduced, but the internal structure of these jets requires the resummation of multiple-gluon effects. The most successful method for achieving such a resummation is to apply the parton-shower language, where explicit final states can be generated, with full respect for energy–momentum conservation and other constraints. By introducing some low fixed cut-off scale $Q_0 \approx 1$ GeV, the very soft and nonperturbative régime of QCD can be factored off and put in a universal hadronization description, such as the Lund string fragmentation model [1]. With this approach, it is possible to obtain a quite accurate description of essentially all hadronic final-state properties of $\mathrm{e^+e^-}$ annihilation events. The physics is more complicated in a hadron collider environment, with additional effects e.g. from initial-state QCD radiation and underlying events, so the level of ambition may have to be set accordingly. However, this applies to all conceivable descriptions, so again we expect a realistic description of jets to be most easily achieved with the help of the parton-shower language.

Heavy quarks radiate less than light ones in the soft-gluon region, so in some respects QCD multiple-emission corrections are not as crucial. The b is sufficiently light that it still radiates profusely, but top and supersymmetric particles may be heavy enough that multiple-gluon emission effects are limited. Furthermore, for particles that are very short-lived, the width will provide a cut-off on soft-gluon emission [2]. So for new-particle searches, higher-order QCD effects may be less of an issue. However, whenever higher precision is required, like for a mass determination of a new state, it may still be necessary to model whatever soft-gluon emission effects there are. And, of course, the decays of these new states will bring further radiation, e.g. like $\mathrm{t} \to \mathrm{bW}^+$, where the radiation off the t and off the b become intertwined, and where width effects may become important for short-lived particles. The aim of the current article is precisely to improve the description of gluon radiation off b and c quarks as well as off heavier objects, in order to allow higher-precision physics studies.

The starting point is the calculation of a large number of first-order matrix elements, for gluon emission in decay processes, often generalizing on results already found in the literature. The processes thereby covered include gluon emission e.g. in $\gamma^*/\mathrm{Z}^0/\mathrm{h}^0/\mathrm{A}^0 \to \mathrm{b}\overline{\mathrm{b}}$ (with differences between a vector, axial vector, scalar and pseudoscalar source of the b's), $\mathrm{t} \to \mathrm{bW}^+$, and various supersymmetric reactions. Quite apart from the implementation in the shower framework, these calculations can also be used to assess the degree of (non)universality, i.e. the dependence on the colour and spin structure of the processes under identical kinematical conditions. In particular, we will show that the 'dead cone' picture can be quite misleading for the emission of more energetic gluons.

These matrix elements are taken as input to an improved version of an existing shower algorithm [3], which primarily has been used for radiation off lighter quarks and gluons. This shower algorithm tends to slightly overestimate the amount of gluon radiation for $\mathrm{e}^+\mathrm{e}^- \to \gamma^*/\mathrm{Z}^0 \to \mathrm{q}\overline{\mathrm{q}}\mathrm{g}$ when q is massless, so a simple rejection procedure can be used to match the hardest emission to the massless matrix elements. The radiation off heavier quarks is underestimated in the collinear region, however. Or, put differently, the dead cone [4] effects are exaggerated. In order to allow a corresponding approach for heavy flavours, the evolution variable therefore has been modified to bring up the emission rate. It therefore becomes possible to use the process-specific matrix elements as rejection factors also here, and furthermore to do it in all stages of the shower.

The one place where precision tests are possible is in studies of b production at LEP1 [5]. We therefore study this topic in detail here, and use it as a test bed for different possible variations of the basic shower algorithm. Other studies include Higgs, top and supersymmetric particle production and decay. Furthermore, we also include some plots to illustrate differences between gluon radiation off sources of different spin.

While not the main thrust of this article, we note that new data on gluon branching to heavy flavours, $\mathrm{g} \to \mathrm{c}\overline{\mathrm{c}}$ and $\mathrm{g} \to \mathrm{b}\overline{\mathrm{b}}$, has been presented by the LEP collaborations [5]. We therefore also discuss what implications this might have for the shower algorithm, and whether the data could be accommodated by reasonable modifications.

The plan of the article is as follows. In Section 5.2, the existing older shower algorithm is explained, together with a few intermediate variants thereof. The new approach is described in Section 5.3. A survey of the matrix-element calculations and the consequent radiation patterns is given in Section 5.4. Some applications are then presented in Section 5.5. The separate topic of gluon splitting is discussed in Section 5.6. Finally, a summary and outlook is given in Section 5.7.

5.2 Previous Models

Several shower algorithms have been proposed in the literature. Today the three most commonly used ones probably are those found in PYTHIA/JETSET [3, 6], HERWIG [7, 8] and ARIADNE [9]. The studies in this article will be based on the former one.

The PYTHIA final-state shower consists of an evolution in the squared mass m^2 of a parton. That is, emissions are ordered in decreasing mass of the radiating parton, and the Sudakov form factor [10] is defined as the no-emission rate in the relevant mass range. Such a choice is not as sophisticated as the angular one in HERWIG or the transverse momentum one in ARIADNE, but usually the three tend to give similar results for e^+e^- annihilation events. An exception, where small but significant differences were found, is the emission of photons in the shower [11]. In general, comparisons between the three are helpful in estimating a range of theoretical uncertainty, in interpretations of existing data or in predictions for the future.

One of the advantages of the PYTHIA algorithm is that a mapping between the parton-shower and matrix-element variables is rather straightforward to $\mathcal{O}(\alpha_s)$ for massless quarks, and that already the basic shower populates the full phase space region very closely the same way as the matrix element. It is therefore possible to introduce a simple correction to the shower to bring the two into agreement. Also in ARIADNE the massless matrix-element matching is straightforward. By contrast, the HERWIG angular-ordered approach does not automatically cover the full $q\overline{q}g$ phase space, which means that a subset of three-jet events are not generated at all. This leads to problems in the description of LEP data, that were overcome by separately adding the missing class of three-jet events [12], in addition to matching to the matrix elements in the allowed region. More recently, a similar approach has been applied to top decay [13], where again HERWIG did not populate the full phase space.

5.2.1 The Massless Shower

In addition to mass, the other main variable in the PYTHIA shower is z, as used in the splitting kernels. It is defined as the energy fraction taken by the first daughter in the CM frame of the event. That is, in a branching $a \to b + c$, $E_b = zE_a$ and $E_c = (1-z)E_a$. In the original choice of z, which is done at the same time as m_a is selected, the b and c masses are not yet known, and are therefore imagined massless, also in cases where either of them is known to have a non-vanishing on-shell mass. A cut-off scale $m_{\mathrm{min}} = Q_0 \approx 1$ GeV is used to constrain the allowed phase space, so that only branchings with $m_a > m_{\mathrm{min}}$ are allowed. For a massive quark, the cut-off is shifted to

$$m_{a,\mathrm{min}} = \sqrt{m_a^2 + \frac{Q_0^2}{4}} + \frac{Q_0}{2} \ . \tag{5.1}$$

The allowed z range, $z_- < z < z_+$, then becomes

$$z_\pm = \frac{1}{2}\left\{1 \pm \beta_a \Theta(m_a - m_{a,\mathrm{min}})\right\} \ , \tag{5.2}$$

with $\beta_a = |\mathbf{p}_a|/E_a$ the a velocity and $\Theta(x)$ the step function.

At a later stage of the evolution, when m_b and m_c are being selected, possibly well above Q_0, the previously found z may be incompatible with these masses. The adopted solution is to take into account mass effects by reducing the magnitude of the three-momenta $\mathbf{p}_b = -\mathbf{p}_c$ in the rest frame of a. Expressed in terms of four-momenta in an arbitrary frame, this is equivalent to

$$\begin{aligned} p_b &= (1-k_b)p_b^{(0)} + k_c p_c^{(0)} \ , \\ p_c &= (1-k_c)p_c^{(0)} + k_b p_b^{(0)} \ , \end{aligned} \tag{5.3}$$

where $p_b^{(0)}$ and $p_c^{(0)}$ are the original massless momenta and p_b and p_c the modified massive ones. The parameters k_b and k_c are found from the constraints $p_b^2 = m_b^2$ and $p_c^2 = m_c^2$:

$$k_{b,c} = \frac{m_a^2 - \lambda_{abc} \pm (m_c^2 - m_b^2)}{2m_a^2} \ , \tag{5.4}$$

with

$$\lambda_{abc} = \sqrt{(m_a^2 - m_b^2 - m_c^2)^2 - 4m_b^2 m_c^2} \ . \tag{5.5}$$

The relation between the preliminary and final energy sharing thus is given by

$$\begin{aligned} z' &= \frac{E_b}{E_a} = (1-k_b)z + k_c(1-z) \\ &= \frac{m_a^2 - \lambda_{abc} + m_b^2 - m_c^2}{2m_a^2} + \frac{\lambda_{abc}}{m_a^2} z \ , \end{aligned} \tag{5.6}$$

with $z = E_b^{(0)}/E_a$ as above. The transverse momentum $p_\perp$ of b and c with respect to the a direction is given by

$$p_\perp^2 = \frac{\lambda_{abc}^2}{m_a^2}\left\{\frac{z(1-z)}{\beta_a^2} - \frac{1-\beta_a^2}{4\beta_a^2}\right\} \ , \tag{5.7}$$

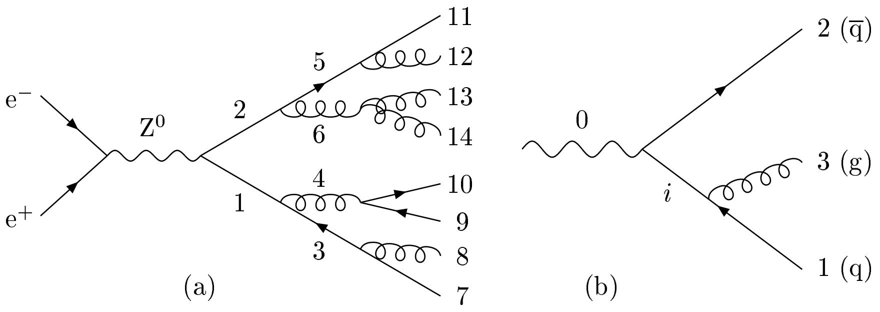

Figure 5.1: Example of showers, with the notations used in the text. (a) A generic shower. (b) A shower giving a three-jet event.

but is approximated by $p_\perp^2 \approx z(1-z)m_a^2$ when used as argument in $\alpha_{\mathrm{s}}(p_\perp^2)$ for the shower.

Angular ordering is not automatic, but is implemented by vetoing emissions that don't correspond to decreasing opening angles. The opening angle of a branching $a \to b + c$ is calculated approximately as

$$\begin{aligned} \theta &\approx \frac{p_{\perp b}}{E_b} + \frac{p_{\perp c}}{E_c} \\ &\approx \sqrt{z(1-z)}m_a \left(\frac{1}{zE_a} + \frac{1}{(1-z)E_a} \right) = \frac{1}{\sqrt{z(1-z)}} \frac{m_a}{E_a} . \end{aligned} \tag{5.8}$$

The procedure thus is the following, Fig. 5.1a. In the γ^*/Z^0 decay, the two original partons 1 and 2 are produced, back-to-back in the rest frame of the pair. In a first step, they are evolved downwards from a maximal mass equal to the CM energy, with the restriction that the two masses together should be below this CM energy. When the two branchings are found, they define m_1 and m_2 and the z values of $1 \to 3 + 4$ and $2 \to 5 + 6$. These branchings obviously have smaller opening angles than the 180° one between 1 and 2, so no angular-ordering constraints appear here. A matching procedure to the matrix element is used to correct the branchings, however, as will be described below. In subsequent steps, a pair of partons like 3 and 4 are evolved in parallel, from maximum masses given by the smaller of the mother (1) mass and the respective daughter (3 or 4) energy. Here angular ordering restricts the region of allowed z values in their branchings, but there are no matrix-element corrections. Once m_3 and m_4 are fixed, the kinematics of the $1 \to 3 + 4$ branching needs to be modified according to eq. (5.3). This is the reason why the evolution is always done for a pair of partons (whereof not both need branch further, however), and why the final kinematics of a branching is postponed to a later stage than the choice of z value.

Several other aspects of the shower could be discussed, such as the choice of non-isotropic azimuthal angles to improve the coherence description and include gluon spin effects, the possibility also to emit photons, or the option to force some branchings in order to match higher-order matrix elements [14]. These are of less interest here and thus not covered.

5.2.2 The Massless Matrix Element Correction

Let us now compare the parton-shower (PS) population of three-jet phase space with the matrix-element (ME) one, for the case of $\mathrm{e^+e^-}$ annihilation to massless quarks. With the conventional ME numbering $\mathrm{q}(1)\,\overline{\mathrm{q}}(2)\,\mathrm{g}(3)$, with $x_j = 2E_j/E_{\mathrm{CM}}$, the matrix element is of the form [15]

$$\frac{1}{\sigma_0}\frac{\mathrm{d}\sigma_{\mathrm{ME}}}{\mathrm{d}x_1\,\mathrm{d}x_2} = \frac{\alpha_{\mathrm{s}}}{2\pi}\,C_F\,\frac{x_1^2+x_2^2}{(1-x_1)(1-x_2)}\ , \tag{5.9}$$

with the colour factor $C_F = 4/3$. We have normalized to the lowest-order cross section σ_0, so that the expression can be interpreted as a probability distribution. For future reference, we will use the notation

$$\frac{1}{\sigma_0}\frac{\mathrm{d}\sigma}{\mathrm{d}x_1\,\mathrm{d}x_2} = \frac{\alpha_{\mathrm{s}}}{2\pi}\,C_F\,\frac{N(x_1,x_2,r)}{(1-x_1)(1-x_2)}\ , \tag{5.10}$$

where $r = m_{\mathrm{q}}/E_{\mathrm{CM}} = m_{\overline{\mathrm{q}}}/E_{\mathrm{CM}}$. Thus $N_{\mathrm{ME}}(x_1,x_2,0) = x_1^2 + x_2^2$.

There are two shower histories that could give such a three-jet event. One is $\gamma^*/\mathrm{Z}^0(0) \to \mathrm{q}(i)\overline{\mathrm{q}}(2) \to \mathrm{q}(1)\overline{\mathrm{q}}(2)\mathrm{g}(3)$, i.e. with an intermediate (i) quark branching $\mathrm{q}(i) \to \mathrm{q}(1)\mathrm{g}(3)$, illustrated in Fig. 5.1b. This gives

$$\begin{aligned} Q^2 &= m_i^2 = (p_0 - p_2)^2 = (1-x_2)E_{\mathrm{CM}}^2\ , && (5.11)\\ z &= \frac{p_0p_1}{p_0p_i} = \frac{E_1}{E_i} = \frac{x_1}{x_1+x_3} = \frac{x_1}{2-x_2}\ , && (5.12)\\ &\Rightarrow\ \frac{\mathrm{d}Q^2}{Q^2}\,\frac{\mathrm{d}z}{1-z} = \frac{\mathrm{d}x_2}{1-x_2}\,\frac{\mathrm{d}x_1}{x_3}\ . && (5.13) \end{aligned}$$

The parton-shower probability for such a branching is

$$\begin{aligned} &\frac{\alpha_{\mathrm{s}}}{2\pi}\,C_F\,\frac{1+z^2}{1-z}\,\mathrm{d}z\,\frac{\mathrm{d}Q^2}{Q^2} = \\ &\frac{\alpha_s}{2\pi}\,C_F\left[1+\left(\frac{x_1}{2-x_2}\right)^2\right]\frac{1-x_1}{x_3}\,\frac{\mathrm{d}x_1\,\mathrm{d}x_2}{(1-x_1)(1-x_2)}\ . \end{aligned} \tag{5.14}$$

In the second shower history, the rôles of q and $\overline{\mathrm{q}}$ are interchanged, i.e. $x_1 \leftrightarrow x_2$. This is the same set of Feynman graphs as in the matrix-element description, except that the shower does not include any interference between the two diagrams. The two shower expressions can therefore be added to give the overall shower population of the three-jet phase space, of the form in eq. (5.10) but with

$$N_{\mathrm{PS}}(x_1, x_2, 0) = \frac{1-x_1}{x_3}\left(1+\left(\frac{x_1}{2-x_2}\right)^2\right) + \frac{1-x_2}{x_3}\left(1+\left(\frac{x_2}{2-x_1}\right)^2\right) , \quad (5.15)$$

In spite of N_{PS} being lengthier than N_{ME}, it turns out that the two almost exactly agree over the whole phase space, but with the shower rate somewhat above, see e.g. Fig. 5.2. It is therefore straightforward and efficient to use the ratio

$$R_{\mathrm{ME/PS}}(x_1, x_2, 0) = \frac{\mathrm{d}\sigma_{\mathrm{ME}}}{\mathrm{d}\sigma_{\mathrm{PS}}} = \frac{N_{\mathrm{ME}}(x_1, x_2, 0)}{N_{\mathrm{PS}}(x_1, x_2, 0)} \quad (5.16)$$

as an acceptance factor inside the shower evolution, in order to correct the first emission of the quark and antiquark to give a sum in agreement with the matrix element.

Clearly, the shower will contain further branchings that modify the simple result, e.g. by the emission both from the q and the $\overline{\mathrm{q}}$, but these effects are formally of $\mathcal{O}(\alpha_{\mathrm{s}}^2)$ and thus beyond the accuracy we strive to match. One should also note that the shower modifies the distribution in three-jet phase space by the appearance of Sudakov form factors, and by using a running $\alpha_{\mathrm{s}}(p_\perp^2)$ rather than a fixed one. In both these respects, however, the shower should be an improvement over the fixed-order result.

5.2.3 The Massive Matrix Element Correction

The prescription of correcting the first branchings by the factor in eq. (5.16) was the original one, used up until Jetset 7.3, for massless and massive quarks alike, where the $x_i = 2E_i/E_{\mathrm{CM}}$ variables were defined with masses included. In version 7.4 an intermediate 'improvement' was introduced, in that the massive matrix element expression was used, as given for a vector source like the γ^* [16]:

$$N_{\mathrm{ME}}(x_1, x_2, r) = x_1^2 + x_2^2 - 4r^2 x_3 - 8r^4 - (2r^2 + 4r^4)\left(\frac{1-x_2}{1-x_1} + \frac{1-x_1}{1-x_2}\right) . \quad (5.17)$$

The shower algorithm itself was not changed, nor the assumed shower weight, i.e. an acceptance factor $N_{\mathrm{ME}}(x_1, x_2, r)/N_{\mathrm{PS}}(x_1, x_2, 0)$ was applied for the first branching on either side. (The older behaviour remained as an option.)

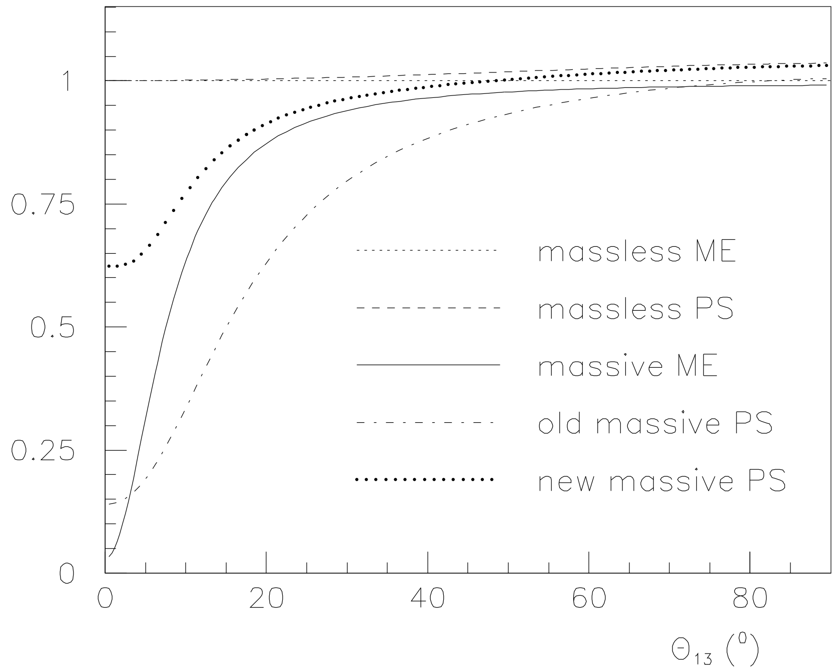

Figure 5.2: The gluon emission rate as a function of emission angle $\theta_{13} = \theta_{\mathrm{qg}}$, for a 10 GeV gluon energy at $E_{\mathrm{CM}} = 91$ GeV, and with $m_b = 4.8$ GeV. All curves are normalized to the massless matrix-element expression, eq. (5.9), here thus represented by the small-dotted line at unity. Dashed: the massless shower before correction, $N_{\mathrm{PS}}(x_1, x_2, 0)/N_{\mathrm{ME}}(x_1, x_2, 0) = 1/R_{\mathrm{ME/PS}}(x_1, x_2, 0)$. Full: the rate from massive matrix elements, $N_{\mathrm{ME}}(x_1, x_2, r)/N_{\mathrm{ME}}(x_1, x_2, 0)$. Dash-dotted: the rate from massive parton shower, $N_{\mathrm{PS}}(x_1, x_2, r)/N_{\mathrm{ME}}(x_1, x_2, 0)$. Large dots: the new rate from massive parton showers, $N'_{\mathrm{PS}}(x_1, x_2, r)/N_{\mathrm{ME}}(x_1, x_2, 0)$.

The mass suppression in the matrix element is illustrated in Fig. 5.2. We remind that, in the soft-gluon limit, a spin-independent (and thus universal) eikonal expression holds [8]:

$$\begin{aligned} \frac{\mathrm{d}\sigma_{\mathrm{q\overline{q}g}}}{\sigma_{\mathrm{q\overline{q}}}} &\propto (-1)\left(\frac{p_1}{p_1p_3} - \frac{p_2}{p_2p_3}\right)^2 \frac{\mathrm{d}^3p_3}{E_3} \\ &= \left(\frac{2p_1p_2}{(p_1p_3)(p_2p_3)} - \frac{m_1^2}{(p_1p_3)^2} - \frac{m_2^2}{(p_2p_3)^2}\right) E_3\mathrm{d}E_3\,\mathrm{d}\cos\theta_{13}\ . \end{aligned} \tag{5.18}$$

In the limit of small angles θ_{13} this gives a mass suppression factor

$$\frac{\mathrm{d}\sigma(x_3,\theta_{13},r)}{\mathrm{d}\sigma(x_3,\theta_{13},0)} \approx \left(\frac{\theta_{13}^2}{\theta_{13}^2+4r^2}\right)^2 , \tag{5.19}$$

i.e. the characteristic dead cone of opening angle approximately $2r = m_\mathrm{q}/E_\mathrm{q}$. Note that the mapping between (x_1, x_2) and (x_3, θ_{13}) depends on r, so eq. (5.19) is not quite the same as $N_\mathrm{ME}(x_1, x_2, r)/N_\mathrm{ME}(x_1, x_2, 0)$.

5.2.4 The Massive Phase Space Correction in the Shower

More recently [5], the issue of masses in the shower was further studied, since the expression for $N_\mathrm{PS}(x_1, x_2, 0)$ had not been touched when N_ME was improved.

In the derivation of $N_\mathrm{PS}(x_1, x_2, r)$, one can start from the ansatz

$$\begin{aligned} x_2 &= 1 - \frac{m_i^2 - m_\mathrm{q}^2}{E_\mathrm{CM}^2} , \\ x_1 &= \left(1 + \frac{m_i^2 - m_\mathrm{q}^2}{E_\mathrm{CM}^2}\right)((1-k_1)z + k_3(1-z)) , \\ x_3 &= \left(1 + \frac{m_i^2 - m_\mathrm{q}^2}{E_\mathrm{CM}^2}\right)((1-k_3)(1-z) + k_1 z) . \end{aligned} \tag{5.20}$$

The quark mass enters both in the energy sharing between the intermediate quark i and the antiquark 2, and in the correction procedure of eq. (5.3) for the splitting of energy in the branching $q(i) \to q(1)g(3)$. The constraints $p_1^2 = m_\mathrm{q}^2$ and $p_3^2 = 0$ give $k_1 = 0$ and $k_3 = m_\mathrm{q}^2/m_i^2$. One then obtains

$$Q^2 = m_i^2 = (1 - x_2 + r^2)E_\mathrm{CM}^2 , \tag{5.21}$$

$$z = \frac{1}{2-x_2}\left(x_1 - r^2\,\frac{x_3}{1-x_2}\right) , \tag{5.22}$$

$$\Rightarrow \frac{\mathrm{d}Q^2}{Q^2}\,\frac{\mathrm{d}z}{1-z} = \frac{\mathrm{d}x_2}{1-x_2+r^2}\,\frac{\mathrm{d}x_1}{x_3} . \tag{5.23}$$

This gives the answer

$$\begin{aligned} N_\mathrm{PS}(x_1, x_2, r) &= \frac{1-x_1}{x_3}\,\frac{1-x_2}{1-x_2+r^2}\left[1 + \frac{1}{(2-x_2)^2}\left(x_1 - r^2\frac{x_3}{1-x_2}\right)^2\right] \\ &+ \{x_1 \leftrightarrow x_2\} , \end{aligned} \tag{5.24}$$

where the second term comes from the graph where the antiquark radiates.

The mass effects go in the 'right' direction, $N_{\mathrm{PS}}(x_1, x_2, r) < N_{\mathrm{PS}}(x_1, x_2, 0)$, but actually so much so that $N_{\mathrm{PS}}(x_1, x_2, r) < N_{\mathrm{ME}}(x_1, x_2, r)$ in major regions of phase space. This is illustrated in Fig. 5.2. Very crudely, one could say that the massive shower exaggerates the angle of the dead cone by about a factor of two, in this rather typical example. There is no dead cone as such built in, however, but a rather more coincidental mass suppression mainly generated by the factor $(1 - x_2)/(1 - x_2 + r^2)$.

Thus the amount of gluon emission off massive quarks is underestimated already in the original prescription, where masses entered in the kinematics but not in the ME/PS correction factor. When the intermediate 'correction' ratio $N_{\mathrm{ME}}(x_1, x_2, r)/N_{\mathrm{PS}}(x_1, x_2, 0)$ is applied, the net result is a distribution even more off from the correct one, by a factor $N_{\mathrm{PS}}(x_1, x_2, r)/N_{\mathrm{PS}}(x_1, x_2, 0)$. Thus it would have been better not to introduce the mass correction in JETSET 7.4.

Based on the results above, one can now instead use the correct ME/PS factor $N_{\mathrm{ME}}(x_1, x_2, r)/N_{\mathrm{PS}}(x_1, x_2, r)$. A technical problem is that this ratio can exceed unity, in the example of Fig. 5.2 by up to almost a factor of two. This could be solved e.g. by enhancing the raw rate of emissions by this factor. However, another trick was applied, based on the facts that the shift of eqs. (5.3) and (5.20) implies that smaller-energy gluons would be allowed for a massive quark than a massless one, and additionally that the accessible z range is overestimated in the original ansatz. Therefore, without any (noticeable) loss of phase space, z can be rescaled to a z' according to

$$(1 - z') = (1 - z)^k \ , \quad \text{with} \quad k = \frac{\ln(r^2)}{\ln(Q_0^2/E_{\mathrm{CM}}^2)} < 1 \ . \tag{5.25}$$

The ME/PS correction factor then has to be compensated by k, and thereby comes below unity almost everywhere — the remaining weighting errors are too small to be relevant.

This procedure, default since PYTHIA version 6.130, improves the shower description of mass effects in the amount of three-jet events [5]. Mass effects are only included correctly for the first branching of the q and $\overline{\mathrm{q}}$ in the shower, however. Subsequent emissions involve no correction procedure. Instead the dead cone effect is exaggerated, similarly to what was shown in Fig. 5.2. Furthermore, even for the first branchings, only the possibility of a vector source decaying to two identical-mass quarks is included, while the Z^0 actually is a mixture of vector and axial vector, and e.g. the $\mathrm{W}^{\pm}$ would decay to two unequal-mass quarks. We will therefore next try to develop a more powerful and general approach.

5.3 A New Approach

One of the advantages of the Monte Carlo approach is that, so long as some upper estimate can be found that allows simple generation, rejection down to a more complex expression is straightforward. In particular, for an evolution in some variable Q with a (Sudakov) form factor built up from the no-emission probability, the 'veto algorithm' [6] can be used, in which the initial overestimate of the emission rate is compensated by the possibility of a rejection, with a continued evolution downwards in Q^2 from the rejected value onwards. As we have seen, the current set of Q^2 and z variables is not so convenient, since the emission rate off massive quarks is an underestimate of the correct rate, and therefore the standard procedure does not work except after some extra tricks. We will therefore pick another set of variables, preferably such that they reduce to the old ones in the massless limit. Several approaches could have been taken, but here we have chosen the minimal one of retaining the z definition and thereby the existing kinematics machinery. As we will show, a modification for the branching $a \to bc$ from $Q^2 = m_a^2$ to $Q^2 = m_a^2 - (m_a^2)_{\mathrm{on-shell}}$ is enough to do the job.

5.3.1 The Choice of Shower Variables

Again consider $\mathrm{e^+e^-} \to \gamma^*/\mathrm{Z}^0 \to \mathrm{q}(1)\,\overline{\mathrm{q}}(2)\,\mathrm{g}(3)$, and the formulae of eq. (5.20), but now assume $Q^2 = m_i^2 - m_\mathrm{q}^2 = m_i^2 - m_1^2$ for the $\mathrm{q}(i) \to \mathrm{q}(1)\mathrm{g}(3)$ branching. That corresponds to $1/Q^2$ being the propagator of the off-shell parton 1. Then eq. (5.22) is unchanged while

$$
\begin{aligned}
Q^2 &= m_i^2 - m_1^2 = (1 - x_2) E_{\mathrm{CM}}^2 \ , && (5.26)\\
&\Rightarrow \frac{\mathrm{d}Q^2}{Q^2}\,\frac{\mathrm{d}z}{1-z} = \frac{\mathrm{d}x_2}{1-x_2}\,\frac{\mathrm{d}x_1}{x_3} \ . && (5.27)
\end{aligned}
$$

So, with this simple trick, we have recovered the Jacobian of the massless case, eq. (5.13). This means that there is little mass suppression left in the shower evolution proper:

$$
\begin{aligned}
N'_{\mathrm{PS}}(x_1, x_2, r) &= \frac{1-x_1}{x_3}\left[1 + \frac{1}{(2-x_2)^2}\left(x_1 - r^2\frac{x_3}{1-x_2}\right)^2\right] \\
&+ \ \{x_1 \leftrightarrow x_2\} \ , \qquad (5.28)
\end{aligned}
$$

as can be seen in Fig. 5.2. In particular, note that $N'_{\mathrm{PS}}(x_1, x_2, r)$ reduces to $N_{\mathrm{PS}}(x_1, x_2, 0)$, eq. (5.14), in the soft limit $x_3 \to 0$. Therefore a matrix-element correction now is even more required, but also simpler to implement, to bring down the rate to a reasonable level.

So far, we have assumed decay to two equal-mass quarks, like in Z^0 decay. For many of the examples to be discussed, like $\mathrm{W}^\pm$ or t decay, the two decay products have unequal masses. It is also convenient to allow slightly unequal masses for particles with non-negligible widths, e.g. in $\mathrm{e^+e^-} \to \mathrm{t\bar{t}}$. We will therefore generalize to the case with $r_1 = m_1/E_{\mathrm{CM}} = m_{\mathrm{q}}/E_{\mathrm{CM}} \neq r_2 = m_2/E_{\mathrm{CM}} = m_{\overline{\mathrm{q}}}/E_{\mathrm{CM}}$. The range of kinematically allowed x_i values is then $2r_1 \leq x_1 \leq 1 + r_1^2 - r_2^2$, $2r_2 \leq x_2 \leq 1 + r_2^2 - r_1^2$, $0 \leq x_3 \leq 1 - (r_1 + r_2)^2$, with the joint condition that

$$(2 - 2x_1 - 2x_2 + x_1 x_2 + 2r_1^2 + 2r_2^2)^2 \leq (x_1^2 - 4r_1^2)(x_2^2 - 4r_2^2) \ . \tag{5.29}$$

The ansatz of eq. (5.20) is modified by $m_{\mathrm{q}} \to m_2$ while $k_3 \to m_1^2/m_i^2$. Furthermore

$$\begin{aligned} Q^2 &= m_i^2 - m_1^2 = (p_0 - p_2)^2 - m_1^2 = (1 + r_2^2 - r_1^2 - x_2) E_{\mathrm{CM}}^2 \ , &(5.30)\\ z &= \frac{1}{2 - x_2} \left(x_1 - r_1^2 \, \frac{x_3}{1 + r_2^2 - r_1^2 - x_2} \right) \ , &(5.31)\\ \Rightarrow \ & \frac{\mathrm{d}Q^2}{Q^2} \, \frac{\mathrm{d}z}{1 - z} = \frac{\mathrm{d}x_2}{1 + r_2^2 - r_1^2 - x_2} \, \frac{\mathrm{d}x_1}{x_3} \ . &(5.32) \end{aligned}$$

When a colourless particle decays to two colour triplets, the two possible one-gluon-emission shower histories then add up to give

$$\frac{1}{\sigma_0} \, \frac{\mathrm{d}\sigma_{\mathrm{PS}}}{\mathrm{d}x_1 \, \mathrm{d}x_2} = \frac{\alpha_{\mathrm{s}}}{2\pi} \, C_F \left\{ \frac{1 + z_1^2}{x_3 (1 + r_2^2 - r_1^2 - x_2)} + \frac{1 + z_2^2}{x_3 (1 + r_1^2 - r_2^2 - x_1)} \right\} \ . \tag{5.33}$$

Here z_1 is given by eq. (5.31) and z_2 is obtained by exchanging $1 \leftrightarrow 2$. Since the numerators $1 \leq 1 + z_i^2 \leq 2$, their exact form is not a main concern for the qualitative discussions. As it turns out, the Monte Carlo procedure is simplified if the shower is generated with a numerator 2 instead of $1 + z_i^2$, so we will make this replacement in the following, with the matrix element correction procedure compensating this overestimate.

5.3.2 The Matrix Element Correction

Next, one should try to relate this to the structure of the matrix elements under similar conditions. We may expect graphs where either of the partons can radiate a gluon and therefore can give a propagator $1/Q_1^2 = 1/(m_{13}^2 - m_1^2)$, cf. eq. (5.30), or $1/Q_2^2 = 1/(m_{23}^2 - m_2^2)$, depending on which side radiates. (Diagrams with a four-boson vertex, such as $\gamma^*/\mathrm{Z}^* \to \tilde{\mathrm{t}}\bar{\tilde{\mathrm{t}}}\mathrm{g}$, are not singular and therefore do not affect the discussion.) After summing and squaring, the cross section then should have the form

$$
\begin{aligned}
\frac{1}{\sigma_0}\,\frac{\mathrm{d}\sigma_{\mathrm{ME}}}{\mathrm{d}x_1\,\mathrm{d}x_2} &= \frac{\alpha_{\mathrm{s}}}{2\pi}\,C_F\left\{\frac{E_{\mathrm{CM}}^4 A(x_1,x_2)}{(m_{13}^2-m_1^2)^2}+\frac{E_{\mathrm{CM}}^4 B(x_1,x_2)}{(m_{23}^2-m_2^2)^2}\right. \\
&\quad \left.+\frac{E_{\mathrm{CM}}^4 C(x_1,x_2)}{(m_{13}^2-m_1^2)(m_{23}^2-m_2^2)}\right\} \\
&= \frac{\alpha_{\mathrm{s}}}{2\pi}\,C_F\left\{\frac{A(x_1,x_2)}{(1+r_2^2-r_1^2-x_2)^2}+\frac{B(x_1,x_2)}{(1+r_1^2-r_2^2-x_1)^2}\right. \\
&\quad \left.+\frac{C(x_1,x_2)}{(1+r_2^2-r_1^2-x_2)(1+r_1^2-r_2^2-x_1)}\right\}\,. \qquad (5.34)
\end{aligned}
$$

The individual functions A, B and C depend on the gauge choice, but the total cross section of course is gauge-independent. It also has some general features, which can be seen in the soft-gluon limit expression, eq. (5.19). Here the interference term is giving a positive expression and the seemingly quadratically-divergent terms are negative and drive the cross section to zero in the collinear limit, the dead cone. In order to have an upper estimate of the cross section, for Monte Carlo applications, it is thus enough to have the singularity structure of the interference term modelled, and no need to worry about quadratic divergences.

As before, we could now compare the total shower and total matrix element rates, and define a corrective factor between the two. To simplify some of the continued studies, however, we have adopted an alternative approach. Instead of adding the two shower histories to compare with the full matrix element, one can split the matrix element in two, such that each part can be compared with only one shower history. Such a subdivision of course is arbitrary, but should still be sensible. A gluon emitted close to the p_1 direction should predominantly be emitted by parton 1, and vice versa. A suitable such subdivision is in the proportions given by the propagators, $1/Q_1^2 : 1/Q_2^2$, which also is the proportions between the two shower histories (in the $1+z^2 \to 2$ approximation). For massless partons, and going to the soft-gluon limit, this means a probability $(1+\cos\theta_{13})/2 = (1-\cos\theta_{23})/2$ for emission off parton 1 and the rest for emission off parton 2.

In the description of the gluon emission rate off parton 1, a matrix element fraction

$$
W_{\mathrm{ME},1}(x_1,x_2) = \frac{Q_2^2}{Q_1^2+Q_2^2}\,\frac{1}{\sigma_0}\,\frac{\mathrm{d}\sigma_{\mathrm{ME}}}{\mathrm{d}x_1\,\mathrm{d}x_2} = \frac{1+r_1^2-r_2^2-x_1}{x_3}\,\frac{1}{\sigma_0}\,\frac{\mathrm{d}\sigma_{\mathrm{ME}}}{\mathrm{d}x_1\,\mathrm{d}x_2} \qquad (5.35)
$$

should be compared with the first half of the total parton shower expression in eq. (5.33),

$$
W_{\mathrm{PS},1}(x_1,x_2) = \frac{\alpha_{\mathrm{s}}}{2\pi}\,C_F\,\frac{2}{x_3(1+r_2^2-r_1^2-x_2)}\,. \qquad (5.36)
$$

The ME/PS correction factor then becomes

$$\begin{aligned} R_1(x_1,x_2) &= \frac{W_{\mathrm{ME},1}(x_1,x_2)}{W_{\mathrm{PS},1}(x_1,x_2)} \\ &= \frac{(1+r_2^2-r_1^2-x_2)(1+r_1^2-r_2^2-x_1)}{2}\left(\frac{\alpha_{\mathrm{s}}}{2\pi}\,C_F\right)^{-1}\frac{1}{\sigma_0}\,\frac{\mathrm{d}\sigma_{\mathrm{ME}}}{\mathrm{d}x_1\,\mathrm{d}x_2}\,, \end{aligned} \tag{5.37}$$

which reduces to $R_1(x_1,x_2) = N_{\mathrm{ME}}(x_1,x_2,r)/2$ for $r_1 = r_2 = r$.

The intention is that $R_1(x_1,x_2)$ should be finite and well-behaved over all of phase space, with one factor of each divergence now multiplied on to the matrix element expression. We will illustrate the behaviour later on, but the key observation is that, for all the matrix elements we will study, searches over the full mass parameter plane and phase space have failed to find any point where the ratio is above unity. R_1 therefore serves well as simple rejection factor. (Without the replacement $1+z^2 \to 2$ in the shower description one would find $R_1(x_1,x_2) > 1$, and some extra precautions would be necessary.) The correction factor R_2 for the other shower history looks the same. Put another way, the relative probability for a gluon to be emitted by parton 1 or by parton 2 is unchanged by the matrix element correction procedure.

The above procedure works not only for quarks, but also e.g. for squarks. The numerator of the splitting kernel would have been $2z$ rather than $1+z^2$ [18], but both are equally well approximated from above by 2. For a gluino, the colour charge is N_C rather than C_F, so the assumed shower emission rate has to be scaled up by a factor $N_C/C_F = 9/4$ (also for the recoiling colour triplet parton, since the separation of radiation is not perfect), with no other change required.

We will also encounter processes where the decaying particle carries colour, like in $\mathrm{t} \to \mathrm{bW}^+$. Then gluon emission off this particle has to be considered, i.e. graphs like $\mathrm{t}(0) \to \mathrm{t}(i)\,\mathrm{g}(3) \to \mathrm{b}(1)\,\mathrm{W}^+(2)\,\mathrm{g}(3)$, proceeding via an intermediate off-shell top. Neglecting the top width, this introduces a new kind of inverse propagators

$$|Q_0^2| = m_0^2 - m_i^2 = m_{123}^2 - m_{12}^2 = 2(p_1+p_2)p_3 = x_3\,E_{\mathrm{CM}}^2\,. \tag{5.38}$$

The leading term of the matrix element, proportional to $1/(Q_0^2 Q_1^2)$, will therefore have the same singularity structure as the shower rate in eq. (5.36). In a shower description, where only the b is allowed to radiate, there is thus no problem in principle of letting that radiation account for the full emission pattern of the matrix elements, i.e.

$$\begin{aligned} R_1(x_1,x_2) &= \frac{W_{\mathrm{ME}}(x_1,x_2)}{W_{\mathrm{PS},1}(x_1,x_2)} \\ &= \frac{x_3(1+r_2^2-r_1^2-x_2)}{2}\left(\frac{\alpha_{\mathrm{s}}}{2\pi}\,C_F\right)^{-1}\frac{1}{\sigma_0}\,\frac{\mathrm{d}\sigma_{\mathrm{ME}}}{\mathrm{d}x_1\,\mathrm{d}x_2}\,. \end{aligned} \tag{5.39}$$

Since also here the shower rate turns out to exceed the matrix element one, a simple rejection approach should work well.

5.3.3 Subsequent Branchings

So far, we have considered matrix elements as providing the probability of exclusive three-jet events. An alternative interpretation, however, would be in terms of an inclusive density of gluon emissions, with the possibility of several such per event. This interpretation works well in the soft-gluon limit, while the emission of a hard gluon reduces the phase space for subsequent emissions and thus ruins the picture of independent emissions. Furthermore, the possibility for gluons to branch in their turn leads to the need to include coherence effects [17] that constrain allowed emissions. Nevertheless, the matrix elements can be used to extract important information, not only on the emission rate of hard gluons, but also on that of soft and collinear ones.

Historically, different approaches have therefore been taken. In the JETSET/PYTHIA procedure used until now, only the first branching is corrected by matrix-element information. Subsequent emissions involve no corrections, but only the process-independent splitting kernels, and therefore give the wrong emission rate off heavy quarks that has already been noted. In the HERWIG routine, a correction is performed for every emission that is the hardest so far [12] — whereas JETSET emissions tend to be ordered in hardness, this is less likely in HERWIG, so the distinction is then relevant. ARIADNE, finally, imposes a correction at all steps of the cascade.

Since our new algorithm does not have the correct dead-cone behaviour built in from the onset, it is clear that some correction procedure will be required. Rather than imposing the process-independent collinear behaviour, we have chosen to base ourselves on the matrix elements also in this region. This offers a smooth interpolation between the hard process-specific and the soft collinear universal behaviours, and sidesteps the issue of which emissions are to be considered the hardest so far [12]. Thus the shower rate will be corrected to the matrix element one at every step of the shower off the original partons. The gluon cascading $\mathrm{g} \to \mathrm{gg}$ is unaffected, since there are no gluon-mass effects or matrix elements to be considered here. Light quarks (in γ^*/Z^0 decay) are also essentially unaffected, since there the shower matches so well with the matrix elements anyway.

The kinematics of the cascade changes in each emission, as the energy of the radiating parton is reduced by the previous emissions. The mapping of an emission on to the matrix element variables is thereby not unique. However, from the dead cone formula, eq. (5.19), we see that the emission angle and the mass-to-energy ratio of the emitting quark should be represented faithfully in the choice of matching matrix element variables. For the branchings subsequent to the first one, say $3 \to 7 + 8$ in Fig. 5.1a, the mother energy E_3 is fixed. The choice of a $Q^2 = m_3^2 - m_7^2$ and a z of the branching maps onto four-momenta p_7 and p_8 as described in eqs. (5.3)–(5.7), with $p_7^2 = m_{\mathrm{q}}^2 > 0$ and $p_8^2 = 0$. In order to make contact with the matrix element variables, now construct a hypothetical recoiling parton $2'$, such that $\mathbf{p}'_2 = -\mathbf{p}_3$ and ${p'_2}^2 = m_{\overline{\mathrm{q}}}^2$. The CM energy of this reduced system is then given by

$$E'_{\mathrm{CM}} = E_3 + E'_2 = E_3 + \sqrt{\mathbf{p}_3^2 + m_{\overline{\mathrm{q}}}^2} = E_3 + \sqrt{E_3^2 - Q^2 - m_{\mathrm{q}}^2 + m_{\overline{\mathrm{q}}}^2}\,. \quad (5.40)$$

Now matrix element and parton shower weights can be evaluated for $x'_1 = 2E_7/E'_{\mathrm{CM}}$, $x'_2 = 2E'_2/E'_{\mathrm{CM}}$, $r'_1 = m_{\mathrm{q}}/E'_{\mathrm{CM}}$ and $r'_2 = m_{\overline{\mathrm{q}}}/E'_{\mathrm{CM}}$. Note that, in the limit $E_4 \to 0$, also $E'_{\mathrm{CM}} \to E_{\mathrm{CM}}$, and the ordinary matrix elements are recovered.

The above procedure is not unique. As an alternative, one could retain the original E_{CM}, but construct an off-shell p'_2 to carry all the energy and momentum of the system except for $p_3 = p_7 + p_8$, i.e. $p'_2 = p_2 + p_4$ in the case of Fig. 5.1a. This gives equivalent results so long as the gluon energy already emitted is not too large, and else gives a somewhat lower rate of wide-angle emission, reflecting that the parton $2'$ then is assigned such a large mass that it radiates less. The overall picture therefore is less appealing, even if results in practical applications are almost equivalent.

In this article, emphasis is put on the gluon emission off the primary quarks (or other primary particles). The subsequent branchings $\mathrm{g} \to \mathrm{gg}$ have not been affected by the mass considerations, so are not discussed here. The rate of $\mathrm{g} \to \mathrm{q\overline{q}}$ branchings is another topic of some interest, given that LEP results do not quite agree with predictions [5]. This issue is further discussed in Sect. 6.

However, given that such a secondary $\mathrm{c\overline{c}}$ or $\mathrm{b\overline{b}}$ pair has been produced, the possibility of further gluon emission off this pair should be considered, even if most pairs are produced at such a low mass that the phase space left for further radiation is limited. In order to provide a sensible behaviour in the collinear region, again matrix-element input is applied, calculated for the decay of a colour octet source. (Process 66 of Table 5.1, so with the wrong spin of the source, but correct for the radiating parton, which is the main point.) To first approximation, this means that radiation occurs independently off the q and $\overline{\mathrm{q}}$; see the discussion on radiation patterns below. The kinematics for the matrix element corrections is set up about as described above, i.e. by mapping onto a reduced system at rest with preserved energy for the radiating parton. A simplification is that here the recoiling parton always has the same mass as the radiating one.

5.3.4 Additional Issues

In the older shower algorithm, the decay products of a branching $a \to bc$ were assumed massless until assigned a mass by some subsequent step. This meant that the $p_\perp^2$ of a branching, eq. (5.7) with $\beta_a = 1$ as a first simplification, was simplified further to $p_\perp^2 \approx z(1-z)m_a^2$ when used as argument in $\alpha_\mathrm{s}(p_\perp^2)$. In a branching $\mathrm{q} \to \mathrm{qg}$, where the q is assumed to have a non-vanishing rest mass, one would instead obtain $p_\perp^2 \approx z(1-z)m_a^2(1-m_b^2/m_a^2)^2$. (This follows from eq. (5.7) or alternatively from the rescaling of x_3 in eq. (5.20).) A smaller $p_\perp^2$ estimate implies a larger α_s and emission rate for a given kinematical configuration, but also that more phase space is cut out by the requirement $p_\perp^2 > Q_0^2/4$, where Q_0 is the soft cut-off scale of the cascade. The net result of such a change is therefore not obvious, and we will study it later on.

Also the calculation of the approximate opening angle of a branching $a \to bc$, eq. (5.8), would be affected by the same considerations. The massive parton energy E_b is increased at the expense of E_c, as given by eq. (5.20). Since the common $p_\perp$ is also decreased, the ratio $p_\perp/E_c$ is preserved, while $p_\perp/E_b$ is decreased. The net result is a decrease of the opening angle by a factor $(1 + (m_b^2/m_a^2)(1-z)/z)^{-1}$. As another option, we will then consider the consequences of such a decrease in the decay opening angle, without any change of the production angle, as a way of minimally relaxing the angular ordering condition off massive quarks.

While our choice of $Q^2 \approx m^2$ variable has significant advantages for the matching to matrix-element expressions, it does not offer as neat an implementation of coherence effects as the angular variable of HERWIG or the transverse momentum one of ARIADNE. Without any further constraints, the amount of radiation is overestimated. Therefore, by default, angular ordering of emissions is imposed as a further constraint. This, on the other hand, tends to restrict emissions somewhat too much. The bulk of these ambiguities affect rather soft gluons, which do not give rise to separate jets. For the precision studies in Section 5.5.1, however, also small effects could be of interest. We have therefore introduced a new "intermediate" coherence option, as compared to the minimal modification above, wherein no angular constraint is imposed on emissions off the primary $\mathrm{q\overline{q}}$ pair. These emissions thus are ordered only in mass. Angular ordering is still imposed in the cascades initiated by the gluons emitted off the primary quarks. In particular each such cascade is restricted to a cone given by the emission angle of the initiating gluon. In this option, generic event properties are only slightly changed compared with the default procedure.

So far, we have mainly considered configurations where a colour singlet decays to stable particles, e.g. $\gamma^*/\mathrm{Z}^0 \to \mathrm{b\overline{b}}$. Another class of events involve sequential decays of coloured objects. The obvious example would be $\gamma^*/\mathrm{Z}^* \to \mathrm{t\overline{t}} \to \mathrm{bW^+\overline{b}W^-}$. Even leaving aside the continued fate of the W's, e.g. assuming they decay leptonically, the event now contains four colour charges that may radiate. In the limit $\Gamma_\mathrm{t} \to 0$, the radiation in the top production stage $\gamma^*/\mathrm{Z}^* \to \mathrm{t\overline{t}}$ decouples completely from that in the top decays. For a finite Γ_t, gluons with energies below or around this scale can receive contributions from many colour sources, however, leading to complex radiation patterns [2]. Close to the $\mathrm{t\bar{t}}$ threshold, the main sources are the respective top decays, described by dipoles $\widehat{\mathrm{tb}}$ and $\widehat{\mathrm{\bar{t}\bar{b}}}$, and radiation off the $\widehat{\mathrm{b\bar{b}}}$ dipole created after the t and $\mathrm{\bar{t}}$ have decayed. Gluons with energies above (below) Γ_{t} predominantly feel the former (latter) dipoles. The radiation pattern can be written as

$$\frac{E_{\mathrm{g}}^2}{\Gamma_{\mathrm{t}}^2 + E_{\mathrm{g}}^2}\left(\widehat{\mathrm{tb}} + \widehat{\mathrm{\bar{t}\bar{b}}}\right) + \frac{\Gamma_{\mathrm{t}}^2}{\Gamma_{\mathrm{t}}^2 + E_{\mathrm{g}}^2}\widehat{\mathrm{b\bar{b}}} \ . \tag{5.41}$$

Thus the reduced radiation induced by the top finite lifetime is compensated by the radiation from new sources that would not have been present for a long-lived top. The $\widehat{\mathrm{b\bar{b}}}$ dipole introduces a dependence on the opening angle between the b and the $\mathrm{\bar{b}}$ that is not there in the separate top decays, so the compensation is not complete. On the perturbative level, this gives a dipole effect [19] that could be observed at low momenta. However, even in the approximation of allowing radiation only within each top quark decay separately, the string fragmentation picture [1] would imply that a nonperturbative colour string should be stretched between the b and $\mathrm{\bar{b}}$ (or their respective cascades), and this would introduce a string effect [20] of almost equal character and magnitude [21]. Thus only very careful studies, e.g. for high-precision measurements of the top mass, would be sensitive to the detailed nature of the soft-gluon emission source. The critical transition is the one between a top long-lived enough to produce top hadrons and one decaying too rapidly for that, where the hadronic final state does change character.

The shower algorithm contains options that allows it to be run, either with soft or with hard emission dampened according to the respective factors in eq. (5.41). However, currently the PYTHIA program contains no machinery to detect when a description of this kind is required, nor a prescription how to combine all possible sources of radiation. This is obviously an interesting task for the future, but one that will be required primarily for particles with a width significantly larger than that of the top.

The normal generation sequence therefore contains a set of separated showers. For instance, in the top example above, the $\gamma^*/\mathrm{Z}^* \to \mathrm{t\bar{t}}$ induces a first cascade, whereby the t and $\mathrm{\bar{t}}$ shower down to the mass shell. Thereafter follows the respective top decay, $\mathrm{t} \to \mathrm{bW}^+$ and $\mathrm{\bar{t}} \to \mathrm{\bar{b}W}^-$, and the separate radiation in those decays. At some yet later stage, the two W's may decay to quarks that again radiate. Anytime a colour singlet is exchanged, like the W's above, there is a clean separation into disjoint QCD subsystems, while the exchange of a coloured state like the top will hook up separately showering systems to the strings that later will produce the observable hadrons. Interconnection effects [22] could complicate this picture, but so far the evidence is that any such effects would be small.

In hadronic collisions, more complex processes would occur, and also initial-state QCD radiation has to be considered as a potential source of further interference effects. In this article we will not address these additional complications, but defer that for some future study. Currently such interference is almost completely neglected, except for some angular restrictions [23].

Even if Γ_{t} is neglected in the showering, for the sake of providing a unique separation of radiation before and after the top propagator, this does not mean that all top quarks have to have the same mass. Instead, resonance masses are chosen according to the relevant Breit-Wigners, convoluted with the respective cross section formulae. In particular, this means that the t and $\overline{\mathrm{t}}$ masses of an event would be unequal. The shower algorithm described above then operates on these event-by-event masses, without any reference to their nominal on-shell equivalents.

The hadronization of a partonic configuration, obtained by the chain of decays and showers outlined above, is described by the Lund string model [1]. All coloured partons belong to strings, stretched from a quark endpoint via a number of intermediate gluons to an antiquark one. (Also diquark endpoints and closed gluon loops can be considered, but are of no relevance in this article.) Normally each such string would have a reasonably large invariant mass, enough to produce several hadrons. However, occasionally a string could come to have a small mass, e.g. by the splitting of a string in two by shower branchings $\mathrm{g} \to \mathrm{q}\overline{\mathrm{q}}$. Then a special treatment may be required for one- or two-hadron decays. While the normal string algorithm has remained essentially unchanged over a number of years, this low-mass 'cluster' treatment has recently been improved [24]. The direct consequences for the topics studied here are minimal, except that quark mass values have now been optimized, especially to describe charm asymmetries in fixed-target experiments. The current default values thus are $m_{\mathrm{u}} = m_{\mathrm{d}} = 0.33$ GeV, $m_{\mathrm{s}} = 0.5$ GeV, $m_{\mathrm{c}} = 1.5$ GeV and $m_{\mathrm{b}} = 4.8$ GeV.

5.4 Matrix Elements

As input and starting point for our shower studies, we will need the matrix elements for the processes of interest. In this article this essentially means the two-body decay of a particle, with associated gluon radiation. Some of the formulae are available in the literature, but most are not, or at least not easily found. We have therefore calculated a number of processes. This also gives us a chance to test the degree of universality of the radiation patterns in channels of different colour and spin structure, but with the same masses. These results are interesting in their own right.

colour	spin	γ_5	example	codes
$1 \to 3 + \overline{3}$	—	—	(eikonal)	6 – 9
$1 \to 3 + \overline{3}$	$1 \to \frac{1}{2} + \frac{1}{2}$	$1, \gamma_5, 1 \pm \gamma_5$	$\mathrm{Z}^0 \to \mathrm{q}\overline{\mathrm{q}}$	11 – 14
$3 \to 3 + 1$	$\frac{1}{2} \to \frac{1}{2} + 1$	$1, \gamma_5, 1 \pm \gamma_5$	$\mathrm{t} \to \mathrm{bW}^+$	16 – 19
$1 \to 3 + \overline{3}$	$0 \to \frac{1}{2} + \frac{1}{2}$	$1, \gamma_5, 1 \pm \gamma_5$	$\mathrm{H}^0 \to \mathrm{q}\overline{\mathrm{q}}$	21 – 24
$3 \to 3 + 1$	$\frac{1}{2} \to \frac{1}{2} + 0$	$1, \gamma_5, 1 \pm \gamma_5$	$\mathrm{t} \to \mathrm{bH}^+$	26 – 29
$1 \to 3 + \overline{3}$	$1 \to 0 + 0$	1	$\mathrm{Z}^0 \to \tilde{\mathrm{q}}\overline{\tilde{\mathrm{q}}}$	31 – 34
$3 \to 3 + 1$	$0 \to 0 + 1$	1	$\tilde{\mathrm{q}} \to \tilde{\mathrm{q}}'\mathrm{W}^+$	36 – 39
$1 \to 3 + \overline{3}$	$0 \to 0 + 0$	1	$\mathrm{H}^0 \to \tilde{\mathrm{q}}\overline{\tilde{\mathrm{q}}}$	41 – 44
$3 \to 3 + 1$	$0 \to 0 + 0$	1	$\tilde{\mathrm{q}} \to \tilde{\mathrm{q}}'\mathrm{H}^+$	46 – 49
$1 \to 3 + \overline{3}$	$\frac{1}{2} \to \frac{1}{2} + 0$	$1, \gamma_5, 1 \pm \gamma_5$	$\tilde{\chi} \to \mathrm{q}\overline{\tilde{\mathrm{q}}}$	51 – 54
$3 \to 3 + 1$	$0 \to \frac{1}{2} + \frac{1}{2}$	$1, \gamma_5, 1 \pm \gamma_5$	$\tilde{\mathrm{q}} \to \mathrm{q}\tilde{\chi}$	56 – 59
$3 \to 3 + 1$	$\frac{1}{2} \to 0 + \frac{1}{2}$	$1, \gamma_5, 1 \pm \gamma_5$	$\mathrm{t} \to \tilde{\mathrm{t}}\tilde{\chi}$	61 – 64
$8 \to 3 + \overline{3}$	$\frac{1}{2} \to \frac{1}{2} + 0$	$1, \gamma_5, 1 \pm \gamma_5$	$\tilde{\mathrm{g}} \to \mathrm{q}\overline{\tilde{\mathrm{q}}}$	66 – 69
$3 \to 3 + 8$	$0 \to \frac{1}{2} + \frac{1}{2}$	$1, \gamma_5, 1 \pm \gamma_5$	$\tilde{\mathrm{q}} \to \mathrm{q}\tilde{\mathrm{g}}$	71 – 74
$3 \to 3 + 8$	$\frac{1}{2} \to 0 + \frac{1}{2}$	$1, \gamma_5, 1 \pm \gamma_5$	$\mathrm{t} \to \tilde{\mathrm{t}}\tilde{\mathrm{g}}$	76 – 79
$1 \to 8 + 8$	—	—	(eikonal)	81 – 84

Table 5.1: The processes that have been calculated, also with one extra gluon in the final state. Colour is given with 1 for singlet, 3 for triplet and 8 for octet. See the text for an explanation of the γ_5 column and further comments.

5.4.1 Calculations

A number of matrix elements have been calculated, using COMPHEP [25] for the actual calculation, including an extension package for Supersymmetric processes [26], and MATHEMATICA [27] for subsequent simplification of the expressions. The list of lowest-order (LO) processes is given in Table 5.1. The LO expression gives the two-body decay rate of a particle, i.e. $a \to bc$, and the matching first-order (FO) one the same decay with an additional gluon in the final state, $a \to bc\mathrm{g}$.

While the matrix element calculations in this section have been performed from scratch, some checks are based on results in the literature. These include: $V \to \mathrm{q}\overline{\mathrm{q}}$ for $m_{\mathrm{q}} = m_{\overline{\mathrm{q}}}$ [16], $\mathrm{H}^0 \to \mathrm{q}\overline{\mathrm{q}}$ for $m_{\mathrm{q}} = m_{\overline{\mathrm{q}}}$ [28], $V \to \tilde{\mathrm{q}}\overline{\tilde{\mathrm{q}}}$ for $m_{\tilde{\mathrm{q}}} = m_{\overline{\tilde{\mathrm{q}}}}$ [18], and $\mathrm{t} \to \mathrm{bW}^+$ for $m_{\mathrm{b}} = 0$ [13]. No doubt, many more are available, without our knowledge.

The process selection is based on the particle content of the Minimal Supersymmetric Standard Model (MSSM), i.e. includes squarks $\tilde{\mathrm{q}}$, gluinos $\tilde{\mathrm{g}}$, neutralinos and charginos $\tilde{\chi}$, and Higgs states h^0, H^0, A^0 and $\mathrm{H}^{\pm}$. The idea, however, is that these situations could represent also a number of other non-standard particles. For instance, the decay of a spin 0 leptoquark $\mathrm{L_Q} \to \mathrm{q}\ell$ is closely similar to $\tilde{\mathrm{q}} \to \mathrm{q}\tilde{\chi}$.

All calculations have been performed in the zero-width limit of the decaying state and the decay products, in order to allow a gauge invariant separation of radiation in the production and decay stages. (As explained above, the Monte Carlo simulation of processes does include mass selection according to the appropriate Breit-Wigners, so we here only comment on the width dependence of the additional gluon radiation, i.e. in the ratio of first to leading order cross sections.) Such a separation occurs naturally for exchanged colourless particles, so is then no problem. For a coloured particle of width Γ, this is a poor approximation in the region of gluon energies (in the particle rest frame) below Γ. The t is still sufficiently narrow that the production–decay interference is not a major problem, see above, but for heavier squarks and gluinos a more complex description may be required. The lowest coloured SUSY states, e.g. stop, tend to have small widths, however, and it is on such states we will concentrate our studies. The additional complications for very wide particles will be deferred to some future study.

The classification by colour and spin is fairly obvious, but that does not completely specify the structure of the process. Consider e.g. $\mathrm{e}^+\mathrm{e}^- \to \gamma^*/\mathrm{Z}^0 \to \mathrm{q}\overline{\mathrm{q}}$. The cross section (neglecting mass effects) is then

$$\sigma_0 \propto e_{\mathrm{e}}^2\, e_{\mathrm{q}}^2 + 2\, e_{\mathrm{e}} v_{\mathrm{e}}\, \Re\mathrm{e}\Xi\, e_{\mathrm{q}} v_{\mathrm{q}} + (v_{\mathrm{e}}^2 + a_{\mathrm{e}}^2)\, |\Xi|^2\, (v_{\mathrm{q}}^2 + a_{\mathrm{q}}^2) \; , \tag{5.42}$$

where

$$\Xi = \frac{1}{16 \sin^2\theta_W \cos^2\theta_W}\, \frac{s}{s - m_{\mathrm{Z}}^2 + i m_{\mathrm{Z}} \Gamma_{\mathrm{Z}}} \tag{5.43}$$

represents the ratio between the Z^0 and the γ propagators and couplings. The term proportional to a_{q}^2 corresponds to the $\mathrm{q}\overline{\mathrm{q}}$ pair coming from an axial vector source, the rest to it coming from a vector source. Since the QCD radiation from these two is somewhat different, we need to include the proper mixture, which depends on the CM energy, $s = E_{\mathrm{CM}}^2$. It has then been simplest to perform the calculations for a pure vector source and a pure axial vector source, represented by 1 and γ_5 in Table 5.1, and mix in the proportions required. We note that this mixing strategy is possible since the total cross section does not contain any interference terms of the character $v_{\mathrm{q}}a_{\mathrm{q}}$. (Such terms do arise when the forward–backward charge asymmetry is considered.) The pure left-handed mixture $V - A = 1 - \gamma_5$ is of special interest, since it represents the $\mathrm{W}^{\pm}$ bosons. Therefore it has been calculated separately, and is denoted by $1 \pm \gamma_5$ in Table 5.1; as we already noted the sign (of the interference term in the squared matrix element) is irrelevant for the QCD emission aspects. In total, four alternatives are therefore open in our implementation: to have a pure vector source, a pure axial vector, an arbitrary mixture $\alpha V + (1-\alpha)A$ and the special equal mixture. In this order, that gives the four codes 11 – 14 in Table 5.1, according to the numbering scheme used in the PYTHIA function `PYMAEL` introduced in version 6.153. (This routine takes as input the process code, x_1, x_2, r_1, r_2 and α, and returns the ratio $(1/\sigma_0)\,\mathrm{d}\sigma/\mathrm{d}x_1\,\mathrm{d}x_2$, omitting a factor of $(\alpha_{\mathrm{s}}/2\pi)C_F$.)

Correspondingly, also most other processes can come either with or without γ_5 factors in the amplitude, or in arbitrary mixtures thereof. In the Higgs sector, normally the h^0 and H^0 are scalar, the A^0 pseudoscalar and the $\mathrm{H}^{\pm}$ a parameter-dependent mixture of 1 and γ_5. If the coupling structure is generalized, also the neutral Higgses could be mixtures, however. The $\tilde{\mathrm{q}}_L$ and $\tilde{\mathrm{q}}_R$ squark partners of the left- and right-handed quarks come with wave function factors $1 - \gamma_5$ and $1 + \gamma_5$, respectively. The squark mass eigenstates will be mixtures of these, with significant mixing expected especially in the third generation. With two squarks in a process, $\gamma_5^2 = 1$ ensures that the matrix element still can be written as a sum $\alpha\,1 + (1-\alpha)\gamma_5$. Again, therefore, we have chosen to perform most of the calculations with and without a γ_5 factor and then leave open to have the mixing depend on the current parameter choice. As a further simplification, the $1 \pm \gamma_5$ mixture is used whenever the correct choice is not known, since this mixture represents an average behaviour. In some instances, further restrictions exist, e.g. a pseudoscalar cannot decay to two scalars, at least among the MSSM processes at our disposal.

The process at the top of Table 5.1 is the spin-independent eikonal answer of eq. (5.19), extended from the soft region where it is intended to be valid:

$$\begin{aligned}\frac{1}{\sigma_0}\,\frac{\mathrm{d}\sigma}{\mathrm{d}x_1\,\mathrm{d}x_2} \quad &= \quad \frac{\alpha_{\mathrm{s}}}{2\pi}\,C_F \left\{ \frac{2(x_1 + x_2 - 1 - r_1^2 - r_2^2)}{(1 + r_1^2 - r_2^2 - x_1)(1 + r_2^2 - r_1^2 - x_2)} \right. \\ &\left. - \frac{2r_1^2}{(1 + r_2^2 - r_1^2 - x_2)^2} - \frac{2r_2^2}{(1 + r_1^2 - r_2^2 - x_1)^2} \right\} . \quad (5.44)\end{aligned}$$

The first numerator, $2(x_1 + x_2 - 1 - r_1^2 - r_2^2)$, here is based on an evaluation of the $2p_1p_2$ numerator of eq. (5.19) with p_1 and p_2 given by their values after the emission of p_3. Away from the soft-gluon limit, however, there is some leeway in this assumption. If instead the p_1 and p_2 values before the emission of p_3 had been used, one would have obtained $x_1 + x_2 - 1 = 1 - x_3 \to 1$. Such a seemingly minor substitution has quite dramatic effects for collinear emission even at rather small x_3, however, and is not really an option. In order to have a not too unrealistic alternative to compare with, we therefore only allow deviations proportional to x_3^2. (This is also what comes out of the $x_1^2 + x_2^2$ numerator of the massless process $V \to \mathrm{q\overline{q}g}$.) The extreme in this direction would be $x_1 + x_2 - 1 \to 1 - x_3 + x_3^2$, but we will also allow arbitrary admixtures $x_1 + x_2 - 1 \to 1 - x_3 + \alpha x_3^2$, with α as a free parameter, obviously in no physics relation to the α introduced above.

In all the formulae, the decay product mass ratios are kept as free parameters, $r_1 = m_b/m_a$ and $r_2 = m_c/m_a$, while the gluon is massless. Since we are not interested in cross sections per se, but in the probability for gluon emission, in the LO cross sections only the mass dependence is retained, normalized to unity for $r_1 = r_2 = 0$, e.g.

$$
\begin{aligned}
&\sigma_0(V, A \to \mathrm{q_1\overline{q}_2}) = \\
&\frac{1}{2}\left\{2 - (r_1^2 - r_2^2)^2 - r_1^2 - r_2^2 \pm 6 r_1 r_2\right\} \sqrt{(1 - r_1^2 - r_2^2)^2 - 4 r_1^2 r_2^2}\ .
\end{aligned}
\tag{5.45}
$$

What is omitted is then some set of couplings and propagators. Exactly the same set is also omitted from the first-order $\mathrm{d}\sigma/\mathrm{d}x_1\,\mathrm{d}x_2$, thereby leaving the ratio unchanged. Additionally the common factor $(\alpha_\mathrm{s}/2\pi)C_F$, is omitted, to leave the choice of $\alpha_\mathrm{s}(p_\perp^2)$ free to be made elsewhere. The ratio of the first to leading order cross sections then gives the assumed differential gluon-emission rate. In the case of a mixture without and with γ_5 factors, the sum has to be taken for numerator and denominator separately, e.g.

$$
\begin{aligned}
&\frac{1}{\sigma_0}\,\frac{\mathrm{d}\sigma}{\mathrm{d}x_1\,\mathrm{d}x_2}(\mathrm{e}^+ e^- \to \gamma^*/\mathrm{Z}^0 \to \mathrm{q\overline{q}}) = \\
&\frac{\alpha\,\mathrm{d}\sigma^V/\mathrm{d}x_1\,\mathrm{d}x_2 + (1-\alpha)\,\mathrm{d}\sigma^A/\mathrm{d}x_1\,\mathrm{d}x_2}{\alpha\,\sigma_0^V + (1-\alpha)\,\sigma_0^A}\ .
\end{aligned}
\tag{5.46}
$$

The vector fraction α can here be read off from the lowest-order expression in eq. (5.42), where the mass factors of eq. (5.46) were omitted. The mass effects are instead included in the individual $\mathrm{d}\sigma/\mathrm{d}x_1\,\mathrm{d}x_2$ and σ_0 terms of eq. (5.47). This standard e.g. means that $V - A$ corresponds to $\alpha = 1/2$, which then because of mass effects gives a somewhat larger vector than axial fraction.

Note that first-order corrections to the total cross section are not included in the σ_0 denominator. This is not a unique choice, but a rather natural one: if we consider the gluon emission rate as the ratio of two cross sections, then including $\mathcal{O}(\alpha_\mathrm{s})$ corrections to one but not the other is not likely to improve the overall accuracy of the calculation. In the soft-gluon limit, it would even break the spin independence of the radiation pattern (cf. the next subsection), i.e. give the wrong physics. And since a complete one-loop calculation of both quantities is well beyond the scope of this article, we remain with lowest non-trivial order for both quantities. Furthermore, if the total cross section is written in the form $\sigma_{\text{tot}} = \sigma_0(1 + a\alpha_{\text{s}}/\pi)$, then decay rates calculated so far tend to give a values of order unity [28, 29], i.e. small effects. An exception would be Coulomb corrections in the threshold region, but there the phase space for real gluon emission is vanishingly small anyway, so of no physical interest. By contrast, one-loop corrections to three-jet rates tend to be larger [30], although most of that is absorbed by the parton-shower choice of a smaller kinematics-dependent scale like $p_\perp^2$ [30, 31].

5.4.2 Radiation Patterns

Before applying the matrix elements to specific physics situations, it is interesting to compare them between each other under similar conditions. This will provide an understanding of the amount of spin and colour dependence in the matrix elements, and thus the extent to which a process-dependent Monte Carlo implementation can be expected to provide an improvement over a process-blind one, e.g. based on some simple dead cone formula.

Fig. 5.3 is intended to provide a first qualitative glimpse of differences. The amount of detail may be bewildering, but at this point the idea is to bring up differences and similarities in a broad sense, without concentrating on each process specifically.

First consider the full curves in Figs. 5.3a–c, which are all for the colour structure $1 \to 3+\overline{3}$ and the same kinematics, and only differ by the spin pattern: $1 \to 1/2+1/2, 0 \to 1/2+1/2, 1 \to 0+0, 0 \to 0+0$, and $1/2 \to 1/2+0$, in relevant cases with and without a γ_5 (but no intermediate mixtures such as $1 \pm \gamma_5$). In the first frame, where the gluon is soft, these curves almost completely overlap. At smaller x_3 the agreement becomes even better, and one can then truly speak of a universal soft-gluon emission pattern, with a characteristic dead cone of opening angle $\theta \approx 2r = 0.4 = 23°$ in this example. By contrast, when x_3 is increased, the curves tend to disagree more and more. At $x_3 = 0.3$, the dead cone is still visible, although it is starting to fill in, but at $x_3 = 0.6$ it is completely gone. Note that the vertical scale changes significantly between the three frames; in absolute numbers the differences between the curves is about a factor two larger at $x_3 = 0.1$ than at 0.6, but in relative terms the differences are negligible at small x_3.

This should bring home the message that the dead cone concept can only be used at small gluon energies, and is irrelevant for energetic gluons. It is only the lowest of the full curves, the completely spinless process $0 \to 0 + 0$, that does preserve the exact dead cone concept, i.e. has a cross section that always vanishes in the collinear limit (in the rest frame of the decaying particle).

The lower dotted curve is the eikonal expression of eq. (5.44), which is constructed to have an exact dead cone. It does agree fairly well with the spinless process, but not with anything else. The upper dotted curve is the

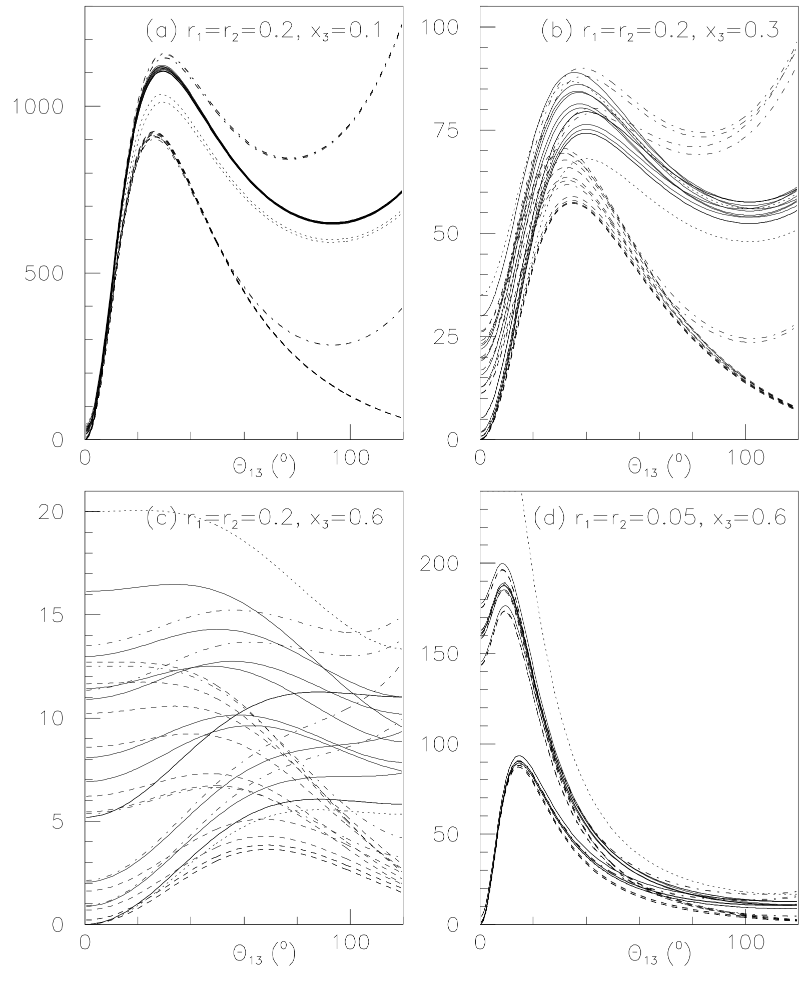

Figure 5.3: The gluon emission rate as a function of the emission angle θ_{13}. Specifically, the vertical axis gives $(1/\sigma_0)\mathrm{d}\sigma/\mathrm{d}x_1\,\mathrm{d}x_2$ with a normalization factor $(\alpha_\mathrm{s}/2\pi)C_F$ removed. This three-jet phase space density differs from $\mathrm{d}\sigma/\mathrm{d}\theta_{13}\,\mathrm{d}x_3$ by a simple Jacobian. A variety of different processes are compared: decay of a colour singlet to a triplet plus an antitriplet full curves, ditto in the eikonal approximation dotted, decay of a triplet to a triplet plus singlet dashed, and gluino processes dash-dotted. The four frames differ in the scaled masses $r_i = m_i/E_\mathrm{CM}$ of the two decay products, and in the gluon energy fraction x_3. Further explanations are given in the text.

colour	spin	γ_5	$\int x_3$	$\int (1-x_1)(1-x_2)$	$\int \theta(y_{\mathrm{D}}-0.1)$
$1 \to 3 + \overline{3}$	$1 \to \frac{1}{2} + \frac{1}{2}$	1	1.000	1.000	1.000
		γ_5	1.056	1.112	1.133
	$0 \to \frac{1}{2} + \frac{1}{2}$	1	1.134	1.293	1.376
		γ_5	1.093	1.207	1.271
	$1 \to 0 + 0$	1	1.073	1.205	1.310
	$0 \to 0 + 0$	1	0.875	0.758	0.720
	$\frac{1}{2} \to \frac{1}{2} + 0$	1	0.953	0.918	0.916
		γ_5	1.057	1.132	1.179
$1 \to 3 + \overline{3}$	eikonal	—	0.802	0.695	0.659
	eikonal $+x_3^2$	—	1.201	1.518	1.670

Table 5.2: Three measures on the amount of gluon radiation in different processes, for mass ratios $r_1 = r_2 = 0.2$. For clarity, results have been normalized to the process in the top line. See the text for a detailed explanation. (this table is continued on the next page).

modified eikonal, with an x_3^2 term added. It tends to overshoot all processes at small angles, while some intermediate mixture, $\alpha \approx 0.5$, would do a sensible job for many processes in the small-angle region. For medium small gluon energies and large angles, both eikonal forms undershoot, however. In general, one may conclude that the eikonal formula is not particularly useful for practical considerations, and that the process-specific matrix elements need to be used.

Of course, the detailed pattern depends on the masses. In Fig. 5.3d these are lower than in the first three, and representative for $\mathrm{Z}^0 \to \mathrm{b}\overline{\mathrm{b}}$. Then the dead cone concept works up to somewhat larger gluon energies, and a trace of it is still left at $x_3 = 0.6$. It is again preserved exactly for $0 \to 0 + 0$ and the eikonal, and also approximately for $1 \to 0 + 0$.

In order to quantify the difference in the total amount of gluon radiation, we compare three measures on the three-jet phase space. Since the total three-jet cross section contains a soft-gluon divergence, this soft region has to be avoided. One measure is thus to integrate the total amount of radiated gluon

colour	spin	γ_5	$\int x_3$	$\int(1-x_1)(1-x_2)$	$\int \theta(y_\mathrm{D}-0.1)$
$3 \to 3+1$	$\frac{1}{2} \to \frac{1}{2}+1$	1	0.323	0.306	0.287
		γ_5	0.356	0.365	0.349
	$\frac{1}{2} \to \frac{1}{2}+0$	1	0.312	0.284	0.258
		γ_5	0.357	0.363	0.344
	$0 \to 0+1$	1	0.287	0.242	0.218
	$0 \to 0+0$	1	0.279	0.224	0.194
	$0 \to \frac{1}{2}+\frac{1}{2}$	1	0.359	0.379	0.375
		γ_5	0.347	0.354	0.346
	$\frac{1}{2} \to 0+\frac{1}{2}$	1	0.294	0.257	0.239
		γ_5	0.314	0.302	0.298
$3 \to 3+8$	$0 \to \frac{1}{2}+\frac{1}{2}$	1	1.634	1.833	1.922
		γ_5	1.574	1.712	1.775
	$\frac{1}{2} \to 0+\frac{1}{2}$	1	1.385	1.320	1.291
		γ_5	1.549	1.664	1.675
$8 \to 3+\overline{3}$	$\frac{1}{2} \to \frac{1}{2}+0$	1	0.561	0.493	0.445
		γ_5	0.621	0.607	0.574

Table 5.2: continued.

energy, in shorthand

$$\int x_3 = \int x_3 \, \frac{1}{\sigma_0} \, \frac{\mathrm{d}\sigma}{\mathrm{d}x_1 \, \mathrm{d}x_2} \, \mathrm{d}x_1 \, \mathrm{d}x_2 \ . \tag{5.47}$$

Correspondingly we define a shorthand $\int(1-x_1)(1-x_2)$ as an alternative removal of the denominator of the matrix elements (generalized to $\int(1+r_1^2-r_2^2-x_1)(1+r_2^2-r_1^2-x_2)$ for unequal masses). Finally a Durham distance [32] $y_{ij} = \min(x_i^2, x_j^2)(1-\cos\theta_{ij})/2$ is used to define a hard three-jet region for which $y_\mathrm{D} = \min(y_{12}, y_{13}, y_{23}) > 0.1$ and a corresponding three-jet rate $\int \theta(y_\mathrm{D}-0.1)$, where θ is the step function. To simplify a comparison between the processes, all results have arbitrarily been normalized to those for the $V \to \mathrm{q\overline{q}}$ process.

As can be seen in Table 5.2, the three measures give about the same message, namely that differences between the processes are significant. In $\int x_3$ the ratio between the two extremes is a factor 1.30, in $\int (1-x_1)(1-x_2)$ 1.70, and in $\int \theta(y_\mathrm{D} - 0.1)$ 1.91. This shows a steady progression of larger ratios the more one is biased towards the hard three-jet region. The eikonal expression is below all the calculated processes, and the modified eikonal (full blast) above.

The results in Table 5.2 are for the case where the daughter masses constitute a significant fraction of the energy available. The other limit, where instead the daughters are massless, is shown in Table 5.3. The main message is that the process dependence remains also in the latter case, even if normally reduced in magnitude by about a factor of two between the extremes. The detailed picture is not so simple, however. Some processes agree in the massless limit when they do not for nonvanishing masses while, in the other extreme, others disagree even more for vanishing masses.

The set of processes with colour structure $3 \to 3 + 1$ can be viewed as crossed versions of the $1 \to 3 + \overline{3}$ ones, but the differences in kinematics result in another overall picture. Examples of radiation patterns are shown by dashed curves in Fig. 5.3. The small-angle behaviour displays the universal dead cone effect at small x_3 and again diverges wildly at larger x_3. Note that we have oriented all processes so that the radiating daughter colour charge is at $0°$, wherefore the radiation continues to drop off at large angles. This is unlike the previous set of curves, which turn around at or near the mid angle to the other radiating daughter. (For small x_3 the two daughters are almost back-to-back, i.e. a bisector at $90°$, while an x_3 of 0.6 allows an almost symmetric configuration with $120°$ between all three.)

It is here interesting to remind of the QED answer for the process $V \to \mathrm{f\overline{f}}\gamma$ with $m_\mathrm{f} = m_{\overline{\mathrm{f}}} = 0$ [33]

$$\frac{1}{\sigma_0} \frac{\mathrm{d}\sigma}{\mathrm{d}x_1\,\mathrm{d}x_2} = \frac{\alpha_\mathrm{em}}{2\pi} \frac{x_1^2 + x_2^2}{(1-x_1)(1-x_2)} \left(e_\mathrm{f} \frac{1-x_1}{x_3} - e_{\overline{\mathrm{f}}} \frac{1-x_2}{x_3} \right)^2 , \tag{5.48}$$

where $e_V = e_\mathrm{f} + e_{\overline{\mathrm{f}}}$ has been used to eliminate the explicit appearance of terms corresponding to radiation off the V. For $e_V = 0$, $e_\mathrm{f} = -e_{\overline{\mathrm{f}}}$ this is the QED analogue of eq. (5.9), while the current case corresponds to $e_{\overline{\mathrm{f}}} = 0$, $\alpha_\mathrm{em} e_\mathrm{f}^2 \to \alpha_\mathrm{s} C_F$:

$$\begin{aligned} \frac{1}{\sigma_0} \frac{\mathrm{d}\sigma}{\mathrm{d}x_1\,\mathrm{d}x_2} &= \frac{\alpha_\mathrm{s}}{2\pi} C_F \frac{x_1^2 + x_2^2}{(1-x_1)(1-x_2)} \left(\frac{1-x_1}{x_3} \right)^2 \\ &= \frac{\alpha_\mathrm{s}}{2\pi} C_F \frac{x_1^2 + x_2^2}{x_3(1-x_2)} \frac{1-x_1}{x_3} . \end{aligned} \tag{5.49}$$

Here the first part of the final expression essentially is the shower answer of eq. (5.36). In the soft-gluon limit $(1-x_1)/x_3 \approx (1+\cos\theta_{13})/2 \approx (1-\cos\theta_{23})/2$,

colour	spin	$\int(1-x_1)(1-x_2)$	$\int\theta(y_{\mathrm{D}}-0.1)$
$1\to 3+\overline{3}$	$1\to\frac{1}{2}+\frac{1}{2}$	1.000	1.000
	$0\to\frac{1}{2}+\frac{1}{2}$	1.167	1.184
	$1\to 0+0$	1.000	1.141
	$0\to 0+0$	0.667	0.773
	$\frac{1}{2}\to\frac{1}{2}+0$	0.917	0.979
$1\to 3+\overline{3}$	eikonal	0.667	0.773
	eikonal $+x_3^2$	1.667	1.595
$3\to 3+1$	$\frac{1}{2}\to\frac{1}{2}+1$	0.347	0.282
	$\frac{1}{2}\to\frac{1}{2}+0$	0.347	0.282
	$0\to 0+1$	0.222	0.214
	$0\to 0+0$	0.222	0.214
	$0\to\frac{1}{2}+\frac{1}{2}$	0.389	0.328
	$\frac{1}{2}\to 0+\frac{1}{2}$	0.264	0.260
$3\to 3+8$	$0\to\frac{1}{2}+\frac{1}{2}$	1.701	1.659
	$\frac{1}{2}\to 0+\frac{1}{2}$	1.389	1.384
$8\to 3+\overline{3}$	$\frac{1}{2}\to\frac{1}{2}+0$	0.573	0.487

Table 5.3: Two measures on the amount of gluon radiation in different processes, for mass ratios $r_1 = r_2 = 0$, cf. Table 5.2. For massless daughters the γ_5 factor makes no difference, and so those results are not shown separately. The $\int x_3$ measure now is collinear divergent and therefore not shown.

so this extra factor gives a further dampening at large emission angles, above the shower ansatz (which in itself is dampened by one such angular factor relative to the colour singlet decay). A main consequence of this extra factor is that the three-jet activity in a colour $3\to 3+1$ event is less than half of that of a $1\to 3+\overline{3}$ one, a pattern which remains when masses are included, see Table 5.2.

Finally we come to the processes with a gluino, denoted by dash-dotted lines

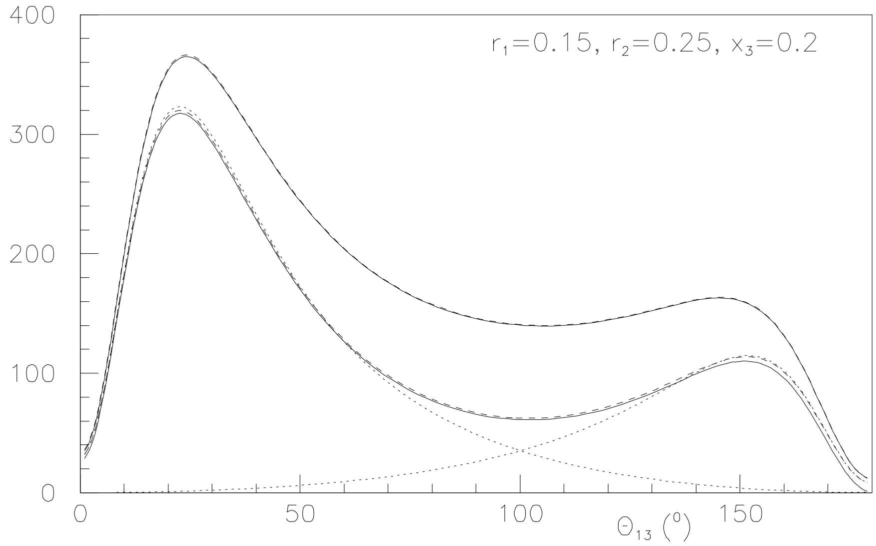

Figure 5.4: Test of the additivity of gluon emission rates, $\mathrm{d}\sigma/\mathrm{d}x_1\,\mathrm{d}x_2$ with a normalization factor $\sigma_0\,C_F\,\alpha_\mathrm{s}/2\pi$ removed. The dotted curves show two processes with colour flow $3 \to 3+1$ and $3 \to 1+3$, respectively (and spin $1/2 \to 1/2+1$). The upper and lower full curves give the complete expressions for $1 \to 3+\overline{3}$ (spin $1 \to 1/2+1/2$) and $8 \to 3+\overline{3}$ (spin $1/2 \to 1/2+0$) processes, respectively. The two dashed curves, almost completely hidden by the full ones, are the same processes according to the additive approximations in eq. (5.50).

in Fig. 5.3. In the limit of infinitely many colours N_C, the process $3 \to 3+8$ may be viewed as one colour flowing through from the initial triplet to the gluino, and a different colour-anticolour pair created between the final triplet and the gluino, i.e. as the sum of $3 \to 1+3$ and $1 \to 3+\overline{3}$. Interference terms between the two colour flows would be suppressed by a factor $1/N_C^2$, just as in the radiation pattern for the colour-related process $V \to \mathrm{q}\overline{\mathrm{q}}\mathrm{g}$ [19]. This process therefore shows the most three-jet activity of the ones studied, especially in the not-displayed gluino hemisphere.

By the same token, $8 \to 3+\overline{3}$ may be approximated by the incoherent sum of a $3 \to 3+1$ and a $\overline{3} \to 1+\overline{3}$ radiation pattern, which gives less radiation than the $1 \to 3+\overline{3}$ processes. The QED formula, eq. (5.48), may here offer a convenient starting point. The $1 \to 3+\overline{3}$ process corresponds to $e_\mathrm{f} = -e_{\overline{\mathrm{f}}}$, so that the interference term $-e_\mathrm{f}e_{\overline{\mathrm{f}}}$ is positive. The $8 \to 3+\overline{3}$ process, e.g. $\tilde{\mathrm{g}} \to \mathrm{q}\overline{\mathrm{q}}$, can instead be emulated in QED by $e_\mathrm{f} = e_{\overline{\mathrm{f}}}$, i.e. a doubly-charged gluino [34]. The interference term then is negative, although suppressed by a colour factor $1/N_C^2$ in the QCD case.

Thus, given a radiation pattern $f_1(\theta_{13})$ for emission off parton 1 like in a colour $3 \to 3+1$ process, and a corresponding $f_2(\theta_{13})$ for a colour $3 \to 1+3$ one (essentially obtainable by swapping the kinematics of the above process, $x_1 \leftrightarrow x_2$, $r_1 \leftrightarrow r_2$) one may guess at the radiation pattern for the $1 \to 3+\overline{3}$ and $8 \to 3+\overline{3}$ processes:

$$\begin{aligned} f_{1\to 3+\overline{3}}(\theta_{13}) &= f_1(\theta_{13}) + f_2(\theta_{13}) + 2\sqrt{f_1(\theta_{13})f_2(\theta_{13})}\ , \\ f_{8\to 3+\overline{3}}(\theta_{13}) &= f_1(\theta_{13}) + f_2(\theta_{13}) - \frac{2}{9}\sqrt{f_1(\theta_{13})f_2(\theta_{13})}\ . \end{aligned} \tag{5.50}$$

This turns out to be a good approximation up to fairly large x_3 values, i.e. so long as the spin structure is not too important, see e.g. Fig. 5.4. The importance of the interference term also gives a simple explanation for the difference between the height of the peaks in the full and dashed curves in Fig. 5.3a–b.

5.4.3 Parity Dependence

Let us further quantify differences induced by having or not a γ_5 factor in the matrix element, i.e. between vector (V) and axial vector (A) sources, between scalar (S) and pseudoscalar (P) ones, etc. We will use a measure which is the mean of the matrix element ratios over the whole phase space for gluon emission. Since the matrix elements with and without the γ_5 coupling both have the same divergence structures the ratio is well-behaved everywhere. All phase space points are here given equal weight, so large differences may not always be reflected in significant changes of the radiation pattern. To be specific, we study the function

$$\langle Q\rangle(r_1,r_2) = \frac{1}{\int \mathrm{d}x_1\mathrm{d}x_2}\int Q(x_1,x_2,r_1,r_2)\mathrm{d}x_1\mathrm{d}x_2, \tag{5.51}$$

where

$$Q(x_1,x_2,r_1,r_2) = \frac{\sigma_0^1}{\sigma_0^{\gamma_5}}\frac{\mathrm{d}\sigma^{\gamma_5}/\mathrm{d}x_1\mathrm{d}x_2}{\mathrm{d}\sigma^1/\mathrm{d}x_1\mathrm{d}x_2}. \tag{5.52}$$

$Q(x_1,x_2,0,0)$ is equal to unity in all of phase space and in most cases $Q(x_1,x_2,r,0)$ is also equal to unity. The exception is when the $r=0$ mass is a boson (spin 0 or 1) and the $r \neq 0$ one is spin $\frac{1}{2}$. All the processes in Table 5.1 which have both non-γ_5 and γ_5 couplings are represented in Fig. 5.5. Processes with the same spin structure have the same ratio, where both the spin of the initial and final states, as well as the order of the decay products, are of importance. We notice that the difference between e.g. vector and axial

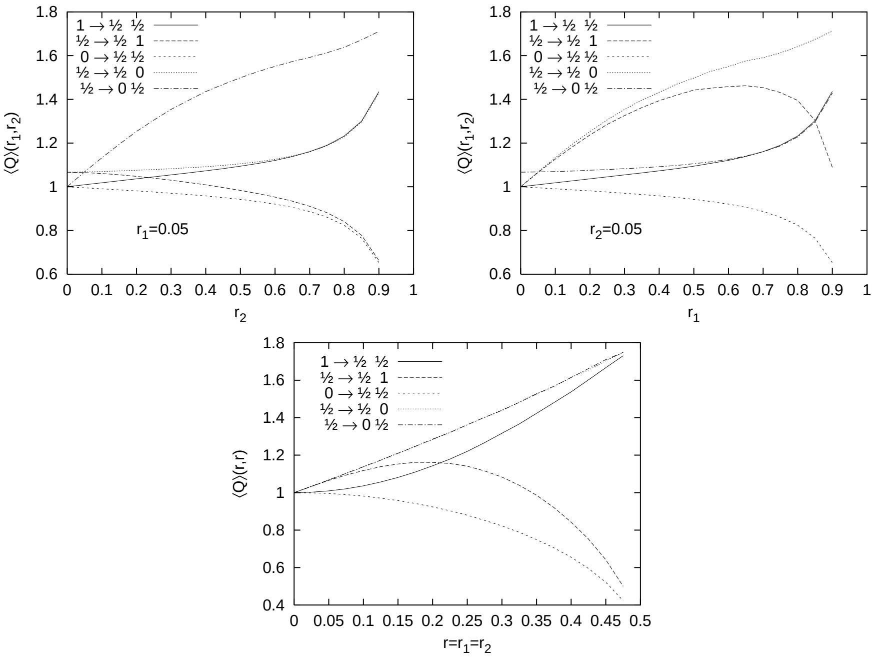

Figure 5.5: $\langle Q\rangle(r_1, r_2)$, eq. (5.51), with r_1 fixed, r_2 fixed, or $r = r_1 = r_2$. The processes are grouped according to spin structure.

vector couplings can be rather large in some cases, even for small and intermediate masses. The most important case, however, with two fermions in the final state, show small differences for $r < 0.5$, so this aspect will only be significant in the case of top production. Physical consequences will be investigated in Section 5.5.

5.5 Applications

In this section, the matrix element corrected shower is used to study some processes at current and future colliders. It is not to be seen as a comprehensive review, but as simple examples intended to illustrate the main features.

5.5.1 Bottom in Z^0 Decay

We start by examining a process where data with good statistics already exists and detailed comparisons are possible, namely gluon radiation off bottom quarks produced in the process $e^+e^- \to Z^0 \to b\overline{b}$ at the Z^0 pole. Gluons are not observed directly in the final state, instead they materialize as jets of hadrons. We will mainly consider jets on the parton level, but we also study the effects of hadronization and decays. The experimental data with which our results are compared have already been corrected to the parton level, using, among others, the same model for fragmentation which we will use.

Jets are constructed by considering all pairs of particles (i, j) in an event, where the particles can be hadrons, partons or clusters of hadrons or partons, finding the pair with the smallest "distance" y_{ij}. If this number is smaller than the "jet resolution" parameter, y_c, the pair is joined into a new cluster by summing up their four-momenta. This procedure is repeated until all y_{ij} are larger than y_c. The resulting clusters are the jets in the event at the resolution scale y_c. Jet algorithms differ mainly by the definition of y_{ij}, and several jet measures have been proposed in the literature [32, 35]. Following the lead of the LEP analyses we want to compare with, we have settled on the DURHAM [32] algorithm which defines

$$y_{ij} = \frac{2\min(E_i^2, E_j^2)(1-\cos\theta_{ij})}{E_{\mathrm{vis}}^2}. \tag{5.53}$$

For small angles, this is approximately the relative transverse momentum squared of the pair, scaled to the visible energy in the event. If jets are constructed with a large y_c, only the most energetic partons will be resolved, and most events will become 2-jet events. When y_c is decreased, smaller structures will start to emerge and multi-parton final states become more important. It is in this region that the parton shower approach to gluon radiation is most useful.

For a primary quark flavour q, the n-jet rate is defined as

$$R_n^q(y_c) = \frac{\sigma_{\mathrm{q\overline{q}}\to n\ \mathrm{jets}}(y_c)}{\sigma_{\mathrm{q\overline{q}}\to\mathrm{hadrons}}}, \tag{5.54}$$

which for $n > 2$ is generally a decreasing function of y_c. We want to study the difference between gluon radiation off b quarks and off light quarks. A suitable observable is then the ratio between the respective n-jet rates

$$R_n^{bl}(y_c) = \frac{R_n^b(y_c)}{R_n^l(y_c)}, \text{ with } l = \mathrm{u,\ d\ or\ s}. \tag{5.55}$$

Experiments at LEP [36, 37] have found both R_3^{bl} and R_4^{bl} to be smaller than one, approaching unity for large y_c. This can be understood qualitatively as a consequence of the well-known dead cone effect [4], stating that the radiation of collinear gluons off heavy quarks is suppressed. The production of well separated jets, however, is not significantly suppressed and should approach that of the light quarks for large y_c.

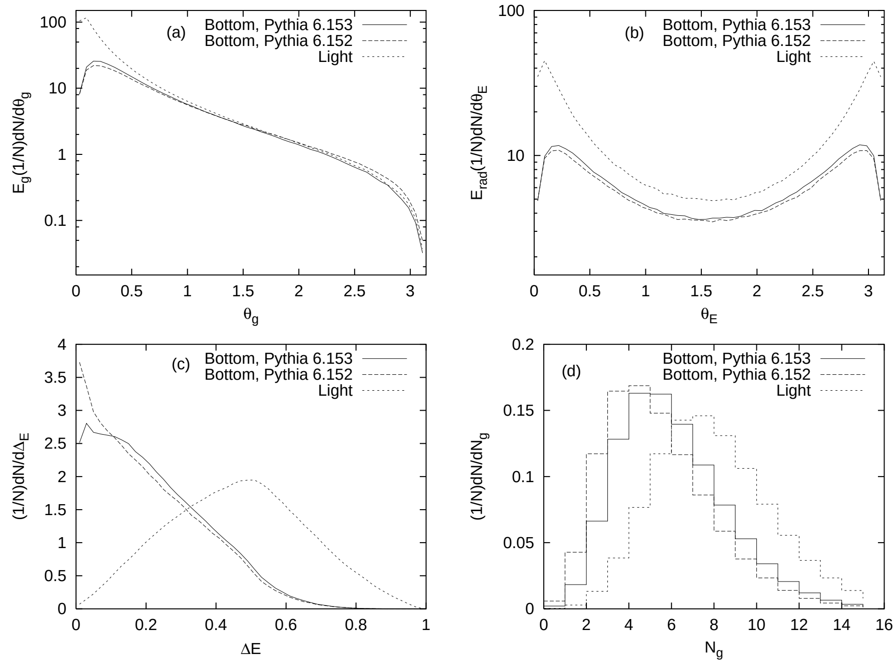

Figure 5.6: Gluon radiation and energy flow in the process $e^+e^- \to Z^0 \to q\overline{q}$, where q is either a light (u, d, s) quark or a b quark. The b-mass is here set to the default in PYTHIA, 4.8 GeV. (a) Energy weighted gluon angle distribution. (b) Energy flow. (c) Radiated energy fraction, $\Delta E = E_{\mathrm{rad}}/E_{\mathrm{CM}}$. (d) Gluon multiplicity.

We want to study this effect more quantitatively by using our improved, matrix element corrected, parton shower. The new approach, described in Section 5.3, has been implemented in PYTHIA 6.153. This is compared to PYTHIA 6.152 containing the older approach of Section 5.2.4, which includes the correct massive matrix element correction in the first emission only. As a reference, we also include results from the algorithm implemented in PYTHIA 6.129, where mass-effects are incorrectly included in the matrix element correction of the first emission, cf. Section 5.2.3.

The jet rate reflects both the amount of energy radiated and the direction in which it is radiated. Fig. 5.6a shows the gluon radiation pattern in the process $e^+e^- \to Z^0 \to q\overline{q}$ at the Z^0-pole, for the old and the new shower routines both for light (u, d and s) quarks and heavy (bottom) quarks. The angle, θ_g, is defined as the angle between the radiated gluon and the primary quark in the CM system of the primary quark pair. In principle, gluons are radiated by the $q\overline{q}$ dipole as a whole, but in our implementation each radiated gluon is assigned to an initial quark, and in the collinear limit this separation is quite sensible. In the case of the total energy flow, Fig. 5.6b, we add the two contributions, and include the energy taken by quarks produced in gluon splitting, so two symmetrical peaks appear. Fig. 5.6c shows the distribution of $\Delta E = E_{\mathrm{rad}}/E_{\mathrm{CM}}$, i.e. the total energy fraction radiated in the shower. Fig. 5.6d, finally, shows the gluon multiplicity in the shower, which obviously is quite dependent on the lower shower cut-off Q_0.

We note first of all that the difference between light and heavy quarks is largest in the region of small angles, the dead cone, and also that the radiated energy fraction is much larger for light quarks, peaked around 0.5 if $Q_0 = 1$ GeV is used to remove the collinear emission off light quarks. For heavy quarks, this collinear emission is regulated by the mass. For large angles, the light and heavy quark distributions converge as they should. In the new approach, the amount of gluon radiation in b events at small angles is somewhat enhanced relative to the old one, where the dead cone was slightly exaggerated, but differences are small. By the change of evolution variable, eq. (5.26), the fraction of events without any shower at all ($\Delta E = 0$) has decreased by almost a factor of 3 from about 4 per mille to 1.4. As a consequence, the peak at $\Delta E = 0$ has been flattened out. The gluon multiplicity has also increased slightly.

We now want to investigate how the changes in the algorithm affect R_3^{bl} and R_4^{bl}. Since one is studying small deviations from unity, these measures are very sensitive to changes in the gluon radiation pattern. Also, the LEP experiments have large samples of Z^0 events and studies at the per cent level are feasible. We will mostly study the behaviour of the model on the parton level, comparing different alternatives. Here the parton level is defined by the partonic configuration at the shower cut-off scale Q_0, below which no further emissions occur. But first we should comment on the effects of fragmentation. Below the Q_0 scale, the Lund string fragmentation model [1] describes how the partons transform into the primary hadrons. Subsequently these may decay further. Once a Q_0 has been chosen, the parameters of the fragmentation model should be fitted to data. Here we will only study the variation with Q_0, both at the parton level and the hadron level, without any such retuning. At the hadron level, we consider first the primary hadrons and study decay effects separately.

Fig. 5.7a shows the effect of fragmentation and the Q_0 dependence. We calculate $R_3^{bl}(y_c)$ at the parton level and at the level of primary hadrons for $Q_0 = 1$ and 2 GeV, respectively. The Q_0 dependence is largest on the parton level with R_3^{bl} slightly lower for the larger Q_0. This is because the increase in Q_0 increases the 3-jet rate for light quark events, while heavy-quark events are not influenced as much: collinear emissions, which dominate at the end of the

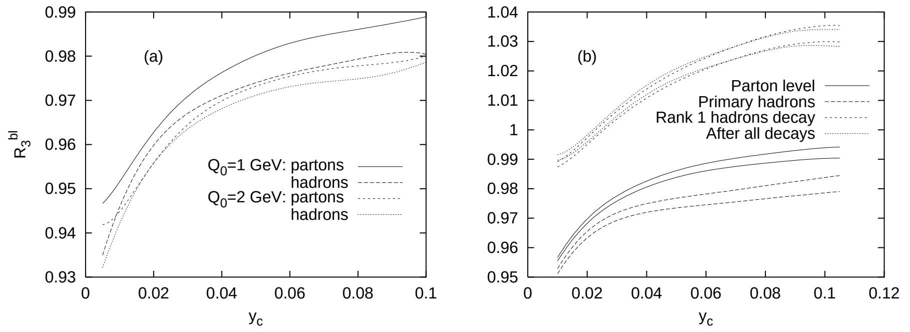

Figure 5.7: Study of fragmentation and decay effects. (a) Effects of changing the cut-off, Q_0, in the shower, both on the parton level and at the level of primary hadrons (i.e. before decays). (b) Effects of hadronization, decay of rank 1 hadrons and decay of all hadrons. In (b) each alternative is represented by the $\pm$ 1σ curves given by the Monte Carlo statistics.

cascade, are suppressed anyway. Intuitively one might have expected the jet rate to be higher for a lower Q_0, since this corresponds to a larger number of partons, but the further partons emitted between 1 and 2 GeV cannot give rise to new jets of their own. They only smear out the energy of the existing jets and possibly make them fall below the cut-off. Furthermore, the hadronization stage tends to decrease the Q_0 dependence because the Lund model is infrared safe and collinear gluon emissions do not affect the string fragmentation process. A retuning of the fragmentation parameters would further limit the effect of small changes in Q_0.

Fig. 5.7b shows the effects of fragmentation and decay. The rank 1 hadrons are the ones that contain the primary quarks from the decay of the Z^0. In the case of bottom production, the rank 1 hadrons will be mainly B mesons and Λ_b baryons. Because of the hard fragmentation function for heavy hadrons, the multiplicity of primary hadrons in b events is smaller than that in a light quark event, reflected in the lower R_3^{bl} curve. However, once the heavy hadrons have decayed, their decay products will more than compensate this. Thus, if the primary hadrons are allowed to decay, the value of R_3^{bl} lies above unity for $y_c > 0.03$. So, on the one hand, heavy hadrons take a large part of the primary quark energy, but they also decay to many particles. For R_3^{bl} there is not a large difference between allowing all primary hadrons to decay or only the rank 1 ones, which can be seen in the small difference between the two top curves in Fig. 5.7b. In the following, we will compare our results to experimental data on the parton level, bearing in mind that this comparison can be ambiguous in

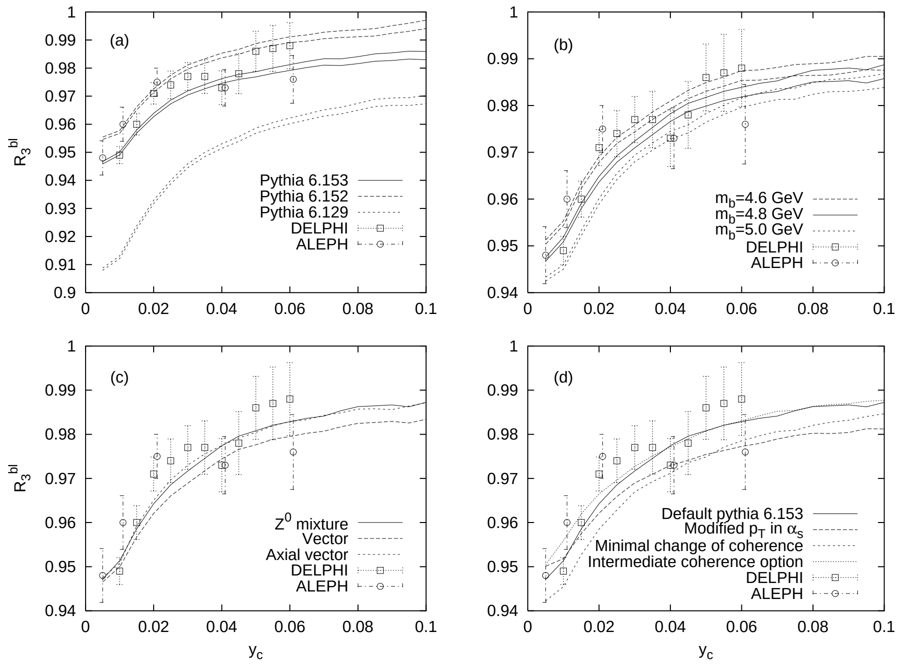

Figure 5.8: $R_3^{bl}(y_c)$ for different model parameters and variations. (a) Different main versions. Some variations of the latest version (6.153): (b) Different bottom masses. (c) Different sources. (d) Other minor variations of the main theme, see the text for details. The data are from [36] and [37]. The data points from Aleph (except the first) have been shifted .001 units in y_c for clarity. In (a) and (b) the $\pm 1\sigma$ curves are given, while only the central value is shown in (c) and (d) for clarity, but the statistics is comparable.

view of the dependence on Q_0. Our aim here is not to achieve a perfect fit to data, but merely ensure that the results are at the right level. As we will see, the data is anyway not good enough to make precise discriminations between all different model variations.

In Figs. 5.8–5.9, R_3^{bl} and R_4^{bl} are shown as functions of y_c for several model variations. Figs. 5.8a, 5.9a show the difference between the old and the modified shower models. An even older version, where mass effects are exaggerated, is also shown as reference. Each model curve is displayed as a one sigma band, showing the size of the Monte Carlo error for $15 \cdot 10^6$ events of each kind. From the increase in multiplicity and energy flow in b events in the new model, one would naively expect the 3- and 4-jet rates to increase for heavy quarks,

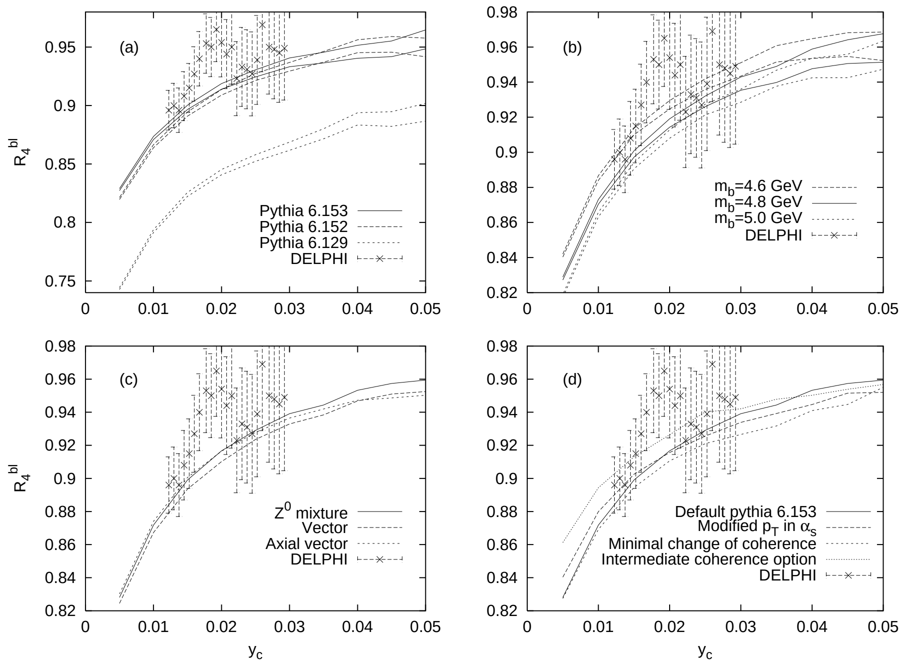

Figure 5.9: $R_4^{bl}(y_c)$ for different model parameters and variations. See caption Fig. 5.8 for details.

thus increasing R_n^{bl}. Actually, the main effect is to reduce the 3-jet rate for heavy quarks, again illustrating that allowing more collinear/soft emissions will not necessarily increase the rate of well separated jets. The naively expected increase of R_4^{bl} (from subsequent branchings) is balanced by a corresponding "smearing" loss as for R_3^{bl}, giving only a small net effect.

As already noted, the old and new models differ mainly in the treatment of subsequent branchings; both include matrix element corrections to the first gluon emission on each side of the event. A clear discrimination between these two versions is not possible, especially in view of the variations that follow below and the relatively large experimental errors. It is clear, however, that the algorithm in Pythia 5.129 is ruled out by the data.

Next we consider variations to the new default, in order to assess the uncertainties of the model:

- The bottom mass.
- Parity dependence (vector vs axial vector source).
- Change of $p_\perp^2$ argument in α_s from $z(1-z)m_a^2$ to $z(1-z)m_a^2(1-m_b^2/m_a^2)^2$

in a branching $a \to bc$, with a being a heavy quark.

- Coherence effects.

The main free parameter is the bottom mass, and Figs. 5.8b, 5.9b show the result of varying this mass between 4.6 GeV and 5 GeV. Fits of NLO QCD calculations to LEP data give a value around 3 GeV for the running bottom mass in the $\overline{\mathrm{MS}}$ renormalization scheme [5, 36, 37] at renormalization scale m_{Z}. Our model is based on LO matrix elements and the mass in our case is the constituent quark mass, so they need not agree. However, a somewhat lower mass than the default seems to be favoured, especially for R_4^{bl}.

In Sections 5.4.2 and 5.4.3 we saw that there are slight differences between different sources. The relevant mixture for Z^0 is given by eq. (5.42), but in Figs. 5.8c, 5.9c we study the two extreme cases of a pure vector source and a pure axial vector one. At the Z^0-pole, the axial vector component dominates, as can be seen in the figure, but at higher energies the vector one will take over. We see that the differences are non-negligible, but not as large as the shown mass dependence, at least for small y_c.

Finally, in Figs. 5.8d, 5.9d, some further aspects of the model, discussed in Section 5.3.4, are varied. Both the modified $p_\perp$ in α_{s} and the "minimal" change of coherence tends to reduce R_3^{bl}, again showing how an increase in the total amount of radiation need not give more separate jets. The "intermediate" coherence option, which still is a realistic alternative, does give an increase, especially of R_4^{bl}. Thereby the overall agreement with data is improved, as much as with a reduced b mass, although uncertainties are sufficiently large that no firm conclusions should be drawn.

Other minor issues could be studied and here we just mention a few. The definition of R_n^{bl} used here is based on a classification of events with heavy or light *primary* quarks. An alternative is to use a ratio between b-tagged and anti b-tagged events. The difference here is in the classification of events with gluon splitting, $\mathrm{g} \to \mathrm{b}\overline{\mathrm{b}}$, in the shower. For the R_3^{bl} ratio this is a minor issue, but it is non-negligible in the case of R_4^{bl} [5]. This uncertainty is currently under study in the DELPHI collaboration, and is not further addressed here. Another issue is the energy dependence of the results. Obviously the mass effects will decrease for larger energies, because of the decrease of $r = m_{\mathrm{b}}/\sqrt{s}$, and this has already been studied at 189 GeV [5]. At the same time, however, the fraction of vector coupling increases significantly above the Z^0-pole, thus decreasing R_3^{bl}, cf. Fig. 5.8c. At intermediate energies this could therefore give rise to a partial cancellation of effects.

5.5.2 Bottom in Higgs Decay

We now turn to gluon radiation in Higgs decay. In the standard model, the decay $\mathrm{H}^0 \to \mathrm{b}\overline{\mathrm{b}}$ is expected to be large, or even dominate, for Higgs masses up

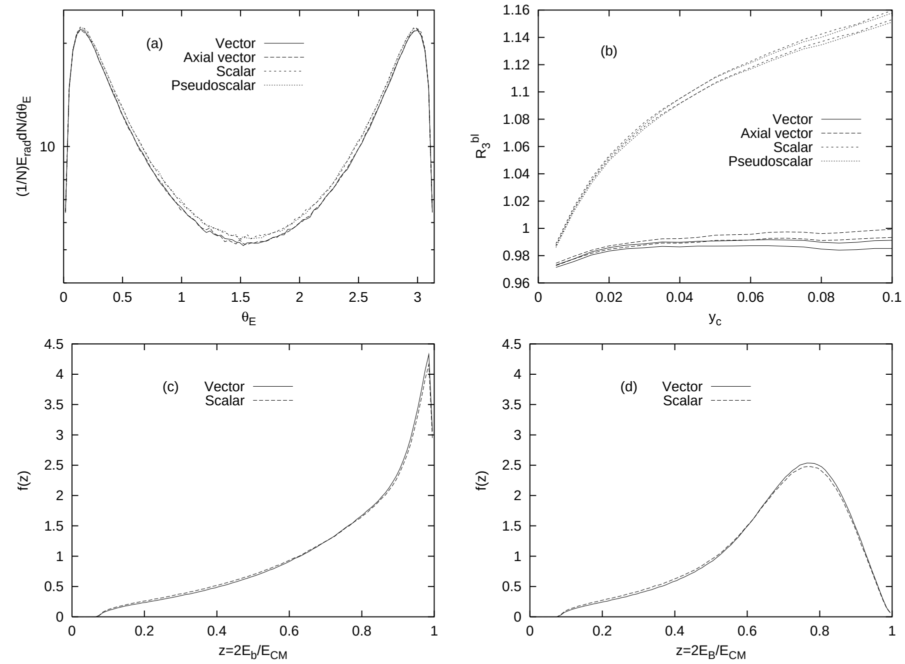

Figure 5.10: Comparison between vector, axial vector, scalar and pseudoscalar sources of $\mathrm{b\overline{b}}$ pairs at 130 GeV. (a) Energy flow in the shower. (b) 3-jet rate, normalized to $\gamma^*/\mathrm{Z}^* \to \mathrm{q\overline{q}}$, i.e. $R_3^{bl}(y_c) = R_3^b(X \to \mathrm{b\overline{b}})/R_3^l(\gamma^*/\mathrm{Z}^* \to \mathrm{q\overline{q}})$, where X is V, A, S or P and q is a light flavour. 1σ Monte Carlo error bands are shown. (c) Distribution of $z_\mathrm{b} = 2E_\mathrm{b}/\sqrt{s}$ at the parton level. (d) Distribution of $z_\mathrm{B} = 2E_\mathrm{B}/\sqrt{s}$, i.e. the fragmentation function, at the hadron level (only primary hadrons are considered).

to the $\mathrm{W^+W^-}$ threshold, and in extensions to the standard model also heavier Higgs states can have significant $\mathrm{b\overline{b}}$ branching ratios. When the fragmentation function for B mesons, i.e. the distribution of $z = 2E_\mathrm{B}/\sqrt{s}$, is measured at LEP1, the b quark is produced from a spin 1 source. If instead the source is a Higgs boson, the difference in gluon radiation could give rise to a changed fragmentation function. Such a change would influence the experimental vertex detection efficiency which, if uncorrected, would give rise to errors in the determination of cross sections. It is therefore important to be able to describe in detail the gluon radiation pattern in this decay. A different measure of the nature of the source is the jet topology, which is also studied in the form of a modified R_3^{bl} ratio, cf. the preceding section.

We choose to study the production of $\mathrm{b\overline{b}}$ pairs at a CM energy of 130 GeV. This number is in the middle between the current lower limit and the $\mathrm{W^+W^-}$ threshold, at around the value expected for the MSSM $\mathrm{h^0}$, but obviously the relative comparison of the sources is only mildly energy-dependent. Five different sources are compared. The first sample is considered as a reference and consists of gluon radiation in the decay $\gamma^*/\mathrm{Z}^* \to \mathrm{q\overline{q}}$, where q is a light u, d or s quark. For simplicity they are assumed to be produced in equal amounts. The other four samples consist of gluon radiation in the decay $X \to \mathrm{b\overline{b}}$, where X is a vector, axial vector, scalar or pseudoscalar source. Clearly the γ^*/Z^* is a mixture, eq. (5.42), and also $\mathrm{h^0/H^0/A^0}$ need not be pure states, but the separation allows us to study the extreme range of possibilities.

Fig. 5.10a shows the angular energy flow. The difference between having or not having a γ_5 in the coupling is negligible, but the radiation at large angles is larger for the spin 0 source than a spin 1 one. The measure in Fig. 5.10b, i.e. the normalized 3-jet rate, is most sensitive and shows that the 3-jet rate is significantly larger for a spin 0 source, especially for well separated jets (large y_c), which is consistent with the larger energy flow at large angles. The parity dependence is very small, on the other hand, and is neglected in the following.

Considering the large spin dependence one could expect the fragmentation function also to change considerably when going from a vector to a scalar source. Fortunately, as can be seen in Figs. 5.10c–d, the changes are minor, indicating that the fragmentation function is mainly sensitive to the bulk of gluons at smaller angles, where the sources give the same emission rate. The larger gluon energy flow for a scalar source is reflected in a slightly smaller $\langle z \rangle$, with a difference of about 1% both at the parton and hadron level. The small effect on the fragmentation function is positive from an experimentalist's point of view, in that fragmentation functions measured at the $\mathrm{Z^0}$ pole can be simply extrapolated also for possible spin 0 sources at higher energies.

5.5.3 Top Production and Decay

For top production around the $\mathrm{t\overline{t}}$ threshold, real gluon emission will be limited because of phase space, so aspects such as the form of the QCD confinement potential, best tackled with other perturbative techniques, will be more relevant [38]. In this section we study the process $\mathrm{e^+e^-} \to \mathrm{t\overline{t}}$ at 500 GeV, where gluon emission will start to become important, and compare the new shower routine with the older versions. We focus on fundamental aspects such as gluon radiation patterns and top mass determinations. In the process we will also study gluon radiation in the decay of the top, and differences in the radiation patterns for the two decay channels $\mathrm{t} \to \mathrm{bW^+}$ and $\mathrm{t} \to \mathrm{bH^+}$ to demonstrate the advertised process dependence of the new shower routine.

We first study gluon radiation in the production of the top. The matrix element used in the correction of the shower is an energy dependent mixture

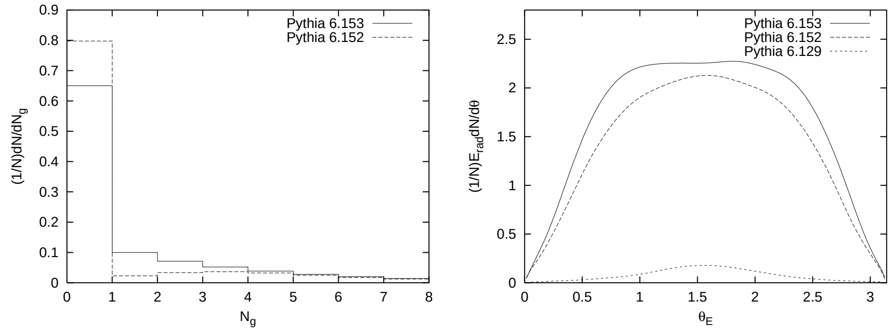

Figure 5.11: Gluon multiplicity and energy flow in the $t\bar{t}$ shower at 500 GeV centre-of-mass.

of vector and axial vector ones. High above the Z^0 pole, the vector part will dominate and at 500 GeV the α parameter, introduced in Section 5.4.1 to parameterize the relative mixture, is about 0.78 for $t\bar{t}$ production. The dead cone effect is expected to be very pronounced in this case, because the scaled mass is large, around $r = 0.35$. Fig. 5.11 shows the gluon multiplicity and the energy flow in the $t\bar{t}$ shower. Most events have no gluon emission, but the no-gluon rate has decreased in the new shower as expected. The result of an even older version, where the dead cone effect is severely exaggerated in all branchings, is shown as a reference. The lesson is that the correct description of the first emission, i.e. the difference between 6.129 and 6.152, is much more important than that of subsequent emissions, between 6.152 and 6.153. Once a gluon is emitted, it tends to be quite energetic and splits into several further gluons. This is the reason for the large spread in the multiplicity and the dip in this distribution for the old shower routine. The total energy flow has also increased in the new shower relative to the older ones. Even if the energy flow seems to be large at large angles, most energy is kept by the original top quarks at $\theta_{\mathrm{E}} = 0$ and π respectively.

The dominant top decay is $t \to bW^+$, where further gluons will be radiated. In the old shower routine, gluon radiation off the b did not take into account the full t–b interference structure. Furthermore, gluon radiation in a hypothetical decay $t \to bH^+$ was the same as in the one above, apart from the difference induced by the different W boson and Higgs masses. In order to separate off this trivial mass effect we put $m_{\mathrm{H}} = m_{\mathrm{W}}$, well aware that this is not realistic.

The matrix element used in the decay $t \to bW^+$ has the familiar $V - A$ coupling, but the $t \to bH^+$ case is less obvious. In the MSSM the vertex factor is proportional to $m_{\mathrm{t}}(1 - \gamma_5) + m_{\mathrm{b}} \tan^2 \beta(1 + \gamma_5)$, i.e. a parameter-dependent mixture of scalar (S) and pseudoscalar (P) couplings. Naively, the $S - P$ one

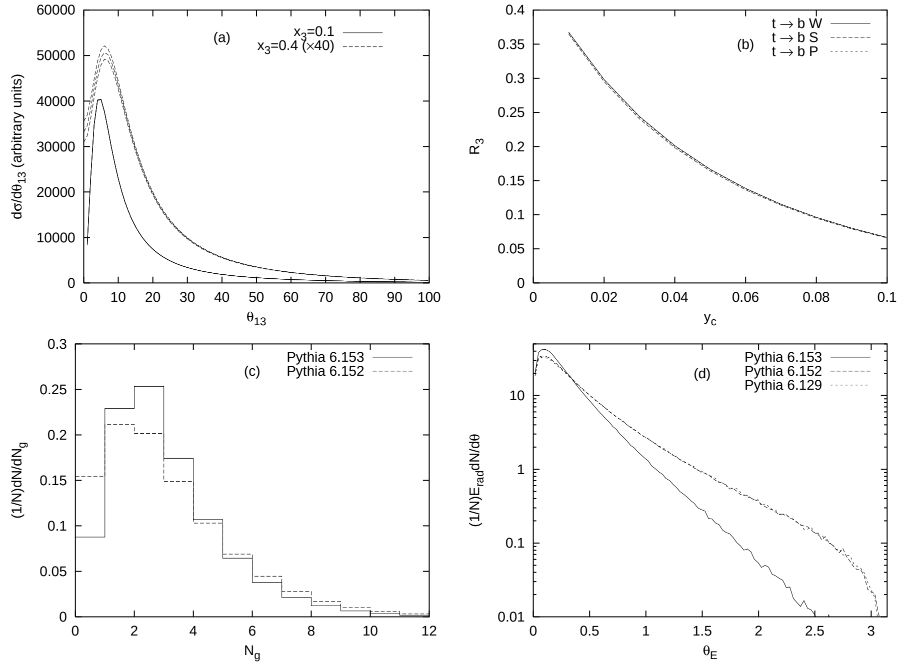

Figure 5.12: (a) The gluon emission rate as a function of the emission angle θ_{13} for top decay, $\mathrm{t} \to \mathrm{b}X$. The emission rate is given for the two gluon energies $x_3 = 0.1$ (full curves) and $x_3 = 0.4$ (dashed). The curves corresponding to the higher energy have been multiplied by a factor of 40 for clarity. Three different curves are shown for each energy: pseudoscalar Higgs, W boson and scalar Higgs (from high to low curves). (b) The 3-jet rate in complete $\mathrm{t\bar{t}}$ events as a function of y_c for the three different cases above, where the W/H are removed from the cluster search. (c–d) Gluon multiplicity and energy flow in the shower induced by the top decay (in the rest-frame of the decaying top with the W at $\theta_{\mathrm{E}} = \pi$).

would be expected to dominate because of the large difference between the top and bottom masses. However, the favoured values of $\tan\beta \gtrsim 3$ could cancel this effect and give rise to an almost pure scalar coupling. We therefore study the two extreme cases of S and P separately. The difference between the matrix elements of this type has been studied in Tables 5.2 and 5.3 and found to be non-negligible for massive daughters but to vanish in the massless limit. For the process $\mathrm{t} \to \mathrm{b}X$, where X is a W^+, pure scalar H^+ or pure pseudoscalar H^+, some differences are visible in the gluon energy flow for larger gluon energies, see Fig. 5.12a, but the differences induced in observables such as the jet rates are small, Fig. 5.12b. That is, we are closer to the massless case of Table 5.3, indicating that the small mass of the radiating b is more important than the large mass of the non-radiating W^+/H^+. In what follows, therefore, only the decay to W^+ is shown. This is the most important case and, as it turns out, the intermediate alternative, cf. Fig. 5.12a.

Figs. 5.12c–d show the gluon multiplicity and energy flow in the decay of the top for the new and the older shower routines. The gluon multiplicity is slightly more peaked in the new shower and the no-gluon rate has been somewhat reduced. The angle θ_E is defined as the angle of emitted energy to the primary bottom quark in the rest frame of the decaying top, which is why no peak appears at large angles, corresponding to the direction of the colour neutral W/H. In the new correction to the shower, gluon radiation at large angles is more severely suppressed. As a consequence, there is more energy left for radiation at small ones, allowing the curves to cross there. This is an effect in addition to the influence of the new matrix element correction scheme, visible e.g. in Fig. 5.6a. The difference between decays to W and H are very small also here (not shown). The result of Pythia 6.129 is similar to 6.152, but the dead cone is slightly more pronounced, as noted before.

In a complete event, gluon emission from the decay and production are added, and also possible radiation in hadronic decays of the W/H must be considered. In principle, these showers will also interfere but, as a realistic first approximation, we work in the zero width limit where these interferences vanish. Considering the two stages of production and decay together, but ignoring the decay products of the W/H, Fig. 5.13a shows the total gluon multiplicity for the new and older shower routines. Since the radiation has increased in the production and decreased in the decay, effects tend to cancel. The net result is a slight increase in the average gluon multiplicity and a somewhat smaller width. The 3-jet rate, however, has decreased, Fig. 5.13b, presumably because of the reduced probability to have gluon emissions at large angles in the top decay, cf. Fig. 5.12d.

The total gluon multiplicity is not a very good measure of the event properties and certainly not an observable. To give a practical example where gluon radiation is important, we consider the reconstruction of the top mass in a simplified scenario, assuming that the W/H can be completely reconstructed in order only to study the effects of gluon emission in the top production and decay. We find two jets and calculate the top mass by considering the two possible combinations of jet+W momenta. The combination which minimizes $(m_1 - m_\mathrm{t})^2 + (m_2 - m_\mathrm{t})^2$, where $m_t = 175$ GeV, gives the reconstructed top masses m_1 and m_2. The distribution of the reconstructed mass is given in Fig. 5.13c, where jets are clustered on the parton level. The reduced radiation level survives in this measure as a slightly narrower peak for the new

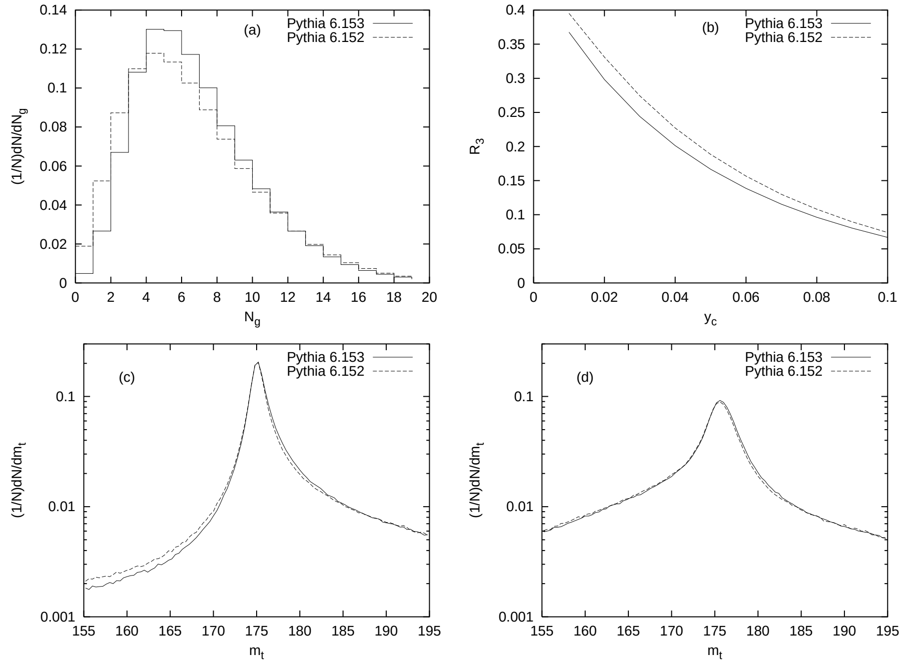

Figure 5.13: $t\bar{t}$ events after top decays. (a) Total gluon multiplicity. (b) The 3-jet rate on the parton level, with W/H removed from the clustering. Initial-state photon radiation is included, but both models are equally affected by this. (c) Reconstructed top mass, parton level. (d) Reconstructed top mass, hadron level.

shower. The effects of fragmentation and decay are quite large for the reconstructed mass, but some differences still survive in the high mass wing, as seen in Fig. 5.13d.

5.5.4 Supersymmetry Production and Decay

In supersymmetric models, a whole new set of processes involving coloured particles is introduced. We have calculated the most important LO matrix elements of the MSSM, listed in Table 5.1, to be used as input to the parton shower routine. In versions of Pythia prior to 6.153, supersymmetric particles did not shower. Because of the large masses of these hypothetical particles, this is a good first approximation. However, if supersymmetric particles are discovered at the LHC or a future linear collider, detailed studies of their properties will profit from a better understanding of QCD radiation patterns.

A complication that appears in the MSSM is significant rates of three body decays involving one or several coloured particles in the initial or final states. Often several interfering diagrams with intermediate off-shell propagators contribute. An example is the decay $\tilde{\chi}^+ \to \tilde{\chi}^0 \mathrm{q}'\overline{\mathrm{q}}$ with either a W or squark propagator. These processes do not fit into the present framework with corrections to matrix elements of the type $a \to bc\mathrm{g}$. As a preliminary solution, the $\mathrm{q}'\overline{\mathrm{q}}$ pair above is assumed to be produced from a $V-A$ source. A new kind of gluon radiation process in the MSSM is from four-vertices such as $\tilde{\mathrm{q}} \to \tilde{\mathrm{q}}'\mathrm{W}^+\mathrm{g}$. These diagrams introduce no new divergences. The interference terms only contribute to the ordinary divergences, and the squared amplitude gives rise to a constant. An upper estimate is again given by the new shower expression, which is corrected by the full matrix element.

As a first example, consider top vs. stop production at a linear $\mathrm{e}^+\mathrm{e}^-$ collider and the decay $\mathrm{t} \to \mathrm{bW}^+$ vs. $\tilde{\mathrm{t}} \to \mathrm{b}\tilde{\chi}^+$. Again, identical masses are assumed and consequently $m_{\tilde{\mathrm{t}}} = m_{\mathrm{t}}$ and $m_{\tilde{\chi}} = m_{\mathrm{W}}$ are used. As usual, the $\mathrm{t}\overline{\mathrm{t}}$ source is an energy dependent mixture of vector and axial vector. Only a scalar coupling is possible for $\mathrm{Z}^0 \to \tilde{\mathrm{t}}\overline{\tilde{\mathrm{t}}}$, so no ambiguity here either. The top decay has the $V-A$ coupling, while the stop one is a parameter dependent mixture of scalar and pseudoscalar. Again we consider the two extreme cases separately. While the stop obviously decays isotropically, the current Pythia implementation does not include top polarization information and thus also decays this particle isotropically. Initial-state photon radiation has not been included in the comparison, since the different threshold behaviours of the $\mathrm{t}\overline{\mathrm{t}}/\tilde{\mathrm{t}}\overline{\tilde{\mathrm{t}}}$ cross sections allow more energetic radiation in the former process, which will affect event topologies.

Fig. 5.14a shows the energy flow for top vs. stop production. The multiplicity is the same for both top and stop, but the energy flow is slightly larger for stop at large angles. The difference between the gluon radiation patterns in the top and stop decays is negligible (not shown). As a result of the increased gluonic energy flow, the 3-jet rate at the parton level, with the $\mathrm{W}/\tilde{\chi}$ removed from the cluster analysis, is slightly larger for stop, Fig. 5.14b. We notice further that the parity dependence is negligible also in this case. The differences between supersymmetric and standard model processes is not large in this example, at least when mass effects are neglected, and the ambiguity in the coupling structure is negligible. This is all good news, but since gluon emission from supersymmetric particles is a completely new feature, many more tests should be done.

As a last example we consider a full simulation of gluino pair production (via $\mathrm{gg} \to \tilde{\mathrm{g}}\tilde{\mathrm{g}}$) at a 14 TeV pp collider. Since we have not developed a full shower formalism for $2 \to 2$ processes, as a first approximation the eikonal expression will be used for radiation off the $\tilde{\mathrm{g}}\tilde{\mathrm{g}}$ system, including a colour factor rescaling

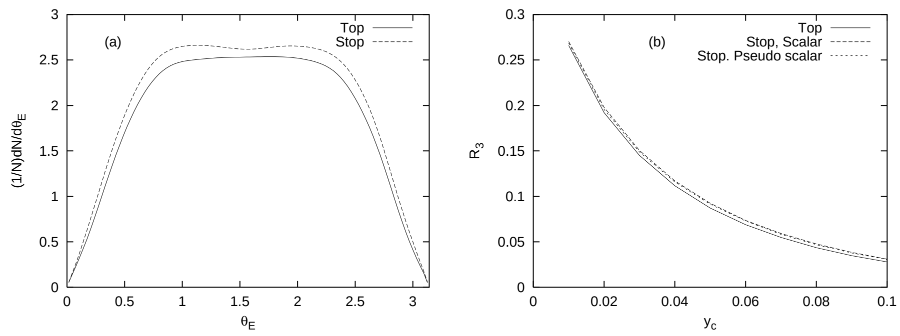

Figure 5.14: Top vs. stop production and decay at a 500 GeV e^+e^- collider. (a) energy flow in the $t\bar{t}$ ($\tilde{t}\bar{\tilde{t}}$) shower. (b) 3-jet rate on the parton level for the production and decay taken together, with the $W/\tilde{\chi}$ removed from the clustering.

by $N_C/C_F = 9/4$. Initial state radiation is studied separately and multiple interactions are neglected. A scenario with $m_{\tilde{g}} = 450$ GeV, $m_{\tilde{b}_1} = 250$ GeV and $m_{\tilde{t}_1} = 200$ GeV is used. The dominant gluino decays are then $\tilde{g} \to \tilde{b}_1\bar{b}$ ($\tilde{t}_1\bar{t}$) and the squarks decay by processes of the type $\tilde{q} \to \tilde{\chi}b$. If the $\tilde{\chi}$ is a neutralino, which here is the lightest supersymmetric particle, it will not decay further. A chargino decays to a neutralino plus either leptons or quarks in approximately equal amounts. This MSSM scenario is implemented in the PYTHIA event generator [6] and the details are described in the SPYTHIA manual [39].

To assess the importance of gluon radiation off supersymmetric particles in a hadron-hadron collision, we compare the transverse gluon energy flow from SUSY and non-SUSY particles in the final state radiation (FSR), Fig. 5.15a. The additional gluon radiation from coloured SUSY particles is thus seen to be small compared to the ordinary gluon radiation from quarks. In this paper we have only considered QCD final state radiation in e^+e^- annihilation. In a hadron collider environment, gluons can be radiated also from the incoming partons (initial state radiation, ISR). This contribution is almost as large as the FSR one, Fig. 5.15a, but the rapidity distribution is different.

In Fig. 5.15b the three PYTHIA versions considered in this paper are compared. Only the FSR component is shown, and the additional radiation from SUSY particles in the latest version gives rise to an increased total transverse gluon energy flow. This increase is, however, slightly compensated by the decrease in gluon radiation in the top and squark decays, cf. Section 5.5.3. In Figs. 5.15c–d the result of a simple cluster search is shown. Particles with a summed transverse energy, $\sum E_\perp > E_{\perp,min}$ inside a $\sqrt{(\Delta\eta)^2 + (\Delta\varphi)^2} < R$

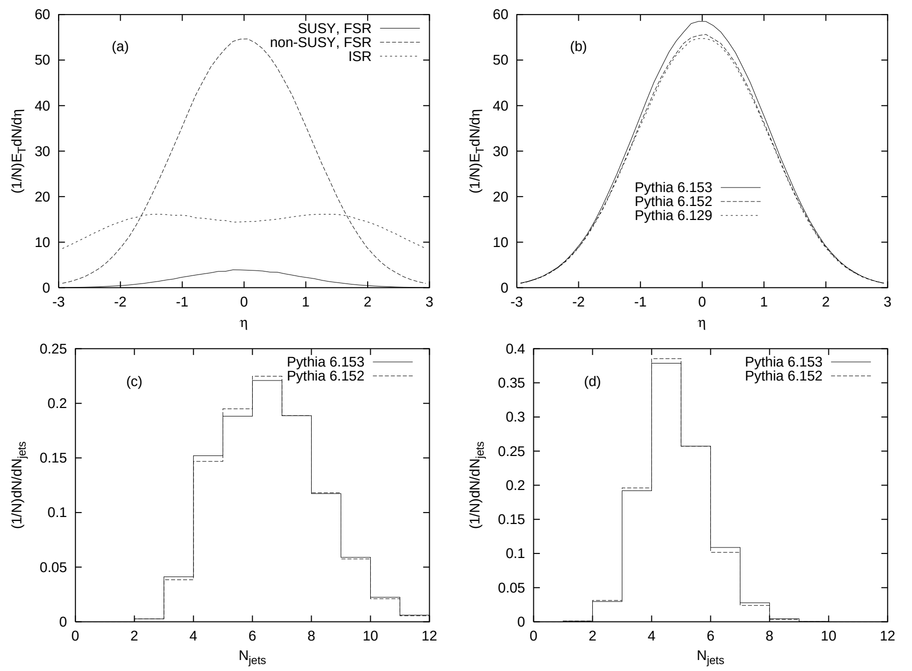

Figure 5.15: Gluino production at a 14 TeV pp collider. (a–b) Transverse gluon energy flow in pseudorapidity, $\eta = \frac{1}{2}\ln((p+p_z)/(p-p_z))$. (c–d) Jet multiplicity for $R = 0.75$, $E_{\perp,min} = 10$ and 40 GeV respectively.

cone are joined in a cluster. For large $E_{\perp,min}$, the jet multiplicity is slightly increased when gluon radiation from supersymmetric particles is included. This could be caused by energetic gluons radiated off the gluinos. For small $E_{\perp,min}$, on the other hand, smaller structures are probed and the radiation off b and lighter quarks is most important. In summary, we conclude that gluon radiation off supersymmetric particles at a hadron collider is small compared to the other sources, and of importance mainly in high-precision studies.

5.6 Gluon Splitting to Heavy Quarks

Data at LEP1 show a larger rate of secondary charm and bottom production than predicted in most shower descriptions [5, 40], or in analytical studies [41]. We therefore comment on a few of the issues in the Monte Carlo simulation and how a relaxation of some demands would affect rates.

α_{s}	coherence	$\mathrm{g} \to \mathrm{q}\overline{\mathrm{q}}$ (%)	$\mathrm{g} \to \mathrm{c}\overline{\mathrm{c}}$ (%)	$\mathrm{g} \to \mathrm{b}\overline{\mathrm{b}}$ (%)
$\alpha_{\mathrm{s}}(p_{\perp}^2)$	full	14.3	1.26	0.15
$\alpha_{\mathrm{s}}(p_{\perp}^2)$	intermediate	14.8	1.27	0.16
$\alpha_{\mathrm{s}}(p_{\perp}^2)$	reduced	21.1	1.92	0.26
$\alpha_{\mathrm{s}}(p_{\perp}^2)$	none	38.8	3.06	0.31
$\alpha_{\mathrm{s}}(m_{\mathrm{g}}^2/4)$	full	12.9	1.15	0.15
$\alpha_{\mathrm{s}}(m_{\mathrm{g}}^2/4)$	intermediate	13.3	1.17	0.15
$\alpha_{\mathrm{s}}(m_{\mathrm{g}}^2/4)$	reduced	20.0	1.78	0.28
$\alpha_{\mathrm{s}}(m_{\mathrm{g}}^2/4)$	none	43.3	3.47	0.46

Table 5.4: The rate of gluon splitting to quarks, in Z^0 decay at 91.2 GeV with the normal primary flavour mixture. q denotes a light quark flavour.

5.6.1 Strong Coupling Argument and Kinematics

The default behaviour in PYTHIA is to let α_{s} have $p_{\perp}^2$ as argument. Actually, the exact kinematics has not yet been reconstructed when α_{s} is invoked, so the approximate expression $p_{\perp}^2 \approx z(1-z)m_a^2$ is used, see discussion at eq. (5.7). Since α_{s} blows up when its argument approaches Λ_{QCD}, this translates into a requirement on $p_{\perp}^2$ or on z and m_a, restricting allowed emissions to $p_{\perp} > Q_0/2$, where Q_0 is the shower cut-off scale. Also when full kinematics is reconstructed, this is reflected in a suppression of branchings with small $p_{\perp}$. Therefore, in $\mathrm{g} \to \mathrm{q}\overline{\mathrm{q}}$ branchings analyzed in the g rest frame, the quarks do not come out with the $1+\cos^2\theta$ angular distribution (with respect to the direction of motion of the gluon) one might expect away from threshold, or a somewhat more isotropic one closer to threshold, but are rather peaked at 90° and dying out at 0° and 180°.

For $\mathrm{g} \to \mathrm{q}\overline{\mathrm{q}}$ branchings, the soft-gluon results that lead to the choice of $p_{\perp}^2$ as scale [42] are no longer compelling, however. One could instead use some other scale that does not depend on z but only on $m_a = m_{\mathrm{g}}$, i.e the off-shellness of the branching gluon, and remove the $p_{\perp}$ cut. A reasonable choice, even if not unique, is to use $m_{\mathrm{g}}^2/4$, where the factor $1/4$ ensures continuity with $p_{\perp}^2$ for $z = 1/2$. This possibility has been added as a new option.

Actually, the change of α_{s} argument in itself leads to a reduced $\mathrm{g} \to \mathrm{q}\overline{\mathrm{q}}$ splitting rate, while the removal of the $p_{\perp} > Q_0/2$ requirement increases it. The net result is a decrease by about 10%, Table 5.4. The topologies of the events are changed somewhat, so rates within experimental cuts could be more affected. However, the changes are not as big as might have been expected — see the following.

5.6.2 Coherence

In the above subsection, it appears as if the $1+\cos^2\theta$ distribution would be recovered in the new $\alpha_{\mathrm{s}}(m_{\mathrm{g}}^2/4)$ option. However, this neglects the coherence condition, which is imposed as a requirement in the shower that successive opening angles in branchings become smaller. Such a condition actually disfavours branchings with z close to 0 or 1, since the opening angle becomes large in this limit, eq. (5.8). It should be noted that the opening angle discussed here is not the true one, but the one based on approximate kinematics, including neglect of masses. More generally, the coherence formalism is not really developed with this kind of configurations in mind, especially not with a heavy quark pair close to threshold.

As a means to exploring consequences, two new coherence level options have thus been introduced. In the first, the $p_{\perp}^2$ of a $\mathrm{g} \to \mathrm{q}\overline{\mathrm{q}}$ branching is reduced by the correct mass-dependent factor, $1-4m_{\mathrm{q}}^2/m_{\mathrm{g}}^2$, while the massless approximation is kept for the longitudinal momentum. This is fully within the uncertainty of the game, and no less reasonable than the default. In the second, no angular ordering at all is imposed on $\mathrm{g} \to \mathrm{q}\overline{\mathrm{q}}$ branchings. This is certainly an extreme scenario, and should be viewed with caution. However, it is still interesting to see what it leads to.

In Section 5.3.4 another "intermediate" coherence variation of the default "full" one was introduced, affecting the rate of gluon emission off the primary quarks but not the subsequent gluon cascades. This variation has negligible consequences for the secondary quark rate at LEP energies and is not considered further.

It turns out that the decay angle distribution of the gluon is much more distorted by the coherence than by the α_{s} and kinematics considerations described earlier. Both modifications are required if one would like to have a $1+\cos^2\theta$ shape, however. Also other distributions, like gluon mass and energy, are affected by the choice of options.

The most dramatic effect appears in the total gluon branching rate, however, Table 5.4. Already the reduced angular ordering requirement can boost the $\mathrm{g} \to \mathrm{b}\overline{\mathrm{b}}$ rate by almost a factor of two. The effects are even bigger without any angular ordering constraints at all. It is difficult to know what to make of these big effects. Experimental information on the angular distribution of secondary $\mathrm{c}\overline{\mathrm{c}}/\mathrm{b}\overline{\mathrm{b}}$ pairs might help understand what is going on, but probably that is not possible experimentally. Anyway, the measured (but still uncertain) values are fully bracketed by the range of the models, indicating that there need not be a conflict between theory and experiment.

5.7 Summary and Outlook

We have in this article studied QCD radiation off heavy particles, both based on the calculation of a wide set of first-order matrix elements and by the usage of these matrix elements as input to a parton-shower description of multiple-gluon emission.

The matrix-element calculations provide at least two important insights. One is the significant spin dependence on the rate of gluon emission, given identical kinematical conditions. Some such effects could be expected simply from the different shape of the splitting kernel of a quark and a squark, say, but equally important is the spin of the decaying particle, and the parity of the process (combining that of mother and daughters). The best illustration is the difference between a vector and a scalar colour singlet source each decaying to a pair of squarks, where the gluon emission rate differs by up to a factor of 1.8 in our limited study, and is likely to reach even higher levels in other observables. The γ_5 dependence disappears in the massless limit, but the bulk of other effects remain also there, so this is not only an issue for the production of heavy flavours. This process dependence would not be caught by the traditional parton-shower philosophy, where the universal aspects of gluon emission are emphasized.

The other insight is that the 'dead cone' concept is one that only applies universally for soft gluon emission. Only one process provides an exact zero in the collinear emission rate while, for reasonably hard gluons, some processes show no dip at all at small angles. And, while soft gluons may be ideologically interesting, the experimentally observable event shapes are often more crucially dependent on some intermediate range of gluon energies. Again, therefore, the message is that a universal shower description may be misleading.

Fortunately, it is not impossible to combine the shower picture with a process dependence of the kind noted above. We have in this article developed one approach to the problem, wherein matrix element information is provided for all shower branchings of the primary particles. This combines a process dependent resummation of gluon emission off these particles with the traditional strengths of the shower formalism, such as providing exclusive final states with exact energy–momentum conservation.

To illustrate this formalism, a few physics examples have been studied. For bottom production at the Z^0 pole, detailed comparisons with data are possible. We find the new shower routine to be in good agreement with current data if the uncertainties in both model and data are taken into account. A significant dependence on coherence options were found both for jet rates and gluon splitting rates in the shower. It has further been possible to rule out an older version of the shower routine where mass effects were not correctly accounted for.

Differences in jet rates were found for different coupling structures in Higgs decay to bottom, whereas the influence on the fragmentation function is minor. Both the production and decay of the top quark is dependent on the matrix element correction, influencing e.g. the mass reconstruction of the top quark. Again the jet rate was found to be most sensitive.

Gluon radiation off supersymmetric particles, squarks and gluinos, has been introduced, but the effect of this additional radiation is small in high energy processes, especially at hadron colliders, because of the background from initial state radiation and showers off the standard model decay products. Differences between top and stop events are small if equal masses are assumed, but many more comparisons between standard model and supersymmetric processes could be envisaged.

From this limited study we conclude that gluon emission off b and lighter quarks dominate the picture. If this component is modelled well, the rest is less important, but still of ideological interest. Since the scaled bottom mass $r = m_{\mathrm{b}}/m_X$, in the decay of a resonance X, is small in most cases, we see little if any parity dependence. In Z^0 decays this effect is less than 1%, but it could be visible in a high-precision study. Also for the spin dependence, effects are small in most cases, although the $\mathrm{H}^0 \to \mathrm{b}\overline{\mathrm{b}}$ example shows they need not be quite as small. It thus turns out that the new process dependence will mainly be important when high precision is strived at.

We note that the current study is not the end of the story. While we have sampled a fair selection of colour and spin structures, more are likely to turn up even in the simple context of two-body decays considered here. The MSSM also allows a significant rate for three-body decays, normally as a sequence of two consecutive two-body ones with an intermediate off-shell propagator, and with the possibility of interference between several such intermediate states. The real challenge, however, may well be provided by the more complex production processes at hadron colliders, where the concept of a sequence of s-channel processes need no longer be valid, e.g. squark production $\mathrm{gg} \to \tilde{\mathrm{q}}\overline{\tilde{\mathrm{q}}}$ with a t-channel squark propagator. The large rate of initial-state radiation also implies that the initial–final state interference terms may be more important than the final-state radiation off the heavy particles themselves. Much work therefore lies ahead, if one desires a good description of QCD effects in many processes of interest at the LHC.

References

[1] B. Andersson, G. Gustafson, G. Ingelman and T. Sjöstrand, Phys. Rep. **97** (1983) 31;
T. Sjöstrand, Nucl. Phys. **B248** (1984) 469.

[2] Yu.L. Dokshitzer, V.A. Khoze, L.H. Orr and W.J. Stirling, Nucl. Phys. **B403** (1993) 65.

[3] M. Bengtsson and T. Sjöstrand, Phys. Lett. **B185** (1987) 435, Nucl. Phys. **B289** (1987) 810.

[4] Yu.L. Dokshitzer, V.A. Khoze and S.I. Troyan, J. Phys. **G17** (1991) 1602.

[5] A Ballestrero et al., hep-ph/0006259, to appear in the Proceedings of the LEP2 Monte Carlo Workshop.

[6] T. Sjöstrand, Comput. Phys. Commun. **82** (1994) 74, LU TP 95–20 (hep-ph/9508391).

[7] G. Marchesini and B.R. Webber, Nucl. Phys. **B238** (1984) 1;
G. Marchesini, B.R. Webber, G. Abbiendi, I.G. Knowles, M.H. Seymour and L. Stanco, Comput. Phys. Commun. **67** (1992) 465.

[8] G. Marchesini and B.R. Webber, Nucl. Phys. **B330** (1990) 261.

[9] G. Gustafson and U. Pettersson, Nucl. Phys. **B306** (1988) 746;
L. Lönnblad, Comput. Phys. Commun. **71** (1992) 15.

[10] V.V. Sudakov, Zh. E.T.F. **30** (1956) 87.

[11] Workshop on Photon Radiation from Quarks, ed. S. Cartwright, CERN 92–04.

[12] M.H. Seymour, Z. Phys. **C56** (1992) 161, Comput. Phys. Commun. **90** (1995) 95.

[13] G. Corcella and M.H. Seymour, Phys. Lett. **B442** (1998) 417.

[14] J. André and T. Sjöstrand, Phys. Rev. **D57** (1998) 5767.

[15] J. Ellis, M.K. Gaillard and G.G Ross, Nucl. Phys. **B111** (1976) 253.

[16] B.L. Ioffe, Phys. Lett. **78B** (1978) 277.

[17] A.H. Mueller, Phys. Lett. **104B** (1981) 161;
B.I. Ermolaev and V.S. Fadin, JETP Lett. **33** (1981) 269.

[18] W. Beenakker, R. Höpker and P.M. Zerwas, Phys. Lett. **B349** (1995) 463.

[19] Ya.I. Azimov, Yu.L. Dokshitzer, V.A. Khoze and S.I. Troyan, Phys. Lett. **165B** (1985) 147.

[20] B. Andersson, G. Gustafson and T. Sjöstrand, Phys. Lett. **94B** (1980) 211.

[21] V.A. Khoze and T. Sjöstrand, Phys. Lett. **B328** (1994) 466.

[22] G. Gustafson, U. Pettersson and P. Zerwas, Phys. Lett. **B209** (1988) 90;
T. Sjöstrand and V.A. Khoze, Z. Phys. **C62** (1994) 281, Phys. Rev. Lett. **72** (1994) 28;
L. Lönnblad and T. Sjöstrand, Phys. Lett. **B351** (1995)293, Eur. Phys. J. **C2** (1998) 165.

[23] CDF Collaboration, F. Abe et al., Phys. Rev. **D50** (1994) 5562.

[24] E. Norrbin and T. Sjöstrand, Phys. Lett. **B442** (1998) 407, LU TP 00–16 (hep-ph/0005110), to appear in Eur. Phys. J. **C**.

[25] A. Pukhov et al., preprint INP MSU 98–41/542 (hep-ph/9908288).

[26] A. Arhib, M.C. Peyranere and G. Moultaka, Phys. Lett. **B341** (1995) 313.

[27] Wolfram Research, Inc., MATHEMATICA, Version 2.2, Champaign, IL (1993).

[28] P. Janot, Phys. Lett. **B223** (1989) 110.

[29] J. Jersak, E. Laermann and P.M. Zerwas, Phys. Lett. **98B** (1981) 363;
M. Jeżabek and J.H. Kühn, Nucl. Phys. **B314** (1989) 1.

[30] R.K. Ellis, D.A. Ross and A.E. Terrano, Nucl. Phys. **B178** (1981) 421.

[31] Z. Kunszt, Phys. Lett. **99B** (1981) 429.

[32] S. Catani, Yu.L. Dokshitzer, M. Olsson, G. Turnock and B.R. Webber, Phys. Lett. **B269** (1991) 432.

[33] T.R. Grose and K.O. Mikaelian, Phys. Rev. **D23** (1981) 123.

[34] Yu.L. Dokshitzer, V.A. Khoze, A.H. Mueller and S.I. Troyan, Rev. Mod. Phys. **60** (1988) 373.

[35] JADE Collaboration, W. Bartel et al., Z. Phys. **C33** (1986) 23;
JADE Collaboration, S. Bethke et al., Phys. Lett. **B213** (1988) 235;
N. Brown and W.J. Stirling, Z. Phys. **C53** (1992) 629;
Y.L. Dokshitzer, G.D. Leder, S. Moretti and B.R. Webber, JHEP **9708** (1997) 001;
L. Lönnblad, S. Moretti and T. Sjöstrand, JHEP **9808** (1998) 001.

[36] Delphi Collaboration, P. Abreu et al., Phys. Lett. **B418** (1998) 430; P. Bambade, private communication.

[37] Aleph Collaboration, R. Barate et al., CERN-EP/2000-093 (hep-ex/0008013).

[38] A.H. Hoang et al., Eur. Phys. J. direct **C3** (2000) 1 (hep-ph/0001286), to appear in the proceedings of the workshop "Physics Studies for a Future Linear Collider", Top Quark WG.

[39] S. Mrenna, Comput. Phys. Commun. **101** (1997) 232.

[40] M.L. Mangano, in International Europhysics Conference on High Energy Physics, eds. K. Huitu et al. (IOP Publishing, Bristol, 2000), p. 33.

[41] M.H. Seymour, Nucl. Phys. **B436** (1995) 163; D.J. Miller and M.H. Seymour, Phys. Lett. **B435** (1998) 213.

[42] D. Amati, A. Bassetto, M. Ciafaloni, G. Marchesini and G. Veneziano, Nucl. Phys. **B173** (1980) 429.

High-Energy-Physics Event Generation with PYTHIA 6.1

Paper VI

High-Energy-Physics Event Generation with PYTHIA 6.1

Torbjörn Sjöstrand[1], Patrik Edén[2], Christer Friberg[1], Leif Lönnblad[1], Gabriela Miu[1], Stephen Mrenna[3] and Emanuel Norrbin[1]

1) Department of Theoretical Physics, Lund University, Sölvegatan 14A, S-223 62 Lund, Sweden

2) NORDITA, Blegdamsvej 17, DK-2100 Copenhagen, Denmark

3) Physics Department, University of California at Davis, One Shields Avenue, Davis, CA 95616, USA

LU TP 00–30 (hep-ph/0010017)
Accepted for publication in *Computer Physics communications*

PYTHIA version 6 represents a merger of the PYTHIA 5, JETSET 7 and SPYTHIA programs, with many improvements. It can be used to generate high-energy-physics 'events', i.e. sets of outgoing particles produced in the interactions between two incoming particles. The objective is to provide as accurate as possible a representation of event properties in a wide range of reactions. The underlying physics is not understood well enough to give an exact description; the programs therefore contain a combination of analytical results and various models. The emphasis in this article is on new aspects, but a few words of general introduction are included. Further documentation is available on the web.

New Version Summary

Title of program: PYTHIA
Version number: 6.154

Catalogue identifier: —

Distribution format: uuencoded compressed tar file

References to most recent previous versions:
Computer Physics Communications **82** (1994) 74 and
Computer Physics Communications **101** (1997) 232, respectively

Catalogue identifiers of most recent previous versions: ACTU

Authors of most recent previous versions:
T. Sjöstrand and S. Mrenna, respectively

Does the new version supersede the previous versions?: yes

Computers for which the new program is designed and others on which it has been tested:
Computer:
DELL Precision 210 and any other machine with a Fortran 77 compiler
Installation: Lund University
Operating system under which the new program has been tested:
Red Hat Linux 6.2

Programming language used: Fortran 77; is also fully compatible with Fortran 90, i.e. does not make use of any obsolescent features of the Fortran 90 standard

Memory required to execute with typical data: about 800 kwords

No. of bits in word: 32 (double precision real uses two words)

No. of processors used: 1

Has the code been vectorized or parallelized?: no

No. of bytes in distributed program: about 1.8 Mb

Keywords:
QCD, standard model, beyond standard model, hard scattering, e^+e^- annihilation, leptoproduction, photoproduction, hadronic processes, high-$p_\perp$ scattering, prompt photons, gauge bosons, Higgs physics, parton distribution functions, jet production, parton showers, fragmentation, hadronization, beam remnants, multiple interactions, particle decays, event measures

Nature of physical problem:
high-energy collisions between elementary particles normally give rise to complex final states, with large multiplicities of hadrons, leptons, neutrinos and photons. The relation between these final states and the underlying physics description is not a simple one, for two main reasons. Firstly, we do not even in principle have a complete understanding of the physics. Secondly, any analytical approach is made intractable by the large multiplicities.

Method of solution:
complete events are generated by Monte Carlo methods. The complexity is mastered by a subdivision of the full problem into a set of simpler separate tasks. All main aspects of the events are simulated, such as hard-process selection, initial- and final-state radiation, beam remnants, fragmentation, decays, and so on. Therefore events should be directly comparable with experimentally observable ones. The programs can be used to extract physics from comparisons with existing data, or to study physics at future experiments.

Restrictions on the complexity of the problem: depends on the problem studied

Typical running time: 10–1000 events per second, depending on process studied

Unusual features of the program: none

6.1 Introduction

The PYTHIA and JETSET programs [1] are frequently used for event generation in high-energy physics. The emphasis is on multiparticle production in collisions between elementary particles. This in particular means hard interactions in e^+e^-, pp and ep colliders, although also other applications are envisaged. The programs can be used both to compare with existing data, for physics studies or detector corrections, and to explore possibilities at present or future experiments. The programs are intended to generate complete events, in as much detail as experimentally observable ones, within the bounds of our current understanding of the underlying physics. The quantum mechanical variability between events in nature is here replaced by Monte Carlo methods, to obtain 'correctly' both the average behaviour and the amount of fluctuations. Many of the components of the programs represent original research, in the sense that models have been developed and implemented for a number of aspects not covered by standard theory.

Although originally conceived separately, the PYTHIA [2] and JETSET [3] programs today are so often used together that they have here been joined under the PYTHIA header. To this has been added the code of SPYTHIA [4], an extension of PYTHIA that also covers the generation of supersymmetric processes. The current article is not intended to give a complete survey of all the program elements or all the physics — we refer to the long manual and further documentation on the PYTHIA web page

`http://www.thep.lu.se/~torbjorn/Pythia.html`

for this. Instead the objective is to give a survey of new features since the latest official publications, with some minimal amount of background material to tie the story together. Many of the advances are related to physics studies, which are further described in separate articles. Others are of a more technical nature, or have been of too limited a scope to result in individual publications (so far).

Some of the main topics are:

- An improved simulation of supersymmetric physics, with several new processes.
- Many new processes of beyond-the-standard-model physics, in areas such as technicolor and doubly-charged Higgses.
- An expanded description of QCD processes in virtual-photon interactions, combined with a new machinery for the flux of virtual photons from leptons.
- Initial-state parton showers are matched to the next-to-leading order matrix elements for gauge boson production.
- Final-state parton showers are matched to a number of different first-order matrix elements for gluon emission, including full mass dependence.
- The hadronization description of low-mass strings has been improved, with

consequences especially for heavy-flavour production.
- An alternative baryon production model has been introduced.
- Colour rearrangement is included as a new option, and several alternative Bose-Einstein descriptions are added.

Many further examples will be given. In the process, the total size of the program code has almost doubled in the six years since the previous main publication.

The report is subdivided so that the physics news are highlighted in Section 6.2 and the programming ones (plus a few more physics ones) in Section 6.3. Section 6.4 contains some concluding remarks and an outlook.

6.2 Physics News

For the description of a typical high-energy event, an event generator should contain a simulation of several physics aspects. If we try to follow the evolution of an event in some semblance of a time order, one may arrange these aspects as follows:

1. Initially two beam particles are coming in towards each other. Normally each particle is characterized by a set of parton distributions, which defines the partonic substructure in terms of flavour composition and energy sharing.
2. One shower initiator parton from each beam starts off a sequence of branchings, such as $\mathrm{q} \to \mathrm{qg}$, which build up an initial-state shower.
3. One incoming parton from each of the two showers enters the hard process, where then a number of outgoing partons are produced, usually two. It is the nature of this process that determines the main characteristics of the event.
4. The hard process may produce a set of short-lived resonances, like the $\mathrm{Z}^0/\mathrm{W}^{\pm}$ gauge bosons, whose decay to normal partons has to be considered in close association with the hard process itself.
5. The outgoing partons may branch as well, to build up final-state showers.
6. In addition to the hard process considered above, further semihard interactions may occur between the other partons of two incoming hadrons.
7. When a shower initiator is taken out of a beam particle, a beam remnant is left behind. This remnant may have an internal structure, and a net colour charge that relates it to the rest of the final state.
8. The QCD confinement mechanism ensures that the outgoing quarks and gluons are not observable, but instead fragment to colour neutral hadrons.
9. Normally the fragmentation mechanism can be seen as occurring in a set of separate colour singlet subsystems, but interconnection effects such as colour rearrangement or Bose–Einstein may complicate the picture.
10. Many of the produced hadrons are unstable and decay further.

In the following subsections, we will survey updates of the above aspects, not in the same order as given here, but rather in the order in which they appear in the program execution, i.e. starting with the hard process.

6.2.1 Physics Subprocesses

Process Classifications

PYTHIA contains a rich selection of physics scenarios, with well above 200 different subprocesses, see Tables 6.1, 6.2, 6.3 and 6.4. The process number space has tended to become a bit busy, so processes are not always numbered logically. Some processes are closely related variants of the same basic process (e.g. the production of a neutralino pair in processes 216–225), others are alternative formulations (e.g. $\mathrm{Z}^0\mathrm{Z}^0 \to \mathrm{h}^0$ has to be convoluted with the flux of Z^0's around fermions, and thus is an approximation to $\mathrm{f}_i\mathrm{f}_j \to \mathrm{f}_i\mathrm{f}_j\mathrm{h}^0$; when the latter was implemented the former was still kept). A process may also have hidden further layers of processes (e.g. $\mathrm{H}^{\pm}$ can be produced in top decays, whichever way top is produced).

One classification of the subprocesses is according to the physics scenario. The following major groups may be distinguished:

- Hard QCD processes, i.e. leading to jet production.
- Soft QCD processes, such as diffractive and elastic scattering, and minimum-bias events. Hidden in this class is also process 96, which is used internally for the merging of soft and hard physics, and for the generation of multiple interactions.
- Heavy-flavour production, both open and hidden (i.e. as bound states like the J/ψ). Hadronization of open heavy flavour will be discussed in Section 6.2.4. Some new processes have been added for closed heavy flavour, but we remind that data here are yet not fully understood, and have given rise to models extending on the more conventional PYTHIA treatment [5].
- W/Z production. A first-order process such as $\mathrm{f}_i\overline{\mathrm{f}}_j \to \mathrm{gW}^{\pm}$ is now quite accurately modeled by the initial-state shower acting on $\mathrm{f}_i\overline{\mathrm{f}}_j \to \mathrm{W}^{\pm}$, see Section 6.2.2, but the former can still be useful for a dedicated study of the high-$p_{\perp}$ tail.
- Prompt-photon production.
- Photon-induced processes, including Deep Inelastic Scattering. A completely new machinery for $\gamma^*\mathrm{p}$ and $\gamma^*\gamma^*$ physics has been constructed here, see Section 6.2.1.
- Standard model Higgs production, where the Higgs is reasonably light and narrow, and can therefore still be considered as a resonance.
- Gauge boson scattering processes, such as $\mathrm{W_L W_L} \to \mathrm{W_L W_L}$ (L = longitudinal), when the standard model Higgs is so heavy and broad that resonant

and non-resonant contributions have to be considered together.

- Non-standard Higgs particle production, within the framework of a two-Higgs-doublet scenario with three neutral (h^0, H^0 and A^0) and two charged ($H^{\pm}$) Higgs states. Normally associated with SUSY (see below), but does not have to be. The Higgs pair production processes were previously hidden in process 141, but are now included explicitly.
- Production of new gauge bosons, such as a Z', W' and R (a horizontal boson, coupling between generations).
- Technicolor production, as an alternative scenario to the standard picture of electroweak symmetry breaking by a fundamental Higgs. Processes 149, 191, 192 and 193 may be considered obsolete, since the other processes now include the decays to the allowed final states of the $\rho^0_{\mathrm{tc}}/\omega^0_{\mathrm{tc}}/\rho^{\pm}_{\mathrm{tc}}$ bosons, also including interferences with $\gamma/Z^0/W^{\pm}$. The default scenario is based on [6].
- Compositeness is a possibility not only in the Higgs sector, but may also apply to fermions, e.g. giving d^* and u^* production. At energies below the threshold for new particle production, contact interactions may still modify the standard behaviour; this is implemented not only for processes 165 and 166, but also for 11, 12 and 20.
- Left–right symmetric models give rise to doubly charged Higgs states, in fact one set belonging to the left and one to the right SU(2) gauge group. Decays involve right-handed W's and neutrinos. The existing scenario is based on [7].
- Leptoquark (L_Q) production is encountered in some beyond-the-standard-model scenarios.
- Supersymmetry (SUSY) is probably the favourite scenario for physics beyond the standard model. A rich set of processes are allowed, even if one obeys R-parity conservation. The supersymmetric machinery and process selection is inherited from SPYTHIA [4], however with many improvements in the event generation chain. Relative to the SPYTHIA process repertoire, the main new additions is sbottom production, where a classification by mass eigenstates is necessary and many Feynman graphs are related to the possibility to have incoming b quarks. Many different SUSY scenarios have been proposed, and the program is flexible enough to allow input from several of these, in addition to the ones provided internally.

Table 6.1: Subprocesses, part 1: standard model, according to the subprocess numbering of PYTHIA. 'f' denotes a fermion (quark or lepton), 'Q' a heavy quark and 'F' a heavy fermion.

No.	Subprocess
Hard QCD processes:	
11	$f_i f_j \to f_i f_j$
12	$f_i \overline{f}_i \to f_k \overline{f}_k$
13	$f_i \overline{f}_i \to gg$
28	$f_i g \to f_i g$
53	$gg \to f_k \overline{f}_k$
68	$gg \to gg$
Soft QCD processes:	
91	elastic scattering
92	single diffraction (XB)
93	single diffraction (AX)
94	double diffraction
95	low-$p_\perp$ production
Open heavy flavour: (also fourth generation)	
81	$f_i \overline{f}_i \to Q_k \overline{Q}_k$
82	$gg \to Q_k \overline{Q}_k$
83	$q_i f_j \to Q_k f_l$
84	$g\gamma \to Q_k \overline{Q}_k$
85	$\gamma\gamma \to F_k \overline{F}_k$
Closed heavy flavour:	
86	$gg \to J/\psi g$
87	$gg \to \chi_{0c} g$
88	$gg \to \chi_{1c} g$
89	$gg \to \chi_{2c} g$
104	$gg \to \chi_{0c}$
105	$gg \to \chi_{2c}$
106	$gg \to J/\psi \gamma$
107	$g\gamma \to J/\psi g$
108	$\gamma\gamma \to J/\psi \gamma$

No.	Subprocess
W/Z production:	
1	$f_i \overline{f}_i \to \gamma^*/Z^0$
2	$f_i \overline{f}_j \to W^\pm$
22	$f_i \overline{f}_i \to Z^0 Z^0$
23	$f_i \overline{f}_j \to Z^0 W^\pm$
25	$f_i \overline{f}_i \to W^+ W^-$
15	$f_i \overline{f}_i \to g Z^0$
16	$f_i \overline{f}_j \to g W^\pm$
30	$f_i g \to f_i Z^0$
31	$f_i g \to f_k W^\pm$
19	$f_i \overline{f}_i \to \gamma Z^0$
20	$f_i \overline{f}_j \to \gamma W^\pm$
35	$f_i \gamma \to f_i Z^0$
36	$f_i \gamma \to f_k W^\pm$
69	$\gamma\gamma \to W^+ W^-$
70	$\gamma W^\pm \to Z^0 W^\pm$
Prompt photons:	
14	$f_i \overline{f}_i \to g\gamma$
18	$f_i \overline{f}_i \to \gamma\gamma$
29	$f_i g \to f_i \gamma$
114	$gg \to \gamma\gamma$
115	$gg \to g\gamma$
Deep inelastic scatt.:	
10	$f_i f_j \to f_i f_j$
99	$\gamma^* f_i \to f_i$
Photon-induced:	
33	$f_i \gamma \to f_i g$
34	$f_i \gamma \to f_i \gamma$
54	$g\gamma \to f_k \overline{f}_k$
58	$\gamma\gamma \to f_k \overline{f}_k$

Table 6.2: Subprocesses, part 2: standard model continued and Higgs production in a two-doublet scenario, with notation as above.

No.	Subprocess
131	$\mathrm{f}_i\gamma^*_\mathrm{T} \to \mathrm{f}_i\mathrm{g}$
132	$\mathrm{f}_i\gamma^*_\mathrm{L} \to \mathrm{f}_i\mathrm{g}$
133	$\mathrm{f}_i\gamma^*_\mathrm{T} \to \mathrm{f}_i\gamma$
134	$\mathrm{f}_i\gamma^*_\mathrm{L} \to \mathrm{f}_i\gamma$
135	$\mathrm{g}\gamma^*_\mathrm{T} \to \mathrm{f}_i\overline{\mathrm{f}}_i$
136	$\mathrm{g}\gamma^*_\mathrm{L} \to \mathrm{f}_i\overline{\mathrm{f}}_i$
137	$\gamma^*_\mathrm{T}\gamma^*_\mathrm{T} \to \mathrm{f}_i\overline{\mathrm{f}}_i$
138	$\gamma^*_\mathrm{T}\gamma^*_\mathrm{L} \to \mathrm{f}_i\overline{\mathrm{f}}_i$
139	$\gamma^*_\mathrm{L}\gamma^*_\mathrm{T} \to \mathrm{f}_i\overline{\mathrm{f}}_i$
140	$\gamma^*_\mathrm{L}\gamma^*_\mathrm{L} \to \mathrm{f}_i\overline{\mathrm{f}}_i$
80	$\mathrm{q}_i\gamma \to \mathrm{q}_k\pi^\pm$
Light SM Higgs:	
3	$\mathrm{f}_i\overline{\mathrm{f}}_i \to \mathrm{h}^0$
24	$\mathrm{f}_i\overline{\mathrm{f}}_i \to \mathrm{Z}^0\mathrm{h}^0$
26	$\mathrm{f}_i\overline{\mathrm{f}}_j \to \mathrm{W}^\pm\mathrm{h}^0$
102	$\mathrm{gg} \to \mathrm{h}^0$
103	$\gamma\gamma \to \mathrm{h}^0$
110	$\mathrm{f}_i\overline{\mathrm{f}}_i \to \gamma\mathrm{h}^0$
121	$\mathrm{gg} \to \mathrm{Q}_k\overline{\mathrm{Q}}_k\mathrm{h}^0$
122	$\mathrm{q}_i\overline{\mathrm{q}}_i \to \mathrm{Q}_k\overline{\mathrm{Q}}_k\mathrm{h}^0$
123	$\mathrm{f}_i\mathrm{f}_j \to \mathrm{f}_i\mathrm{f}_j\mathrm{h}^0$
124	$\mathrm{f}_i\mathrm{f}_j \to \mathrm{f}_k\mathrm{f}_l\mathrm{h}^0$
Heavy SM Higgs:	
5	$\mathrm{Z}^0\mathrm{Z}^0 \to \mathrm{h}^0$
8	$\mathrm{W}^+\mathrm{W}^- \to \mathrm{h}^0$
71	$\mathrm{Z}^0_\mathrm{L}\mathrm{Z}^0_\mathrm{L} \to \mathrm{Z}^0_\mathrm{L}\mathrm{Z}^0_\mathrm{L}$
72	$\mathrm{Z}^0_\mathrm{L}\mathrm{Z}^0_\mathrm{L} \to \mathrm{W}^+_\mathrm{L}\mathrm{W}^-_\mathrm{L}$
73	$\mathrm{Z}^0_\mathrm{L}\mathrm{W}^\pm_\mathrm{L} \to \mathrm{Z}^0_\mathrm{L}\mathrm{W}^\pm_\mathrm{L}$
76	$\mathrm{W}^+_\mathrm{L}\mathrm{W}^-_\mathrm{L} \to \mathrm{Z}^0_\mathrm{L}\mathrm{Z}^0_\mathrm{L}$
77	$\mathrm{W}^\pm_\mathrm{L}\mathrm{W}^\pm_\mathrm{L} \to \mathrm{W}^\pm_\mathrm{L}\mathrm{W}^\pm_\mathrm{L}$

No.	Subprocess
BSM Neutral Higgses:	
151	$\mathrm{f}_i\overline{\mathrm{f}}_i \to \mathrm{H}^0$
152	$\mathrm{gg} \to \mathrm{H}^0$
153	$\gamma\gamma \to \mathrm{H}^0$
171	$\mathrm{f}_i\overline{\mathrm{f}}_i \to \mathrm{Z}^0\mathrm{H}^0$
172	$\mathrm{f}_i\overline{\mathrm{f}}_j \to \mathrm{W}^\pm\mathrm{H}^0$
173	$\mathrm{f}_i\mathrm{f}_j \to \mathrm{f}_i\mathrm{f}_j\mathrm{H}^0$
174	$\mathrm{f}_i\mathrm{f}_j \to \mathrm{f}_k\mathrm{f}_l\mathrm{H}^0$
181	$\mathrm{gg} \to \mathrm{Q}_k\overline{\mathrm{Q}}_k\mathrm{H}^0$
182	$\mathrm{q}_i\overline{\mathrm{q}}_i \to \mathrm{Q}_k\overline{\mathrm{Q}}_k\mathrm{H}^0$
156	$\mathrm{f}_i\overline{\mathrm{f}}_i \to \mathrm{A}^0$
157	$\mathrm{gg} \to \mathrm{A}^0$
158	$\gamma\gamma \to \mathrm{A}^0$
176	$\mathrm{f}_i\overline{\mathrm{f}}_i \to \mathrm{Z}^0\mathrm{A}^0$
177	$\mathrm{f}_i\overline{\mathrm{f}}_j \to \mathrm{W}^\pm\mathrm{A}^0$
178	$\mathrm{f}_i\mathrm{f}_j \to \mathrm{f}_i\mathrm{f}_j\mathrm{A}^0$
179	$\mathrm{f}_i\mathrm{f}_j \to \mathrm{f}_k\mathrm{f}_l\mathrm{A}^0$
186	$\mathrm{gg} \to \mathrm{Q}_k\overline{\mathrm{Q}}_k\mathrm{A}^0$
187	$\mathrm{q}_i\overline{\mathrm{q}}_i \to \mathrm{Q}_k\overline{\mathrm{Q}}_k\mathrm{A}^0$
Charged Higgs:	
143	$\mathrm{f}_i\overline{\mathrm{f}}_j \to \mathrm{H}^+$
161	$\mathrm{f}_i\mathrm{g} \to \mathrm{f}_k\mathrm{H}^+$
Higgs pairs:	
297	$\mathrm{f}_i\overline{\mathrm{f}}_j \to \mathrm{H}^\pm\mathrm{h}^0$
298	$\mathrm{f}_i\overline{\mathrm{f}}_j \to \mathrm{H}^\pm\mathrm{H}^0$
299	$\mathrm{f}_i\overline{\mathrm{f}}_i \to \mathrm{A}^0\mathrm{h}^0$
300	$\mathrm{f}_i\overline{\mathrm{f}}_i \to \mathrm{A}^0\mathrm{H}^0$
301	$\mathrm{f}_i\overline{\mathrm{f}}_i \to \mathrm{H}^+\mathrm{H}^-$

Table 6.3: Subprocesses, part 3: beyond the standard model non-SUSY, with notation as above.

No.	Subprocess
New gauge bosons:	
141	$\mathrm{f}_i\overline{\mathrm{f}}_i \to \gamma/\mathrm{Z}^0/\mathrm{Z}'^0$
142	$\mathrm{f}_i\overline{\mathrm{f}}_j \to \mathrm{W}'^+$
144	$\mathrm{f}_i\overline{\mathrm{f}}_j \to \mathrm{R}$
Technicolor:	
149	$\mathrm{gg} \to \eta_{\mathrm{tc}}$
191	$\mathrm{f}_i\overline{\mathrm{f}}_i \to \rho^0_{\mathrm{tc}}$
192	$\mathrm{f}_i\overline{\mathrm{f}}_j \to \rho^+_{\mathrm{tc}}$
193	$\mathrm{f}_i\overline{\mathrm{f}}_i \to \omega^0_{\mathrm{tc}}$
194	$\mathrm{f}_i\overline{\mathrm{f}}_i \to \mathrm{f}_k\overline{\mathrm{f}}_k$
195	$\mathrm{f}_i\overline{\mathrm{f}}_j \to \mathrm{f}_k\overline{\mathrm{f}}_l$
361	$\mathrm{f}_i\overline{\mathrm{f}}_i \to \mathrm{W}^+_{\mathrm{L}}\mathrm{W}^-_{\mathrm{L}}$
362	$\mathrm{f}_i\overline{\mathrm{f}}_i \to \mathrm{W}^\pm_{\mathrm{L}}\pi^\mp_{\mathrm{tc}}$
363	$\mathrm{f}_i\overline{\mathrm{f}}_i \to \pi^+_{\mathrm{tc}}\pi^-_{\mathrm{tc}}$
364	$\mathrm{f}_i\overline{\mathrm{f}}_i \to \gamma\pi^0_{\mathrm{tc}}$
365	$\mathrm{f}_i\overline{\mathrm{f}}_i \to \gamma{\pi'}^0_{\mathrm{tc}}$
366	$\mathrm{f}_i\overline{\mathrm{f}}_i \to \mathrm{Z}^0\pi^0_{\mathrm{tc}}$
367	$\mathrm{f}_i\overline{\mathrm{f}}_i \to \mathrm{Z}^0{\pi'}^0_{\mathrm{tc}}$
368	$\mathrm{f}_i\overline{\mathrm{f}}_i \to \mathrm{W}^\pm\pi^\mp_{\mathrm{tc}}$
370	$\mathrm{f}_i\overline{\mathrm{f}}_j \to \mathrm{W}^\pm_{\mathrm{L}}\mathrm{Z}^0_{\mathrm{L}}$
371	$\mathrm{f}_i\overline{\mathrm{f}}_j \to \mathrm{W}^\pm_{\mathrm{L}}\pi^0_{\mathrm{tc}}$
372	$\mathrm{f}_i\overline{\mathrm{f}}_j \to \pi^\pm_{\mathrm{tc}}\mathrm{Z}^0_{\mathrm{L}}$
373	$\mathrm{f}_i\overline{\mathrm{f}}_j \to \pi^\pm_{\mathrm{tc}}\pi^0_{\mathrm{tc}}$
374	$\mathrm{f}_i\overline{\mathrm{f}}_j \to \gamma\pi^\pm_{\mathrm{tc}}$
375	$\mathrm{f}_i\overline{\mathrm{f}}_j \to \mathrm{Z}^0\pi^\pm_{\mathrm{tc}}$
376	$\mathrm{f}_i\overline{\mathrm{f}}_j \to \mathrm{W}^\pm\pi^0_{\mathrm{tc}}$
377	$\mathrm{f}_i\overline{\mathrm{f}}_j \to \mathrm{W}^\pm{\pi'}^0_{\mathrm{tc}}$

No.	Subprocess
Compositeness:	
146	$\mathrm{e}\gamma \to \mathrm{e}^*$
147	$\mathrm{dg} \to \mathrm{d}^*$
148	$\mathrm{ug} \to \mathrm{u}^*$
167	$\mathrm{q}_i\mathrm{q}_j \to \mathrm{d}^*\mathrm{q}_k$
168	$\mathrm{q}_i\mathrm{q}_j \to \mathrm{u}^*\mathrm{q}_k$
169	$\mathrm{q}_i\overline{\mathrm{q}}_i \to \mathrm{e}^\pm\mathrm{e}^{*\mp}$
165	$\mathrm{f}_i\overline{\mathrm{f}}_i(\to \gamma^*/\mathrm{Z}^0) \to \mathrm{f}_k\overline{\mathrm{f}}_k$
166	$\mathrm{f}_i\overline{\mathrm{f}}_j(\to \mathrm{W}^\pm) \to \mathrm{f}_k\overline{\mathrm{f}}_l$
Doubly-charged Higgs:	
341	$\ell_i\ell_j \to \mathrm{H}^{\pm\pm}_L$
342	$\ell_i\ell_j \to \mathrm{H}^{\pm\pm}_R$
343	$\ell^\pm_i\gamma \to \mathrm{H}^{\pm\pm}_L\mathrm{e}^\mp$
344	$\ell^\pm_i\gamma \to \mathrm{H}^{\pm\pm}_R\mathrm{e}^\mp$
345	$\ell^\pm_i\gamma \to \mathrm{H}^{\pm\pm}_L\mu^\mp$
346	$\ell^\pm_i\gamma \to \mathrm{H}^{\pm\pm}_R\mu^\mp$
347	$\ell^\pm_i\gamma \to \mathrm{H}^{\pm\pm}_L\tau^\mp$
348	$\ell^\pm_i\gamma \to \mathrm{H}^{\pm\pm}_R\tau^\mp$
349	$\mathrm{f}_i\overline{\mathrm{f}}_i \to \mathrm{H}^{++}_L\mathrm{H}^{--}_L$
350	$\mathrm{f}_i\overline{\mathrm{f}}_i \to \mathrm{H}^{++}_R\mathrm{H}^{--}_R$
351	$\mathrm{f}_i\mathrm{f}_j \to \mathrm{f}_k\mathrm{f}_l\mathrm{H}^{\pm\pm}_L$
352	$\mathrm{f}_i\mathrm{f}_j \to \mathrm{f}_k\mathrm{f}_l\mathrm{H}^{\pm\pm}_R$
Leptoquarks:	
145	$\mathrm{q}_i\ell_j \to \mathrm{L}_{\mathrm{Q}}$
162	$\mathrm{qg} \to \ell\mathrm{L}_{\mathrm{Q}}$
163	$\mathrm{gg} \to \mathrm{L}_{\mathrm{Q}}\overline{\mathrm{L}}_{\mathrm{Q}}$
164	$\mathrm{q}_i\overline{\mathrm{q}}_i \to \mathrm{L}_{\mathrm{Q}}\overline{\mathrm{L}}_{\mathrm{Q}}$

Table 6.4: Subprocesses, part 4: SUSY, with notation as above. A trailing + on a final state indicates that the charge-conjugated one is included as well.

No.	Subprocess
SUSY:	
201	$\mathrm{f}_i\overline{\mathrm{f}}_i \to \tilde{\mathrm{e}}_L\tilde{\mathrm{e}}_L^*$
202	$\mathrm{f}_i\overline{\mathrm{f}}_i \to \tilde{\mathrm{e}}_R\tilde{\mathrm{e}}_R^*$
203	$\mathrm{f}_i\overline{\mathrm{f}}_i \to \tilde{\mathrm{e}}_L\tilde{\mathrm{e}}_R^*+$
204	$\mathrm{f}_i\overline{\mathrm{f}}_i \to \tilde{\mu}_L\tilde{\mu}_L^*$
205	$\mathrm{f}_i\overline{\mathrm{f}}_i \to \tilde{\mu}_R\tilde{\mu}_R^*$
206	$\mathrm{f}_i\overline{\mathrm{f}}_i \to \tilde{\mu}_L\tilde{\mu}_R^*+$
207	$\mathrm{f}_i\overline{\mathrm{f}}_i \to \tilde{\tau}_1\tilde{\tau}_1^*$
208	$\mathrm{f}_i\overline{\mathrm{f}}_i \to \tilde{\tau}_2\tilde{\tau}_2^*$
209	$\mathrm{f}_i\overline{\mathrm{f}}_i \to \tilde{\tau}_1\tilde{\tau}_2^*+$
210	$\mathrm{f}_i\overline{\mathrm{f}}_j \to \tilde{\ell}_L\tilde{\nu}_\ell^*+$
211	$\mathrm{f}_i\overline{\mathrm{f}}_j \to \tilde{\tau}_1\tilde{\nu}_\tau^*+$
212	$\mathrm{f}_i\overline{\mathrm{f}}_j \to \tilde{\tau}_2\tilde{\nu}_\tau{}^*+$
213	$\mathrm{f}_i\overline{\mathrm{f}}_i \to \tilde{\nu}_\ell\tilde{\nu}_\ell{}^*$
214	$\mathrm{f}_i\overline{\mathrm{f}}_i \to \tilde{\nu}_\tau\tilde{\nu}_\tau^*$
216	$\mathrm{f}_i\overline{\mathrm{f}}_i \to \tilde{\chi}_1\tilde{\chi}_1$
217	$\mathrm{f}_i\overline{\mathrm{f}}_i \to \tilde{\chi}_2\tilde{\chi}_2$
218	$\mathrm{f}_i\overline{\mathrm{f}}_i \to \tilde{\chi}_3\tilde{\chi}_3$
219	$\mathrm{f}_i\overline{\mathrm{f}}_i \to \tilde{\chi}_4\tilde{\chi}_4$
220	$\mathrm{f}_i\overline{\mathrm{f}}_i \to \tilde{\chi}_1\tilde{\chi}_2$
221	$\mathrm{f}_i\overline{\mathrm{f}}_i \to \tilde{\chi}_1\tilde{\chi}_3$
222	$\mathrm{f}_i\overline{\mathrm{f}}_i \to \tilde{\chi}_1\tilde{\chi}_4$
223	$\mathrm{f}_i\overline{\mathrm{f}}_i \to \tilde{\chi}_2\tilde{\chi}_3$
224	$\mathrm{f}_i\overline{\mathrm{f}}_i \to \tilde{\chi}_2\tilde{\chi}_4$
225	$\mathrm{f}_i\overline{\mathrm{f}}_i \to \tilde{\chi}_3\tilde{\chi}_4$
226	$\mathrm{f}_i\overline{\mathrm{f}}_i \to \tilde{\chi}_1^\pm\tilde{\chi}_1^\mp$
227	$\mathrm{f}_i\overline{\mathrm{f}}_i \to \tilde{\chi}_2^\pm\tilde{\chi}_2^\mp$
228	$\mathrm{f}_i\overline{\mathrm{f}}_i \to \tilde{\chi}_1^\pm\tilde{\chi}_2^\mp$
229	$\mathrm{f}_i\overline{\mathrm{f}}_j \to \tilde{\chi}_1\tilde{\chi}_1^\pm$
230	$\mathrm{f}_i\overline{\mathrm{f}}_j \to \tilde{\chi}_2\tilde{\chi}_1^\pm$

No.	Subprocess
231	$\mathrm{f}_i\overline{\mathrm{f}}_j \to \tilde{\chi}_3\tilde{\chi}_1^\pm$
232	$\mathrm{f}_i\overline{\mathrm{f}}_j \to \tilde{\chi}_4\tilde{\chi}_1^\pm$
233	$\mathrm{f}_i\overline{\mathrm{f}}_j \to \tilde{\chi}_1\tilde{\chi}_2^\pm$
234	$\mathrm{f}_i\overline{\mathrm{f}}_j \to \tilde{\chi}_2\tilde{\chi}_2^\pm$
235	$\mathrm{f}_i\overline{\mathrm{f}}_j \to \tilde{\chi}_3\tilde{\chi}_2^\pm$
236	$\mathrm{f}_i\overline{\mathrm{f}}_j \to \tilde{\chi}_4\tilde{\chi}_2^\pm$
237	$\mathrm{f}_i\overline{\mathrm{f}}_i \to \tilde{\mathrm{g}}\tilde{\chi}_1$
238	$\mathrm{f}_i\overline{\mathrm{f}}_i \to \tilde{\mathrm{g}}\tilde{\chi}_2$
239	$\mathrm{f}_i\overline{\mathrm{f}}_i \to \tilde{\mathrm{g}}\tilde{\chi}_3$
240	$\mathrm{f}_i\overline{\mathrm{f}}_i \to \tilde{\mathrm{g}}\tilde{\chi}_4$
241	$\mathrm{f}_i\overline{\mathrm{f}}_j \to \tilde{\mathrm{g}}\tilde{\chi}_1^\pm$
242	$\mathrm{f}_i\overline{\mathrm{f}}_j \to \tilde{\mathrm{g}}\tilde{\chi}_2^\pm$
243	$\mathrm{f}_i\overline{\mathrm{f}}_i \to \tilde{\mathrm{g}}\tilde{\mathrm{g}}$
244	$\mathrm{gg} \to \tilde{\mathrm{g}}\tilde{\mathrm{g}}$
246	$\mathrm{f}_i\mathrm{g} \to \tilde{\mathrm{q}}_{iL}\tilde{\chi}_1$
247	$\mathrm{f}_i\mathrm{g} \to \tilde{\mathrm{q}}_{iR}\tilde{\chi}_1$
248	$\mathrm{f}_i\mathrm{g} \to \tilde{\mathrm{q}}_{iL}\tilde{\chi}_2$
249	$\mathrm{f}_i\mathrm{g} \to \tilde{\mathrm{q}}_{iR}\tilde{\chi}_2$
250	$\mathrm{f}_i\mathrm{g} \to \tilde{\mathrm{q}}_{iL}\tilde{\chi}_3$
251	$\mathrm{f}_i\mathrm{g} \to \tilde{\mathrm{q}}_{iR}\tilde{\chi}_3$
252	$\mathrm{f}_i\mathrm{g} \to \tilde{\mathrm{q}}_{iL}\tilde{\chi}_4$
253	$\mathrm{f}_i\mathrm{g} \to \tilde{\mathrm{q}}_{iR}\tilde{\chi}_4$
254	$\mathrm{f}_i\mathrm{g} \to \tilde{\mathrm{q}}_{jL}\tilde{\chi}_1^\pm$
256	$\mathrm{f}_i\mathrm{g} \to \tilde{\mathrm{q}}_{jL}\tilde{\chi}_2^\pm$
258	$\mathrm{f}_i\mathrm{g} \to \tilde{\mathrm{q}}_{iL}\tilde{\mathrm{g}}$
259	$\mathrm{f}_i\mathrm{g} \to \tilde{\mathrm{q}}_{iR}\tilde{\mathrm{g}}$
261	$\mathrm{f}_i\overline{\mathrm{f}}_i \to \tilde{\mathrm{t}}_1\tilde{\mathrm{t}}_1^*$
262	$\mathrm{f}_i\overline{\mathrm{f}}_i \to \tilde{\mathrm{t}}_2\tilde{\mathrm{t}}_2^*$
263	$\mathrm{f}_i\overline{\mathrm{f}}_i \to \tilde{\mathrm{t}}_1\tilde{\mathrm{t}}_2^*+$

No.	Subprocess
264	$\mathrm{gg} \to \tilde{\mathrm{t}}_1\tilde{\mathrm{t}}_1^*$
265	$\mathrm{gg} \to \tilde{\mathrm{t}}_2\tilde{\mathrm{t}}_2^*$
271	$\mathrm{f}_i\mathrm{f}_j \to \tilde{\mathrm{q}}_{iL}\tilde{\mathrm{q}}_{jL}$
272	$\mathrm{f}_i\mathrm{f}_j \to \tilde{\mathrm{q}}_{iR}\tilde{\mathrm{q}}_{jR}$
273	$\mathrm{f}_i\mathrm{f}_j \to \tilde{\mathrm{q}}_{iL}\tilde{\mathrm{q}}_{jR}+$
274	$\mathrm{f}_i\overline{\mathrm{f}}_j \to \tilde{\mathrm{q}}_{iL}\tilde{\mathrm{q}}_j^*{}_L$
275	$\mathrm{f}_i\overline{\mathrm{f}}_j \to \tilde{\mathrm{q}}_{iR}\tilde{\mathrm{q}}_j^*{}_R$
276	$\mathrm{f}_i\overline{\mathrm{f}}_j \to \tilde{\mathrm{q}}_{iL}\tilde{\mathrm{q}}_j^*{}_R+$
277	$\mathrm{f}_i\overline{\mathrm{f}}_i \to \tilde{\mathrm{q}}_{jL}\tilde{\mathrm{q}}_j^*{}_L$
278	$\mathrm{f}_i\overline{\mathrm{f}}_i \to \tilde{\mathrm{q}}_{jR}\tilde{\mathrm{q}}_j^*{}_R$
279	$\mathrm{gg} \to \tilde{\mathrm{q}}_{iL}\tilde{\mathrm{q}}_i^*{}_L$
280	$\mathrm{gg} \to \tilde{\mathrm{q}}_{iR}\tilde{\mathrm{q}}_i^*{}_R$
281	$\mathrm{bq}_i \to \tilde{\mathrm{b}}_1\tilde{\mathrm{q}}_{iL}$
282	$\mathrm{bq}_i \to \tilde{\mathrm{b}}_2\tilde{\mathrm{q}}_{iR}$
283	$\mathrm{bq}_i \to \tilde{\mathrm{b}}_1\tilde{\mathrm{q}}_{iR} + \tilde{\mathrm{b}}_2\tilde{\mathrm{q}}_{iL}$
284	$\mathrm{b}\overline{\mathrm{q}}_i \to \tilde{\mathrm{b}}_1\tilde{\mathrm{q}}_i^*{}_L$
285	$\mathrm{b}\overline{\mathrm{q}}_i \to \tilde{\mathrm{b}}_2\tilde{\mathrm{q}}_i^*{}_R$
286	$\mathrm{b}\overline{\mathrm{q}}_i \to \tilde{\mathrm{b}}_1\tilde{\mathrm{q}}_i^*{}_R + \tilde{\mathrm{b}}_2\tilde{\mathrm{q}}_i^*{}_L$
287	$\mathrm{q}_i\overline{\mathrm{q}}_i \to \tilde{\mathrm{b}}_1\tilde{\mathrm{b}}_1^*$
288	$\mathrm{q}_i\overline{\mathrm{q}}_i \to \tilde{\mathrm{b}}_2\tilde{\mathrm{b}}_2^*$
289	$\mathrm{gg} \to \tilde{\mathrm{b}}_1\tilde{\mathrm{b}}_1^*$
290	$\mathrm{gg} \to \tilde{\mathrm{b}}_2\tilde{\mathrm{b}}_2^*$
291	$\mathrm{bb} \to \tilde{\mathrm{b}}_1\tilde{\mathrm{b}}_1$
292	$\mathrm{bb} \to \tilde{\mathrm{b}}_2\tilde{\mathrm{b}}_2$
293	$\mathrm{bb} \to \tilde{\mathrm{b}}_1\tilde{\mathrm{b}}_2$
294	$\mathrm{bg} \to \tilde{\mathrm{b}}_1\tilde{\mathrm{g}}$
295	$\mathrm{bg} \to \tilde{\mathrm{b}}_2\tilde{\mathrm{g}}$
296	$\mathrm{b}\overline{\mathrm{b}} \to \tilde{\mathrm{b}}_1\tilde{\mathrm{b}}_2^*+$

Obviously the list is far from exhaustive; it is a major problem to keep up to date with all the new physics scenarios and signals that are proposed and have to be studied. One example of another physics area that has attracted much attention recently is the possibility of extra dimensions on 'macroscopic' scales. Also, a general-purpose program can not be optimized for all kinds of processes. If a generator for some kind of partonic configurations is already available, outside of PYTHIA, there exists the possibility to feed this in for subsequent treatment of showers and hadronization.

Parton Distributions

For cross section calculations, the hard partonic cross section has to be convoluted with the parton distributions of the incoming beam particles. The current default is GRV 94L for protons [8] and SaS 1D for real and virtual photons [9]. Some further parameterizations are available in PYTHIA, such as the recent CTEQ 5 proton ones [10], and a much richer repertoire if the PDFLIB library [11] is linked.

Photon Physics

Since before, a model for the interactions of real photons is available, i.e. for γp and $\gamma\gamma$ events [12]. This has now been improved and extended also to include virtual photons, i.e. γ^*p and $\gamma^*\gamma^*$ events [13]. It is especially geared towards the transition region of rather small photon virtualities $Q^2 \lesssim 10$ GeV^2, where the physics picture is rather complex, while it may be overkill for large Q^2, where the picture again simplifies.

Photon interactions are complicated since the photon wave function contains so many components, each with its own interactions. To first approximation, it may be subdivided into a direct and a resolved part. (In higher orders, the two parts can mix, so one has to provide sensible physical separations between the two.) In the former the photon acts as a pointlike particle, while in the latter it fluctuates into hadronic states. These fluctuations are of $\mathcal{O}(\alpha_{\mathrm{em}})$, and so correspond to a small fraction of the photon wave function, but this is compensated by the bigger cross sections allowed in strong-interaction processes. For real photons therefore the resolved processes dominate the total cross section, while the pointlike ones take over for virtual photons.

The fluctuations $\gamma \to \mathrm{q}\overline{\mathrm{q}}\,(\to \gamma)$ can be characterized by the transverse momentum $k_\perp$ of the quarks, or alternatively by some mass scale $m \simeq 2k_\perp$, with a spectrum of fluctuations $\propto \mathrm{d}k_\perp^2/k_\perp^2$. The low-$k_\perp$ part cannot be calculated perturbatively, but is instead parameterized by experimentally determined couplings to the lowest-lying vector mesons, $V = \rho^0$, ω^0, ϕ^0 and J/ψ, an ansatz called VMD for Vector Meson Dominance. Parton distributions are defined with a unit momentum sum rule within a fluctuation [9], giving rise to total hadronic cross sections, jet activity, multiple interactions and beam remnants as in hadronic interactions. States at larger $k_\perp$ are called GVMD or Generalized VMD, and their contributions to the parton distribution of the photon are called anomalous. Given a dividing line $k_0 \simeq 0.5$ GeV to VMD states, the parton distributions are perturbatively calculable. The total cross section of a state is not, however, since this involves aspects of soft physics and eikonalization of jet rates. Therefore an ansatz is chosen where the total cross section scales like $k_V^2/k_\perp^2$, where the adjustable parameter $k_V \approx m_\rho/2$ for light quarks. The spectrum of states is taken to extend over a range $k_0 < k_\perp < k_1$, where k_1 is identified with the $p_{\perp\mathrm{min}}(s)$ defined in eq. (6.6) below. There is some arbitrariness in that choice, and for jet rate calculations also contributions to the parton distributions from above this region are included.

If the photon is virtual, it has a reduced probability to fluctuate into a vector meson state, and this state has a reduced interaction probability. This can be modeled by a traditional dipole factor $(m_V^2/(m_V^2+Q^2))^2$ for a photon of virtuality Q^2, where $m_V \to 2k_\perp$ for a GVMD state. Putting it all together, the cross section of the GVMD sector then scales like

$$\int_{k_0^2}^{k_1^2} \frac{\mathrm{d}k_\perp^2}{k_\perp^2} \, \frac{k_V^2}{k_\perp^2} \left(\frac{4k_\perp^2}{4k_\perp^2 + Q^2} \right)^2 . \tag{6.1}$$

A real direct photon in a γp collision can interact with the parton content of the proton: $\gamma\mathrm{q} \to \mathrm{qg}$ and $\gamma\mathrm{g} \to \mathrm{q}\overline{\mathrm{q}}$. The $p_\perp$ in this collision is taken to exceed k_1, in order to avoid double-counting with the interactions of the GVMD states. For a virtual photon the DIS (deeply inelastic scattering) process $\gamma^*\mathrm{q} \to \mathrm{q}$ is also possible, but by gauge invariance its cross section must vanish in the limit $Q^2 \to 0$. At large Q^2, the direct processes can instead be considered as the $\mathcal{O}(\alpha_\mathrm{s})$ correction to the lowest-order DIS process. The DIS γ^*p cross section is here proportional to the structure function $F_2(x, Q^2)$ with the Bjorken $x = Q^2/(Q^2+W^2)$. Since normal parton distribution parameterizations are frozen below some Q_0 scale and therefore do not obey the gauge invariance condition, an ad hoc factor $(Q^2/(Q^2+m_\rho^2))^2$ is introduced for the conversion from the parameterized $F_2(x,Q^2) = \sum e_\mathrm{q}^2 \, q(x,Q^2)$ to a $\sigma_{\mathrm{DIS}}^{\gamma^*\mathrm{p}}$. In order to avoid double-counting between DIS and direct events, we decide to introduce a requirement $p_\perp > \max(k_1, Q)$ on direct events. In the remaining DIS ones, thus $p_\perp < Q$. The DIS rate should be reduced accordingly, by a Sudakov form factor giving the probability not to have an interaction above scale Q, which can be approximated by $\exp(-\sigma_{\mathrm{direct}}^{\gamma^*\mathrm{p}}/\sigma_{\mathrm{DIS}}^{\gamma^*\mathrm{p}})$.

Note that the Q^2 dependence of the DIS and direct processes is implemented in the matrix element expressions. This is different from VMD/GVMD, where dipole factors are used to reduce the assumed flux of partons inside a virtual photon relative to those of a real one, but the matrix elements contain no parton virtuality dependence.

After some further minor corrections for double-counting, we arrive at a picture of hadronic γ^*p events as being composed of four main components: VMD, GVMD, direct and DIS. Most of these in their turn have a complicated internal structure, as we have seen. The $\gamma^*\gamma^*$ collision between two inequivalent photons contains 13 components: four when the VMD and GVMD states interact with each other ('double-resolved'), eight with a direct or DIS photon interaction on a VMD or GVMD state on either side ('single-resolved', including the traditional DIS), and one where two direct photons interact by the process $\gamma^*\gamma^* \to \mathrm{q}\overline{\mathrm{q}}$ ('direct', not to be confused with the direct process of γ^*p).

Several further aspects can be added to the above machinery. The impact of resolved longitudinal photons is unknown, except that it has to vanish in the limit $Q^2 \to 0$, and can be approximated by some Q^2-dependent enhancement of the normal transverse one. For a complete description of ep events or $\mathrm{e}^+\mathrm{e}^-$ two-photon ones, a convolution with the x- and Q^2-dependent flux of virtual photons inside an electron is also now provided.

Supersymmetry

PYTHIA simulates the Minimal Supersymmetric Standard Model (MSSM), based on an effective Lagrangian of softly-broken SUSY with parameters defined at the weak scale, which is typically between m_{Z} and 1 TeV. The MSSM particle spectrum is minimal in the sense that it includes only the partners of all Standard Model particles (presently without massive neutrinos), a two-Higgs doublet — one Higgs $\mathrm{H_u}$ coupling only to up-type fermions and one $\mathrm{H_d}$ coupling only to down-type fermions — and partners, and the gravitino. Once the parameters of the softly-broken SUSY Lagrangian are specified, the interactions are fixed, and the sparticle masses can be calculated [14].

The masses of the scalar partners to fermions, sfermions, depend on soft scalar masses, trilinear couplings, the Higgsino mass μ, and $\tan\beta$, the ratio of Higgs vacuum expectation values $\langle \mathrm{H_u} \rangle / \langle \mathrm{H_d} \rangle$. The masses of the fermion partners to the gauge and Higgs bosons, the neutralinos and charginos, depend on soft gaugino masses, μ, and $\tan\beta$. Finally, the properties of the Higgs scalar sector is calculated from the input pseudoscalar Higgs boson mass m_{A}, $\tan\beta$, μ, trilinear couplings and the sparticle properties in an effective potential approach [15]. Of course, these calculations also depend on SM parameters ($m_{\mathrm{t}}, m_{\mathrm{Z}}, \alpha_{\mathrm{s}}$, etc.). Any modifications to these quantities from virtual MSSM effects are not taken into account. In principle, the sparticle masses also acquire loop corrections that depend on all MSSM masses.

R-parity conservation is assumed (at least on the time and distance scale of a typical collider experiment), and only lowest order, sparticle pair production processes are included. Only those processes with $\mathrm{e}^+\mathrm{e}^-, \mu^+\mu^-$, or quark and gluon initial states are simulated. Likewise, only R-parity conserving decays are allowed, so that one sparticle is stable, either the lightest neutralino, the gravitino, or a sneutrino. SUSY decays of the top quark are included, but all other SM particle decays are unaltered.

Various improvements to the simulation are being implemented in stages. Some of these can have a significant impact on the collider phenomenology. Among these are: the generalization to complex-valued soft SUSY-breaking parameters in the neutralino and chargino sector; the same in the Higgs sector, which removes the possibility of CP-even or CP-odd labels; the calculation of neutralino and chargino decay rates which are accurate for large $\tan\beta$; and matrix element weighting of particle distributions in three-body decays.

Strong Dynamics in Electroweak Symmetry Breaking

The simulation of strong dynamics associated with electroweak symmetry breaking in PYTHIA is based on an effective Lagrangian for the lightest resonances of a technicolor (TC)-like model. In TC, the breaking of a chiral symmetry in a new, strongly interacting gauge theory generates the Goldstone bosons necessary for electroweak symmetry breaking. Bound states of technifermions provide a QCD-like spectrum of technipions (π_{tc}), technirhos (ρ_{tc}), techniomegas (ω_{tc}), etc. The mass hierarchies, however, are unlike QCD because of the behavior of the gauge couplings in realistic models of extended TC (ETC). The difficulties of ETC in explaining the top quark mass while suppressing FCNC's is circumvented by the addition of topcolor interactions, which provide the bulk of m_{t}.

In ETC models, hard mass contributions to technipion masses make decays like $\rho_{\mathrm{tc}} \to \pi_{\mathrm{tc}}\pi_{\mathrm{tc}}$ kinematically inaccessible. Instead, decays like $\rho_{\mathrm{tc}}^{\mathrm{ew}} \to \pi_{\mathrm{tc}}^{\mathrm{ew}}\mathrm{W_L}$, for example, dominate, where ew denotes constituent technifermions with only electroweak quantum numbers and $\mathrm{W_L}$ is a longitudinal W bosons. As a result, the ew technirho and techniomega tend to have small total widths.

Effective couplings are derived in the valence technifermion approximation, and the techniparticle decays can be calculated directly [6]. Technirhos and techniomegas are produced through kinematic mixing with gauge bosons, leading to final states containing Standard Model particles and/or pseudo-Goldstone bosons (technipions).

As an additional wrinkle, $\mathrm{SU}_c(3)$ non-singlet states are included along with the coloron of topcolor assisted technicolor. In this case, colored technirhos (and the coloron) can have substantial total widths and enhanced couplings to bottom and top quarks.

6.2.2 QCD Radiation

The matrix-element (ME) and parton-shower (PS) approaches to higher-order QCD corrections both have their advantages and disadvantages. The former offers a systematic expansion in orders of α_{s}, and a powerful machinery to handle multi-parton configurations on the Born level, but loop calculations are tough and lead to messy cancellations at small resolution scales. Resummed matrix elements may circumvent the latter problem for specific quantities, but then do not provide exclusive accompanying events. Parton showers are based on an improved leading-log (almost next-to-leading-log) approximation, and so cannot be accurate for well separated partons, but they offer a simple, process-independent machinery that gives a smooth blending of event classes (by Sudakov form factors) and a sensible match to hadronization. It is therefore natural to try to combine these descriptions, so that ME results are recovered for widely separated partons while the PS sets the sub-jet structure.

For final-state showers in $\mathrm{Z}^0 \to \mathrm{q}\overline{\mathrm{q}}$, where q is assumed essentially massless, such solutions are the standard since long [16], e.g. by letting the shower slightly overpopulate the $\mathrm{q}\overline{\mathrm{q}}\mathrm{g}$ phase space and then using a Monte Carlo veto technique to reduce down to the ME level.

Initial-State Showers

A similar technique is now available for the description of initial-state radiation in the production of a single colour-singlet resonance, such as $\gamma^*/\mathrm{Z}^0/\mathrm{W}^\pm$ [17]. The basic idea is to map the kinematics between the PS and ME descriptions, and to find a correction factor that can be applied to hard emissions in the shower so as to bring agreement with the matrix-element expression. The PYTHIA shower kinematics definitions are based on Q^2 as the spacelike virtuality of the parton produced in a branching and z as the factor by which the $\hat{s}$ of the scattering subsystem is reduced by the branching. Some simple algebra then shows that the two $\mathrm{q}\overline{\mathrm{q}}' \to \mathrm{gW}^\pm$ emission rates disagree by a factor

$$R_{\mathrm{q}\overline{\mathrm{q}}'\to\mathrm{gW}}(\hat{s},\hat{t}) = \frac{(\mathrm{d}\hat{\sigma}/\mathrm{d}\hat{t})_{\mathrm{ME}}}{(\mathrm{d}\hat{\sigma}/\mathrm{d}\hat{t})_{\mathrm{PS}}} = \frac{\hat{t}^2 + \hat{u}^2 + 2m_{\mathrm{W}}^2\hat{s}}{\hat{s}^2 + m_{\mathrm{W}}^4} \ , \tag{6.2}$$

which is always between 1/2 and 1. The shower can therefore be improved in two ways, relative to the old description. Firstly, the maximum virtuality of emissions is raised from $Q^2_{\mathrm{max}} \approx m_{\mathrm{W}}^2$ to $Q^2_{\mathrm{max}} = s$, i.e. the shower is allowed to populate the full phase space. Secondly, the emission rate for the final (which normally also is the hardest) $\mathrm{q} \to \mathrm{qg}$ emission on each side is corrected by the factor $R(\hat{s},\hat{t})$ above, so as to bring agreement with the matrix-element rate in the hard-emission region. In the backwards evolution shower algorithm [18], this is the first branching considered.

The other possible $\mathcal{O}(\alpha_{\mathrm{s}})$ graph is $\mathrm{qg} \to \mathrm{q}'\mathrm{W}^\pm$, where the corresponding correction factor is

$$R_{\mathrm{qg}\to\mathrm{q}'\mathrm{W}}(\hat{s},\hat{t}) = \frac{(\mathrm{d}\hat{\sigma}/\mathrm{d}\hat{t})_{\mathrm{ME}}}{(\mathrm{d}\hat{\sigma}/\mathrm{d}\hat{t})_{\mathrm{PS}}} = \frac{\hat{s}^2 + \hat{u}^2 + 2m_{\mathrm{W}}^2\hat{t}}{(\hat{s} - m_{\mathrm{W}}^2)^2 + m_{\mathrm{W}}^4} \ , \tag{6.3}$$

which lies between 1 and 3. A probable reason for the lower shower rate here is that the shower does not explicitly simulate the s-channel graph $\mathrm{qg} \to \mathrm{q}^* \to \mathrm{q}'\mathrm{W}$. The $\mathrm{g} \to \mathrm{q}\overline{\mathrm{q}}$ branching therefore has to be preweighted by a factor of 3 in the shower, but otherwise the method works the same as above. Obviously, the shower will mix the two alternative branchings, and the correction factor for a final branching is based on the current type.

The reweighting procedure prompts some other changes in the shower. In particular, $\hat{u} < 0$ translates into a constraint on the phase space of allowed branchings, not previously implemented.

Our published comparisons with data on the $p_{\perp\mathrm{W}}$ spectrum show quite a good agreement with this improved simulation [17]. A worry was that an unexpectedly large primordial $k_\perp$, around 4 GeV, was required to match the data in the low-$p_{\perp\mathrm{W}}$ region. However, at that time we had not realized that the data were not fully unsmeared. The required primordial $k_\perp$ therefore drops by about a factor of two [19].

The method can also be used for initial-state photon emission, e.g. in the process $\mathrm{e}^+\mathrm{e}^- \to \gamma^*/\mathrm{Z}^0$. There the old default $Q^2_{\mathrm{max}} = m^2_{\mathrm{Z}}$ allowed no emission at large $p_\perp$, $p_\perp \gtrsim m_{\mathrm{Z}}$ at LEP2. This is now corrected by the increased $Q^2_{\mathrm{max}} = s$, and using the R of eq. (6.2) with $m_{\mathrm{W}} \to m_{\mathrm{Z}}$.

The above method does not address the issue of next-to-leading order corrections to the total W cross section, which instead can be studied with more sophisticated matching procedures [20]. Also extensions to other processes can be considered in the future.

There are also some other changes to the initial state radiation algorithm:

- The cut on minimum gluon energy emitted in a branching is modified by an extra factor roughly corresponding to the $1/\gamma$ factor for the boost to the hard subprocess frame. Earlier, when a subsystem was strongly boosted, the minimum energy requirement became quite stringent on the low-energy incoming side, and could cut out much radiation.
- The angular-ordering requirement is now based on ordering $p_\perp/p$ rather than $p_\perp/p_L$, i.e. replacing $\tan\theta$ by $\sin\theta$. Earlier the starting value $(\tan\theta)_{\mathrm{max}} = 10$ could actually be violated by some bona fide emissions for strongly boosted subsystems.
- The Q^2 value of the backwards evolution of a heavy quark like c in a proton beam is by force kept above m^2_{c}, so as to ensure that the branching $\mathrm{g} \to \mathrm{c}\overline{\mathrm{c}}$ is not 'forgotten' by evolving Q^2 below Q^2_0. Thereby the possibility of having a c in the beam remnant proper is eliminated [21]. The procedure is not forced for a photon beam, where charm occurs as part of the valence flavour content.
- For incoming $\mu^\pm$ (or $\tau^\pm$) beams the kinematical variables are better selected to represent the differences in lepton mass, and the lepton-inside-lepton parton distributions are properly defined.

Final-State Showers

The traditional final-state shower algorithm in PYTHIA [16] is based on an evolution in $Q^2 = m^2$, i.e. potential branchings are considered in order of decreasing mass. A branching $a \to bc$ is then characterized by m_a^2 and $z = E_b/E_a$. For the process $\gamma^*/\mathrm{Z}^0 \to \mathrm{q}\overline{\mathrm{q}}$, the first gluon emission off both q and $\overline{\mathrm{q}}$ are corrected to the first-order matrix elements for $\gamma^*/\mathrm{Z}^0 \to \mathrm{q}\overline{\mathrm{q}}\mathrm{g}$. (The α_s and the Sudakov form factor are omitted from the comparison, since the shower procedure here attempts to include higher-order effects absent in the first-order matrix elements.)

This matching is well-defined for massless quarks, and was originally used unchanged for massive ones. A first attempt to include massive matrix elements did not compensate for mass effects in the shower kinematics, and therefore came to exaggerate the suppression of radiation off heavy quarks [22]. Now the shower has been modified to solve this issue, and also improved and extended to cover better a host of different reactions [23].

The starting point is the calculation of processes $a \to bc$ and $a \to bc\mathrm{g}$, where the ratio

$$W_{\mathrm{ME}}(x_1, x_2) = \frac{1}{\sigma(a \to bc)} \frac{\mathrm{d}\sigma(a \to bc\mathrm{g})}{\mathrm{d}x_1\,\mathrm{d}x_2} \qquad (6.4)$$

gives the process-dependent differential gluon-emission rate. Here the phase space variables are $x_1 = 2E_b/m_a$ and $x_2 = 2E_c/m_a$, expressed in the rest frame of parton a. Using the standard model and the minimal supersymmetric extension thereof as templates, a wide selection of colour and spin structures have been addressed, exemplified by $\mathrm{Z}^0 \to \mathrm{q}\overline{\mathrm{q}}$, $\mathrm{t} \to \mathrm{bW}^+$, $\mathrm{H}^0 \to \mathrm{q}\overline{\mathrm{q}}$, $\mathrm{t} \to \mathrm{bH}^+$, $\mathrm{Z}^0 \to \tilde{\mathrm{q}}\overline{\tilde{\mathrm{q}}}$, $\tilde{\mathrm{q}} \to \tilde{\mathrm{q}}'\mathrm{W}^+$, $\mathrm{H}^0 \to \tilde{\mathrm{q}}\overline{\tilde{\mathrm{q}}}$, $\tilde{\mathrm{q}} \to \tilde{\mathrm{q}}'\mathrm{H}^+$, $\tilde{\chi} \to \mathrm{q}\overline{\tilde{\mathrm{q}}}$, $\tilde{\mathrm{q}} \to \mathrm{q}\tilde{\chi}$, $\mathrm{t} \to \tilde{\mathrm{t}}\tilde{\chi}$, $\tilde{\mathrm{g}} \to \mathrm{q}\overline{\tilde{\mathrm{q}}}$, $\tilde{\mathrm{q}} \to \mathrm{q}\tilde{\mathrm{g}}$, and $\mathrm{t} \to \tilde{\mathrm{t}}\tilde{\mathrm{g}}$. The mass ratios $r_1 = m_b/m_a$ and $r_2 = m_c/m_a$ have been kept as free parameters. When allowed, processes have been calculated for an arbitrary mixture of "parities", i.e. without or with a γ_5 factor, like in the vector/axial vector structure of γ^*/Z^0. All the matrix elements are encoded in the new function `PYMAEL(NI,X1,X2,R1,R2,ALPHA)`, where `NI` distinguishes the matrix elements and `ALPHA` is related to the γ_5 admixture.

In order to match to the singularity structure of the massive matrix elements, the evolution variable Q^2 is changed from m^2 to $m^2 - m^2_{\mathrm{on-shell}}$, i.e. $1/Q^2$ is the propagator of a massive particle. Furthermore, the z variable of a branching needs to be redefined, which is achieved by reducing the three-momenta of the daughters in the rest frame of the mother. For the shower history $b \to b\mathrm{g}$ this gives a differential probability

$$\begin{aligned} W_{\mathrm{PS},1}(x_1, x_2) &= \frac{\alpha_\mathrm{s}}{2\pi} C_F \frac{\mathrm{d}Q^2}{Q^2} \frac{2\,\mathrm{d}z}{1-z} \frac{1}{\mathrm{d}x_1\,\mathrm{d}x_2} \\ &= \frac{\alpha_\mathrm{s}}{2\pi} C_F \frac{2}{x_3\,(1 + r_2^2 - r_1^2 - x_2)} \,, \end{aligned} \qquad (6.5)$$

where the numerator $1 + z^2$ of the splitting kernel for $\mathrm{q} \to \mathrm{qg}$ has been replaced by a 2 in the shower algorithm. For a process with only one radiating parton in the final state, such as $\mathrm{t} \to \mathrm{bW}^+$, the ratio $W_{\mathrm{ME}}/W_{\mathrm{PS},1}$ gives the acceptance probability for an emission in the shower. The singularity structure exactly agrees between ME and PS, giving a well-behaved ratio always below unity. If both b and c can radiate, there is a second possible shower history that has to be considered. The matrix element is here split in two parts, one arbitrarily associated with $b \to b\mathrm{g}$ branchings and the other with $c \to c\mathrm{g}$ ones. A convenient choice is $W_{\mathrm{ME},1} = W_{\mathrm{ME}}(1 + r_1^2 - r_2^2 - x_1)/x_3$ and $W_{\mathrm{ME},2} = W_{\mathrm{ME}}(1 + r_2^2 - r_1^2 - x_2)/x_3$, which again gives matching singularity structures in $W_{\mathrm{ME},i}/W_{\mathrm{PS},i}$ and thus a well-behaved Monte Carlo procedure.

Also subsequent emissions of gluons off the primary particles are corrected to W_{ME}. To this end, a reduced-energy system is constructed, which retains the kinematics of the branching under consideration but omits the gluons already emitted, so that an effective three-body shower state can be mapped to an (x_1, x_2, r_1, r_2) set of variables. For light quarks this procedure is almost equivalent with the original one of using the simple universal splitting kernels after the first branching. For heavy quarks it offers an improved modelling of mass effects also in the collinear region.

Some further changes have been introduced, a few minor as default and some more significant ones as non-default options [23]. This includes the description of coherence effects and α_{s} arguments, in general and more specifically for secondary heavy flavour production by gluon splittings.

Further issues remain to be addressed, e.g. radiation off particles with non-negligible width. In general, however, the new shower should allow an improved description of gluon radiation in many different processes.

6.2.3 Beam Remnants and Multiple Interactions

Beam Remnants

In a hadron–hadron collision, the initial-state radiation algorithm reconstructs one shower initiator in each beam, by backwards evolution from the hard scattering. This initiator only takes some fraction of the total beam energy, leaving behind a beam remnant that takes the rest. Since the initiator is coloured, so is the remnant. It is therefore colour-connected to the hard interaction, and forms part of the same fragmenting system. Often the remnant can be complicated, e.g. a g initiator would leave behind a uud proton-remnant system in a colour octet state, which can conveniently be subdivided into a colour triplet quark and a colour antitriplet diquark, each of which are colour-connected to the hard interaction. The energy sharing between these two remnant objects, and their relative transverse momentum, introduces additional nonperturbative degrees of freedom. Some of the default values have recently been updated [21].

One would expect an ep event to have only one beam remnant, and an e^+e^- event none. This is not always correct, e.g. a $\gamma\gamma \to q\overline{q}$ interaction in an e^+e^- event would leave behind the e^+ and e^- as beam remnants. The photons may in their turn leave behind remnants.

It is customary to assign a primordial transverse momentum to the shower initiator, to take into account the motion of quarks inside the original hadron, basically as required by the uncertainty principle. A number of the order of $\langle k_\perp \rangle \approx m_\mathrm{p}/3 \approx 300$ MeV could therefore be expected. However, in hadronic collisions much higher numbers than that are often required to describe data, typically of the order of 1 GeV [24, 19] if a Gaussian parameterization is used. (This number is now the default.) Thus, an interpretation as a purely nonperturbative motion inside a hadron is difficult to maintain.

Instead a likely culprit is the initial-state shower algorithm. This is set up to cover the region of hard emissions, but may miss out on some of the softer activity, which inherently borders on nonperturbative physics. By default, the shower does not evolve down to scales below $Q_0 = 1$ GeV. Any shortfall in shower activity around or below this cutoff then has to be compensated by the primordial $k_\perp$ source, which thereby largely loses its original meaning.

Multiple Interactions

Multiple parton–parton interactions is the concept that, based on the composite nature of hadrons, several parton pairs may interact in a typical hadron–hadron collision [25]. Over the years, evidence for this mechanism has accumulated, such as the recent direct observation by CDF [26]. The occurrences with two parton pairs at reasonably large $p_\perp$ just form the top of the iceberg, however. In the PYTHIA model, most interactions are at lower $p_\perp$, where they are not visible as separate jets but only contribute to the underlying event structure. As such, they are at the origin of a number of key features, like the broad multiplicity distributions, the significant forward–backward multiplicity correlations, and the pedestal effect under jets.

Since the perturbative jet cross section is divergent for $p_\perp \to 0$, it is necessary to regularize it, e.g. by a cut-off at some $p_{\perp\mathrm{min}}$ scale. That such a regularization should occur is clear from the fact that the incoming hadrons are colour singlets — unlike the coloured partons assumed in the divergent perturbative calculations — and that therefore the colour charges should screen each other in the $p_\perp \to 0$ limit. Also other damping mechanisms are possible [27]. Fits to data typically give $p_{\perp\mathrm{min}} \approx 2$ GeV, which then should be interpreted as the inverse of some colour screening length in the hadron.

One key question is the energy-dependence of $p_{\perp\mathrm{min}}$; this may be relevant e.g. for comparisons of jet rates at different Tevatron energies, and even more for any extrapolation to LHC energies. The problem actually is more pressing now than at the time of the original study [25], since nowadays parton distributions are known to be rising more steeply at small x than the flat $xf(x)$ behaviour normally assumed for small Q^2 before HERA. This translates into a more dramatic energy dependence of the multiple-interactions rate for a fixed $p_{\perp\min}$.

The larger number of partons also should increase the amount of screening, however, as confirmed by toy simulations [28]. As a simple first approximation, $p_{\perp\min}$ is assumed to increase in the same way as the total cross section, i.e. with some power $\epsilon \approx 0.08$ [29] that, via reggeon phenomenology, should relate to the behaviour of parton distributions at small x and Q^2. Thus the new default in PYTHIA is

$$p_{\perp\min}(s) = (1.9\ \text{GeV}) \left(\frac{s}{1\ \text{TeV}^2} \right)^{0.08} . \tag{6.6}$$

6.2.4 Fragmentation and Decays

QCD perturbation theory, formulated in terms of quarks and gluons, is valid at short distances. At long distances, QCD becomes strongly interacting and perturbation theory breaks down. In this confinement régime, the coloured partons are transformed into colourless hadrons, a process called either hadronization or fragmentation.

The fragmentation process has yet to be understood from first principles, starting from the QCD Lagrangian. This has left the way clear for the development of a number of different phenomenological models. PYTHIA is intimately connected with string fragmentation, in the form of the time-honoured 'Lund model' [30]. This is the default for all applications. Improvements have been made in some areas, however.

Low-Mass Strings

A hadronic event is conventionally subdivided into sets of partons that form separate colour singlets. These sets are represented by strings, that e.g. stretch from a quark end via a number of intermediate gluons to an antiquark end. Three string mass regions may be distinguished for the hadronization.

1. *Normal string fragmentation.* In the ideal situation, each string has a large invariant mass. Then the standard iterative fragmentation scheme [30, 31] works well. In practice, this approach can be used for all strings above some cut-off mass of a few GeV.
2. *Cluster decay.* If a string is produced with a small invariant mass, maybe only two-body final states are kinematically accessible. The traditional iterative Lund scheme is then not applicable. We call such a low-mass string a cluster, and consider it separately from above. In recent program versions,

the modeling has now been improved to give a smooth match on to the standard string scheme in the high-cluster-mass limit [21].

3. *Cluster collapse.* This is the extreme case of the above situation, where the string mass is so small that the cluster cannot decay into two hadrons. It is then assumed to collapse directly into a single hadron, which inherits the flavour content of the string endpoints. The original continuum of string/cluster masses is replaced by a discrete set of hadron masses. Energy and momentum then cannot be conserved inside the cluster, but must be exchanged with the rest of the event. This description has also been improved [21].

String systems below a threshold mass are handled by the cluster machinery. In it, an attempt is first made to produce two hadrons, by having the string break in the middle by the production of a new $\mathrm{q}\overline{\mathrm{q}}$ pair, with flavours and hadron spins selected according to the normal string rules. If the sum of the hadron masses is larger than the cluster mass, repeated attempts can be made to find allowed hadrons; the default is two tries. If an allowed set is found, the angular distribution of the decay products in the cluster rest framed is picked isotropically near the threshold, but then gradually more elongated along the string direction, to provide a smooth match to the string description at larger masses. This also includes a forward–backward asymmetry, so that each hadron is preferentially in the same hemisphere as the respective original quark it inherits.

If the attempts to find two hadrons fail, one single hadron is formed from the given flavour content. The basic strategy thereafter is to exchange some minimal amount of energy and momentum between the collapsing cluster and other string pieces in the neighbourhood. The momentum transfer can be in either direction, depending on whether the hadron is lighter or heavier than the cluster it comes from. When lighter, the excess momentum is split off and put as an extra ‘gluon’ on the nearest string piece, where ‘nearest’ is defined by a space–time history-based distance measure. When the hadron is heavier, momentum is instead borrowed from the endpoints of the nearest string piece.

The free parameters of the model can be tuned to data, especially to the significant asymmetries observed between the production of D and $\overline{\mathrm{D}}$ mesons in π^-p collisions, with hadrons that share some of the π^- flavour content very much favoured at large x_F in the π^- fragmentation region [32]. These spectra and asymmetries are closely related to the cluster collapse mechanism, and also to other effects of the colour topology of the event (‘beam drag’) [21]. Also other parameters enter the description, however, such as the effective charm mass and the beam remnant structure.

Baryon Production

A new advanced scheme has been introduced for baryon production with the popcorn mechanism [33], plus some minor changes to the older popcorn scheme [34]. These new features currently only appear as options, with the default unchanged, and can be separated into three parts.

Firstly, an improved implementation of SU(6) weights for baryon production. This should not be regarded as a new model, rather a more correct implementation of the old. However, in order to enable the user to see the effects of the SU(6) weighting separately, both procedures are available as different options. The main change is that, if a step $\mathrm{q} \to \mathrm{B} + \overline{\mathrm{qq}}'$ is SU(6)-rejected, the new try may now instead give a $\mathrm{q} \to \mathrm{M} + \mathrm{q}'$ step (where B stands for baryon, M for meson). The old procedure leads to a slightly faster algorithm and a better interpretation of the input parameter for the diquark-to-quark production rate. However, the probability that a quark will produce a baryon and a antidiquark is then flavour independent, which is not in agreement with the model. Further, for $\mathrm{qq} \to \mathrm{M} + \mathrm{qq}'$, SU(6) symmetry is included in the weights for qq', while qq is kept with unit probability. The procedures for $\mathrm{qq} \to \mathrm{B} + \overline{\mathrm{q}}'$ and a final joining $\mathrm{qq} + \mathrm{q} \to \mathrm{B}$ are unchanged.

Secondly, a suppression of diquark vertices occuring at small proper times. This is based on a study of the production dynamics of the three quarks that form a baryon. The main experimental consequence is a suppression of the baryon production rate at large momentum fraction. This in particular implies a smaller rate of first-rank light baryon production, while charm and bottom baryons are less affected (since the production proper time is larger for a heavy hadron than a light one of the same momentum). It thereby substitutes and explains the older brute-force possibility to suppress the production of first-rank baryons.

Thirdly, a completely new flavour algorithm for baryons and popcorn mesons, also using the small-proper-time suppression above. While the old popcorn alternative allowed at most one meson to be produced in between the baryon and the antibaryon, the new model allows an arbitrary number. The new flavour model makes explicit use of the popcorn suppression factor $\exp(-2m_{\perp}M_{\perp}/\kappa)$, where $m_{\perp}$ is the transverse mass of the quark creating the colour fluctuation, $M_{\perp}$ is the total invariant transverse mass of the popcorn meson system, and κ is the string tension constant. Thus two parameters, representing the mean $2m_{\perp}/\kappa$ for light quarks and s-quarks, respectively, govern both diquark and popcorn meson production. A corresponding parameter is introduced for the fragmentation of strings that contain diquarks already from the beginning, i.e. baryon remnants. The new procedure therefore requires far fewer parameters than the old one, and still provides a comparable quality in the description of the various baryon production rates. This was investigated in detail in [35]. (The concluding worry of an "improper treatment" was caused by an unfortunate misunderstanding and can be disregarded.) Other features, such as baryon correlations, are also modified.

Several new routines have been added, and the diquark code has been extended with information about the curtain quark flavour, i.e. the $q\overline{q}$ pair that is shared between the baryon and antibaryon, but this is not visible externally. Some parameters are no longer used, while others have to be given modified values, as described in the long writeup.

Interconnection Effects

The widths of the W, Z and t are all of the order of 2 GeV. A standard model Higgs with a mass above 200 GeV, as well as many supersymmetric and other beyond the standard model particles would also have widths in the multi-GeV range. Not far from threshold, the typical decay times $\tau = 1/\Gamma \approx 0.1\,\mathrm{fm} \ll \tau_{\mathrm{had}} \approx 1\,\mathrm{fm}$. Thus hadronic decay systems overlap, between a resonance and the underlying event, or between pairs of resonances, so that the final state may not contain independent resonance decays.

So far, studies have mainly been performed in the context of W pair production at LEP2. Pragmatically, one may here distinguish three main eras for such interconnection:

1. Perturbative: this is suppressed for gluon energies $\omega > \Gamma$ by propagator/timescale effects; thus only soft gluons may contribute appreciably.
2. Nonperturbative in the hadroformation process: normally modeled by a colour rearrangement between the partons produced in the two resonance decays and in the subsequent parton showers.
3. Nonperturbative in the purely hadronic phase: best exemplified by Bose–Einstein effects.

The above topics are deeply related to the unsolved problems of strong interactions: confinement dynamics, $1/N_{\mathrm{C}}^2$ effects, quantum mechanical interferences, etc. Thus they offer an opportunity to study the dynamics of unstable particles, and new ways to probe confinement dynamics in space and time [36, 37], *but* they also risk to limit or even spoil precision measurements.

The reconnection scenarios outlined in [37] are now available, plus also an option along the lines suggested in [38]. Currently they can only be invoked in process 25, $e^+e^- \to W^+W^- \to q_1\overline{q}_2q_3\overline{q}_4$, which is the most interesting one for the foreseeable future. (Process 22, $e^+e^- \to \gamma^*/Z^0\ \gamma^*/Z^0 \to q_1\overline{q}_2q_3\overline{q}_4$ can also be used, but the travel distance is calculated based only on the Z^0 propagator part.) If normally the event is considered as consisting of two separate colour singlets, $q_1\overline{q}_2$ from the W^+ and $q_3\overline{q}_4$ from the W^-, a colour rearrangement can give two new colour singlets $q_1\overline{q}_4$ and $q_3\overline{q}_2$. It therefore leads to a different hadronic final state, although differences usually turn out to be subtle and difficult to isolate [39]. When also gluon emission is considered, the number of potential reconnection topologies increases. Apart from the overall rate of reconnection, the scenarios in PYTHIA differ in the relative probability assigned to each of these topologies, based on their properties in momentum space and/or space–time. For instance, scenario I is based on an analogy with type I superconductors, with the colour field represented by extended flux tubes. By contrast, scenario II assumes that narrow vortex lines carry all the topological information, like in type II superconductors, even if the full energy is stored over a wider region.

Bose–Einstein effects are simulated in a simplified manner, by introducing small momentum shifts in identical final-state mesons (primarily $\pi^{\pm}$ and π^0) so as to bring them closer to each other [40]. The shifts can be chosen to reproduce a desired BE enhancement shape for small relative momentum $Q = \sqrt{m_{ij}^2 - 4m_i^2}$ between identical bosons i and j. Typically the shape is chosen as a Gaussian, $f_2(Q) = 1 + \lambda \exp(-Q^2R^2)$, with λ and R two free parameters. The input is only exactly reproduced in the limit of an isotropic and low-density initial particle distribution; since these conditions are not completely fulfilled in reality, there are distortions [41], for better or worse. (The nontrivial three-particle correlations in data are described qualitatively, although not quantitatively.)

A major shortcoming of the algorithm is that energy is not automatically conserved, even though three-momentum is. In the original algorithm, this was solved by a uniform rescaling of all three-momenta, with undesirable side effects e.g. when studying BE effects in W^+W^- hadronic final states. In the current version, several new options have been added that, based on different principles, instead shifts pairs apart. The default one, BE_{32}, operates on identical particles, introducing an extra factor

$$1 + \alpha\lambda \exp(-Q^2R^2/9)\left\{1 - \exp(-Q^2R^2/4)\right\} \tag{6.7}$$

to $f_2(Q)$. Here α is a negative number adjusted event by event for overall energy conservation, with $\langle\alpha\rangle \approx -0.25$. This scenario can be viewed as a simplified version of a dampened oscillating correlation function, where only the first peak and dip has been retained. Further new options have also been introduced specifically geared towards studies of W^+W^- hadronic events, e.g. to include the effects of the separated W^+ and W^- decay vertices.

Decays

Two separate decay treatments exist in PYTHIA. One is making use of a set of tables where branching ratios and decay modes are stored, and is used e.g. for hadronic decays, where branching ratios normally cannot be calculated from first principles.

The other treatment is used for a set of fundamental resonances in or beyond the standard model, such as t, Z^0, $W^{\pm}$, h^0, supersymmetric particles, and many more. Characteristic here is that these resonances have perturbatively calculable widths to each of their decay channels. The decay products are typically quarks, leptons, or other resonances. In decays to quarks, parton showers are automatically added to give a more realistic multijet structure, and one may also allow photon emission off leptons. If the decay products in turn are resonances, further decays are necessary. Often spin information is available in resonance decay matrix elements, leading to nonisotropic decays. This part has been improved in several processes, but is still missing in many others.

The routine used to calculate the partial and total width of resonances (now expressed in GeV throughout), has been expanded for all the new particles and decay modes introduced. Some alternative calculation schemes have also been adopted, e.g. based on a simple rescaling of the on-shell widths rather than a complete recalculation (which may at times not be feasible) based on the current mass.

The width to be used in the denominator of a resonance propagator is only well-defined near the peak. Well away from the peak, an unfortunate choice may lead to a loss of cancellation between resonant and nonresonant diagrams. A special problem exists for a massive standard model Higgs, where the width $\Gamma_{\mathrm{h}} \propto m_{\mathrm{h}}^3$ is so large that the choice of $\hat{s}$ dependence of the width significantly influences the resonance peak shape. Following [42], the default now is $\Gamma_{\mathrm{h}} \propto m_{\mathrm{h}}^2 \sqrt{\hat{s}}$.

6.3 Program News

Essentially all of the basic philosophy and framework remain from the previous PYTHIA and JETSET versions, so no user familiar with these should feel at loss with PYTHIA 6.1. Most of the changes and additions instead are under the surface, and are only visible as new options added to the existing repertoire. However, some changes are fairly obvious, and other less obvious ones still of general interest. These will be covered in this section, in fairly general terms. Again we refer to the PYTHIA web page for a detailed documentation.

6.3.1 Coding Conventions

As before, the FORTRAN 77 standard is adhered to. A very few minor extensions may be used in isolated places, like the 7-character names of the PDFLIB routines [11], but are not known to cause problems on any compiler in use.

An obvious consequence of the PYTHIA/JETSET code merging is that the old JETSET routines and commonblocks have been renamed to begin with `PY` (instead of LU or UL), just like the PYTHIA ones. In most cases, the rest of the name is unchanged, but there are a few exceptions, mainly RLU→PYR, KLU→PYK, PLU→PYP and LUXTOT→PYXTEE. Three integer functions now begin with PY, namely PYK, PYCHGE and PYCOMP, and therefore have to be declared extra. The LUDATA block data has been merged into PYDATA, and the test routine LUTEST into PYTEST. For rotations and boosts, the PYROBO routine now requires the range of affected entries to be given, like the old LUDBRB but unlike LUROBO (but 0,0 as range arguments gives back the old LUROBO behaviour).

All real variables are now in DOUBLE PRECISION, which is assumed to mean 64 bits, and also real constants have been promoted to the higher precision. This is required to ensure proper functioning at currently studied energies, such as the LHC and beyond. To take into account this, all routines begin with the declarations

```
C...Double precision and integer declarations.
      IMPLICIT DOUBLE PRECISION(A-H, O-Z)
      IMPLICIT INTEGER(I-N)
      INTEGER PYK,PYCHGE,PYCOMP
```

and users should do the same in their main programs.

On a machine where DOUBLE PRECISION would give 128 bits, it may make sense to use compiler options to revert to 64 bits, since the program is anyway not constructed to make use of 128 bit precision.

The random number generator is the same as in previous versions [43], but has now been expanded to operate with a 48 bit mantissa for the real numbers.

FORTRAN 77 makes no provision for double-precision complex numbers, but since COMPLEX is used only sparingly, no problems should be expected from this omission. For the technicolor processes, some variables are declared COMPLEX*16 in the PYSIGH routine. Should the compiler not accept this, that one declaration can be changed to COMPLEX with some drop in precision for the affected processes.

Several compilers report problems when an odd number of integers precede a double-precision variable in a commonblock. Therefore an extra integer has been introduced as padding in a few instances (NPAD, MSELPD and NGENPD in Table 6.5).

In order to cater for the increased offering of subprocesses, some arrays in commonblocks have been expanded. A few, such as PYINT4, have also been reorganized to represent improvements in the physics modeling. Most commonblocks and commonblock variables are easily recognizable from previous program versions, however. The current complement is given in Table 6.5, omitting some of the less interesting ones.

Since FORTRAN 77 provides no date-and-time routine, PYTIME allows a system-specific routine to be interfaced, with some commented-out examples

Table 6.5: The current form of the main commonblock declarations.

```
COMMON/PYJETS/N,NPAD,K(4000,5),P(4000,5),V(4000,5)
COMMON/PYDAT1/MSTU(200),PARU(200),MSTJ(200),PARJ(200)
COMMON/PYDAT2/KCHG(500,4),PMAS(500,4),PARF(2000),VCKM(4,4)
COMMON/PYDAT3/MDCY(500,3),MDME(4000,2),BRAT(4000),KFDP(4000,5)
COMMON/PYDAT4/CHAF(500,2)
CHARACTER CHAF*16
COMMON/PYDATR/MRPY(6),RRPY(100)
COMMON/PYSUBS/MSEL,MSELPD,MSUB(500),KFIN(2,-40:40),CKIN(200)
COMMON/PYPARS/MSTP(200),PARP(200),MSTI(200),PARI(200)
COMMON/PYINT1/MINT(400),VINT(400)
COMMON/PYINT2/ISET(500),KFPR(500,2),COEF(500,20),ICOL(40,4,2)
COMMON/PYINT3/XSFX(2,-40:40),ISIG(1000,3),SIGH(1000)
COMMON/PYINT4/MWID(500),WIDS(500,5)
COMMON/PYINT5/NGENPD,NGEN(0:500,3),XSEC(0:500,3)
COMMON/PYINT6/PROC(0:500)
CHARACTER PROC*28
COMMON/PYMSSM/IMSS(0:99),RMSS(0:99)
COMMON/PYUPPR/NUP,KUP(20,7),NFUP,IFUP(10,2),PUP(20,5),Q2UP(0:10)
COMMON/PYBINS/IHIST(4),INDX(1000),BIN(20000)
```

given in the code. This routine is only used for cosmetic improvements of the output, however, so can be left at the default with time 0 given.

For a program written to run PYTHIA 5 and JETSET 7, most of the conversion required for PYTHIA 6 is fairly straightforward, and can be automatized. Both a simple FORTRAN routine and a more sophisticated PERL [44] script exists to this end. Some manual checks and interventions may still be required.

6.3.2 Particle Codes and Data

A number of new particle codes `KF` have been introduced, or modified, see Table 6.6. Mostly this is based on the PDG-agreed conventions [45, 46], but some not yet standardized codes appear in the 'empty' range 41–80. Furthermore, the fourth generation fermions and neutral scalar Higgs states have been renamed. The two fermion spartners are labelled left and right, except in the third generation, where an expected larger mixing makes the two mass eigenstates a better choice of classification.

The top hadrons are gone. It is now known that top is too short-lived to form hadronic bound states, so a reasonable description is instead to have the top quarks decay before hadronization is considered. The same is now

Table 6.6: New or modified particle codes or names.

Renamed:	
7	b′
8	t′
17	τ'
18	ν'_τ
25	h^0
35	H^0
Moved:	
100443	ψ'
100553	Υ'
4000001	d^*
4000002	u^*
4000011	e^*
4000012	ν_e^*

Technicolor:	
51	π^0_tc
52	π^+_tc
53	$\pi'^{\,0}_\mathrm{tc}$
54	ρ^0_tc
55	ρ^+_tc
56	ω^0_tc
LR-symmetric:	
61	H_L^{++}
62	H_R^{++}
63	W_R^+
64	$\nu_{R\mathrm{e}}$
65	$\nu_{R\mu}$
66	$\nu_{R\tau}$

SUSY:		SUSY:	
1000001	$\tilde{\mathrm{d}}_L$	2000001	$\tilde{\mathrm{d}}_R$
1000002	$\tilde{\mathrm{u}}_L$	2000002	$\tilde{\mathrm{u}}_R$
1000003	$\tilde{\mathrm{s}}_L$	2000003	$\tilde{\mathrm{s}}_R$
1000004	$\tilde{\mathrm{c}}_L$	2000004	$\tilde{\mathrm{c}}_R$
1000005	$\tilde{\mathrm{b}}_1$	2000005	$\tilde{\mathrm{b}}_2$
1000006	$\tilde{\mathrm{t}}_1$	2000006	$\tilde{\mathrm{t}}_2$
1000011	$\tilde{\mathrm{e}}_L$	2000011	$\tilde{\mathrm{e}}_R$
1000012	$\tilde{\nu}_{\mathrm{e}L}$	2000012	$\tilde{\nu}_{\mathrm{e}R}$
1000013	$\tilde{\mu}_L$	2000013	$\tilde{\mu}_R$
1000014	$\tilde{\nu}_{\mu L}$	2000014	$\tilde{\nu}_{\mu R}$
1000015	$\tilde{\tau}_1$	2000015	$\tilde{\tau}_2$
1000016	$\tilde{\nu}_{\tau L}$	2000016	$\tilde{\nu}_{\tau R}$
1000021	$\tilde{\mathrm{g}}$	1000025	$\tilde{\chi}^0_3$
1000022	$\tilde{\chi}^0_1$	1000035	$\tilde{\chi}^0_4$
1000023	$\tilde{\chi}^0_2$	1000037	$\tilde{\chi}^+_2$
1000024	$\tilde{\chi}^+_1$	1000039	$\tilde{\mathrm{G}}$

assumed about a hypothetical fourth generation. Should the need ever arise in the future to consider a new long-lived coloured object, an effective description of a hadron as a small string with an ordinary colour-matching flavour at the other end should be sufficient. One such example would be leptoquark-hadrons [47].

Bottom hadrons are now defined individually, e.g. the previous common decay scheme is gone in favour of individual branching ratios for each hadron. On the other hand, given the sketchy knowledge of many branching ratios, the default description is still fairly standardized.

Decay data is mainly based on the 1996 PDG edition [48], but with many 'educated guesses' to fill in missing information.

Since running fermion masses are used in an increasing number of processes, e.g. for Higgs couplings, a function `PYMRUN(KF,Q2)` has been introduced to give the mass as a function of Q^2 scale.

The compressed codes, `KC = PYCOMP(KF)`, are completely changed. We remind that `KF` can range up to seven-digit codes, plus a sign. They therefore cannot be used to directly access information in particle data tables. The `KC` codes range between 1 and 500, and give the index to the particle data arrays. Each `KF` code is now one-to-one associated with a `KC` code; the only ambiguity is that `KC` does not distinguish antiparticles from particles. Whereas `KF` codes below 100 still obey `KF = KC`, the mapping of codes above 100 is completely changed. It is no longer hard-coded in PYCOMP, but defined by the fourth component of the KCHG array. Therefore it can be changed or expanded during the course of a run, either by PYUPDA calls or by direct user intervention.

6.3.3 New Options

A large amount of new options have been added, related to almost all the physics changes above and more, and we here only mention some of the more significant ones.

The inclusion of SUSY processes means that all the SPYTHIA PYMSSM commonblock switches and parameters are inherited. New parameters are added also for other new physics scenarios, such as technicolor and doubly-charged Higgses.

The extensions to the physics of virtual photons, outlined in Section 6.2.1, has resulted in two sets of new possibilities. One is in the description of the virtual-photon flux, where new CKIN switches has been introduced, e.g. to set the range of photon x and Q^2. This is available when PYINIT is called with **'gamma/lepton'** as beam or target, to denote that the photon flux inside the lepton has to be considered as a new administrative layer, also documented in the event record. The other is the new physics machinery. Here the main switch is MSTP(14) that sets the assumed nature of the photon or photons, e.g. 'a direct photon from the left collides with a VMD one from the right'. The default is the most general mixture, meaning 4 components for γ^*p and 13 for $\gamma^*\gamma^*$. This is the relevant approach for studies of QCD processes. There is no corresponding automatic mixing machinery for other processes, so then the relevant contributing components have to be handled separately and added afterwards. Further options are available for several of the components, e.g. the DIS process dampening in the $Q^2 \to 0$ limit, the relative normalization of the GVMD spectrum, the scale choice for parton distributions, and the possibility to add the effects of a longitudinal resolved contribution.

The matrix-element options for $\mathrm{e}^+\mathrm{e}^- \to \gamma^*/\mathrm{Z}^0 \to 2$, 3 or 4 partons have previously only been available via the LUEEVT/PYEEVT routine, that suffers from problems of its own in having a rather old-fashioned machinery for QED initial-state radiation and electroweak parameters. Now the QCD matrix-element description is accessible as an option to the shower default for $\mathrm{e}^+\mathrm{e}^-$ events generated with subprocess 1 of the standard PYTHIA machinery.

6.3.4 Interfaces

While PYTHIA contains an extensive library of subprocesses, it is far from up to all the requirements of the experimental community. Both further processes and a more detailed treatment of the existing ones is required at times. In particular, it is not uncommon with a generator dedicated to one specific process, where also higher-order electroweak corrections, absent in PYTHIA, have been included in the cross section. None of these programs are geared to handle the QCD aspects of parton showers and hadronization, however, so it makes sense to combine the individual strengths.

A generic facility to include external processes exists since long in PYTHIA. Here one can feed in partonic configurations from an external generator, together with some basic information on colour flow and which partons are allowed to radiate, and let PYTHIA construct a complete event based on this information. For the simple configurations encountered in $\mathrm{e}^+\mathrm{e}^-$ annihilation events, this would often be overkill, since neither the initial-state QCD radiation nor beam-remnant treatment of the generic (hadronic) collision is present.

Based on the concepts presented in the LEP2 workshop [46], a few simpler alternatives are therefore now provided for this kind of tasks:

- `CALL PY2FRM(IRAD,ITAU,ICOM)` allows a parton shower to develop and partons to hadronize from a given two-fermion starting point. `IRAD` sets whether quarks are allowed also to radiate photons or not, `ITAU` whether τ leptons should be decayed or not, and `ICOM` whether the input and output event record is `HEPEVT` or `PYJETS`. An arbitrary number of photons (e.g. from initial-state radiation) may also be stored with the input.
- `CALL PY4FRM(ATOTSQ,A1SQ,A2SQ,ISTRAT,IRAD,ITAU,ICOM)` allows parton showers to develop and partons to hadronize from a given four-fermion starting point. The extra parameters can be used to select between the two colour pairings allowed for a $\mathrm{q}_1\overline{\mathrm{q}}_2\mathrm{q}_3\overline{\mathrm{q}}_4$ state, according to some different strategies when interference terms do not allow unique probabilities to be found.
- `CALL PY6FRM(P12,P13,P21,P23,P31,P32,PTOP,IRAD,ITAU,ICOM)` allows parton showers to develop and partons to hadronize from a given six-fermion starting point. The `Pij` parameters give the relative probabilities for the six colour pairings allowed for a six-quark state, and `PTOP` the probability that the event originates from a $\mathrm{t}\overline{\mathrm{t}}$ pair (in which case the shower handling has to be different than e.g. in a $\mathrm{Z}^0\mathrm{W}^+\mathrm{W}^-$ event).

The above routines are not set up to handle QCD four-jet events, i.e. events of the types $\mathrm{q}\overline{\mathrm{q}}\mathrm{gg}$ and $\mathrm{q}\overline{\mathrm{q}}\mathrm{q}'\overline{\mathrm{q}}'$, with $\mathrm{q}'\overline{\mathrm{q}}'$ coming from a gluon branching. Such events are generated in normal parton showers, but not necessarily at the right rate (a problem that may be especially interesting for massive quarks like b). Therefore one would like to start a QCD parton shower from a given four-parton configuration. Some time ago, a machinery was developed to handle this kind of occurences [49]. This approach has now been adapted to the current PYTHIA version, in a somewhat modified form. In it, an imagined shower history of two branchings is (re)constructed from the four-parton state, according to relative probabilities derived in the shower language. Thereafter a normal shower is allowed to develop, with branchings chosen at random except for these two predetermined ones. The routine `CALL PY4JET(PMAX,IRAD,ICOM)` takes an original four-parton configuration stored in `HEPEVT` or `PYJETS` and lets a shower develop as described above. `PMAX` can be used to set the maximum virtuality of those parts of the shower not given from the parton configuration itself, either to a fixed value or to the lowest virtuality of the reconstructed shower.

6.3.5 Utilities

The clustering algorithm `PYCLUS` has been extended also to accept the Durham distance measure [50] as an alternative. This is $p_\perp$-based, like the original `LUCLUS` distance measure, but differs in the details.

The `GBOOK` histogramming package was written in 1979 as a lightweight substitute for `HBOOK` [51] before that program was available in FORTRAN 77. The one-dimensional histogram part now appears in the standard distribution, in order to make the sample runs offered on the web a bit more realistic. The main routines are:

- `CALL PYBOOK(ID,TITLE,NX,XL,XU)` to book a one-dimensional histogram with integer identifier `ID` (in the range $1 - 1000$), character title `TITLE` and `NX` bins stretching from `XL` to `XU`.
- `CALL PYFILL(ID,X,W)` to fill histogram `ID` at position `X` with weight `W`.
- `CALL PYFACT(ID,F)` to rescale the contents of histogram `ID` by a factor `F`.
- `CALL PYOPER(ID1,OPER,ID2,ID3,F1,F2)` to perform operations on several histograms, such as adding or dividing them by each other.
- `CALL PYDUMP(MDUMP,LFN,NHI,IHI)` to dump histogram contents to a file from which they could be read in for plotting in another program.
- `CALL PYHIST` to print all histograms in a simple line-printer mode, and thereafter reset histogram contents.

A commonblock of dimension 20000 is used to store the histograms; this size may need to be expanded if many histograms are to be booked.

The `PYUPDA` routine has been expanded with a new option that allows a set of particle data to be read in, in tabular form as before, as an addition to or partial replacement of the existing particle data.

6.4 Summary and Outlook

We have here given a very brief survey of news in the PYTHIA 6.1 program. A more detailed description of physics and programs is available separately [52]. Any serious user should turn to this publication, and to the original physics papers, for further information.

The treasure trove for information is the PYTHIA webpage,

`http://www.thep.lu.se/~torbjorn/Pythia.html` , where one may find the current and previous subversions, with documentation, sample main programs, links to related programs, etc.

The PYTHIA program is continuously being developed. We are aware of many physics shortcomings, which hopefully will be addressed in the future. It is in the nature of a program of this kind never to be finished, at least as long as it is of importance for the high-energy physics experimental community.

The main visible change in the future is the transition to C++ as the programming language for PYTHIA 7. Even if much of the physics will be carried over unchanged, none of the existing code will survive. The structure of the event record and the whole administrative apparatus is completely different from the current one, in order to allow a much more general and flexible formulation of the event generation process. Following the formulation of a strategy document [53], a first proof-of-concept version was released recently [54]. So far it only contains one reasonably complete physics module, however, namely that of string fragmentation. More realistic versions should follow, but it will take a long time to convert all important physics components from PYTHIA 6. The two versions therefore will coexist for several years, with the FORTRAN one used for physics 'production' and the C++ one for exploration of the object-oriented approach that will be standard at the LHC.

Acknowledgements

A large number of persons should be thanked for their contributions. Bo Andersson and Gösta Gustafson are the originators of the Lund model, and strongly influenced the early development of the programs. Hans-Uno Bengtsson is the originator of the PYTHIA program. Mats Bengtsson is the original author of the final-state parton-shower algorithm. Several pieces of code have been donated by other persons. Further comments on the programs have been obtained from users too numerous to be mentioned here, but who are all gratefully acknowledged. To write programs of this size and complexity would be impossible without a strong user feedback.

References

[1] T. Sjöstrand, Comput. Phys. Commun. **82** (1994) 74.

[2] H.-U. Bengtsson, Comput. Phys. Commun. **31** (1984) 323;
H.-U. Bengtsson and G. Ingelman, Comput. Phys. Commun. **34** (1985) 251;
H.-U. Bengtsson and T. Sjöstrand, Comput. Phys. Commun. **46** (1987) 43.

[3] T. Sjöstrand, Comput. Phys. Commun. **27** (1982) 243;
T. Sjöstrand, Comput. Phys. Commun. **28** (1983) 227;
T. Sjöstrand, Comput. Phys. Commun. **39** (1986) 347;
T. Sjöstrand and M. Bengtsson, Comput. Phys. Commun. **43** (1987) 367.

[4] S. Mrenna, Comput. Phys. Commun. **101** (1997) 232.

[5] B. Cano-Coloma and M.A. Sanchis-Lozano, Nucl. Phys. **B508** (1997) 753;
A. Edin, G. Ingelman and J. Rathsman, Phys. Rev. **D56** (1997) 7317.

[6] K. Lane, Phys. Rev. **D60** (1999) 075007;
S. Mrenna, Phys. Lett. **B461** (1999) 352.

[7] K. Huitu, J. Maalampi, A. Pietilä and M. Raidal, Nucl. Phys. **B487** (1997) 27, and private communication;
G. Barenboim, K. Huitu, J. Maalampi and M. Raidal, Phys. Lett. **B394** (1997) 132.

[8] M. Glück, E. Reya and A. Vogt, Z. Phys. **C67** (1995) 433.

[9] G.A. Schuler and T. Sjöstrand, Z. Phys. **C68** (1995) 607, Phys. Lett. **B376** (1996) 193.

[10] CTEQ Collaboration, H.L. Lai et al., Eur. Phys. J. **C12** (2000) 375.

[11] H. Plothow-Besch, Comput. Phys. Commun. **75** (1993) 396.

[12] G.A. Schuler and T. Sjöstrand, Nucl. Phys. **B407** (1993) 539, Z. Phys. **C73** (1997) 677.

[13] C. Friberg and T. Sjöstrand, Eur. Phys. J. **C13** (2000) 151, JHEP **09** (2000) 010 (hep-ph/0007314), LU TP 00–31 (hep-ph/0009003), to appear in Phys. Lett. **B**.

[14] H.E. Haber and G.L. Kane, Phys. Rep. **117** (1985) 75.

[15] M. Carena, J.–R. Espinosa, M. Quiros and C.E.M. Wagner, Phys. Lett. **B355** (1995) 209;
M. Carena, M. Quiros and C.E.M. Wagner, Nucl. Phys. **B461** (1996) 407.

[16] M. Bengtsson and T. Sjöstrand, Phys. Lett. **B185** (1987) 435, Nucl. Phys. **B289** (1987) 810.

[17] G. Miu and T. Sjöstrand, Phys. Lett. **B449** (1999) 313.

[18] T. Sjöstrand, Phys. Lett. **157B** (1985) 321.

[19] C. Bálazs, J. Huston and I. Puljak, hep-ph/0002032.

[20] S. Mrenna, UCD-99-4 (hep-ph/9902471).

[21] E. Norrbin and T. Sjöstrand, Phys. Lett. **B442** (1998) 407, LU TP 00–16 (hep-ph/0005110), to appear in Eur. Phys. J. **C**, DOI 10.1007/s100520000460.

[22] A Ballestrero et al., hep-ph/0006259, to appear in the Proceedings of the LEP2 Monte Carlo Workshop.

[23] E. Norrbin and T. Sjöstrand, LU TP 00–42 (hep-ph/0010012).

[24] EMC Collaboration, M. Arneodo et al., Z. Phys. **C36** (1987) 527;
L. Apanasevich et al., Phys. Rev. **D59** (1999) 074007.

[25] T. Sjöstrand and M. van Zijl, Phys. Rev. **D36** (1987) 2019.

[26] CDF Collaboration, F. Abe et al., Phys. Rev. Lett. **79** (1997) 584.

[27] G. Gustafson and G. Miu, LU TP 99–43 (hep-ph/0002278).

[28] J. Dischler and T. Sjöstrand, LU TP 00–01 (hep-ph/0001237), in preparation.

[29] A. Donnachie and P.V. Landshoff, Phys. Lett. **B296** (1992) 227.

[30] B. Andersson, G. Gustafson, G. Ingelman and T. Sjöstrand, Phys. Rep. **97** (1983) 31.

[31] T. Sjöstrand, Nucl. Phys. **B248** (1984) 469.

[32] WA82 Collaboration, M. Adamovich et al., Phys. Lett. **B305** (1993) 402;
E769 Collaboration, G.A. Alves et al., Phys. Rev. Lett. **72** (1994) 812;
E791 Collaboration, E.M. Aitala et al., Phys. Lett. **B371** (1996) 157.

[33] P. Edén and G. Gustafson, Z. Phys. **C75** (1997) 41;
P. Edén, LUTP 96–29 (hep-ph/9610246).

[34] B. Andersson, G. Gustafson and T. Sjöstrand, Nucl. Phys. **B197** (1982) 45, Physica Scripta **32** (1985) 574.

[35] A. Joly, J. Gascon, P. Taras, Eur. Phys. J. **C6** (1999) 413.

[36] G. Gustafson, U. Pettersson and P. Zerwas, Phys. Lett. **B209** (1988) 90.

[37] T. Sjöstrand and V.A. Khoze, Z. Phys. **C62** (1994) 281, Phys. Rev. Lett. **72** (1994) 28.

[38] G. Gustafson and J. Häkkinen, Z. Phys. **C64** (1994) 659.

[39] E. Norrbin and T. Sjöstrand, Phys. Rev. **D55** (1997) R5;
V.A. Khoze and T. Sjöstrand, Eur. Phys. J. **C6** (1999) 271, EPJdirect **C1** (2000) 1.

[40] L. Lönnblad and T. Sjöstrand, Phys. Lett. **B351** (1995) 293, Eur. Phys. J. **C2** (1998) 165.

[41] R. Muresan, O. Smirnova and B. Lörstad, Eur. Phys. J. **C6** (1999) 629.

[42] M. Seymour, Phys. Lett. **B354** (1995) 409.

[43] G. Marsaglia, A. Zaman and W.-W- Tsang, Stat. Prob. Lett. **9**. (1990) 35; F. James, Comput. Phys. Commun. **60** (1990) 329.

[44] L. Garren, `http://www-pat.fnal.gov/mcgen/lund/convert.pl`.

[45] Particle Data Group, D.E. Groom et al., Eur. Phys. J. **C15** (2000) 1.

[46] I.G. Knowles et al., in 'Physics at LEP2', CERN 96-01, eds. G. Altarelli, T. Sjöstrand and F. Zwirner, Vol. 2, p. 103.

[47] C. Friberg, E. Norrbin and T. Sjöstrand, Phys. Lett. **B403** (1997) 329.

[48] Particle Data Group, R.M. Barnett et al., Phys. Rev. **D54** (1996) 1.

[49] J. André and T. Sjöstrand, Phys. Rev. **D57** (1998) 5767.

[50] S. Catani, Yu.L. Dokshitzer, M. Olsson, G. Turnock and B.R. Webber, Phys. Lett. **B269** (1991) 432.

[51] R. Brun et al., CERN Program Library code Y250.

[52] T. Sjöstrand, LU TP 95–20 (hep-ph/9508391), updated version in preparation.

[53] L. Lönnblad, Comput. Phys. Commun. **118** (1999) 213.

[54] M. Bertini, L. Lönnblad and T. Sjöstrand, LU TP 00–23 (hep-ph/0006152), to appear in Comput. Phys. Commun.